SKB

TECHNICAL REPORT 92-30

Interaction between rock, bentonite buffer and canister. FEM calculations of some mechanical effects on the canister in different disposal concepts

Lennart Börgesson

Clay Technology AB, Lund, Sweden

July 1992

SVENSK KÄRNBRÄNSLEHANTERING AB
SWEDISH NUCLEAR FUEL AND WASTE MANAGEMENT CO

BOX 5864 S-102 48 STOCKHOLM

TEL 08-665 28 00 TELEX 13108 SKB S
TELEFAX 08-661 57 19

INTERACTION BETWEEN ROCK, BENTONITE BUFFER AND CANISTER.
FEM CALCULATIONS OF SOME MECHANICAL EFFECTS ON THE CANISTER IN DIFFERENT DISPOSAL CONCEPTS

Lennart Börgesson

Clay Technology AB, Lund, Sweden

July 1992

This report concerns a study which was conducted for SKB. The conclusions and viewpoints presented in the report are those of the author(s) and do not necessarily coincide with those of the client.

Information on SKB technical reports from 1977-1978 (TR 121), 1979 (TR 79-28), 1980 (TR 80-26), 1981 (TR 81-17), 1982 (TR 82-28), 1983 (TR 83-77), 1984 (TR 85-01), 1985 (TR 85-20), 1986 (TR 86-31), 1987 (TR 87-33), 1988 (TR 88-32), 1989 (TR 89-40), 1990 (TR 90-46) and 1991 (TR 91-64) is available through SKB.

Interaction Between Rock, Bentonite Buffer and Canister

FEM Calculations of Some Mechanical Effects on the Canister in Different Disposal Concepts

July 1992

Lennart Börgesson

Clay Technology AB
IDEON, 223 70 Lund

ABSTRACT

An important task of the buffer of highly compacted bentonite is to offer a mechanical protection to the canister. This role has been investigated by a number of finite element calculations using the complex elasto plastic material models for the bentonite that have been developed on the basis of laboratory tests and adapted to the code ABAQUS.

The following main functions and scenarios have been investigated for some different canister types and repository concepts:

- The effect of the water and swelling pressure
- The effect of a rock shear perpendicular to the canister axis
- The effect of creep in the copper after a rock shear displacement
- The thermomechanical effects when an initially saturated buffer is used

TABLE OF CONTENTS

SUMMARY

The function of the bentonite buffer as a mechanical protection of the canister in a repository has been investigated in a number of finite element calculations. Three canister types (KBS3 HIP canister, KBS3 Cu/Fe composite canister and VLH large canister) and two repository concepts (KBS3 and VLH) have been compared.

The functions and scenarios have been simulated by the finite element code ABAQUS. The bentonite behaves according to the effective stress theory and has been modeled as Porous Elastic and Drucker Prager Plastic according to laboratory investigations.

The most important results from the calculations are:

- the water and swelling pressure will close the gap between the copper and the steel in the composite canisters except at the edges of the lids when the canister has flat ends.

- A rock displacement of 10 cm across the deposition hole will cause some plastic strain in the copper in all concepts and for all canisters investigated but the plastic strain is small with a maximum of 4% which was achieved at a density higher than intended for actual use in repositories.

- the thermomechanical function of an initially water saturated buffer is acceptable if the rock offers drainage of the porewater overpressure in the bentonite. Rock that is too impermeable to let the overpressure dissipate is unsuitable.

1 INTRODUCTION

The highly compacted bentonite, surrounding the canisters in all the Swedish concepts for disposal of nuclear fuel, acts as a mechanical buffer between the rock and the canister. However, there are some scenarios, especially that of rock displacement along a fracture intersecting the deposition hole, that need to be studied further. This report shows some calculations of the following effects on the canister:

- Swelling pressure of the bentonite
- Rock shear through different levels of the canister
- Thermomechanical effects on the canister

Three different types of canisters have been considered:

- KBS3 HIP canister
- KBS3 copper/steel composite canister
- VLH large copper/steel composite canister

Some of the calculations were initiated by SKB's Reference Group for Mechanical Integrity of Canisters for Spent Nuclear Fuel, while some were made in connection with the functional analyses for PASS. The latter calculations only refer to the cases of interest for the canister behavior while other calculations for PASS are described in a separate report.

2 FINITE ELEMENT PROGRAM

All calculations were made with the finite element code ABAQUS, which is specially designed for non-linear analyses. The calculations were performed at FEMTECH in Västerås in close cooperation between the author and Jan Hernelind.

The element models were made either directly by assigning nodes and coordinates to the input files, or by use of the preprocessor PATRAN.

Since the calculations include different materials with very complex material models (especially the bentonite) and coupled processes (e.g. stress, strain, pore water flow, heat flow and thermal expansion) their performance was not straightforward. Thus, any successful calculation was usually preceded by a large number of trials with non-convergent solutions.

The calculations were first conducted with a simple material model and successively developed towards the models and technique used for the ultimate versions. For this reason the material models and the structure model have varied somewhat, but as a whole the calculations are comparable unless otherwise stated in the text.

3 MATERIAL MODELS

3.1 GENERAL

The material models for the bentonite buffer have been developed from the results of many laboratory tests and verification calculations. These models and their status at the end of 1990 are in detail described by Börgesson (1990).

The main choice of modeling the plastic behavior was between Drucker Prager and Cam Clay. None of them is perfect for modeling the behavior of bentonite but a generalized Drucker Prager model has been proved to describe the behavior well in a limited range of average stress.

The elastic part of the Drucker Prager model is well described as Porous Elastic, which means that the relation between the void ratio and the logarithm of the average stress is a straight line.

Since water saturated bentonite is a two-phase material and the pore water plays an important role for the behavior, the pore properties and the soil structure properties are separated and modeled individually. The Effective Stress Theory is the basis for that modeling.

The copper and steel parts of the canister are modeled with traditional elastic-plastic metal models. The rock is either modeled as a rigid surface or as a very stiff elastic porous medium.

3.2 BENTONITE

The models and parameters used for the bentonite can be grouped as follows:

- Modeling of Drucker-Prager Plasticity
- Modeling of Porous Elasticity
- Modeling of Pore and Particle properties
- Modeling of Thermal and Thermomechanical behavior
- Initial conditions

The parameters may vary a little between the individual calculations depending mostly on refinement of the models. The parameters will be described in this chapter and the basic values given.

Drucker Prager Plasticity

In the Drucker-Prager Plasticity model the influence of the average stress (friction angle $\phi \neq 0$) can be taken into account. Cohesion can also be simulated.

The model is illustrated in Fig 3-1, which shows that the stress dependence is caused by the "friction angle" β in the σ_j-p plane and the parameter d illustrating the "cohesion". If the plastic flow $d\varepsilon^{pl}$ is associated, the angle $\psi=\beta$ and the flow is perpendicular to the yield surface. In order to decrease the resulting dilation it is necessary to assume non-associated flow by putting $\psi<\beta$.

When the stress path enters the plastic region ds^{pl} the yield surface is moved upwards until it reaches the failure surface.

The model also includes a constant K which controls the dependence of the yield surface on the inter-

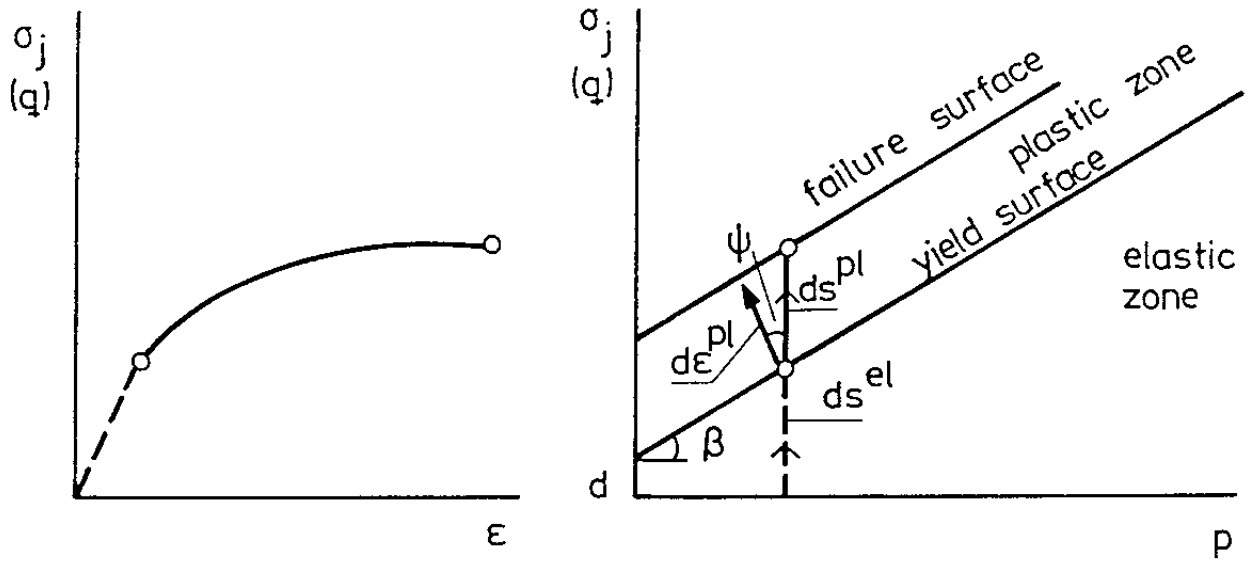

Figure 3-1 Drucker-Prager Plasticity Model

mediate principle stress. The yield surface is defined so that K is the ratio of the yield stress in triaxial tension and the yield stress in triaxial compression. The classical Drucker-Prager model is obtained when K=1.0 and ψ=β.

The parameters needed for the extended Drucker-Prager model are thus β, d, K, ψ and the yield function f. The basic values of those parameters are:

β=20°
d=100 kPa
ψ=2°
K=0.9

Yield function

σ_j (kPa)	ε_y
113	0
138	0.005
163	0.02
188	0.04
213	0.1

σ_j is the Mises stresses and ε_y is the plastic strain at a stress path that corresponds to a uniaxial compression test, i.e. without confining pressure. Linear interpolation is made between the values.

Porous Elasticity

In a porous material, the volume or void ratio can be changed. The stress/void ratio relation can be expressed by use of the porous elasticity model, in which the volumetric behavior is defined according to Eqn 2:6

$$\frac{\kappa}{1+e_0}\ln(p_0/p) = J^{el}-1 \qquad (2:6)$$

where
e_0= initial void ratio
p_0= initial average stress
κ= the inclination of the e-log$p$ relation
J^{el}=the elastic volume ratio

The key parameters are κ, i.e. the logarithmic bulk modulus while Poisson's ratio is also needed. The basic values of these parameters are:

κ=0.21
ν=0.4

Pore and particle properties

The density ρ_w and bulk modulus B_w of the pore water as well as the bulk modulus of the solid particles B_s are:

ρ_w=1.0 t/m^3
B_w=2.1·10^6 kPa
B_s=2.1·10^8 kPa

The flow of water through the clay is modeled by Darcy's law with the hydraulic conductivity k being a function of the void ratio e (interpolation between the values). The following basic relation is used:

e	k (m/s)
0.45	$1.0 \cdot 10^{-14}$ m/s
0.70	$6.0 \cdot 10^{-14}$ m/s
1.00	$3.0 \cdot 10^{-13}$ m/s

Thermal and Thermomechanical behavior

The thermal behavior is modeled by the thermal conductivity λ, the specific heat c and the bulk density ρ. In thermomechanical problems the thermal expansion coefficients of water and solids (α_w and α_s) and the bulk modules (B_w and B_s) are responsible for the behavior. Since $\alpha_w >> \alpha_s$ the latter coefficient has been assumed the be 0. The basic values of the parameters are:

λ=1.4 W/m,K
c=1600 Ws/kg,K
ρ=2100 kg/m^3
$\alpha_w = 3.0 \cdot 10^{-4}$ 1/K
α_s=0 1/K

Initial conditions

Only 4 parameters describing the initial situation in the buffer are needed. They are: 1) the initial void ratio e_0, 2) the initial average effective stress p_0 (corresponding to the swelling pressure), 3) the initial pore water pressure u_0 and 4) the initial tempe-

rature T. In the rock displacement calculations the following values are generally assumed:

e_0=0.65
p_0=8000 kPa
u_0=5000 kPa
T =15 °C

Comments

These models and parameters are not ideal and in the ongoing research activities,the behavior of the bentonite buffer has become more deeply understood, which has led to changes in the models. However, the calculations are made with the best models available at the time for the calculations and it is considered that although some changes in calculated behavior may have resulted, had a new and better set of models been applied, the conclusions would still be the same.

3.3 CANISTER

Although the geometry and composition of the canisters are different in the various concepts, the material components of the canisters are generally modeled in the same way. The models and parameters used can be grouped as follows:

- Modeling of the mechanical behavior applying Linear Elasticity and Metal Plasticity
- Modeling of the Thermal and Thermomechanical behavior

Three materials have been modeled:

- Copper
- Steel
- The interior (UO_2 and Cu) of HIP canisters

The first two will be described here while the latter will be described in connection with the calculation.

Copper

The elastic parameters are the modulus of elasticity E and Poisson's ratio ν:

$$E=114\cdot10^{6}\ \text{kPa}$$
$$\nu=0.35$$

The plastic strain is described by the following yield function in the same way as for the Drucker-Prager model:

σ_j (kPa)	ε_y
$50\cdot10^3$	0
$80\cdot10^3$	0.015
$130\cdot10^3$	0.065
$180\cdot10^3$	0.154
$210\cdot10^3$	0.288

The thermal properties are:

$$\lambda=380\ \text{W/m,K}$$
$$c=390\ \text{Ws/kg,K}$$
$$\rho=8930\ \text{kg/m}^3$$
$$\alpha=1.6\cdot10^{-5}\ \text{1/K}$$

Steel

The elastic parameters are:

$$E=200\cdot10^{6}\ \text{kPa}$$
$$\nu=0.30$$

The plastic strain is described by the following yield function in the same way as for the Drucker-Prager model:

σ_j (kPa)	ε_y
$300\cdot10^{3}$	0
$412\cdot10^{3}$	0.023
$542\cdot10^{3}$	0.078
$697\cdot10^{3}$	0.147

The thermal properties are:

$$\lambda=59\ \text{W/m,K}$$
$$c=460\ \text{Ws/kg,K}$$
$$\rho=7800\ \text{kg/m}^3$$
$$\alpha=1.2\cdot10^{-5}\ \text{1/K}$$

3.4 ROCK

The rock has been modeled as an infinite rigid body in all the rock shear scenarios. In the thermo-mechanical calculation of VLH the rock was modeled as linear elastic with the following parameter values:

$$E=5\cdot10^{6}\ \text{kPa}$$
$$\nu=0.20$$

The thermal properties are:

λ=3.6 W/m,K

c=800 Ws/kg,K

ρ=2700 kg/m^3

α=8.3·10^{-6} 1/K

4 KBS3 HIP CANISTER

4.1 GENERAL

All rock shear calculations imply shear along a fracture oriented perpendicularly to a deposition hole. In most of the calculations the shear was assumed to pass through the center of the canister as illustrated in Fig 4-1. Since the shear plane can then be taken as an anti-symmetry plane, only the upper half of the deposition hole needs to be considered.

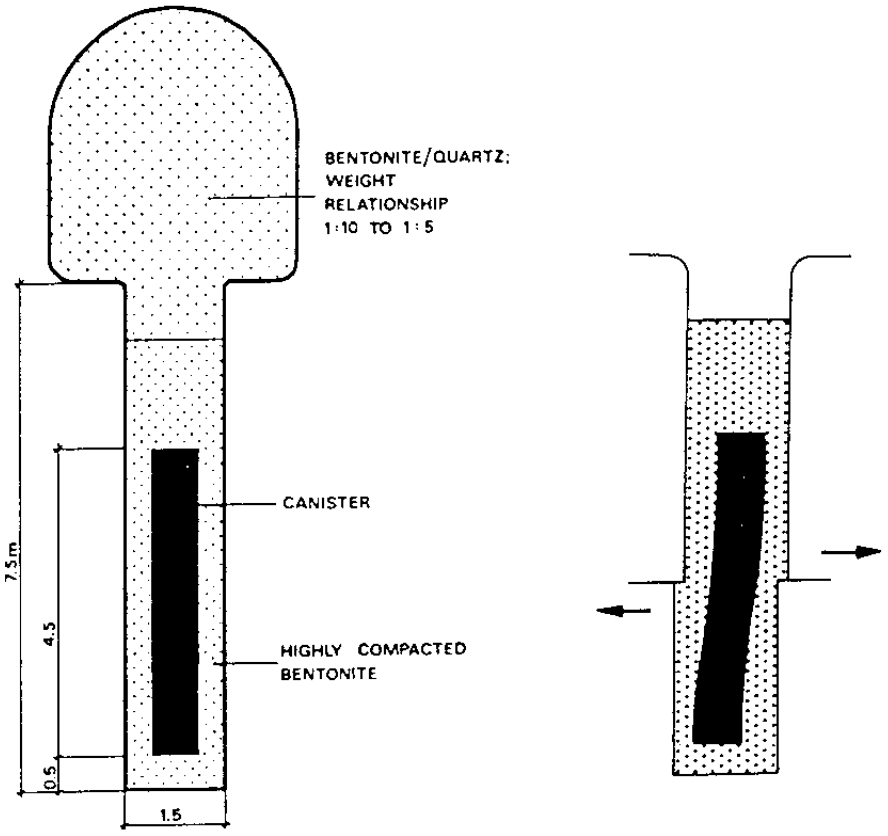

Figure 4-1 Illustration of the rock shear scenario in KBS3

Two types of calculations of the effect of rock shear of KBS3 deposition holes with the HIP (Hot Isostatic Pressure) copper canister have been made. A first series of calculations was made by simulating the canister to be solid copper with no internal stresses, while a second recent set of calculations was made by simulating the internal boxes with BWR elements and the residual stresses in the copper from the HIP process as well. The first series of calculations will be shown very briefly (only for comparison) while the second set will be described in detail.

4.2 INFLUENCE OF ROCK SHEAR ON AN IDEALIZED CANISTER MADE OF SOLID COPPER

These calculations were made with a deposition hole geometry that was scaled 1:10 to the KBS3 geometry with a buffer thickness of 4 cm, in order to compare the calculations with model tests.

Simplified material model

Two kinds of calculations have been made with a canister simulated to consist of pure copper. A set of calculations was made with a simplified material model for the bentonite, i.e. modeling it as an idealized elastic plastic material as for the metals (Metal Plasticity), which corresponds fairly well to the behavior of the clay when the rate of shear is high enough to yield completely undrained conditions.

7 calculations with varying bentonite density and bentonite thickness were made. The main conclusions from these calculations were:

1. At a bentonite density lower than ρ_m=1.9 t/m^3 the copper canister only deformed elastically. At higher density, plastic deformations took place with the highest values obtained for the density ρ_m=2.14 t/m^3 with a maximum plastic strain of 4%.

2. The canister was most affected at the surface 1/4 of the total length from the ends of the canister.

3. The thickness of the bentonite barrier is of minor importance for the stresses in the canister and a change in thickness of +/- 50% did not affect the stresses significantly.

Fig 4-2 shows, as an example the deformed structure and the plastic strain of a canister after a rock displacement of 1.1 cm at the bentonite density ρ_m=2.14 t/m^3. Only the upper quarter was modeled with a vertical symmetry plane and a horizontal anti-symmetry plane which corresponds to the shear plane.

The results of these calculations are given in a separate report by Börgesson (1988) and will not be further dealt with here.

Material model simulating the effective stress theory

A set of calculations was made with combined models of Porous Elasticity (which is based on the effective stress theory) and Critical State Plasticity.
The latter model and the calculations have been described by Börgesson (1990). Three calculations were made dealing with the following items:

1. Completely drained buffer material exposed to rock creep displacements or to very small intermittent rock displacements

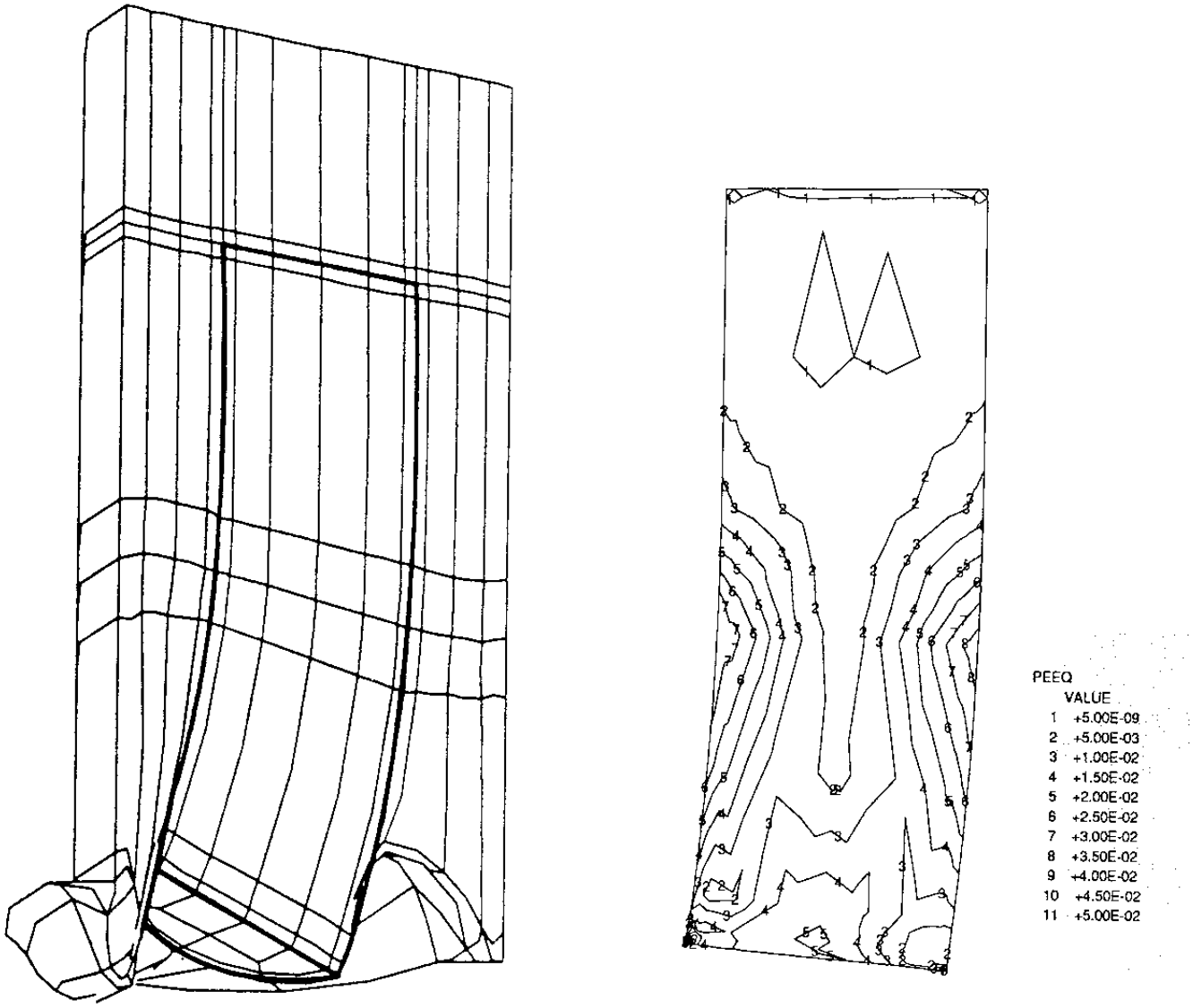

Figure 4-2 Deformed canister (displacement magnification factor F_m=2.5) and achieved plastic strain in the copper canister at the clay density ρ_m=2.14 t/m^3

2. Completely undrained buffer material exposed to fairly rapid rock displacements

3. Partly drained buffer material exposed to rock displacement lasting for some years

The input parameters were not completely relevant in these calculations but the main conclusions were:

* The rock shear scenario can be modeled and calculated by use of the ABAQUS code with the material models that are based on the Effective Stress Theory.

* Even at slow rock displacement lasting for 10 years, the pore pressure generated will be considerable

4.3 ROCK SHEAR OF A CANISTER WITH RESIDUAL STRESSES FROM THE HIP PROCESS

4.3.1 General

The hot isostatic pressure process at the encapsulation of a KBS3 canister yields stresses in the canister due to shrinkage on cooling from temperature 550°C. The residual stresses are caused by the difference in thermal expansion between the copper and the inner part of the canister with BWR elements. A calculation of these stresses was made by ABB (Fryklund 1992). In order to include these stresses as residual stresses in the canister at the rock shear scenario, the HIP process was recalculated with ABAQUS for an element model that was applicable in the rock shear calculation. The result of the HIP calculation was then used as starting point for the rock shear calculation.

4.3.2 Material models

Clay

The material model and the initial conditions for the bentonite clay were in complete agreement with the description in chapter 3.2.

Copper

The material data differed slightly from the general description in chapter 3.3 and a temperature dependence was coupled to the mechanical properties according to Table 4-1.

Table 4-1 Mechanical parameters of copper used in the HIP calculation

Temp °C	E MPa	ν	σ_y MPa	E_T MPa	$\alpha \cdot 10^{-6}$ 1/K
-50	117650	0.33	44	1220	16.8
20	117650	0.33	44	1220	16.8
100	115380	0.33	42	868	17.2
200	96550	0.33	37	625	18.0
300	80650	0.33	32	313	18.7
500	50000	0.33	21	36	19.9
550	40000	0.33	16	36	19.9

UO_2 etc.

The inner part of the canister is composed of several materials and the properties are not known. In the calculation the same temperature-dependant properties were used as those applied by ABB, with plastic properties added that agree with those of the copper. The plastic behavior is an assumption which is conservative in the rock shear.

Table 4-2 Mechanical parameters of the inner part of the canister used in the HIP calculation

Temp °C	E MPa	ν	σ_y MPa	E_T MPa	$\alpha \cdot 10^{-6}$ 1/K
-50	153680	0.32	44	1220	12.3
20	153680	0.32	44	1220	12.3
150	141030	0.32	42	868	12.9
250	126230	0.32	37	625	13.5
350	111130	0.32	32	313	13.7
450	93070	0.32	21	36	14.6
550	75000	0.32	16	36	14.6

4.3.3 Assumptions

Element mesh

The entire canister and surrounding bentonite were simulated with the 3D element mesh shown in Fig 4-3. A symmetry plane runs along the central axis parallel to the shear direction. The shear plane goes perpendicularly to the canister axis and intersects the canister at a distance of 1/4 of the canister length from its end. The diameter of the canister is 800 mm and thickness of the pure copper covering the BWR elements is 128 mm. Thus the geometry of the inner part with the BWR elements is taken to be cylindrical with the same total cross section area as the real one.

Calculation procedure

The calculation was made stepwise in the following manner:

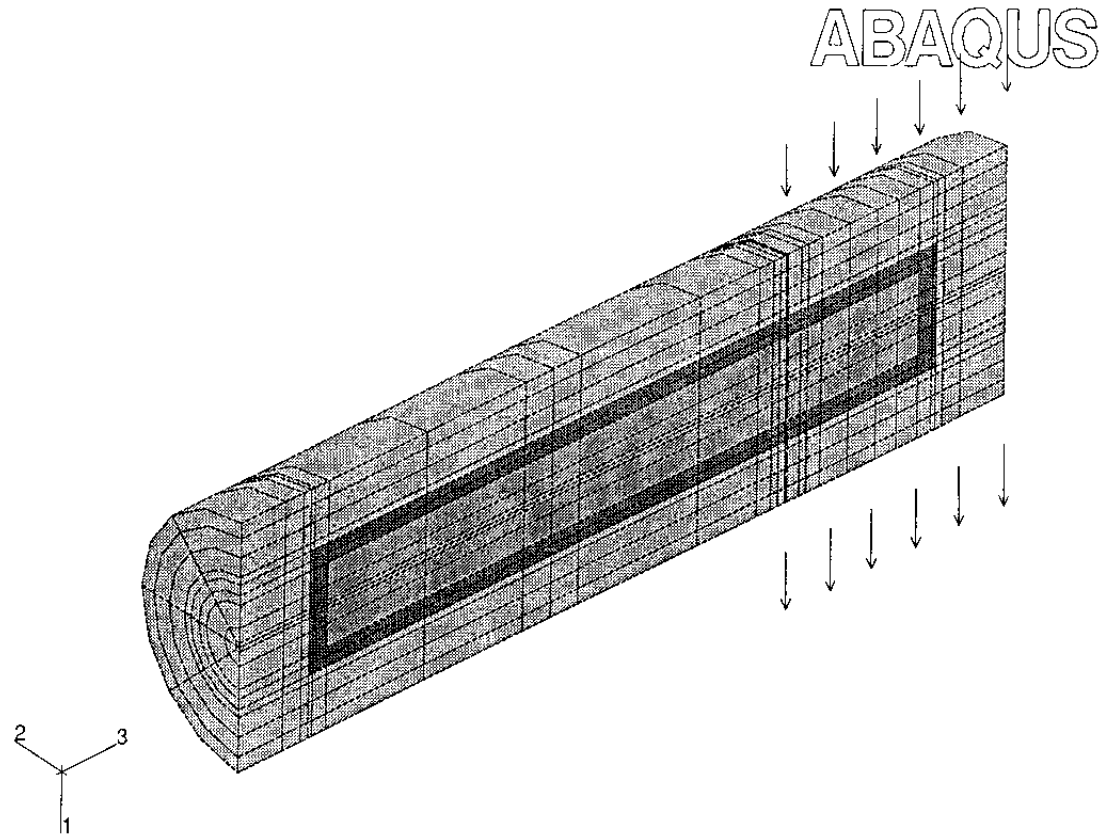

Figure 4-3 Element model for the rock shear calculation of the HIP canister with residual stresses. The shear plane and the rock displacement are indicated in the figure.
Light grey: bentonite
Dark grey: copper
Intermediate grey: UO_2 etc.

1. Calculation of the cooling phase at the HIP process. The calculation only concerned the canister, which was assumed to be free from stresses at 550°C. The cooling from 550°C to 20°C was simulated.

2. Calculation of the consolidation phase of the bentonite buffer starting from its initial conditions and finally reaching a state of equilibrium implying some swelling of the bentonite against the canister and the rock. Drained conditions were assumed in this calculation.

3. Calculation of the influence of rock shear starting with the stresses and strains achieved in the previous calculations. The applied rate of shear was 10 cm in 30 days. The rock was in this step assumed to be undrained meaning that no exchange of water was allowed between the rock and the clay.

4.3.4 Results

HIP process

The cooling period in the HIP process gave residual stresses in the copper which are of the same magnitude as those calculated by ABB. Fig 4-4 shows the Mises stresses and the plastic strain in the copper. The plastic strain at the surface of the copper is 0.3% (ABB: 0.3%) and the maximum plastic strain (developed in the lid) is 0.7%, which is lower than the value achieved by ABB (3.0%) due to the coarse element mesh.

Bentonite buffer swelling

The effect of equalization and swelling of the bentonite differs very little from the effect of an isotropic constant pressure, with a maximum plastic strain in the copper of about 0.001%, since the deformation of the canister is very small.

Rock shear

The rock shear was planned to continue until a a total displacement of 10 cm was reached, i.e. in agreement with the other calculations. However, the calculation process stopped after arriving at a relatively small displacement due to convergence problems. It was not possible to reach more than about 4 cm displacement in spite of several attempts.

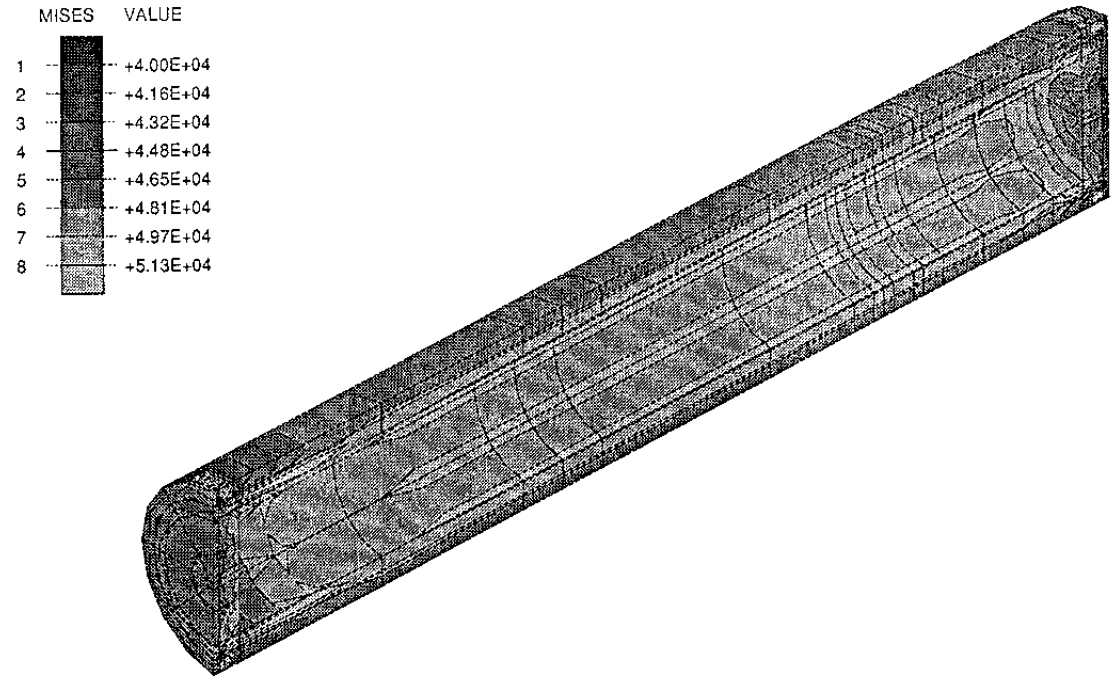

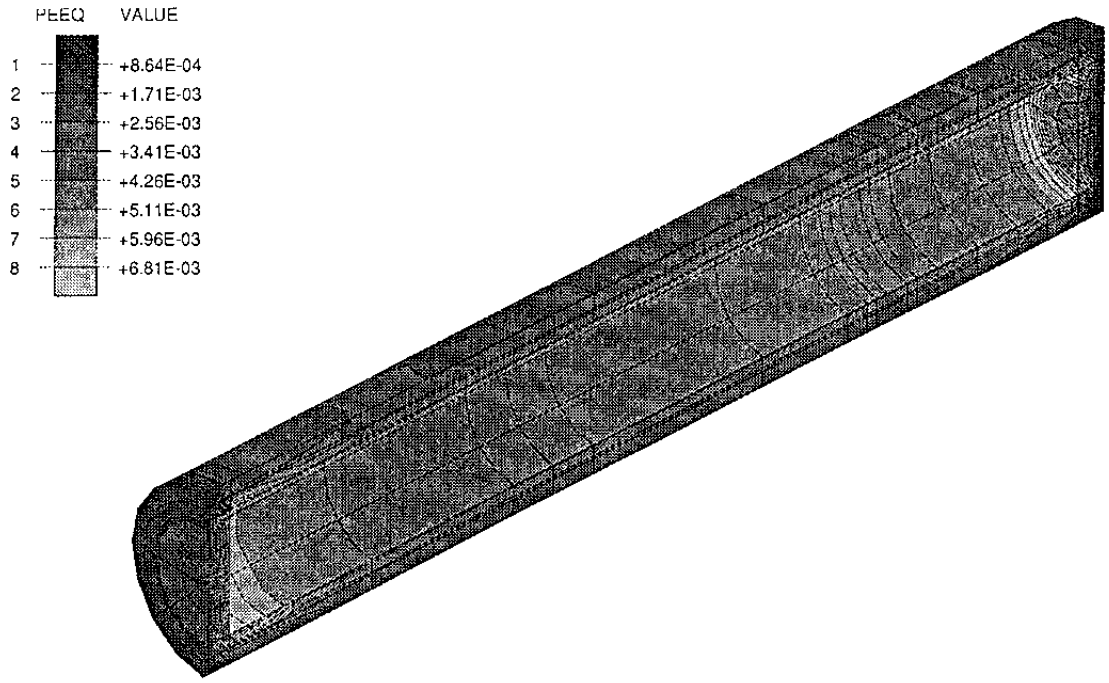

Figure 4-4 The residual Mises stresses (kPa) (upper) and plastic strain in the copper from the HIP process

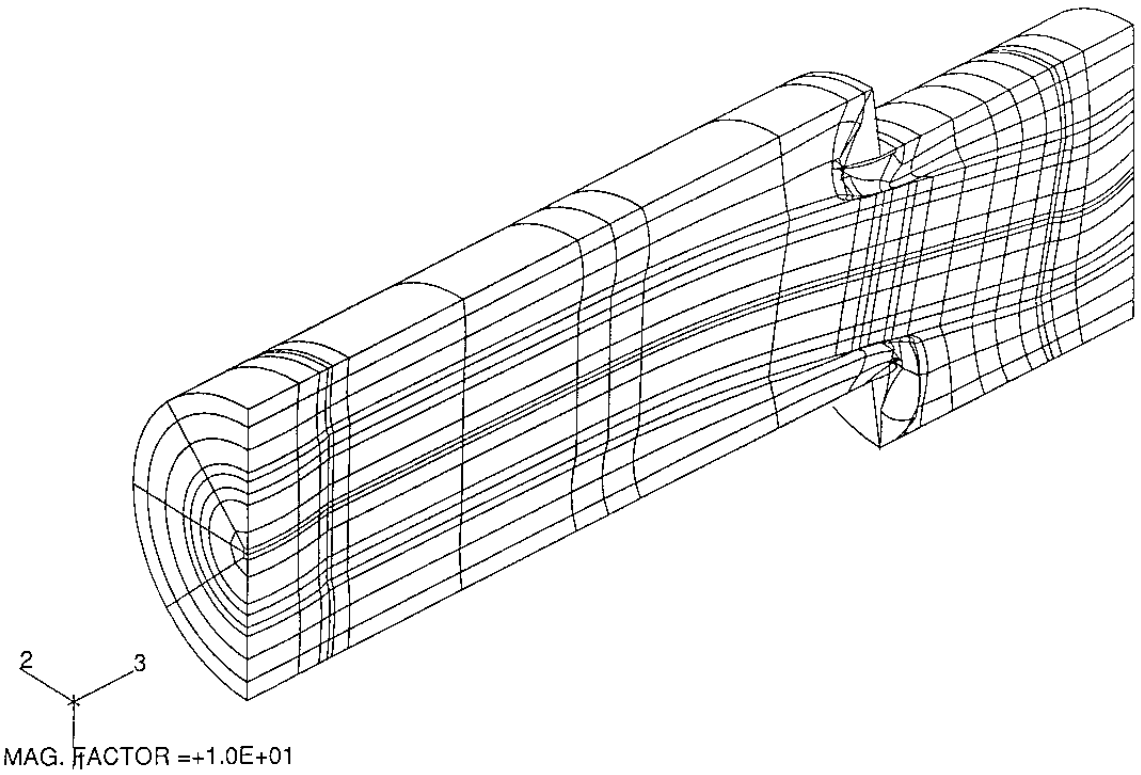

Figure 4-5 Deformed structure after 4 cm rock shear

Although this value is less than half the displacement applied in the other calculations it is probably sufficent for drawing major conclusions.

Fig 4-5 shows the deformed structure with a displacement magnification factor of 10, while Fig 4-6 shows the pore pressure and the plastic strain in the bentonite clay. A very high pore pressure of up to 9 MPa appeared in the compressed parts of the buffer, while a strong decrease in pore pressure from the initial value of 5 MPa to below 1 MPa developed at the opposite sides of the canister. A large plastic strain of the clay of up to 50% took place in the shear zone close to the canister while most of the clay plasticized by a plastic strain less than 5%. These results agree very well with the corresponding results from the copper/steel composite canister if the difference in rock displacements is considered.

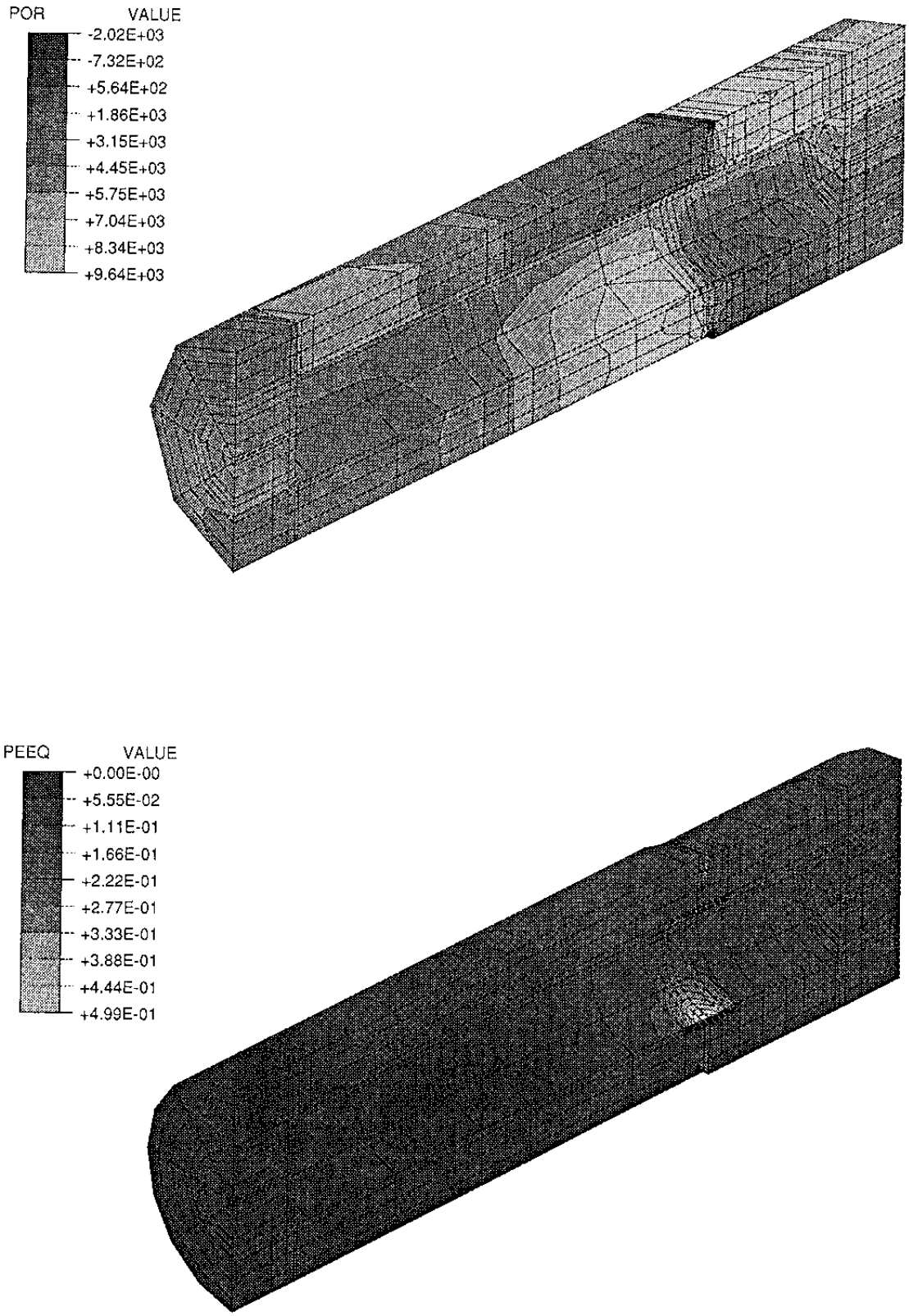

Figure 4-6 Pore pressure in kPa (upper) and plastic strain in the bentonite after 4 cm rock shear

Fig 4-7 shows the deformed copper in the canister and the additional plastic strain from the shear. The canister deforms in an almost identical way as the composite canister (after 5 cm shear) while the maximum plastic strain is about 0.6%, which is somewhat less than for the composite canister (~1.0%).

If the plastic strain in the copper is assumed to be proportional to the rock displacement, which is a reasonable assumption according to the calculations reported in chapter 5.5, the maximum plastic strain at the canister surface, including the plastic strain induced by the HIP process, will be about 1.5%.

According to this calcuation the inner part of the canister plasticized as well, as illustrated by Fig 4-8. The plastic properties of this part are not known but it is probable that the yield stress is higher than the assumed one, which thus means that the plastic strain in the copper is overestimated.

A complete set of results from these calculations is shown in Appendix I.

4.4 CONCLUSIONS

The following main conclusions can be drawn from the calculations of the mechanical effects on the KBS3 HIP canister:

1. The effect of rock shear on the canister strongly depends on the density of the bentonite buffer. The maximum plastic strain was 4% achieved at the density ρ_m=2.14 t/m^3, while no plastic strain was obtained for the density ρ_m=1.93 t/m^3.

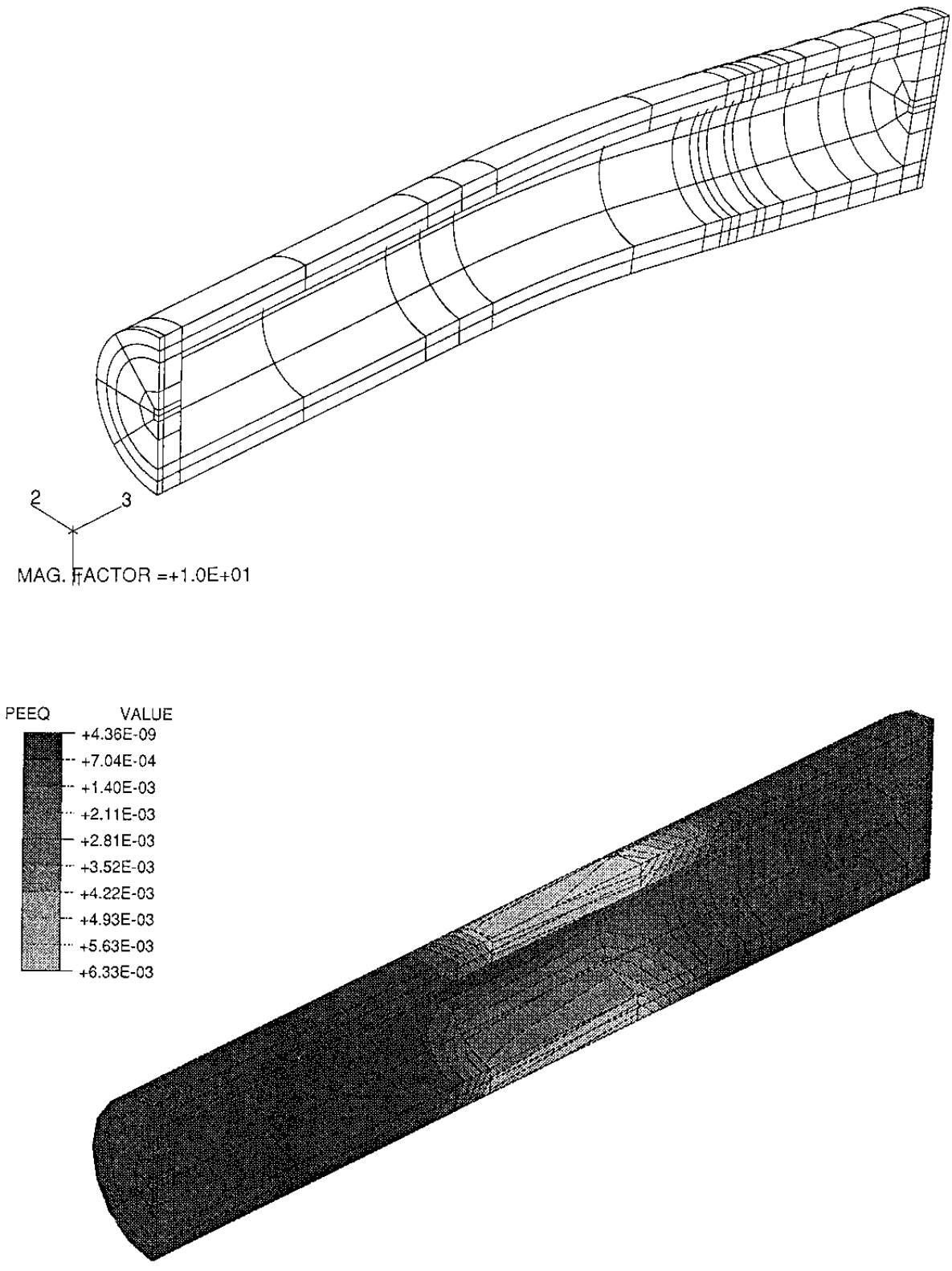

Figure 4-7 The deformed copper elements (upper) and the plastic strain in the copper after 4 cm rock shear

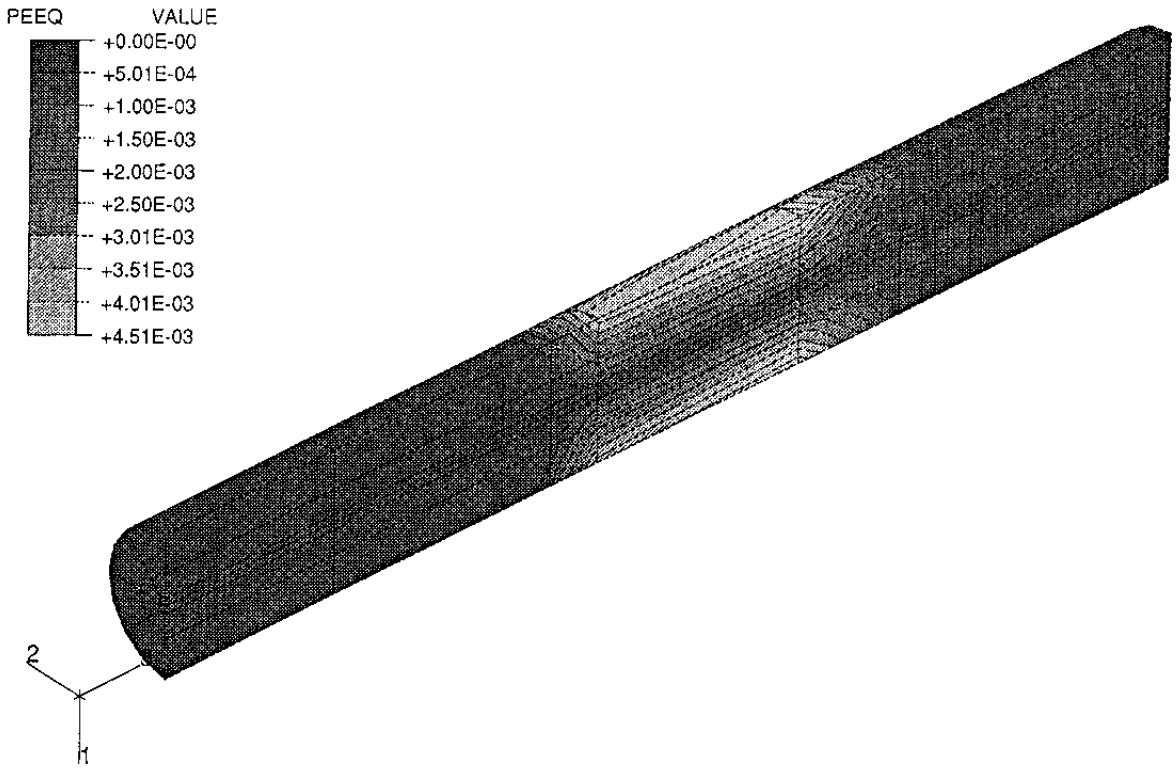

Figure 4-8 Plastic strain in the UO_2 after 4 cm rock shear

2. The HIP process produces 0.3% plastic strain at the canister surface.

3. 10 cm rock shear with the shear plane intersecting the canister asymetrically yields a maximum plastic strain at the canister surface of about 1.5% including the residual stresses from the HIP process when the density of the bentonite buffer is about ρ_m=2.05 t/m^3 (e=0.65).

4. The generated pore pressure in the bentonite during rock shear will, according to the calculations, be strongly increased and reach ~9 MPa on the compressed side of the canister and decreased to ~1 MPa on the opposite side.

5 KBS3 COPPER/STEEL CANISTER

5.1 GENERAL

The stresses and strains in the hollow, double wall copper/steel canister have been studied by conducting the following calculations:

1. The effect of the swelling pressure from the bentonite and the water pressure from the rock

2. The effect of rock shear through the center of the canister (symmetry) with 30 days duration

3. The same as in paragraph 2 adding also the effect of 30 years of consolidation and pore pressure dissipation in the bentonite after the rock shear

4. The same as in the paragraph 3 adding also the effect of creep in the copper

5. The effect of asymmetric rock shear

The geometry of the canister is shown in Fig 5-1. There is a gap of 1 mm between the copper and steel cylinder. The interior of the steel canister was assumed to be empty in the calculations.

5.2 EFFECT OF THE SWELLING PRESSURE FROM THE BENTONITE

Assumptions

The rock shear was assumed to take place after complete saturation, swelling and pore pressure equilibrium. It was thus suitable to let the rock

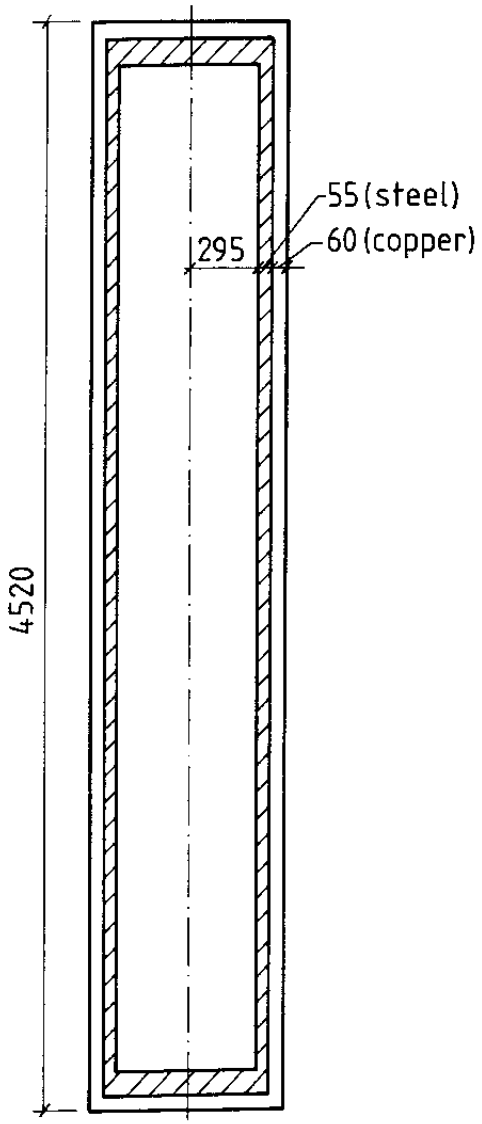

Figure 5-1 Geometry of the double-walled copper/steel canister (mm)

shear calculation be preceded by a calculation of the swelling of the bentonite against the rock and canister, and use the deformed and stressed model as starting-point for the rock shear.

Since the considered case implied equilibrium after long time and complete drainage, the calculation was made assuming no pore pressure in the bentonite elements. The canister and clay were geometrically modeled in a similar way as in the calculation with the idealized HIP canister (chaper 4.2), in which

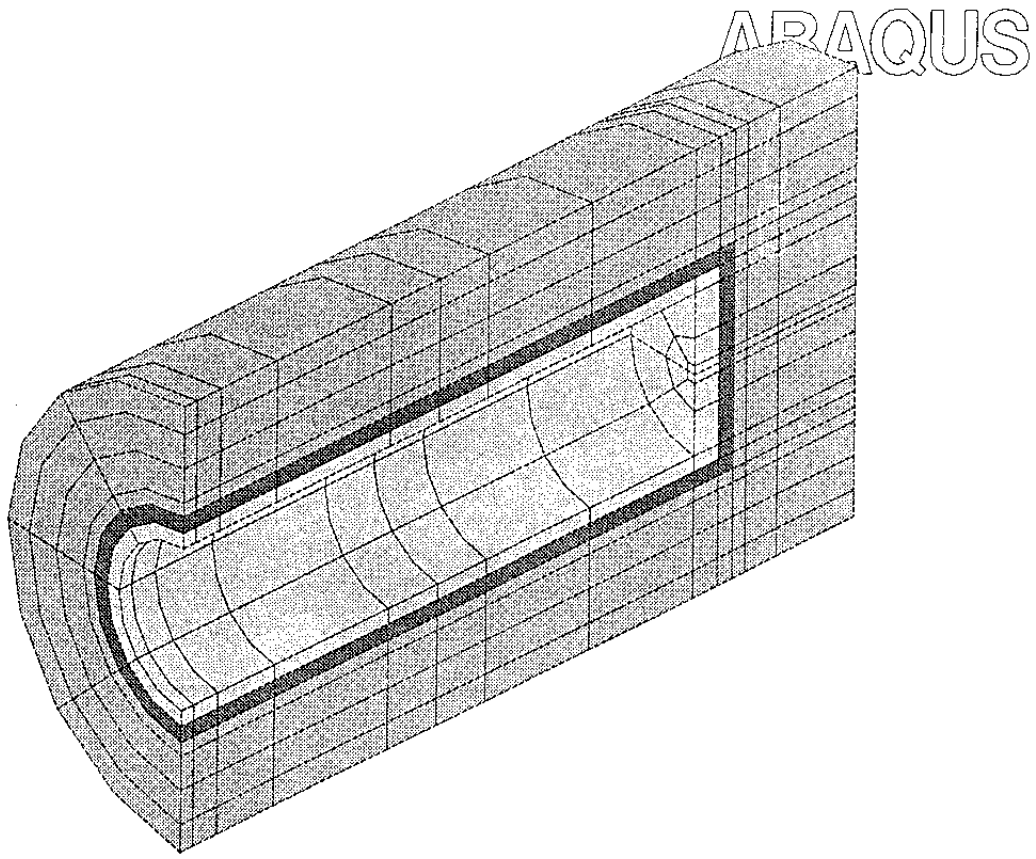

Figure 5-2 Element mesh for the KBS3 calculation with symmetric shear of the copper/steel canister.
Light gray: steel
Dark grey: copper
Intermediate grey: bentonite

only 1/4 of the deposition hole was modeled. Fig 5-2 shows the element mesh with different shading of the different materials. The 1 mm slot between the copper and steel canisters was simulated by interface elements.

The axial plane is one of symmetry, while the radial plane, with 90° intersection with the hole axis, is an anti-symmetry plane, simulating the shear plane. The surrounding rock boundary was mechanically modeled as infinitely stiff. The contact between the bentonite and the rock as well as the canister was modeled as having an infinitely high friction, while there was no friction between the two canisters when

the 1 mm gap was closed, bringing the steel in contact with the copper.

The material models and input parameters are the same as described in chapter 3 except for the porous elasticity parameter κ which, by mistake, was set 10 times too low. The consequence of this is a too low swelling potential of the clay, which will be of minor importance for the rock shear calculation, since the confined volume for the clay will change very little during the shear. The stresses and strains in the canister from the swelling pressure of the bentonite will be somewhat underestimated, since the calculation implied some volume change. However, it was not considered necessary to make new calculations since the difference was estimated to be small.

Results

The resulting void ratio and average stress in the bentonite after complete swelling and drainage are shown in Fig 5-3. The figure shows that the void ratio has increased a little from 0.650 to 0.653 in the central part of the hole, while the change is less than 0.001 close to the end of the canister. The increase in void ratio results in a reduction in average stress, as shown in the same figure. The reduction is about 1 MPa at the most (from 8 to 7 MPa), in spite of the low value of the porous elastic bulk modulus. In practice the reduction will be even lower.

The effect on the copper canister is shown in Fig 5-4. The picture of the deformed canister (with a high displacement magnification factor) shows that the copper canister does not carry the total pressure from the water and the bentonite and that the copper canister is pressed against the steel canister along the entire periphery and also in the central part of

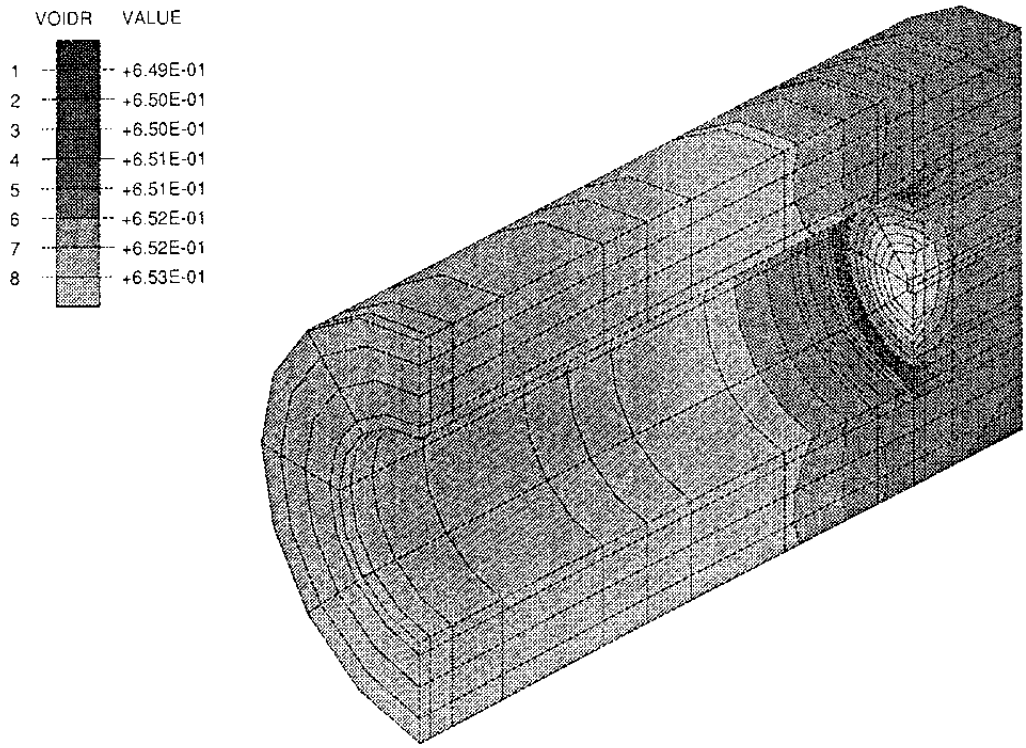

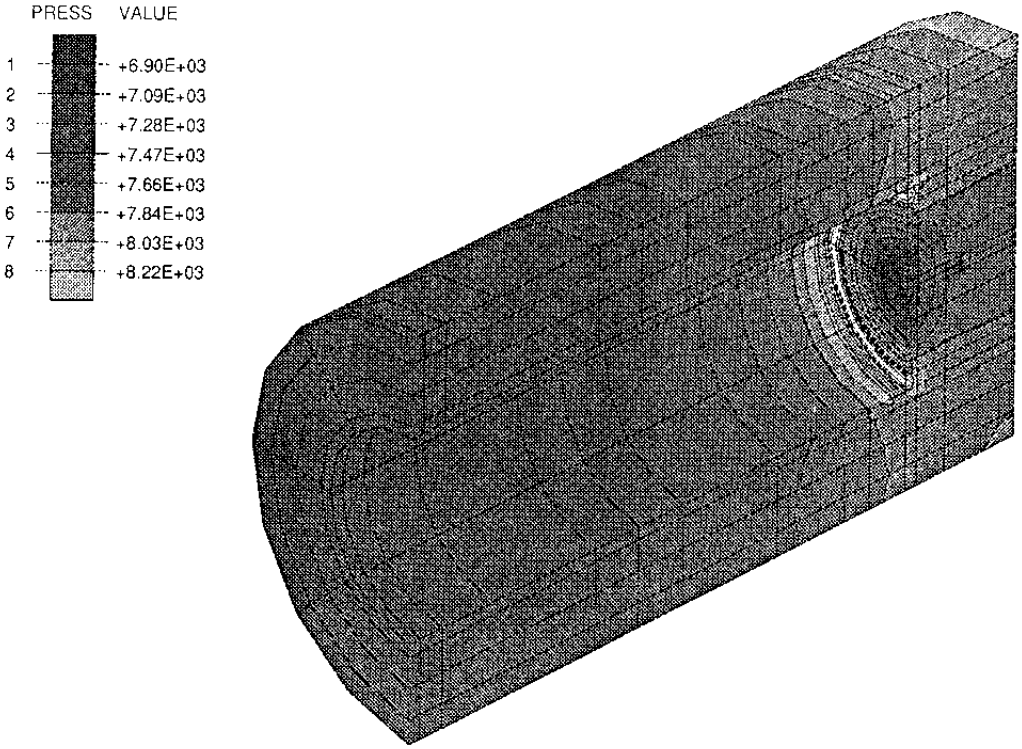

Figure 5-3 The calculated void ratio (upper) and average stress (kPa) in the bentonite clay after swelling equilibrium

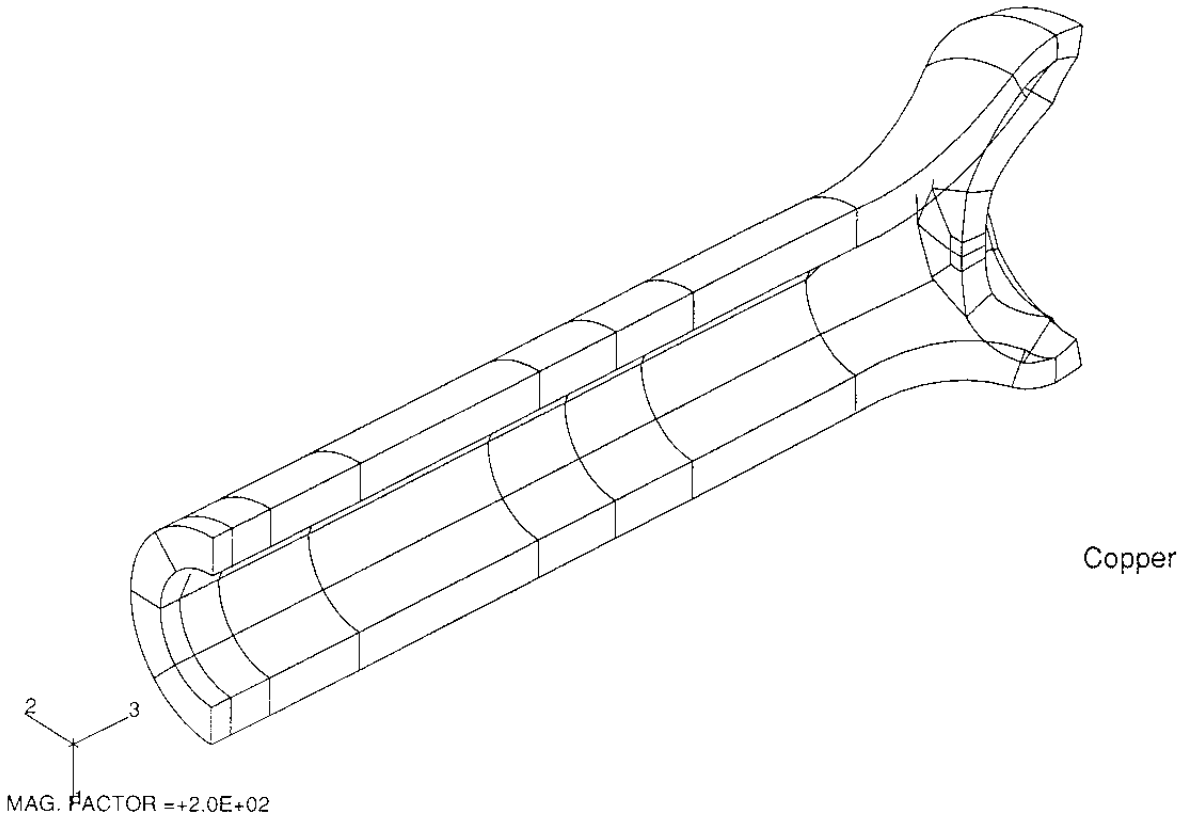

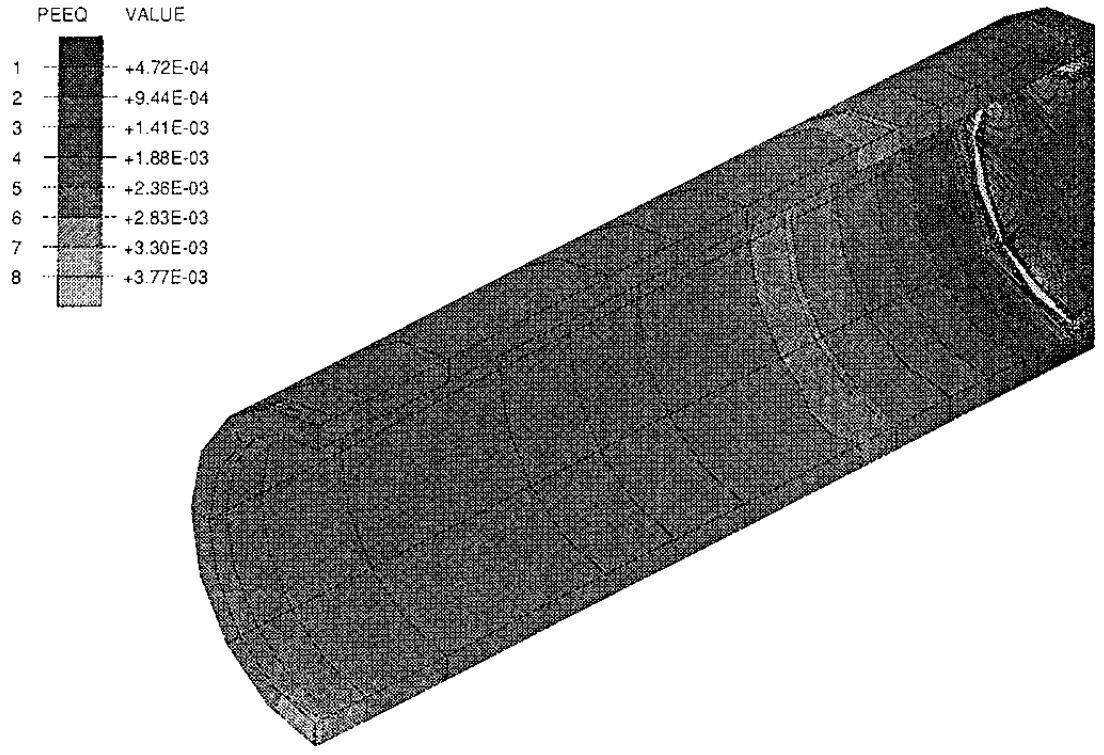

Figure 5-4 Deformed copper canister (F_m=200) and the plastic strain in the copper at equilibrium after swelling

the lid. The lower picture shows that the plastic strain in the copper canister varies between 0.1 and 0.4% with in average of 0.2% along most of the canister. The maximum strain is found to be 0.4% at the connection between the lid and the tube. However, the coarse element mesh does not make it possible to evaluate the exact stress distribution at the edges of the lid.

The closing of the slot between the concentric canisters, and the transfer of stresses from the copper to the steel canister is illustrated in Fig 5-5. The upper picture shows the aperture of the slot (the interface elements). The slot is closed along most of the canister while it is a little more than 1 mm at the edge of the lid. The lower picture shows the Mises stresses in the steel canister. As an average, these stresses are about 10 MPa along a major part of the canister with high stresses locally in the lid.

A complete set of results is shown in Appendix 2.

Conclusions

The main conclusions concerning the effect of the swelling pressure from the bentonite and the water pressure in the rock is:

- the 1 mm slot between the copper and steel will be closed except at the edges of the lid

- the copper canister will plasticize along a large part of the canister with a plastic strain of about 0.2%

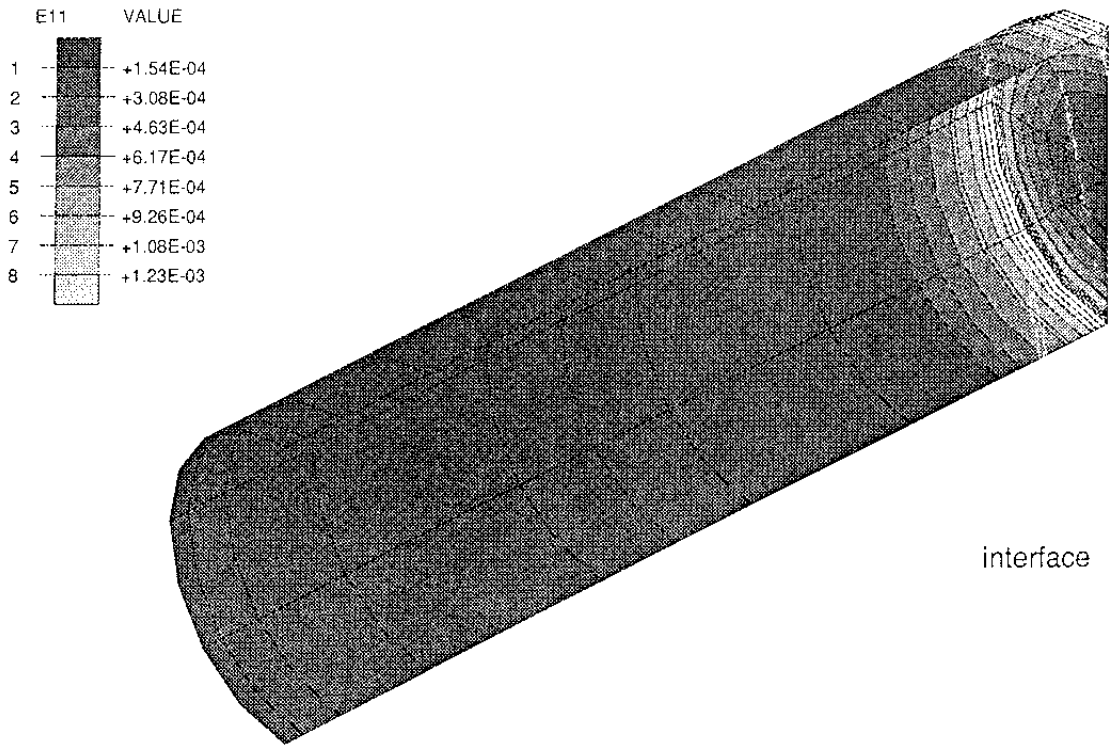

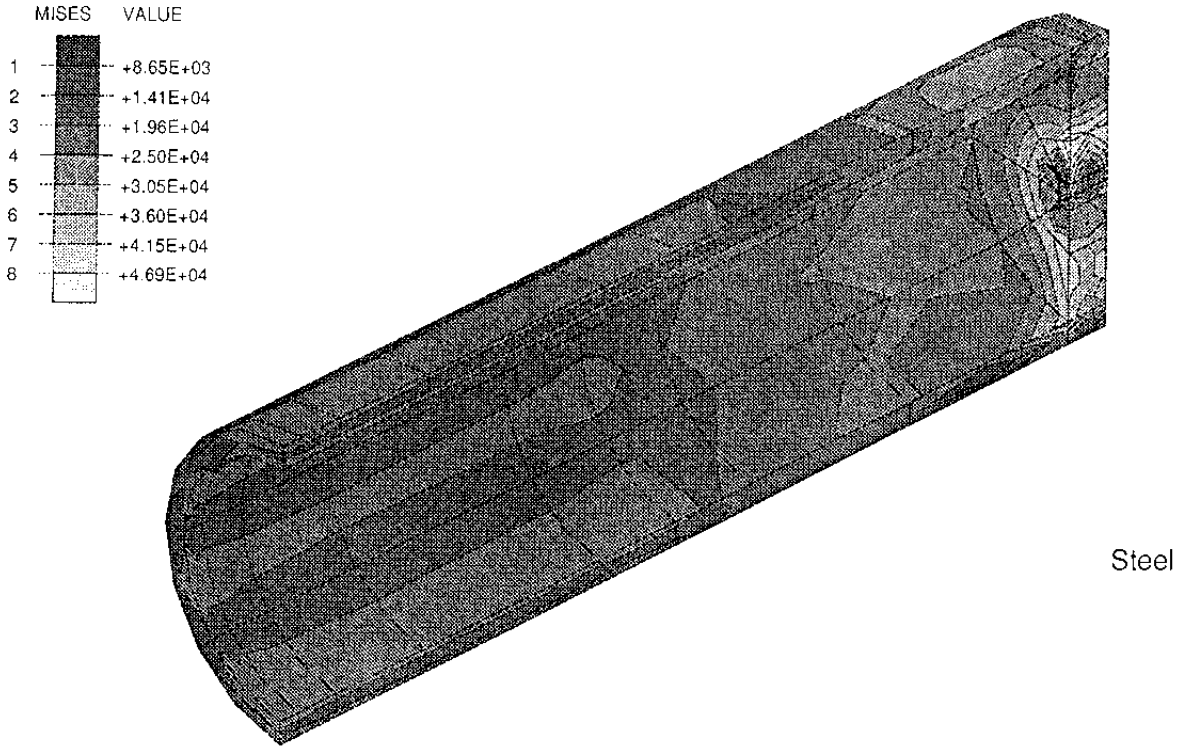

Figure 5-5 Calculated aperture (m) between the canisters (upper) and calculated Mises stresses (kPa) in the steel after swelling equilibrium

5.3 EFFECT OF ROCK SHEAR THROUGH THE CENTER OF THE CANISTER

5.3.1 Assumptions

After development of equilibrium conditions according to the bentonite swelling calculation, the rock shear calculation was started. The material and structure models were identical to those described in chapter 5.2, with the exception that the results from the swelling calculation were used as starting conditions for the rock shear calculation.

The rock shear was simulated as a rather slow rock displacement of totally 10 cm during 30 days with a constant rate of strain. Since the boundary conditions for the pore water pressure were represented by a completely drained rock with a constant pressure of 5 MPa, some drainage was expected to take place of the bentonite.

The shear was, in accordance with the earlier calculations, simulated by displacing the entire rock boundary and the top boundary of the bentonite and at the same time locking the bottom boundary in the tangential and radial directions, i.e. allowing only axial displacements. In this way the bottom boundary simulated an asymmetric plane such that the total rock displacement was twice the applied displacement.

5.3.2 Results

The deformed structure after completed shear is shown in Fig 5-6. The characteristic large axial strain of the clay in contact with the canister close to the shear plane is seen in the figure as well as the tilting of the canister.

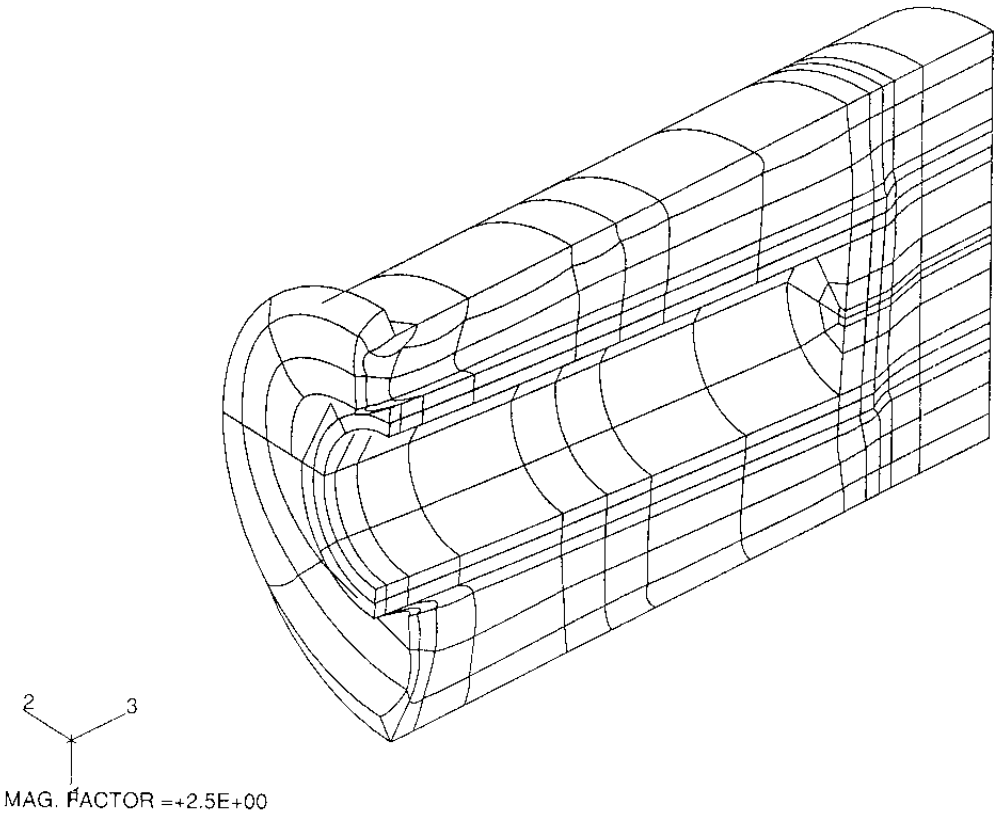

Figure 5-6 Deformed structure after 10 cm total rock shear

Bentonite

The pore pressure and the plastic strain in the bentonite after completed shear 30 days after onset of strain are shown in Fig 5-7. The pore pressure distribution shows the following:

- very high values (>17 MPa) on the compressed side of the canister

- negative values (<-1.5 MPa) on the opposite side of the canister close to the shear plane

- the effect of the drainage into the rock is not very strong (which is confirmed by the small change in void ratio) but clearly seen

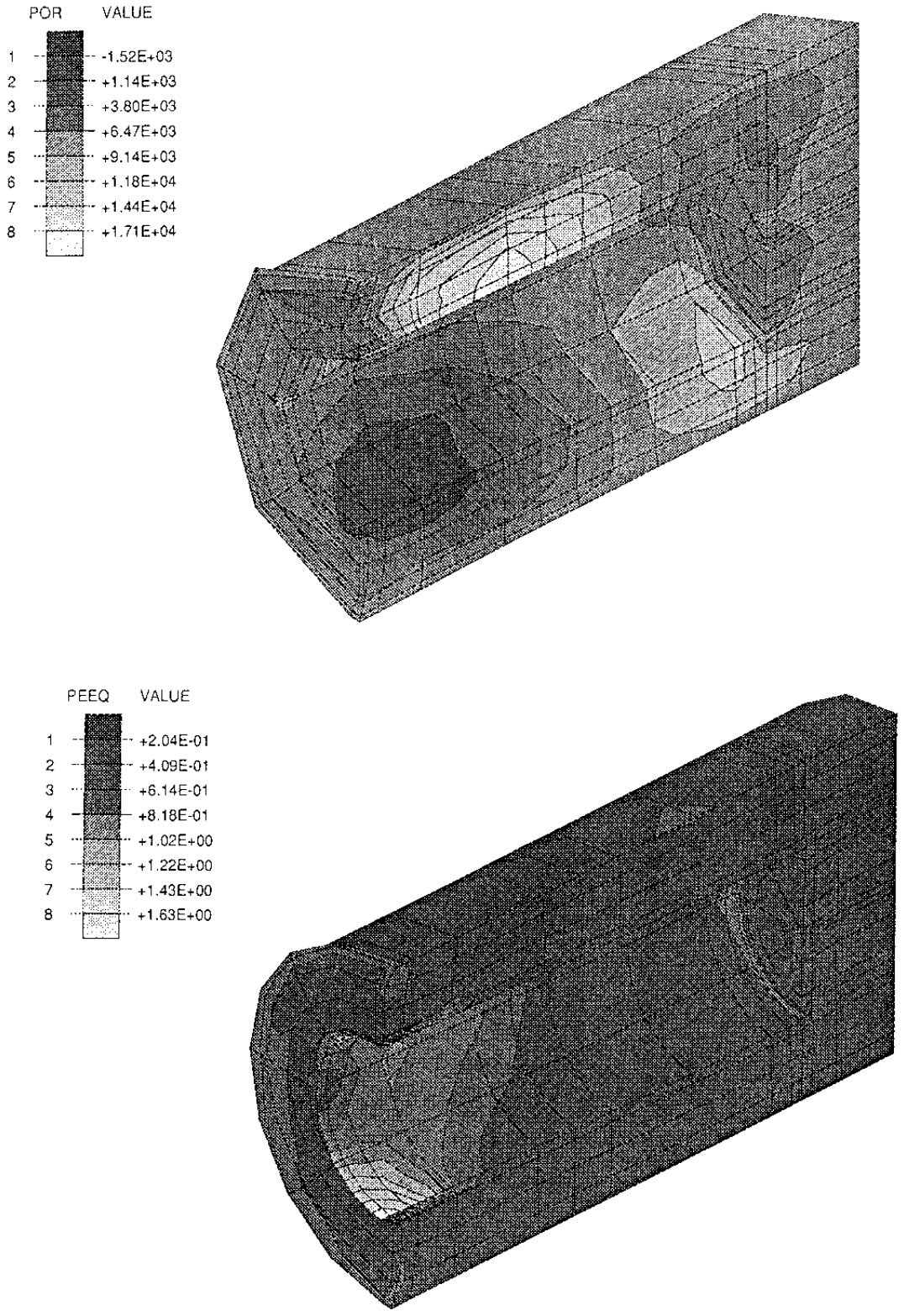

Figure 5-7 The calculated pore pressure in kPa (upper) and plastic strain in the bentonite clay after rock shear

The local high negative pore pressure may be questioned. It is probable (although not certain) that the bentonite will come off the canister and a slot formed between the canister and the bentonite, if the displacement is not extremely slow.

The entire clay is plasticized except close to the rock at the end of the hole. The plot of the plastic equivalent strain shows that some parts close to the canister are strongly plasticized with plastic strains larger than 160%.

Copper canister

The deformed copper canister and the plastic strain in the copper are shown in Fig 5-8. The picture of the deformed mesh shows that bending of the canister is small and hardly visible in spite of the large displacement magnification factor. However, the tilting can be seen if the direction is compared to the direction of the canister in the picture below, in which no magnification of the displacements has been introduced.

The plastic strain shown in the lower picture is significant but not very large; it exceeds 1% inside the tube on the compressed side and outside the tube on the opposite side close to the shear plane. In the rest of the canister the plastic strain is smaller than 0.5% with possible exception of the edges of the lid.

Steel canister

Fig 5-9 shows the normal stresses in the interface elements and the plastic strain in the steel canister. The normal stresses in the interface elements correspond to the radial stresses between the copper and steel canisters. Zero stress thus means that

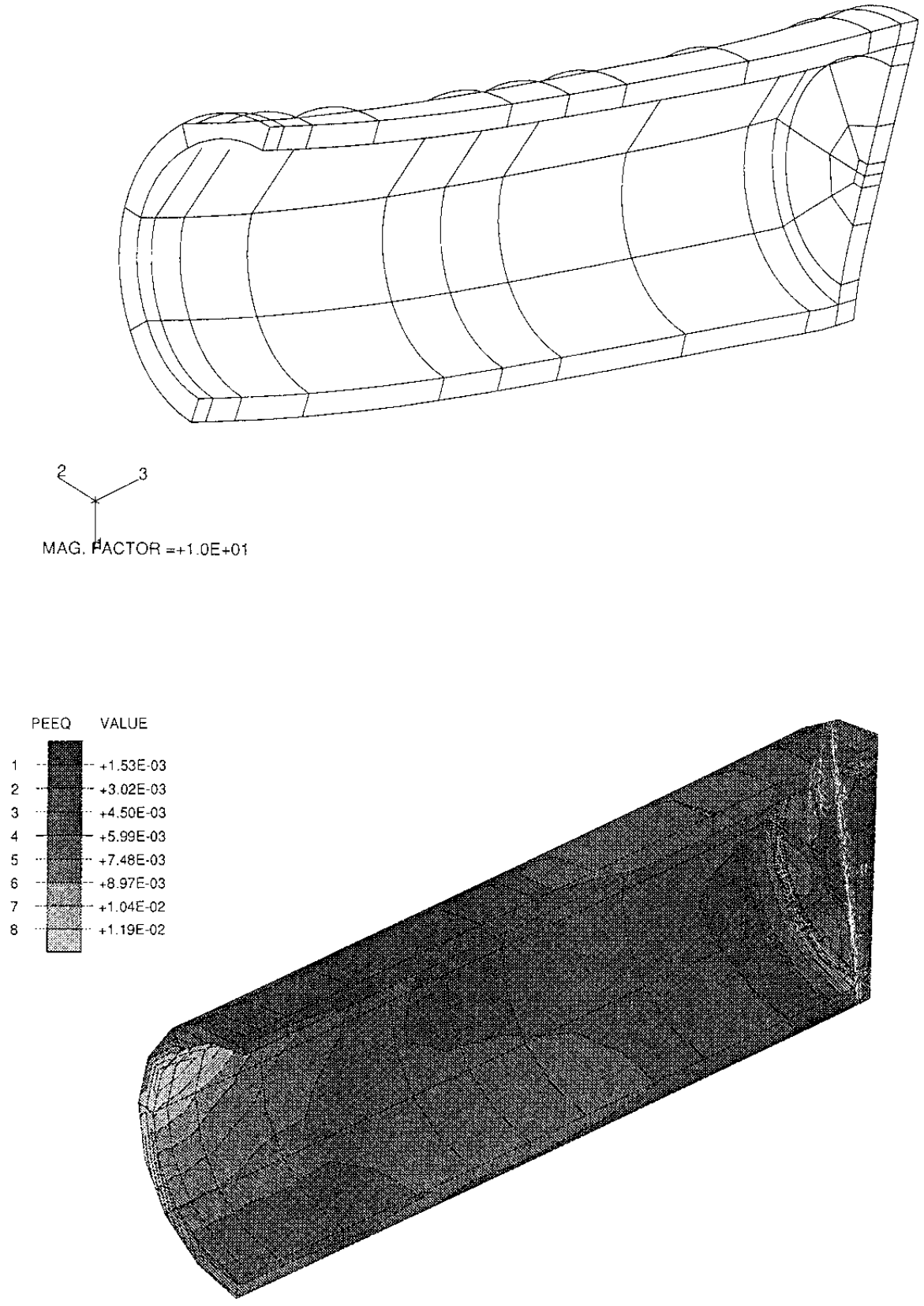

Figure 5-8 Deformed canister (F_m=10) and plastic strain in the copper after rock shear

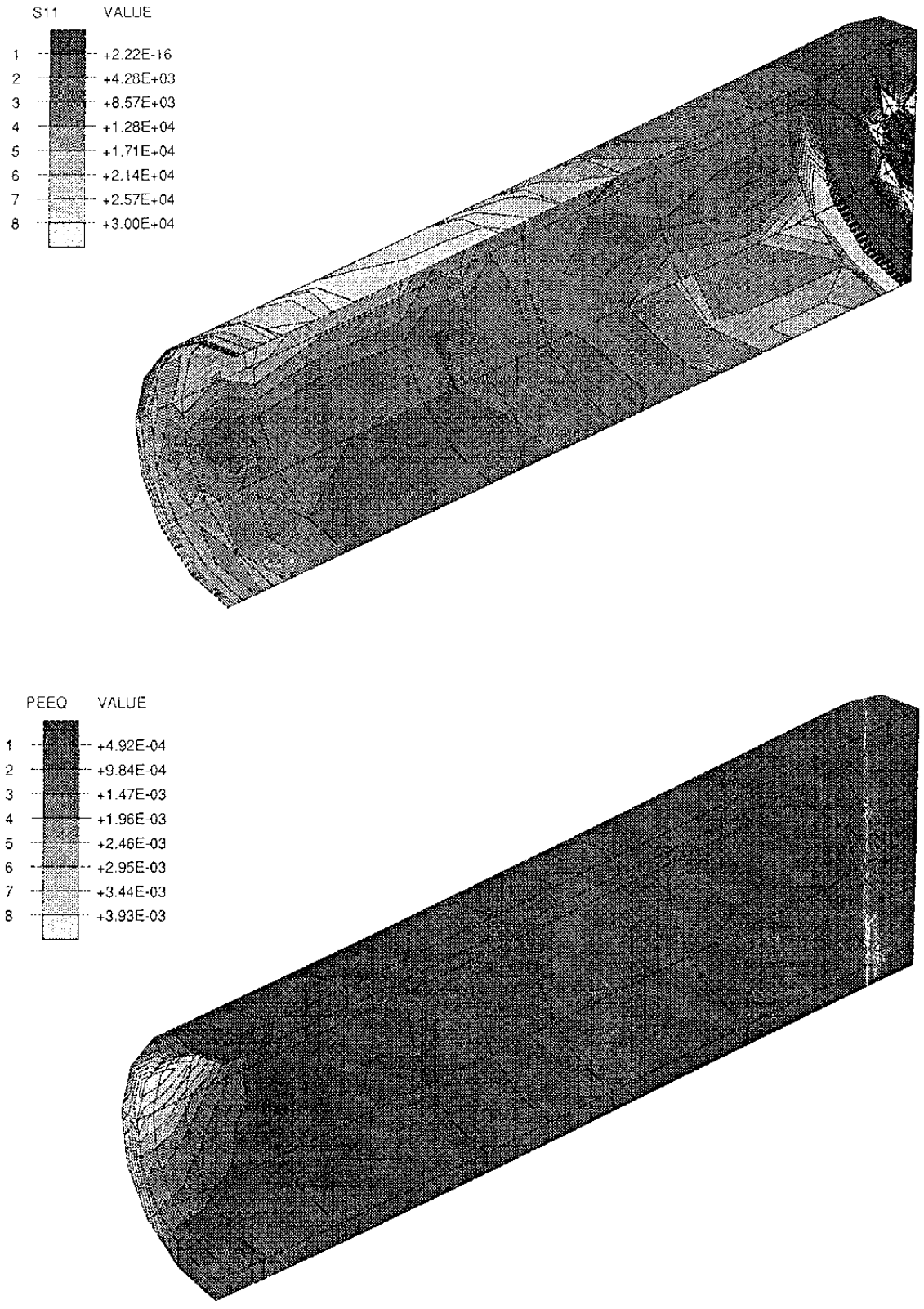

Figure 5-9 Normal stresses (kPa) in the interface elements (upper) and plastic strain in the steel after rock shear

there is no contact between the materials. The figure shows that materials are in contact along almost the entire interface, with maximum normal stresses of about 30 MPa. In the darkest areas on the passive side and in the lid, there is no contact between the materials. The copper that was pressed against the steel through the swelling of the bentonite has thus come off on the passive side at the rock shear.

The steel canister was found to be plasticized close to the shear plane in a similar way as the copper canister. A maximum plastic strain of about 0.4% is concluded to take place inside the canister on the active side and outside the canister on the passive side.

A complete set of results is shown in Appendix 3.

5.3.3 Conclusions

The major conclusions from the calculations of a 10 cm rock displacement through the center of the composite canister are the following:

- the shear will generate very high pore pressures in the clay on the compressed side (≈17 MPa)
- low negative pore pressures will be generated on the passive side which probably will result in a temporary slot between the clay and the canister
- plastic strain in the copper of 1% at maximum
- plastic strain in the steel of 0.4% at maximum
- the contact between the two canisters produced by the swelling of the bentonite will be partly lost on the passive side

5.4 EFFECTS OF CREEP AND CONSOLIDATION AFTER ROCK SHEAR

5.4.1 General

The stresses generated in the bentonite and in the canister will relax with time but also cause creep deformations and pore pressure dissipation in the bentonite. Thus, the following three processes will be involved:

- creep in the copper and in the steel
- consolidation of the bentonite (due to pore pressure dissipation and related change in effective stress)
- creep in the bentonite

The creep in the steel is negligible in comparison to the creep in the copper and will not be taken into consideration. Since both the creep and the consolidation in the bentonite could not be combined in one calculation and since it is probable that the creep effects are smaller than the consolidation effects, it was decided to neglect creep effects in the bentonite and only consider consolidation.

Thus, creep in the copper and consolidation of the clay have been studied in the following two calculations:

- the combined effect of creep in the copper and consolidation of the clay during 10^9 sec (32 years)
- the effect of consolidation of the clay in the same time period

5.4.2 Creep function for copper

The following creep function for the copper was used in the calculations (Pettersson 1991):

$$\dot{\varepsilon}=1.58\cdot10^{-17}\cdot\sigma_j^{3.4} \qquad \sigma_j<130 \text{ MPa} \qquad (5:1)$$

where σ_j = Mises stresses in MPa
$\dot{\varepsilon}$ = rate of creep strain (1/s)

5.4.3 Combined effect of creep and consolidation

In this calculation the rock boundary was fixed to the situation obtained after 10 cm shear displacement. The rock boundary was assumed to be completely drained and the combined effect of consolidation from pore pressure dissipation in the clay and creep deformation of the copper was calculated for a period of time of 10^9 sec. The time had to be restricted since the computer work was very time-consuming because of the creep nature of copper. Since the creep rate does not decrease with time but only with decreasing stress, the time steps in the calculation can not be increased unless the stresses decrease.

Fig 5-10 shows the average effective stress and the plastic strain in the clay at the end of the calculation. The plastic strain is identical to the values just after shear; the average stress has obviously changed very little.

Fig 5-11 shows an example of the normal strain in the shear direction (ε_{11}) in the copper before and after the creep. As seen in the figure the area with a strain $+0.265\% < \varepsilon_{11} < +0.271\%$ on the inside surface has increased considerably. The strain in the lid edges has also increased a lot.

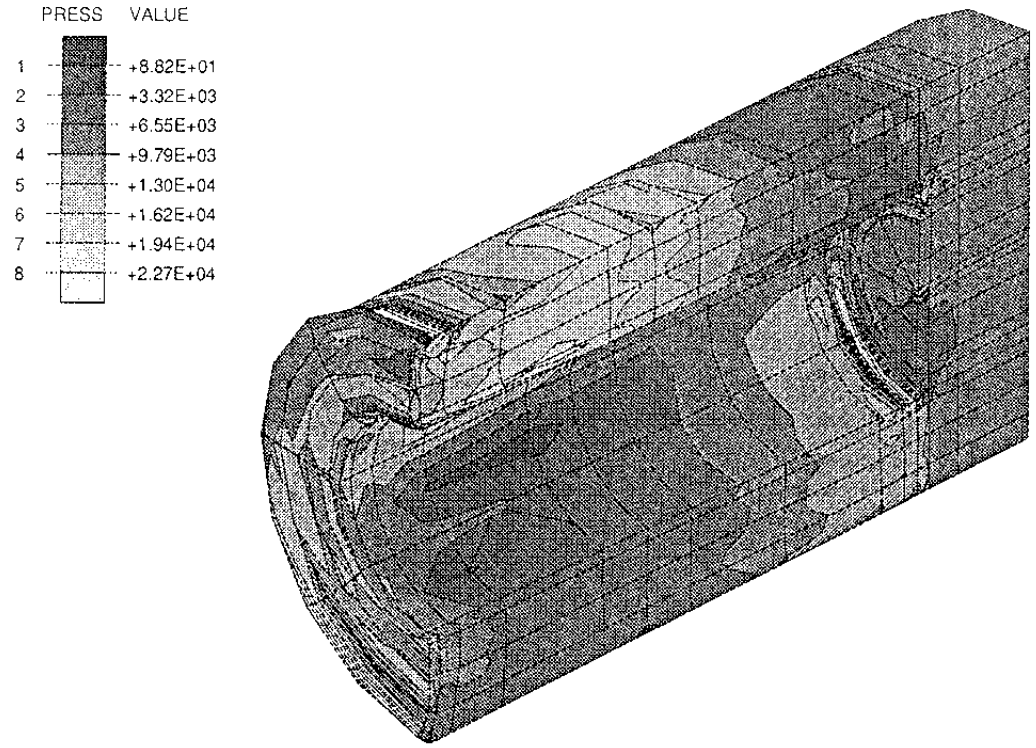

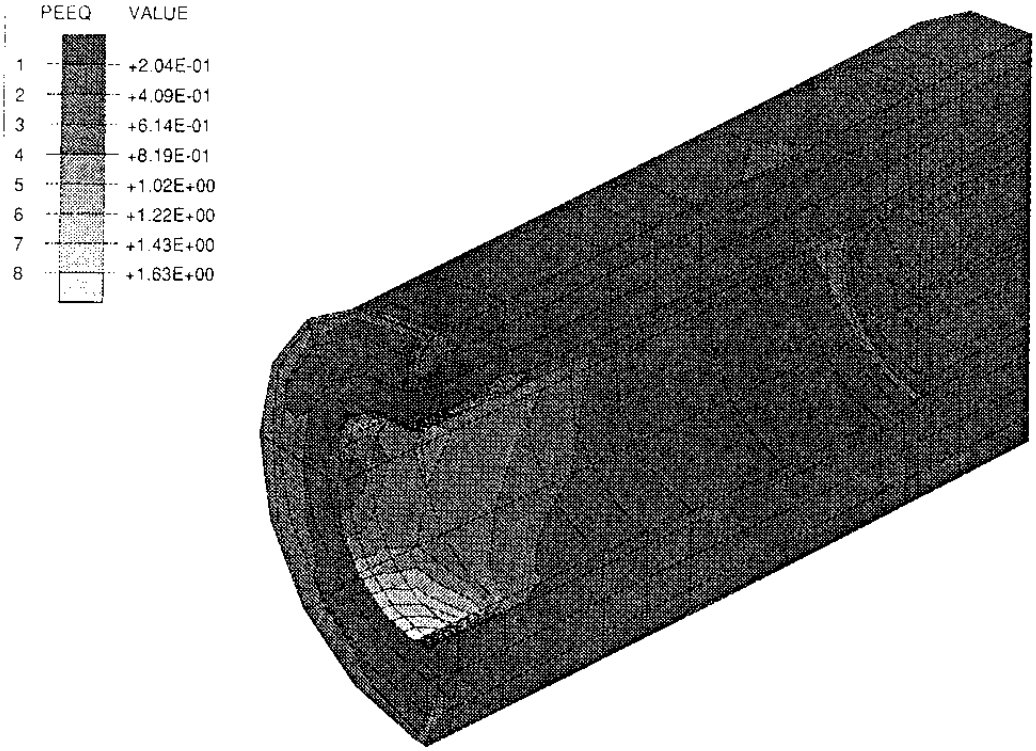

Figure 5-10 Calculated average stress (kPa) (upper) and the plastic strain in the bentonite after 32 years creep and consolidation after rock shear

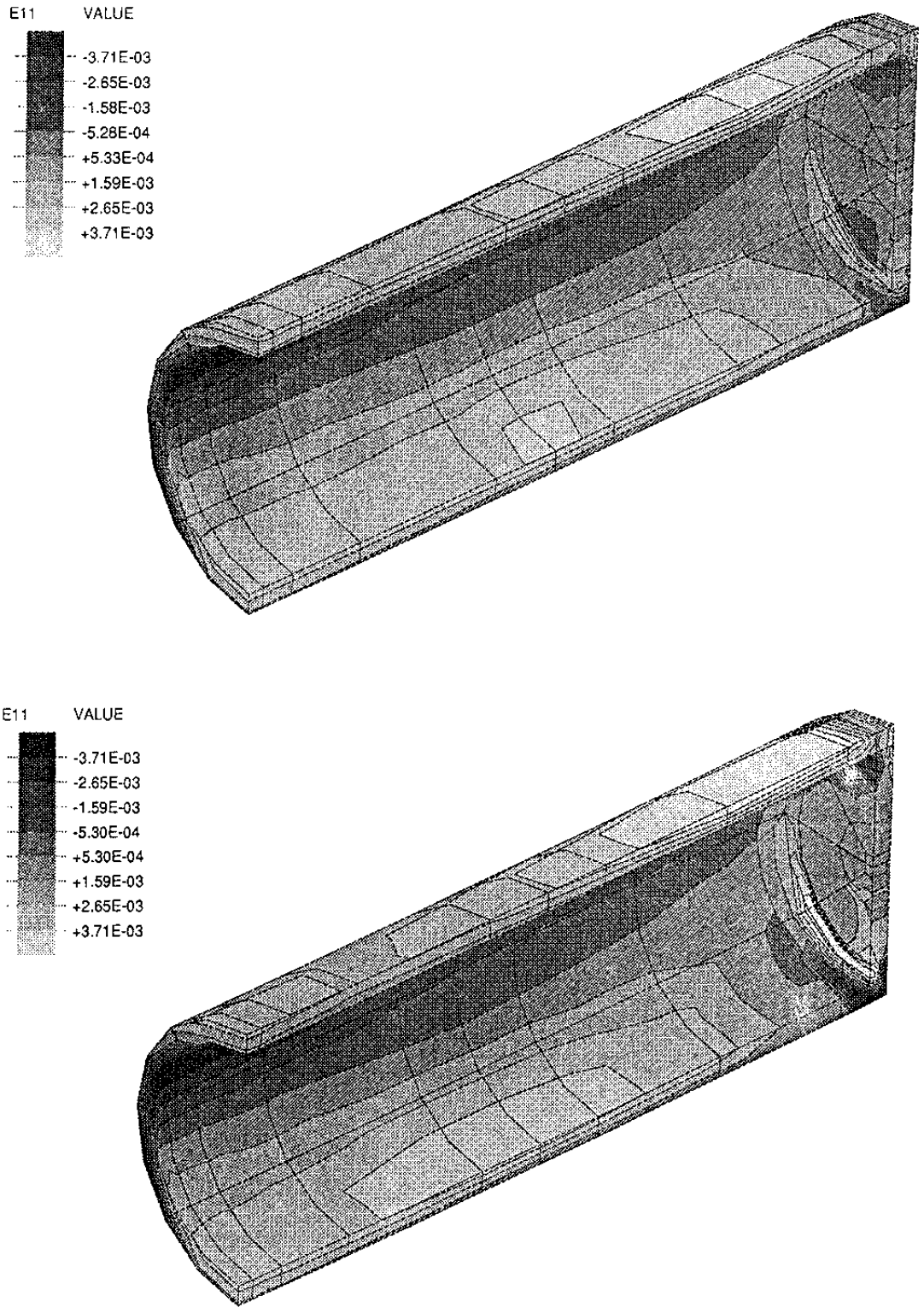

Figure 5-11 The normal strain in the shear direction ε_{11} in the copper before (upper) and after the combined creep in the copper and consolidation of the clay

All strain and displacements in the copper are shown in Appendix 4 (after shear) and Appendix 5 (after creep and consolidation). Two major conclusions can drawn:

- the strain in the long cylinder of the canister has increased about 0.002% at maximum

- the strain at the connection of the cylinder and lid has increased locally to about 0.012%

It is concluded that the effect is very small in the cylindrical part. The local large increase in strain at the edge of the lid is uncertain because of the coarse element mesh.

5.4.4 Effect of consolidation of the clay

The calculation in the previous chapter included two phenomena; creep in the copper and consolidation of the clay. Since the consolidation is finished within the time simulated in the calculation it is not possible to extrapolate over longer periods of time. In order to separate the phenomena a second calculation was made, in which only the consolidation of the clay was considered, neglecting the creep in the copper.

Fig 5-12 shows the same comparison of the strain ε_{11} before and after the consolidation as in Fig 5-11. As can be seen, the difference is much smaller in Fig 5-12 and the conclusion must thus be that the change in strain seen in Fig 5-11 is mainly caused by the creep in the copper.

However, for the shear strain ε_{13} the conclusion will be the opposite. Fig 5-13 shows this strain after shear, after consolidation and creep and after consolidation with no creep. The pictures after consolida-

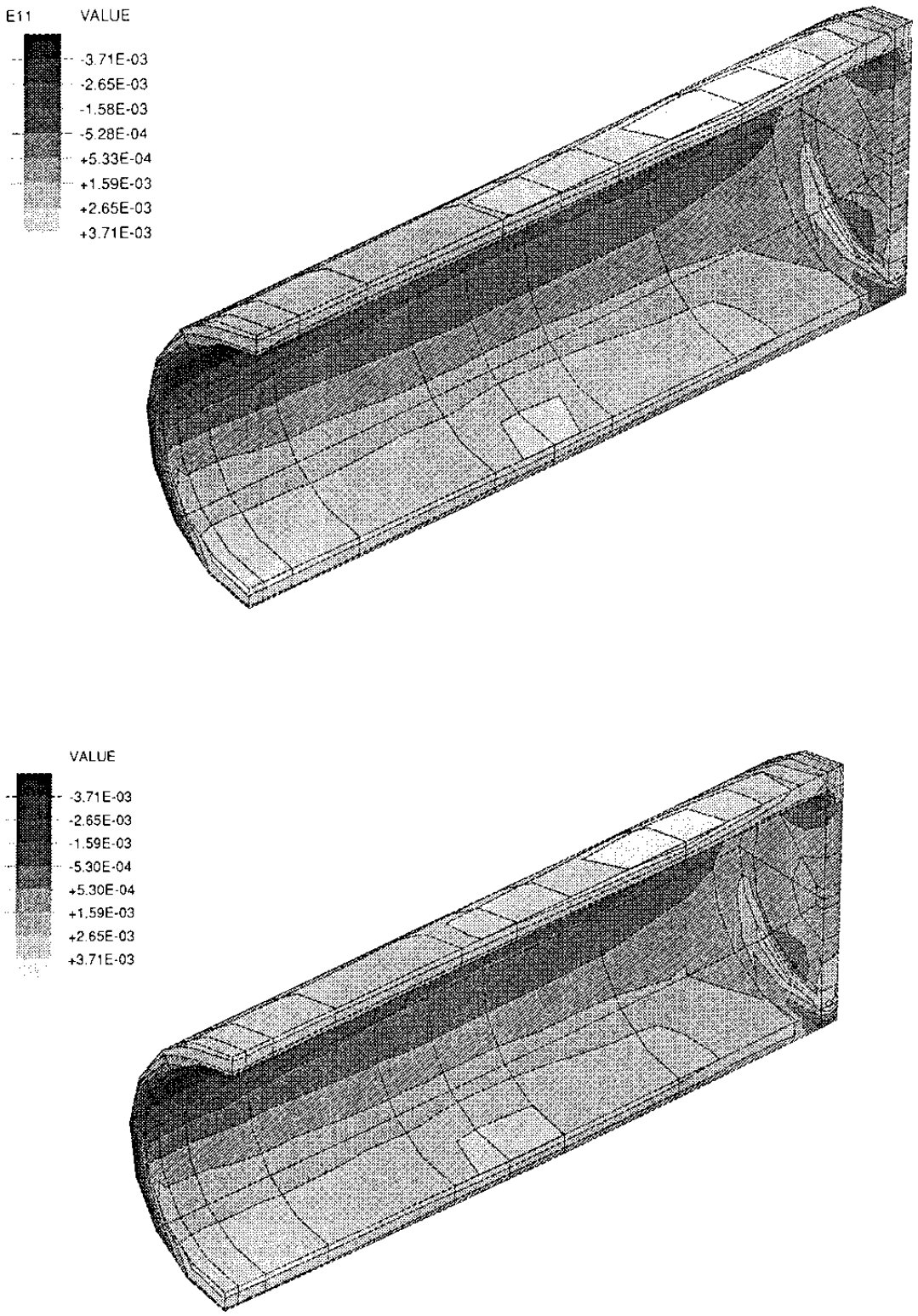

Figure 5-12 The normal strain in the shear direction ε_{11} in the copper before (upper) and after consolidation of the clay

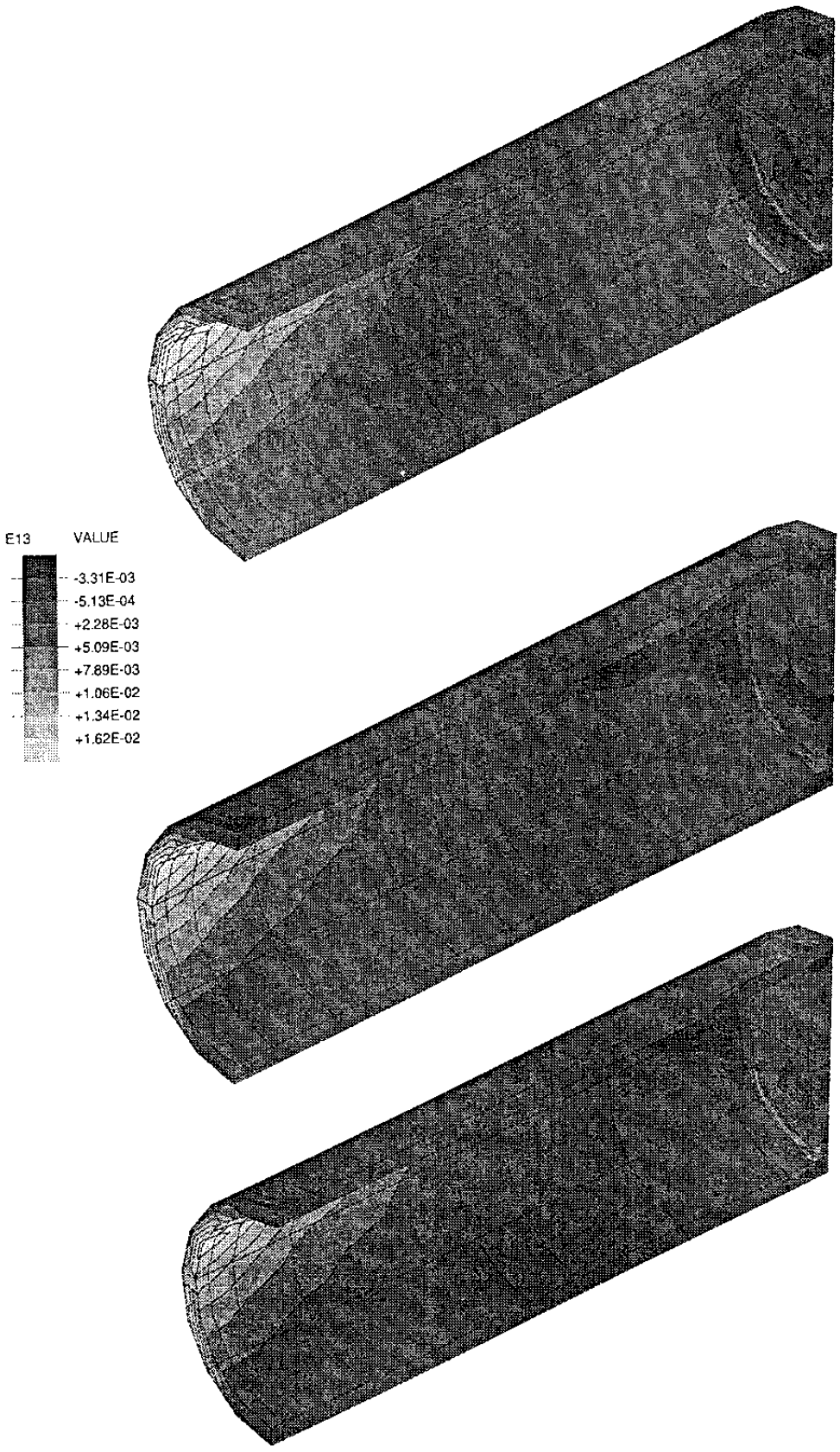

Figure 5-13 The shear strain ε_{11} in the copper before (upper), after creep in the copper and consolidation of the clay (center) and after only consolidation of the clay

tion and creep and after creep only, are almost identical, which means that the change in strain, which is about 0.002% in the cylinder and about 0.012 at the edges of the lid, mainly originates from the consolidation.

Appendix 6 contains a set of results of the strains and displacements in the copper after consolidation only.

5.4.5 Conclusions

The effect on the canister of creep and consolidation during 30 years after rock shear is thus small. However, if the strain rate at the maximum change in strain, that mainly comes from the creep in the simulated period, is linearly extrapolated to 100 000 years, the results would be:

- maximum total creep strain in the cylinder: ε_{11}=6%
- maximum total creep strain at the cylinder/lid connection ε_{11}=36%

Such an extrapolation, which is conservative, shows that the creep in the cylinder after rock shear does not cause failure but that the creep at the cylinder/lid connection may almost yield failure after 100 000 years. However, the coarse element mesh in this part of the canister makes the conclusion very uncertain; a new calculation may be required.

5.5 ASYMETRIC ROCK SHEAR

5.5.1 General

It is probable that rock shear perpendicular to the

axis of the canister creates higher stresses in the canister than any other shear direction, with the possible exception of the stresses in the lid, since the projected length of the canister is largest in the shear direction. However, the most critical shear plane does not necessarily go through the center of the canister, since asymmetric shear will increase resistance to motion at one end of the canister. In order to investigate this effect, a calculation with rock shear at 1/4 of the canister length was made.

5.5.2 Assumptions

The element mesh is shown in Fig 5-14. The dimensions are the same as in the other simulations but the entire canister and buffer had to be modeled because of the asymmetry. The shear plane, which is marked in the figure, passes through the right 1/4-point of the canister. The shear is produced by mechanically fixing the hole boundary to the left of the shear plane and moving the right boundary.

The materials and material models are identical to those described earlier in this chapter, except for the creep function of the copper which was not included.

The calculations were made in the same way as the previous calculations with symmetric shear. The water pressure and the swelling pressure from the bentonite were first simulated, resulting in the same swelling of the bentonite and closure of the slot between the copper and the steel as described in chapter 5.2. After equilibrium, shear (10 cm in 30 days) at constant rate was applied.

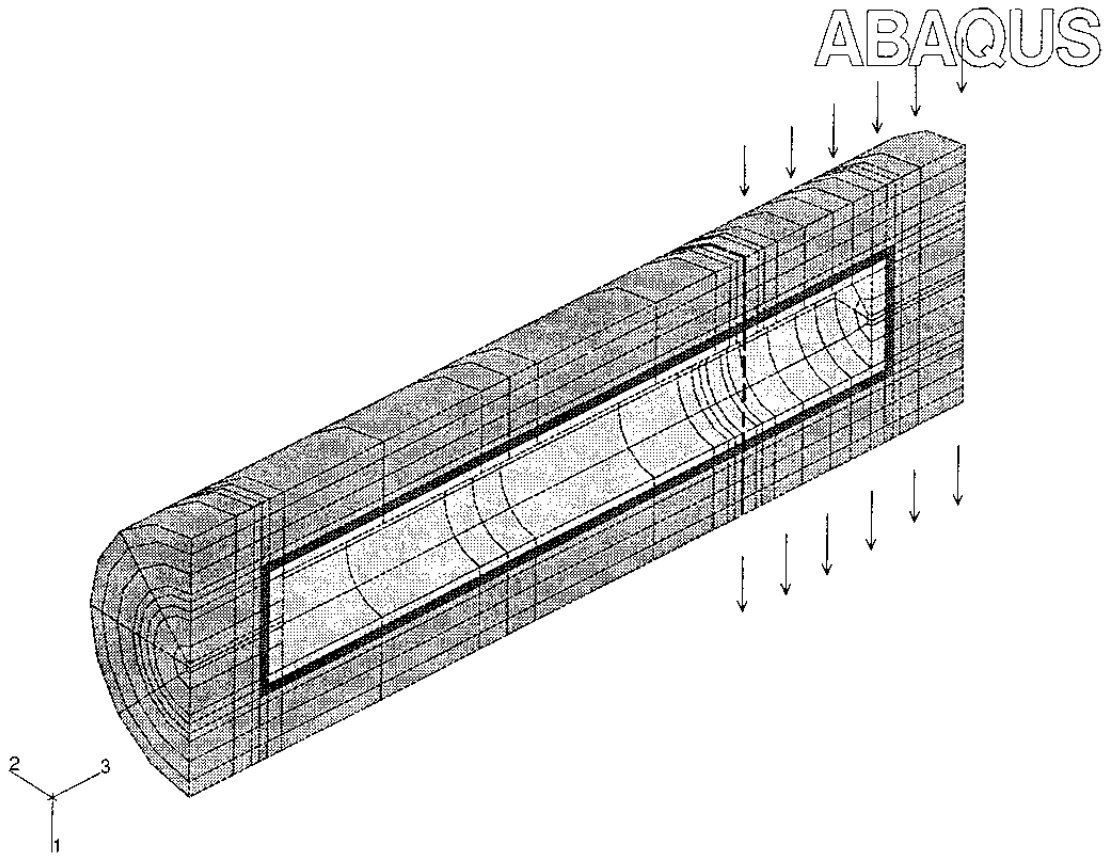

Figure 5-14 Element mesh for asymmetric rock shear

The drainage condition differed from that in the previous calculation since the rock contact was assumed to be completely undrained instead of completely drained. These two types represent the two extremes in a real deposition hole but the different drainage conditions are probably of limited importance since the shear is too fast for the pore pressure to be dissipated.

5.5.3 Results

The deformed structure after 10 cm shear is shown in Fig 5-15. The different resistance to canister movement between the two canister ends is clearly seen. The left part of the asymmetrically sheared canister is completely parallel to the axis of the hole while

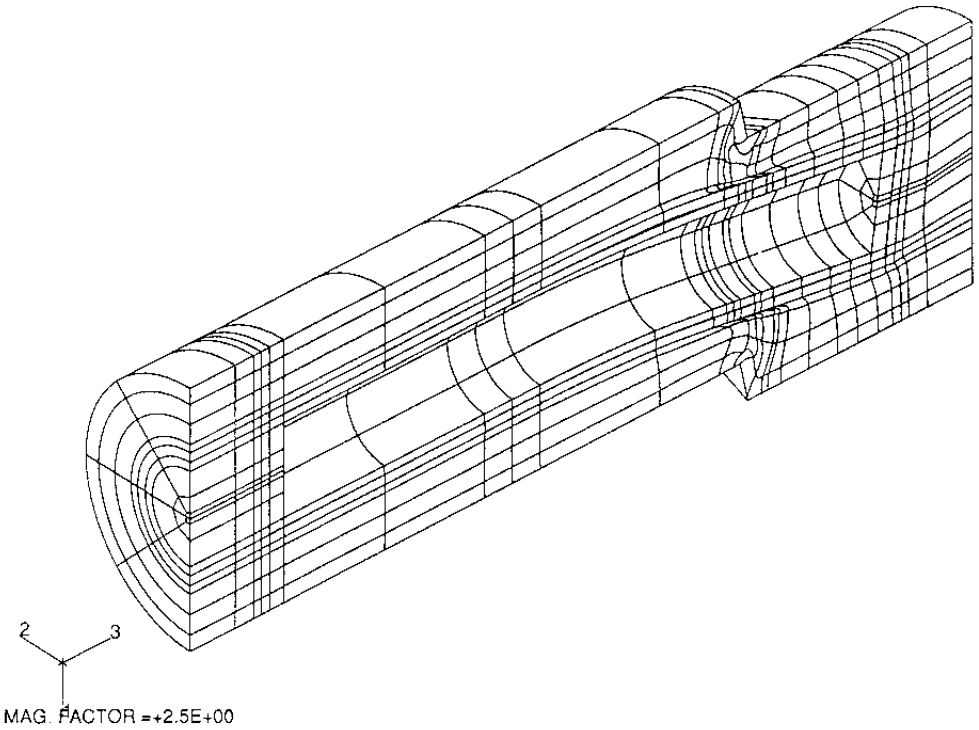

Figure 5-15 Deformed structure after 10 cm asymmetric shear

the right part is strongly inclined. The picture also shows that a gap has been formed between the copper and steel cylinders at the left upper side.

Fig 5-16 shows two pictures of how the shear has affected the clay. The pore pressure in the clay just after completed shear and the produced plastic strain are shown. The plastic strain of up to 170% in the bentonite/canister contact zone close to the shear plane is almost identical to that at symmetric shear, while the pore pressure is considerably lower in the calculation with the asymmetric shear.

The deformed copper canister and its plastic strain are shown in fig 5-17. The big displacement magnification factor in the deformation plot makes the effect of the shear quite clear. The canister is obviously not very much bent close to the shear

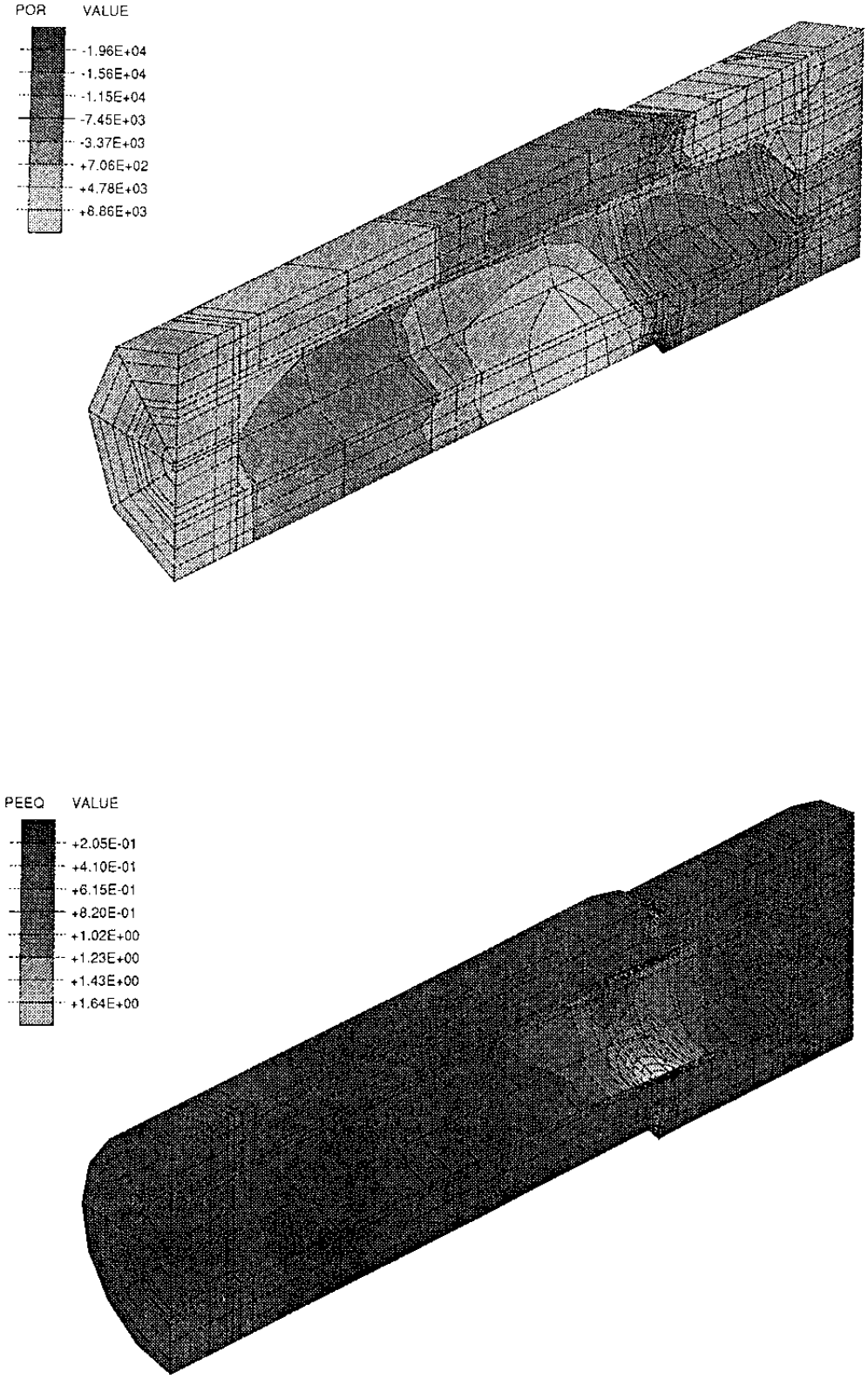

Figure 5-16 Pore pressure (kPa) (upper) and plastic strain in the bentonite after asymmetric shear

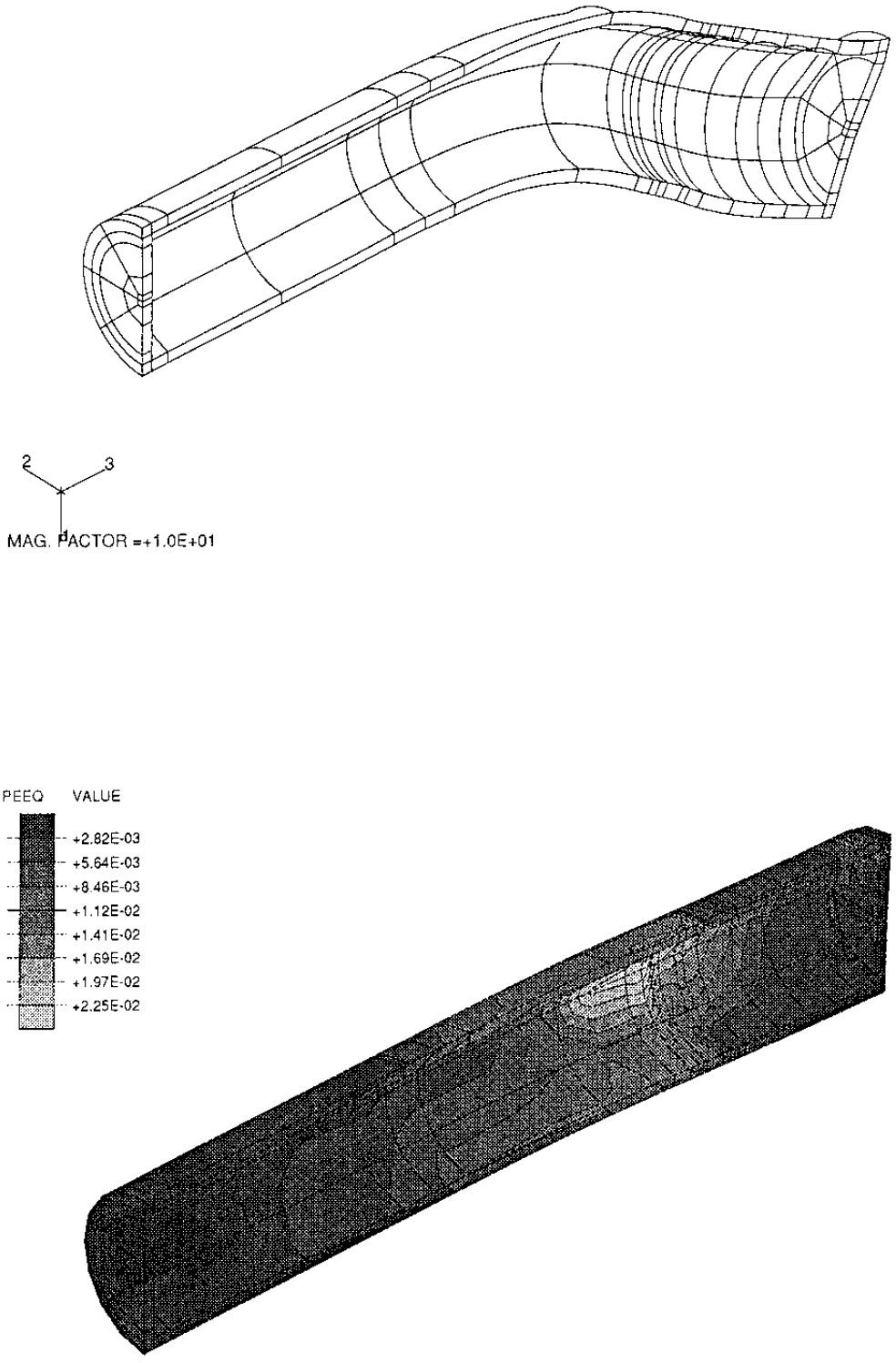

Figure 5-17 Deformed copper canister with F_m=10 (upper) and the plastic strain in the copper after asymmetric rock shear

plane. Most of the bending takes instead place in the central part of the canister. However, this is not reflected in the plastic strain of the copper, which is largest close to the shear plane with a maximum value about 2.5%. This is about twice the plastic strain that was calculated for symmetric shear.

The bending is reflected by the plastic strain in the inner steel canister as shown in Fig 5-18. The plastic strain is quite large (~1.5%) at the center of the inside of the steel canister, i.e. about four times the strain obtained in the calculation of symmetric shear. Fig 5-18 also shows the normal stresses in the interface elements representing the radial stresses between the copper and steel canisters. The darkest parts are where no stresses exist between the canisters indicating that they are not in contact. The gap is largest in the passive parts (maximum ~5 mm) which can be seen in the pictures in Appendix 7. The appendix includes a complete set of results from the calculation. The results are given for 5 and 10 cm rock displacement.

5.5.4 Conclusions

The effect on the canister is stronger at asymmetric than at symmetric rock shear, i.e. the plastic strain is 2-4 times larger. However, the stresses and strain are not sufficiently high to produce failure of the canister.

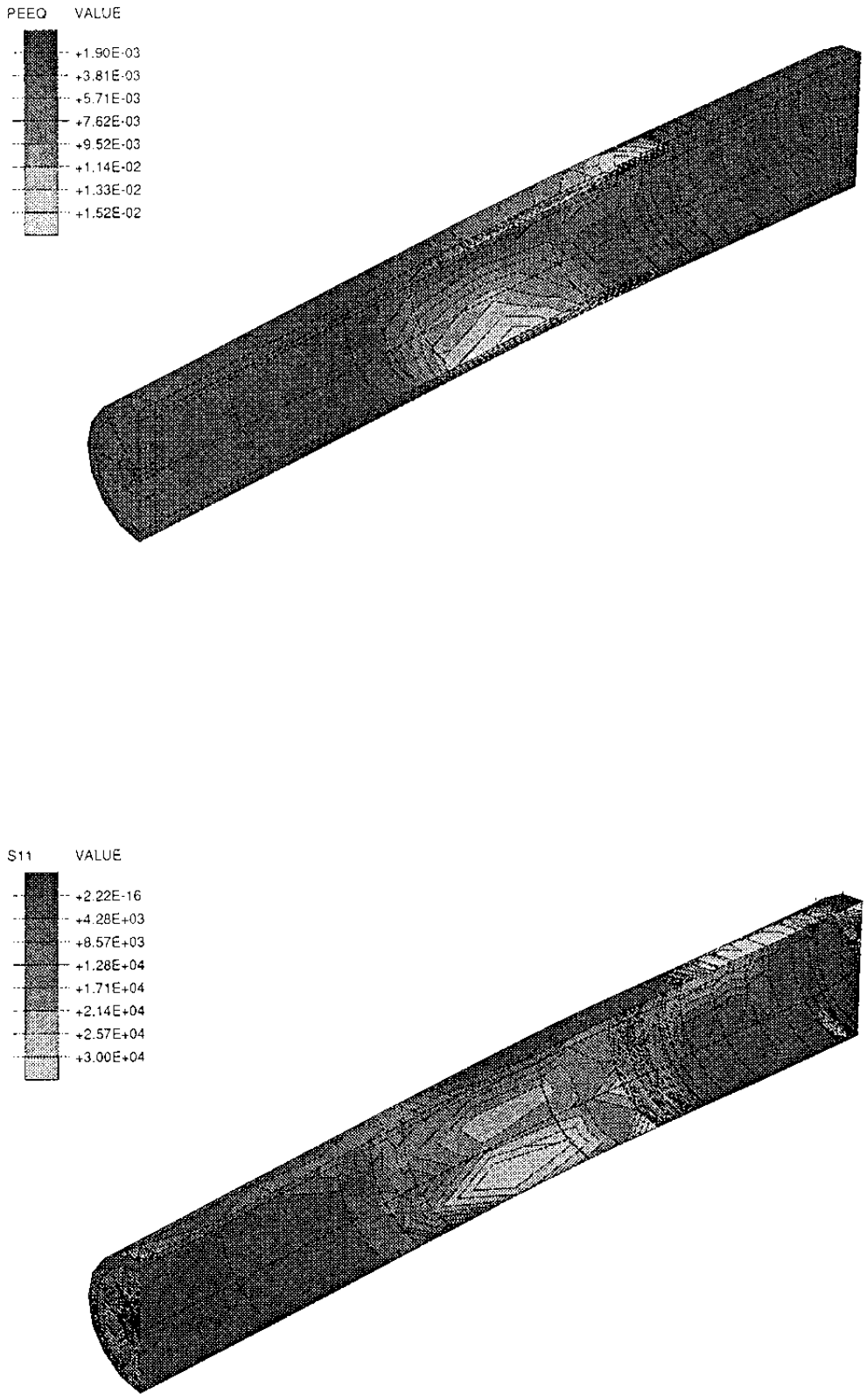

Figure 5-18 Plastic strain in the steel canister (upper) and normal stresses in the interface elements after asymmetric rock shear

6 VLH COPPER/STEEL CANISTER

6.1 GENERAL

The difference in geometry and dimensions between the canisters and between the boreholes in the VLH and KBS3 repositories made it desirable to conduct the same calculations for VLH as for KBS3 except for the creep and the asymmetric shear. Since VLH may require initially water-saturated bentonite buffer, the thermomechanical effects just after emplacement have been investigated as well.

6.2 EFFECT OF WATER AND SWELLING PRESSURE

6.2.1 Calculation assumptions

The geometry differs from KBS3 mainly by the spherical ends and the larger diameter of the canister. Fig 6-1 shows the element mesh. The dimensions are:

Inner diameter of steel canister: 1.26 m
Thickness of steel canister: 0.11 m
Thickness of copper canister: 0.06 m
Thickness of bentonite buffer: 0.40 m
Resulting diameter of dep. hole: 2.40 m
Length of canister: 6.00 m

For symmetry reasons, only 1/4 of the structure has been modeled as in the KBS3 calculations with symmetric shear. The slot between the steel and copper canisters has been modeled by 1 mm thick interface elements with no internal stiffness.

VLH 910402

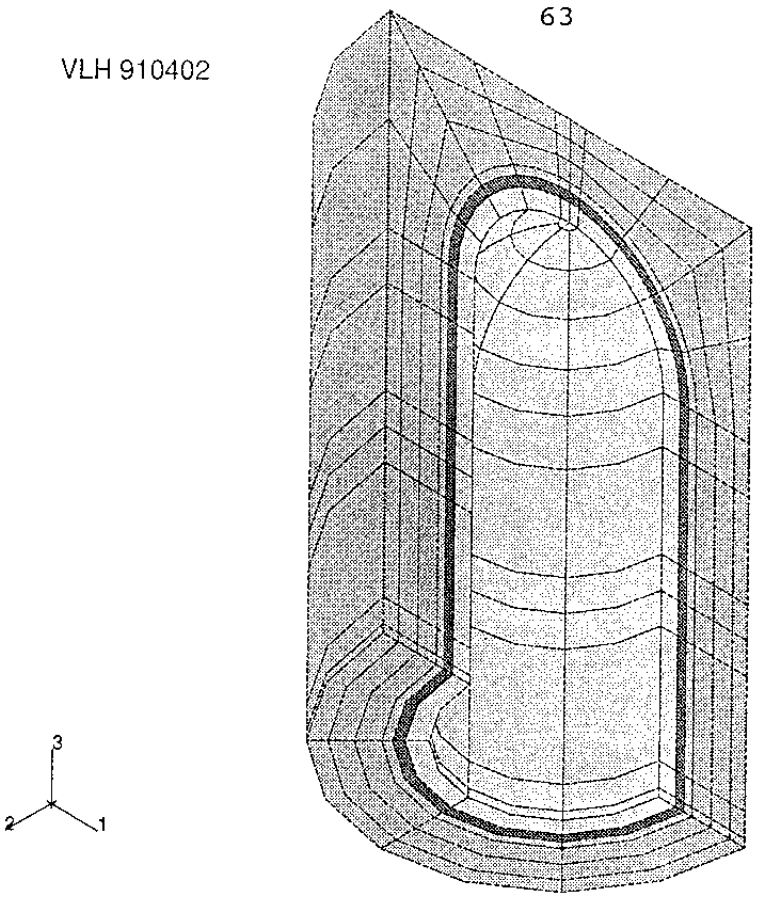

Figure 6-1 Element mesh of the VLH geometry
Light grey: steel
Dark grey: copper
Intermediate grey: bentonite

The material properties are identical to those used in the corresponding KBS3 calculation shown in chapter 5 with exception for the copper, which was modeled with a much lower elastic stiffness of $E=18 \cdot 10^6$ kPa in these calculations. The yield criterion and yield function of the copper were the same in both calculations.

The calculations were made in two steps as in the KBS3 calculations. In the first step the bentonite was allowed to swell and the additional water pressure applied. The result of this calculation describes the long-term state of the canister except for the heat expansion. This state was the starting point of the rock shear calculation.

6.2.2 Results

Figs 6-2 and 6-3 show the effect of the bentonite swelling and the additional hydrostatic pressure on the VLH structure. The bentonite (Fig 6-2) behaves in the same way as in the KBS3 structure, while the shape of the copper canister as well as the contact pressure (Fig 6-3) show that the copper canister is in contact with the steel canister along the entire surface. No plastic strain occurs either in the copper or in the steel and the maximum Mises stresses are about 50 MPa.

A more complete set of results from this calculation is shown in Appendix 8.

6.3 EFFECT OF ROCK SHEAR

6.3.1 Assumptions

The shear was simulated with a constant rate of shear to a total displacement of 5 cm after 1 week. The surrounding rock was assumed to be completely undrained in this calculation. The same element mesh and material properties were used as in the previous swelling calculation.

6.3.2 Results

The deformed structure after 5 cm rock displacement is shown in Fig 6-4 while the generated pore pressures and plastic strain in the clay are shown in Fig 6-5. Very high pore pressures in the bentonite are produced on the compressed side with values up to ~20 MPa and low negative pressures on the opposite side, with values down to ~-8 MPa (locally even lower at the shear plane).

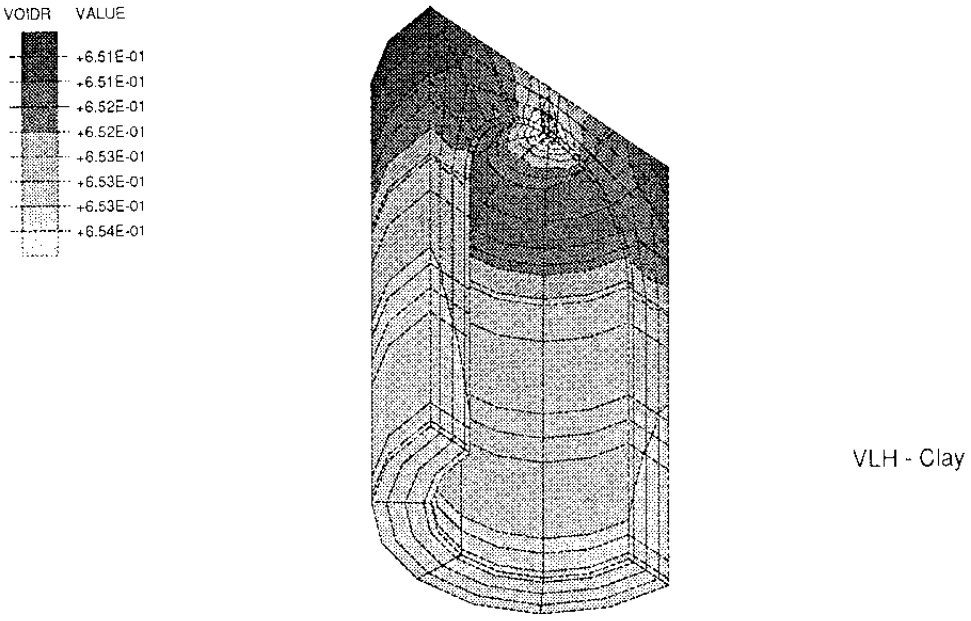

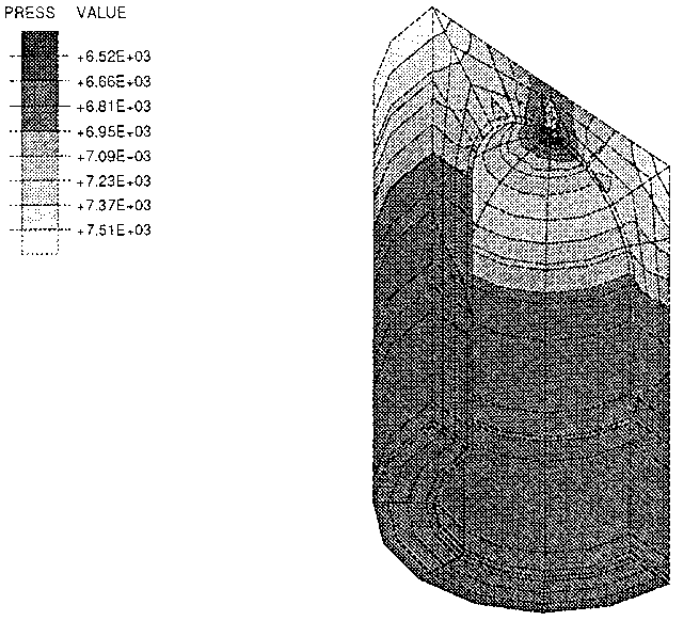

Figure 6-2 The calculated void ratio (upper) and average stress (kPa) in the bentonite after swelling equilibrium

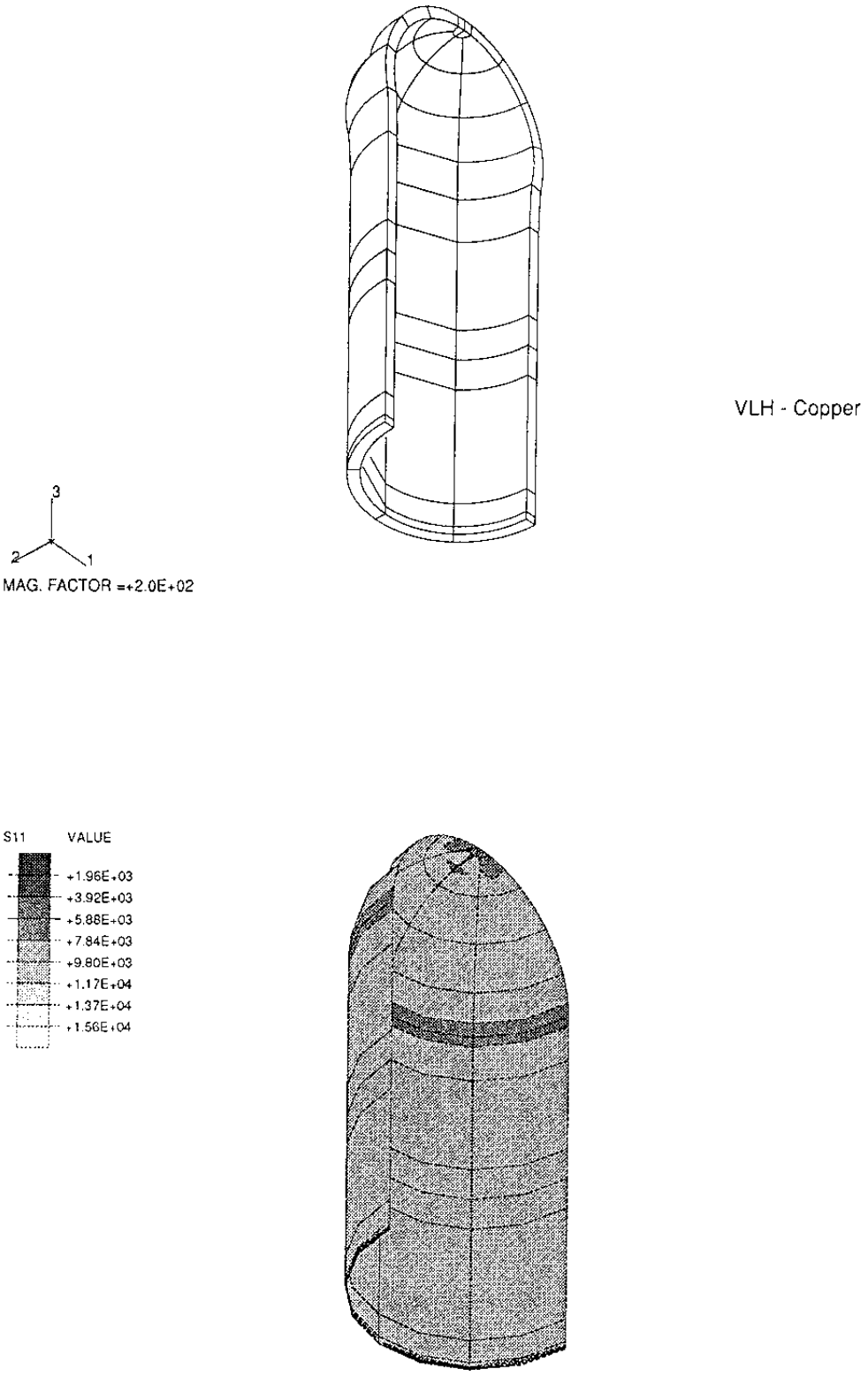

Figure 6-3 The deformed copper canister with F_m=200 (upper) and the normal contact pressure between the steel and copper canisters at equilibrium after swelling

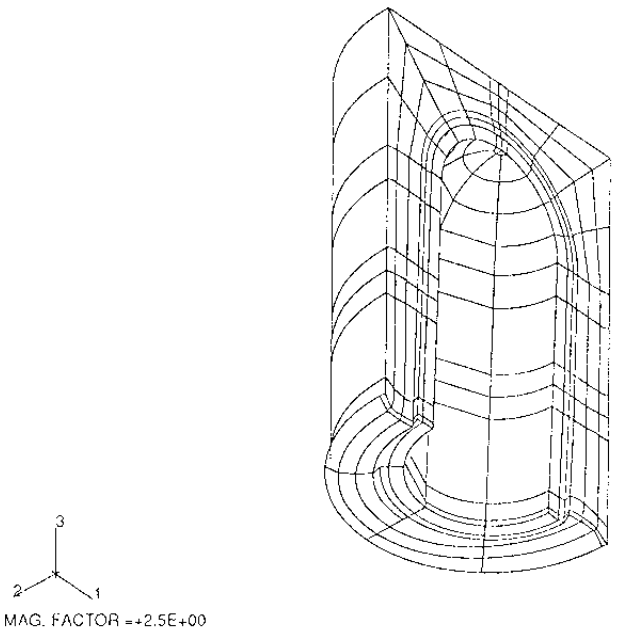

Figure 6-4 Deformed structure after 5 cm rock shear with F_m=2.5

The effect of shear on the copper canister is shown in Fig 6-6. The deformation magnification factor of the plotting of deformations is very large by which two bulges appear on the canister where the contact between the copper and the steel is lost. The canister is not bent but only tilted. The large magnification factor has strongly exaggerated the tilting and is the reason for the strange inclination. The copper is plasticized with up to ~0.7% plastic strain.

The aperture of the slot between the copper and the steel and the Mises stresses in the steel are shown in Fig 6-7. The figure shows the large bulge in the cylindrical part between the shear plane and the spherical end (cf. also Fig 6-6). The aperture is up to 3 mm in the bulge. The Mises stresses in the steel

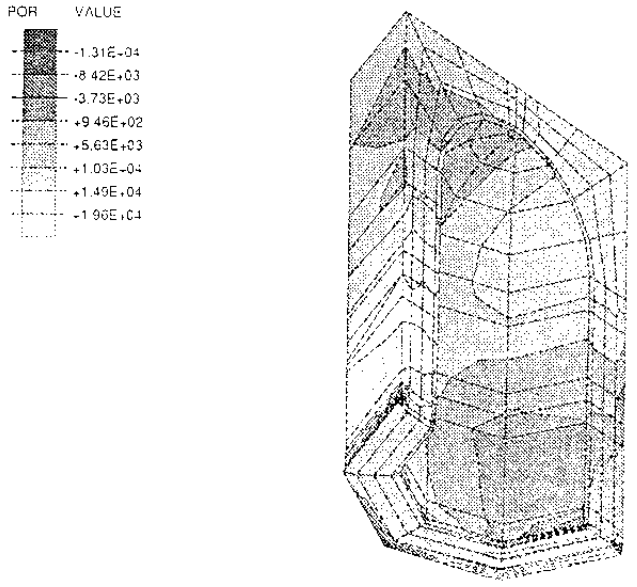

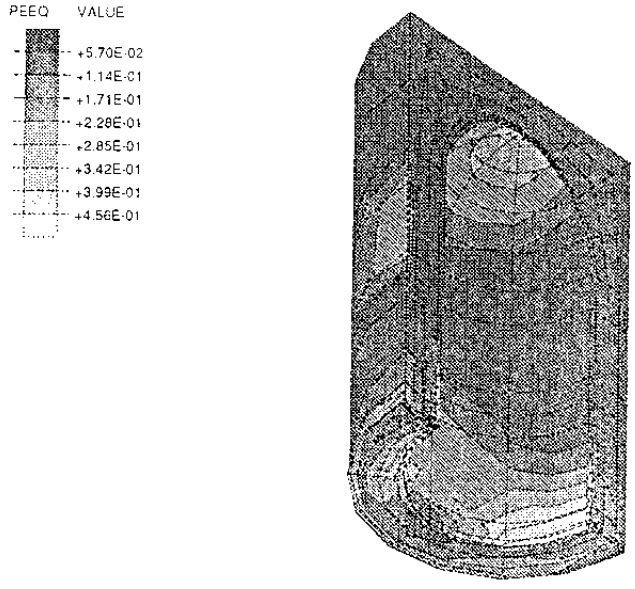

Figure 6-5 Generated pore pressure (kPa) (upper) and plastic strain in the copper after rock shear

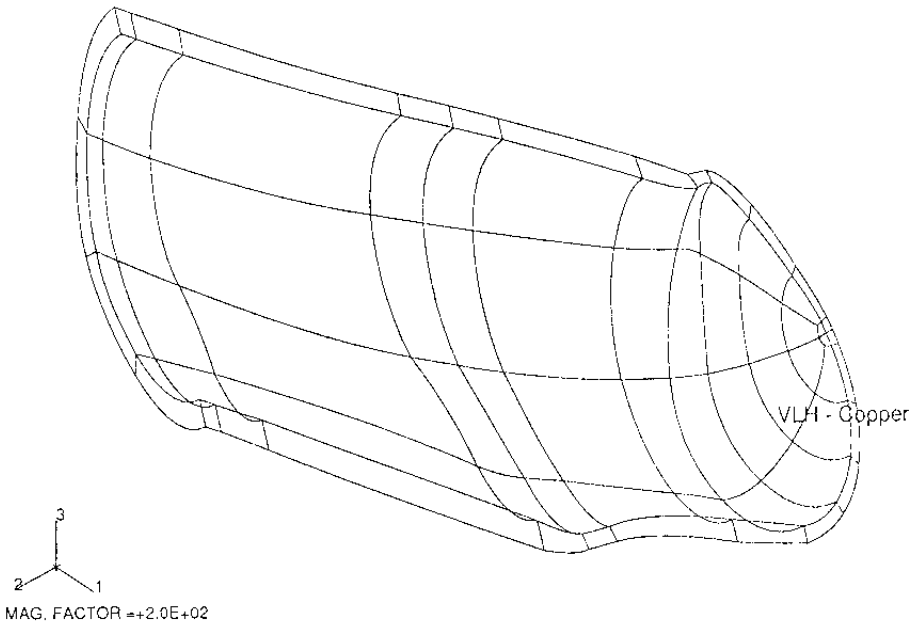

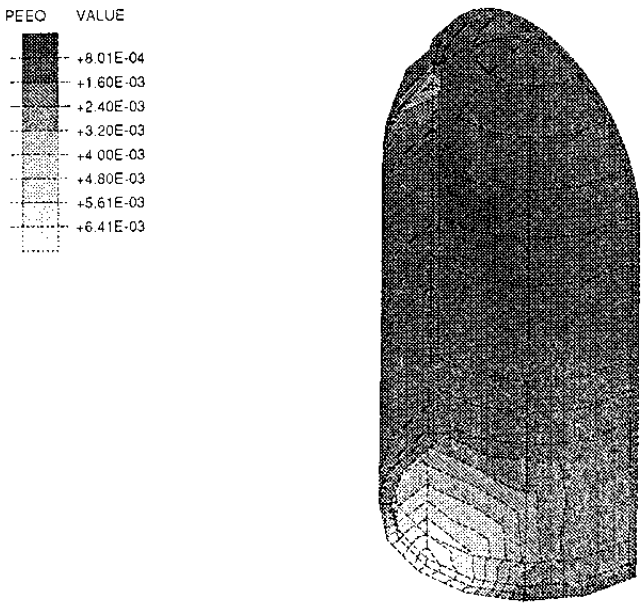

Figure 6-6 Deformed copper canister (upper) and plastic strain in the copper after rock shear

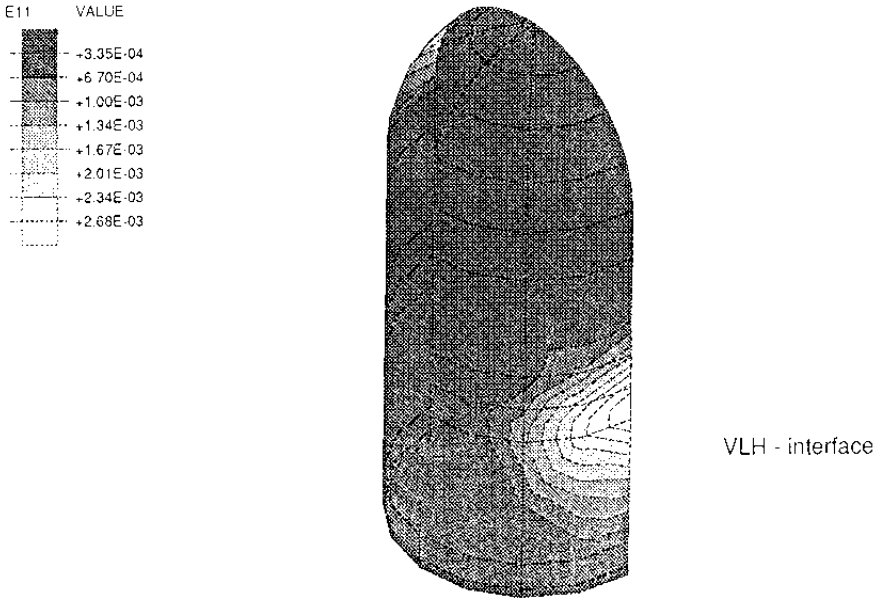

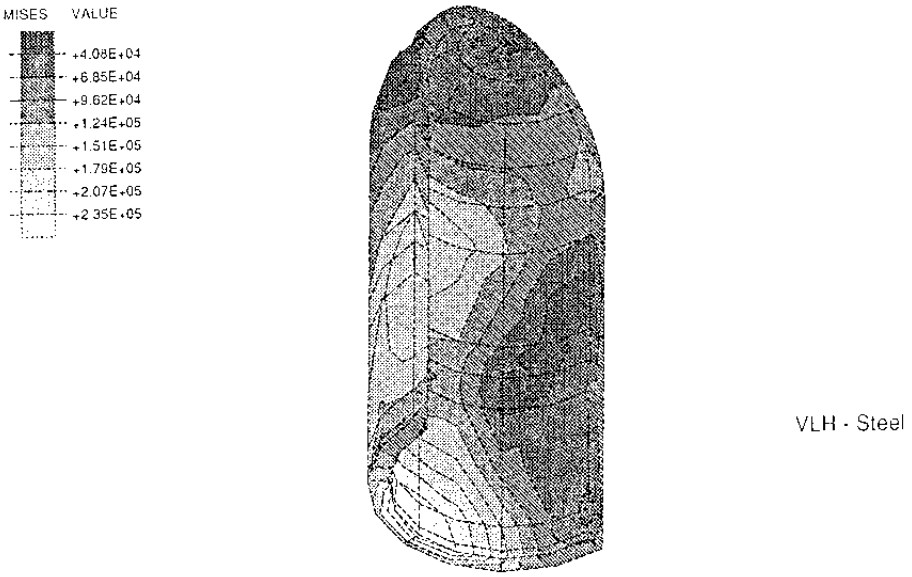

Figure 6-7 Aperture (m) of the slot between the canisters (upper) and the Mises stresses (kPa) in the steel after rock shear

do not exceed the yield stress and are about 250 MPa at maximum. A set of results from this calculation is enclosed in Appendix 9.

6.3.3 Conclusions

The effects of water and swelling pressure and of rock shear on the VLH copper/steel canister are not fatal to the canister. The stress/strain mechanisms are slightly different from those in the KBS3 canister, mainly due to the spherical ends that are more favorable. The most important difference is that the copper in the VLH canister does not plasticize by the water and swelling pressure if the slot between the copper and the steel can be limited to 1 mm.

6.4 THERMOMECHANICAL EFFECTS OF USING AN IN INITIALLY SATURATED BUFFER

6.4.1 General

In its present state the VLH concept implies that the buffer has an initially very high degree of water saturation. The power generated by the waste and the resulting increase in temperature of the near field will however cause an expansion of the materials that may create very high stresses in the canister and the rock. The high coefficient of thermal expansion of the saturated bentonite is the main reason for such high stresses.

Since the expansion of the saturated bentonite is mainly caused by the expansion of the pore water, the increase in stress with temperature is controlled by the drainage of the pore water through the rock. A fundamental question is thus if the drainage is fast enough to prevent unacceptably high pore pressures.

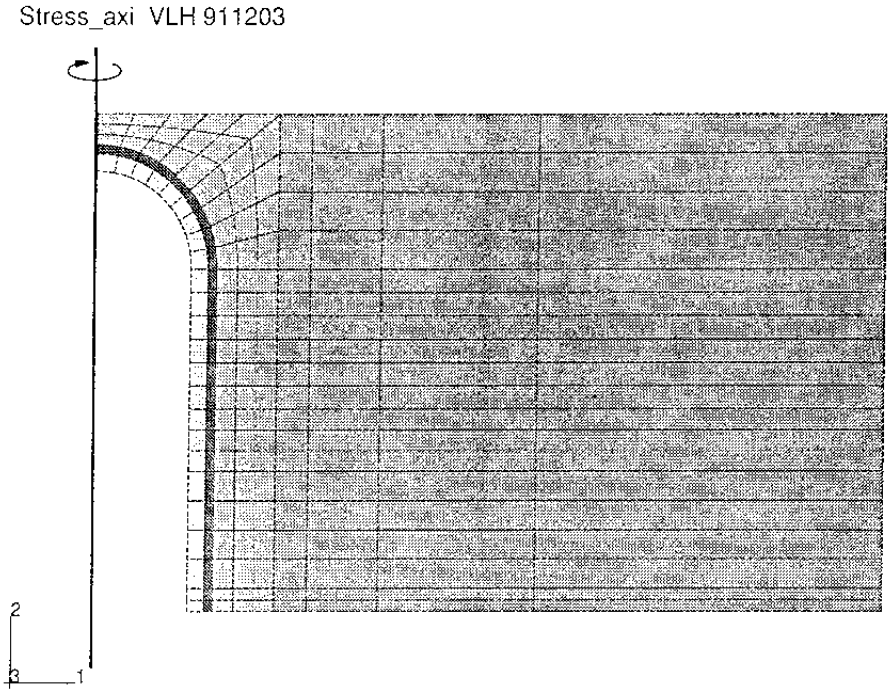

Figure 6-8 Element mesh for the thermomechanical calculation. Axisymmetry around the left boundary. The right boundary extends to 100 m from the axis.
Light light grey: steel
Dark grey: copper
Light grey: bentonite
Intermediate grey: rock

6.4.2 Assumptions

Structure

The VLH repository was simulated by an axisymmetric element mesh. A small part of this mesh is shown in Fig 6-8. The steel and copper canisters, the clay and a few meters of the rock are shown in the figure. The rock extends 100 m from the symmetry axis. The upper and lower boundaries in the figure are symmetry planes and an infinitely long tunnel filled with canisters is thus simulated by modeling only half a

canister. The dimensions are equal those described in chapter 6.2 except for the total thickness of the bentonite layer between two canisters, which is 0.4 m in this calculation instead of 0.8 m. The 1 mm slot between the steel and the copper is not simulated and the materials are assumed to be in close contact (joint surface nodes).

Materials

The materials were modeled according to the description in chapter 3.

Drainage and water pressure conditions

Complete drainage of the rock surface of the tunnel with a pore pressure of 3 MPa is assumed. This is a non-conservative assumption which is probably valid for full-phase drilling but not yet verified.

Calculation

The power of the waste is assumed to decline according to equation (6:1):

$$P=2950\cdot\left(0.769\cdot e^{-0.02T}+0.163\cdot e^{-0.002T}+0.068\cdot e^{-0.0002T}\right) \qquad (6:1)$$

where P is the total power generated by the waste in the canister in watts and T the time in years after deposition. This equation implies that the waste is deposited after 40 years of intermediate storage. The canister contains 24 fuel elements, each with an initial power of 122.9 W.

The calculation was made in two steps. At first the temperature development in the structure was calcula-

ted, since it is a process uncoupled to the mechanical effects. Then, the thermomechanical calculation, coupled to the calculation of the pore water flow and pore water pressure dissipation in the buffer, was made. The calculation referred to a total time of 10^9 seconds, or about 32 years simulated time.

6.4.3 Results

The temperature increase with time for the canister, which is equal to the highest temperature in the buffer, and for a point located in the rock 10 m from the center line, are shown in Fig 6-9. A maximum temperature of the canister is obviously reached after $2.5 \cdot 10^8$ seconds or about 8 years, which is in good agreement with earlier calculations. The temperature distribution in the buffer at the end of the calculation is also shown as an example. The temperature is high not only close to the canister but also between the canisters.

The key question for the thermomechanical calculation is the pore pressure in the bentonite. Fig 6-10 shows the calculated pore pressure distribution in the bentonite at four different times during the period. The maximum pore pressure is as high as about 15 MPa already after $1.7 \cdot 10^6$ sec or 20 days but the overpressure is completely dissipated at the end of the considered time period. The figure also shows that the pore pressure is highest between the canisters, which is logical since the temperature is higher and the distance to the drainage zone longer than anywhere else.

The maximum pore pressure between the canisters is plotted as a function of time in Fig 6-11 for the four occasions shown in Fig 6-10. The maximum pore pressure obviously occurs after about 10^7 sec. or

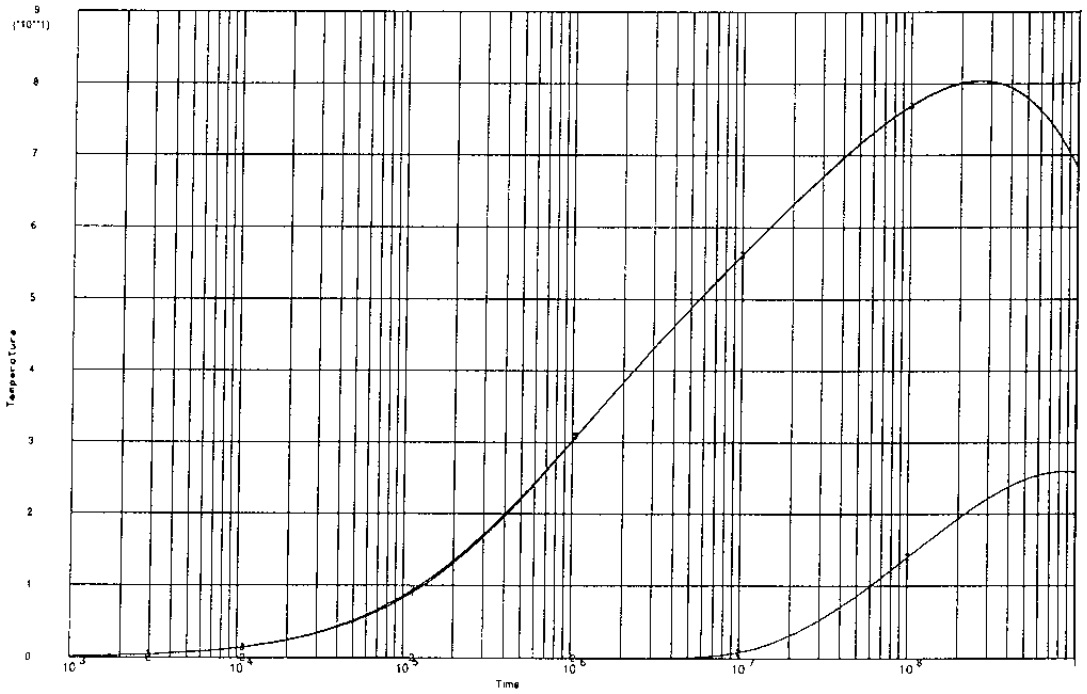

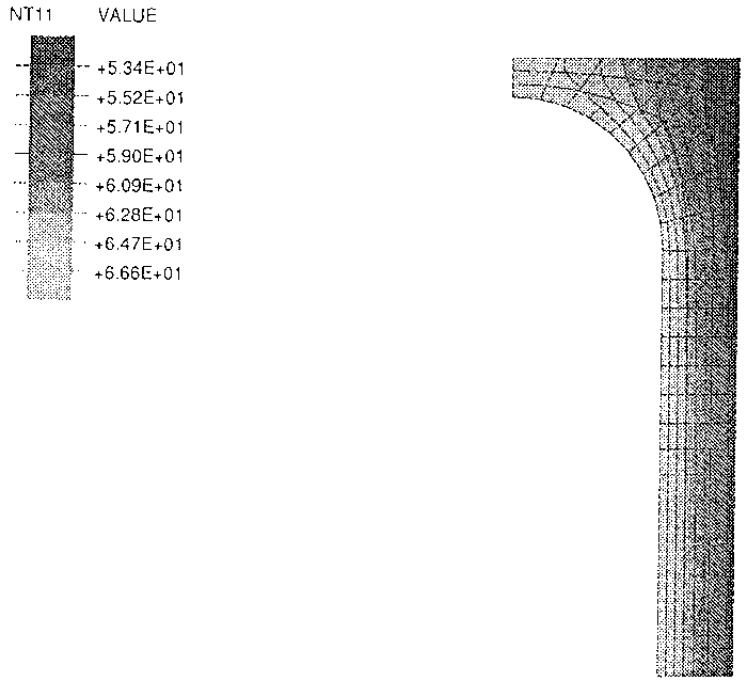

Figure 6-9 Results from the temperature calculation. The upper figure shows the highest temperature in the buffer and the temperature in the rock 10 m from the center line as a function of time. The lower figure shows the temperature distribution in the bentonite after 10^9 sec (32 years)

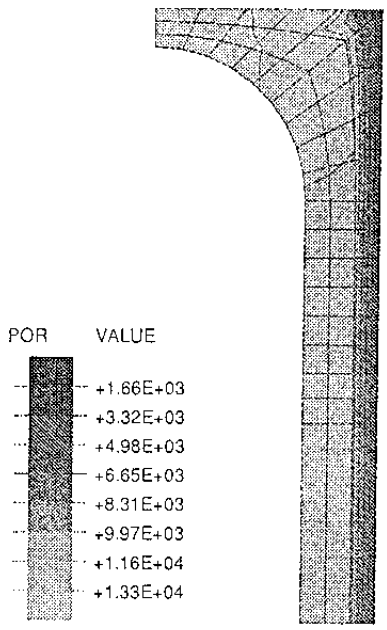

TOTAL ACCUMULATED TIME +1.716E+06

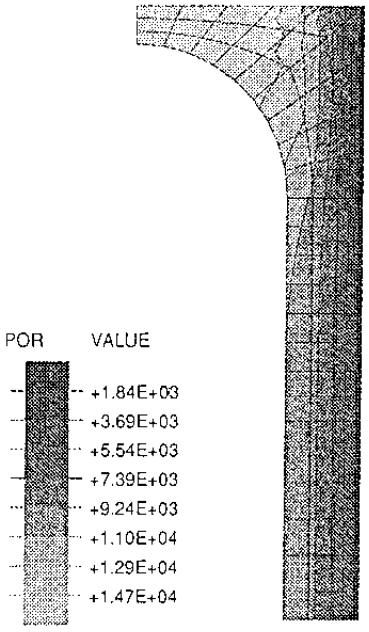

TOTAL ACCUMULATED TIME +1.268E+07

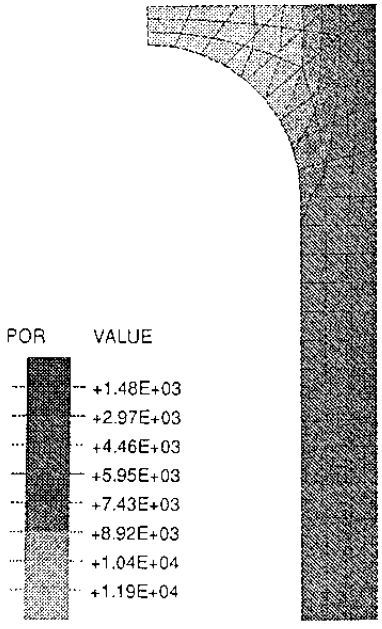

TOTAL ACCUMULATED TIME +4.092E+07

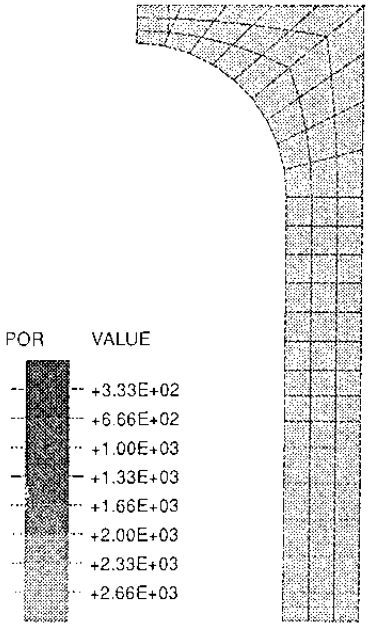

TOTAL ACCUMULATED TIME +1.000E+09

Figure 6-10 Pore pressure (kPa) distribution in the bentonite at different times (sec)

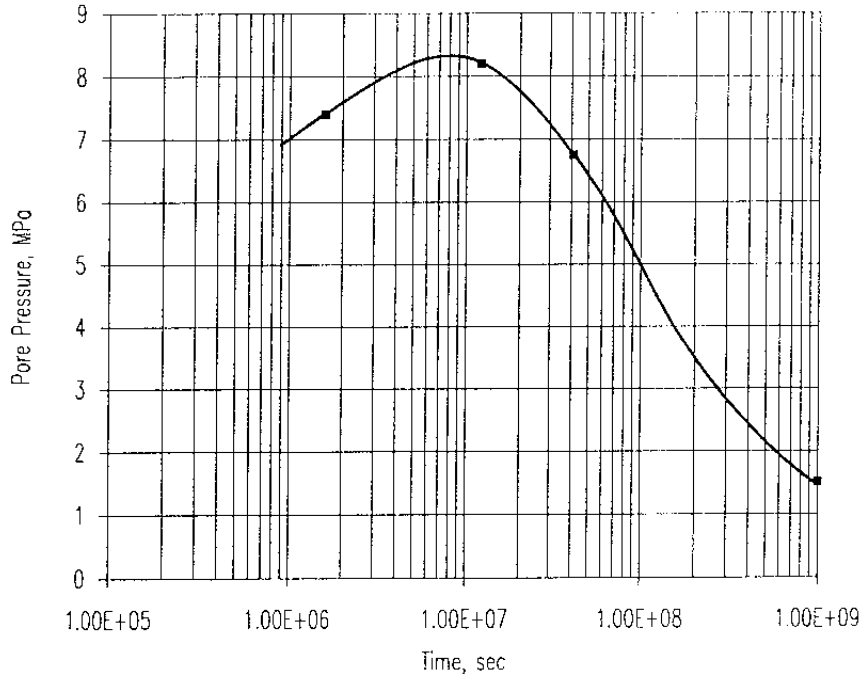

Figure 6-11 Maximum pore pressure in the bentonite as a function of time

100-200 days. The effect on the canister and rock should thus be the highest at about that time. A complete set of results from the time $1.268 \cdot 10^7$ sec is enclosed in Appendix 10.

The deformed canister, the plastic strain in the canister, and Mises stresses in the rock, are shown in Fig 6-12. The displacement magnification factor of the deformed canister is very high (1300) and the real displacements thus quite small but the axial compression of the canister will still be 0.5-1 mm according to this calculation. No plastic strain will occur in the steel but the copper will almost yield with a plastic strain of up to 0.15%. The Mises stresses in the rock will be quite high (up to 25 MPa) and there will be tensile stresses of about 12 MPa close to the tunnel surface. Since no in situ

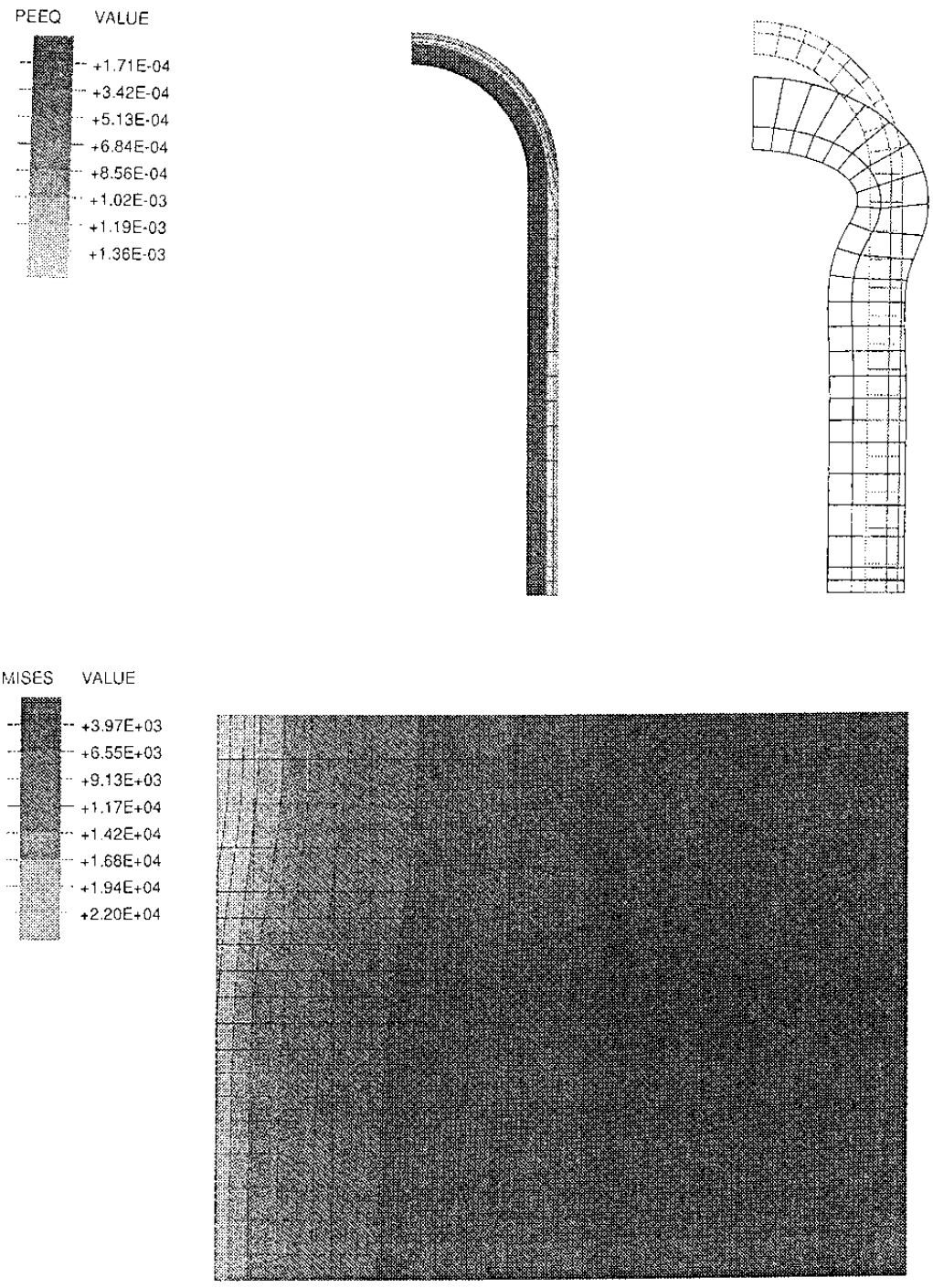

Figure 6-12 The plastic strain in the canister and the deformed canister with F_m=1300 (upper) and the Mises stresses in the rock (kPa) after 147 days

stresses has been applied to the rock, these values represent the change in stress and not absolute stresses.

6.4.4 Conclusions

The thermomechanical calculations show that the drainage is sufficiently effective to yield moderate pore pressures in the saturated buffer. Thus, the highest pressures are reached after 100-200 days, while the highest temperature will not appear until after about 8 years. However, despite the drainage effect, the induced pore pressure will be quite high and the effect on the canister and rock cannot be neglected. The uncertainty respecting the draining capacity of the near field rock makes it desirable to repeat the calculation assuming undrained rock conditions.

7 CONCLUSIONS

The various effects on on different types of canisters can be summarized as in Table 7-1. Shear 1/2 means shear through the central part of the canister (symmetry) while shear 1/4 means shear across the canister at 1/4 of its length from one end (asymmetry)

Table 7-1 Maximum plastic strain in the copper at different processes.

Canister type	Process	ρ_m t/m^3	Pl. strain % Surface	Lid	Rem.
KBS3 HIP	HIP		0.3	3.0	
	Swelling	2.05	0.0+0.3	0.0+3.0	1)
	Shear 1/4	2.05	1.2+0.3	0.0+3.0	1)
	Shear 1/2	1.93	0.0	0.0	
	Shear 1/2	2.14	4.0	0.0	
KBS3	Swelling	2.05	0.2	0.4	
Cu/Fe	Shear 1/2	2.05	1.2	0.7	2)
comp.	Creep 10^5y	2.05	6 (?)	36 (?)	3)
	Shear 1/4	2.05	2.5	1.0	2)
VLH	Swelling	2.05	0.0	0.0	
Cu/Fe	Shear	2.05	1.4	0.5	2)
comp.	Thermom.	2.05	0.15	0.1	2)

1) The first figure is the plastic strain from the process while the second figure is from the HIP process.

2) Including the plastic strain from the swelling

3) After shear 1/2

The following conclusions can be drawn from the calculations shown in the table:

1. The maximum plastic strain in the copper after 10 cm rock displacement is 4%, which refers to the very high bentonite density ρ_m=2.14 t/m^3.

2. The different canisters behave similarly but the KBS3 and VLH Cu/Fe composite canisters seem to be somewhat more affected than the KBS3 HIP canister.

3. The 1/4 shear seems to affect the canister more than the 1/2 shear.

4. The influence of the bentonite density is more important than the influence of the canister type.

Additional conclusions from the calculations are:

5. The 1 mm gap between the copper and steel in the composite canister will be closed after saturation of the bentonite due to the swelling except at the edge of the lid of the KBS3 canister.

6. The shear produces a high pore pressure in the compressed part of the bentonite (10-20 MPa) while the pore pressure will be negative on the opposite side of the canister (-1 to -10 MPa). However, instead of a negative pore pressure there will probably be a temporary gap between the canister and the clay in that part. The gap between the copper and steel in the composite canisters will be opened by 1-5 mm in that part.

One concludes that the various processes are not fatal to the canisters. However, the effects of creep in the copper after shear are not fully known since the strain values are extrapolations from a 30 y calculation. It is recommended to look further into that

effect. It is also recommended to make a supplementary calculation of the thermomechanical effect of a water saturated buffer in the case of completely undrained rock.

REFERENCES

1. Börgesson L. (1988) - Modeling of buffer material behavior. Some examples of material models and performance calculations. SKB Technical Report 88-29.

2. Börgesson L., Hökmark H. and Karnland O. (1988) - Rheological properties of sodium smectite clay. SKB Technical Report 88-26.

3. Börgesson L. (1990) - Interim report on the laboratory and theoretical work in modeling the drained and undrained behavior of buffer materials. SKB Technical Report 90-45.

4. Chen W. F. and Mizuno E. (1990) - Nonlinear analysis in soil mechanics. Theory and implementation. Developments in geotechnical engineering vol. 53. Elsevier.

5. Hibbit, Karlsson and Sorensen. ABAQUS manuals.

6. Pettersson K. (1991) - Personal communication

APPENDIX I-X

Results from ABAQUS calculations

Legend:

MISES = von Mises stresses (kPa)

PEEQ = Plastic strain

PRIN1 = Major principal stress (kPa)

PRIN3 = Minor principal stress (kPa)

VOIDR = Void ratio in the bentonite

POR = Pore pressure in the bentonite (kPa)

PRESS = Average stress $p=(\sigma_1+\sigma_2+\sigma_3)/3$ (kPa)

S = Normal stress (kPa)

E = Total strain

U = Total deformation

NT = Temperature increase ($^{\circ}$C)

APPENDIX Ia

Results from the calculation of the HIP process KBS3 HIP canister with residual stresses

KBS3-HIP 920707

ABAQUS

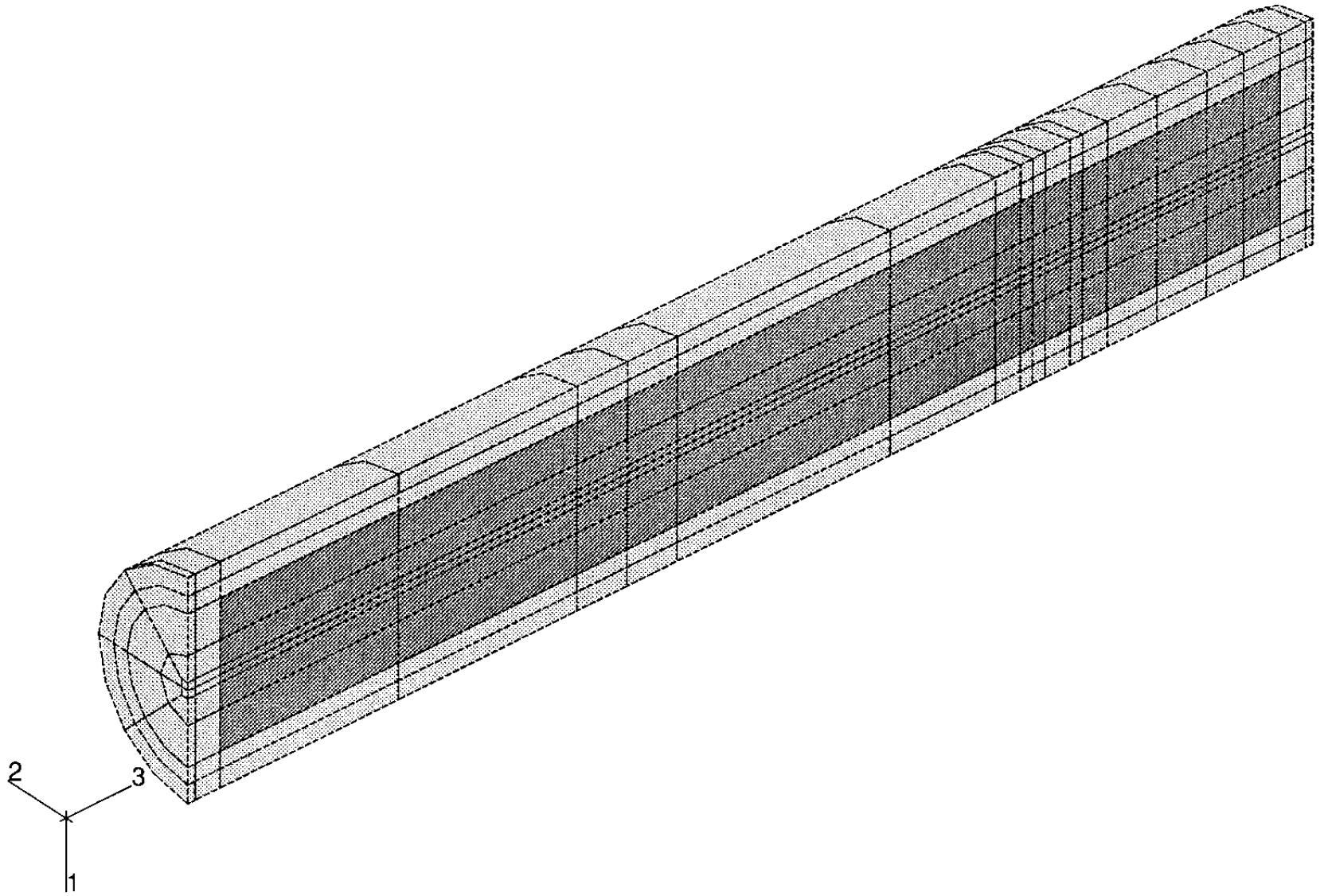

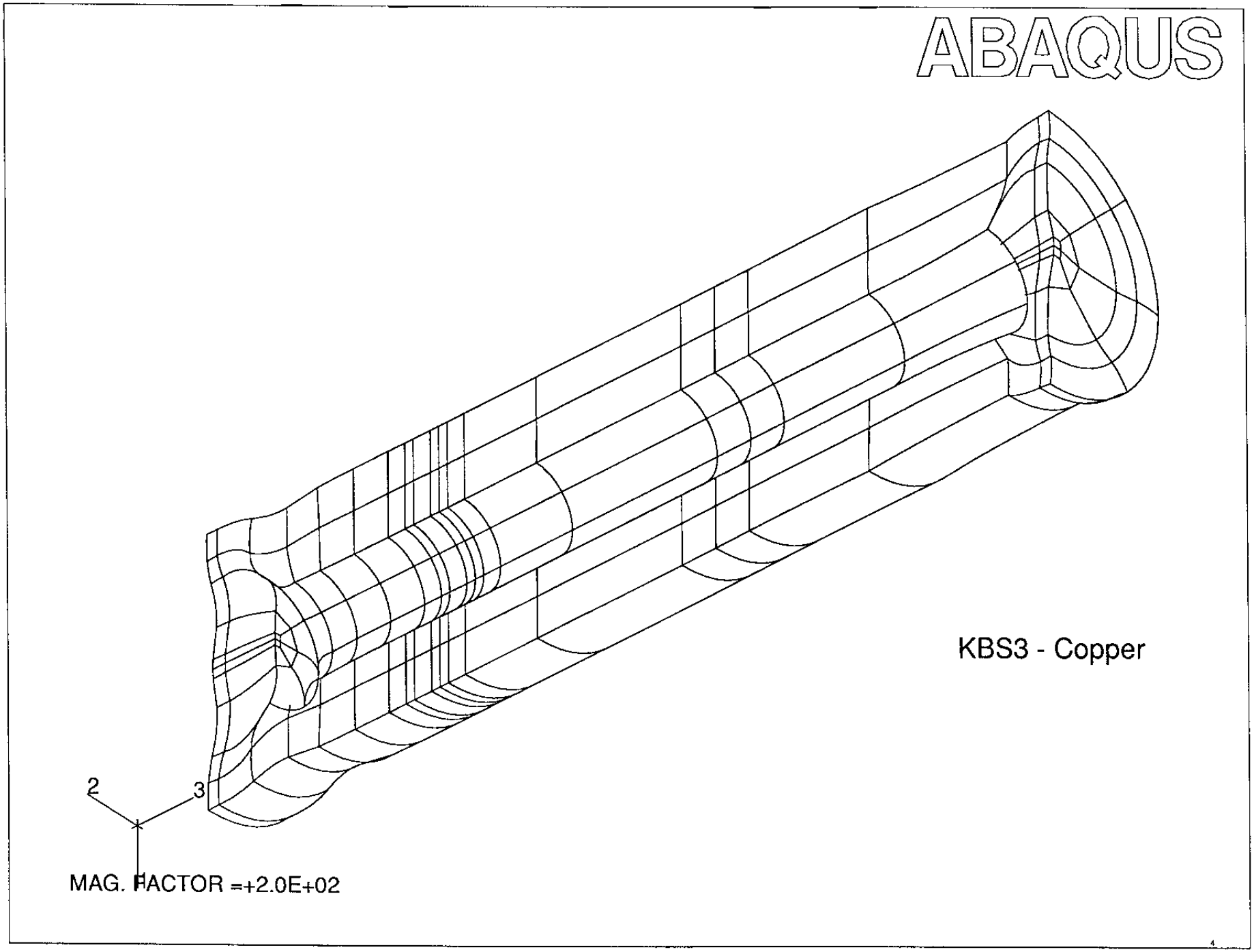
ABAQUS
KBS3 - Copper
2
3
MAG. FACTOR =+2.0E+02

ABAQUS

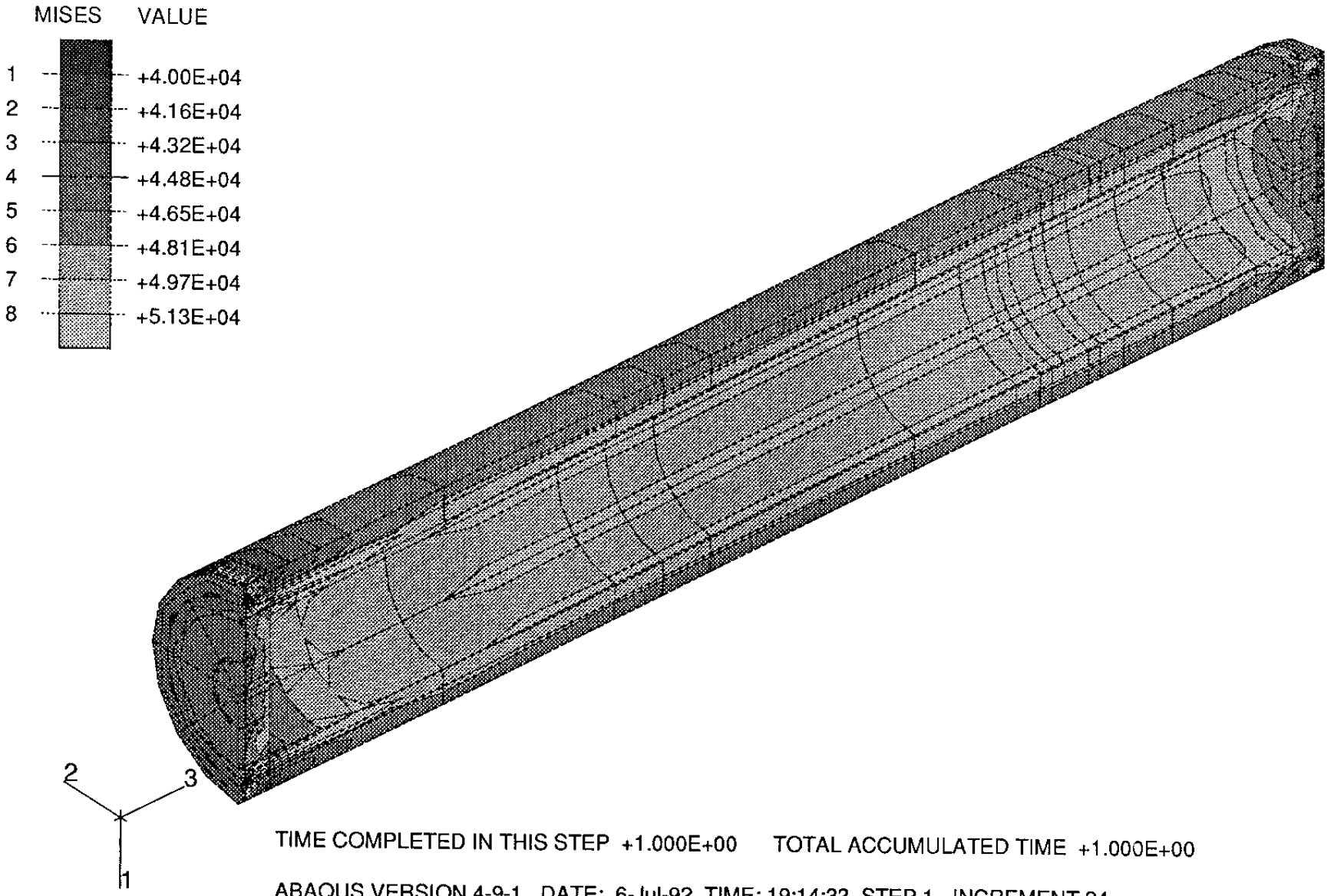

TIME COMPLETED IN THIS STEP +1.000E+00 TOTAL ACCUMULATED TIME +1.000E+00

ABAQUS VERSION 4-9-1 DATE: 6-Jul-92 TIME: 19:14:33 STEP 1 INCREMENT 24

ABAQUS

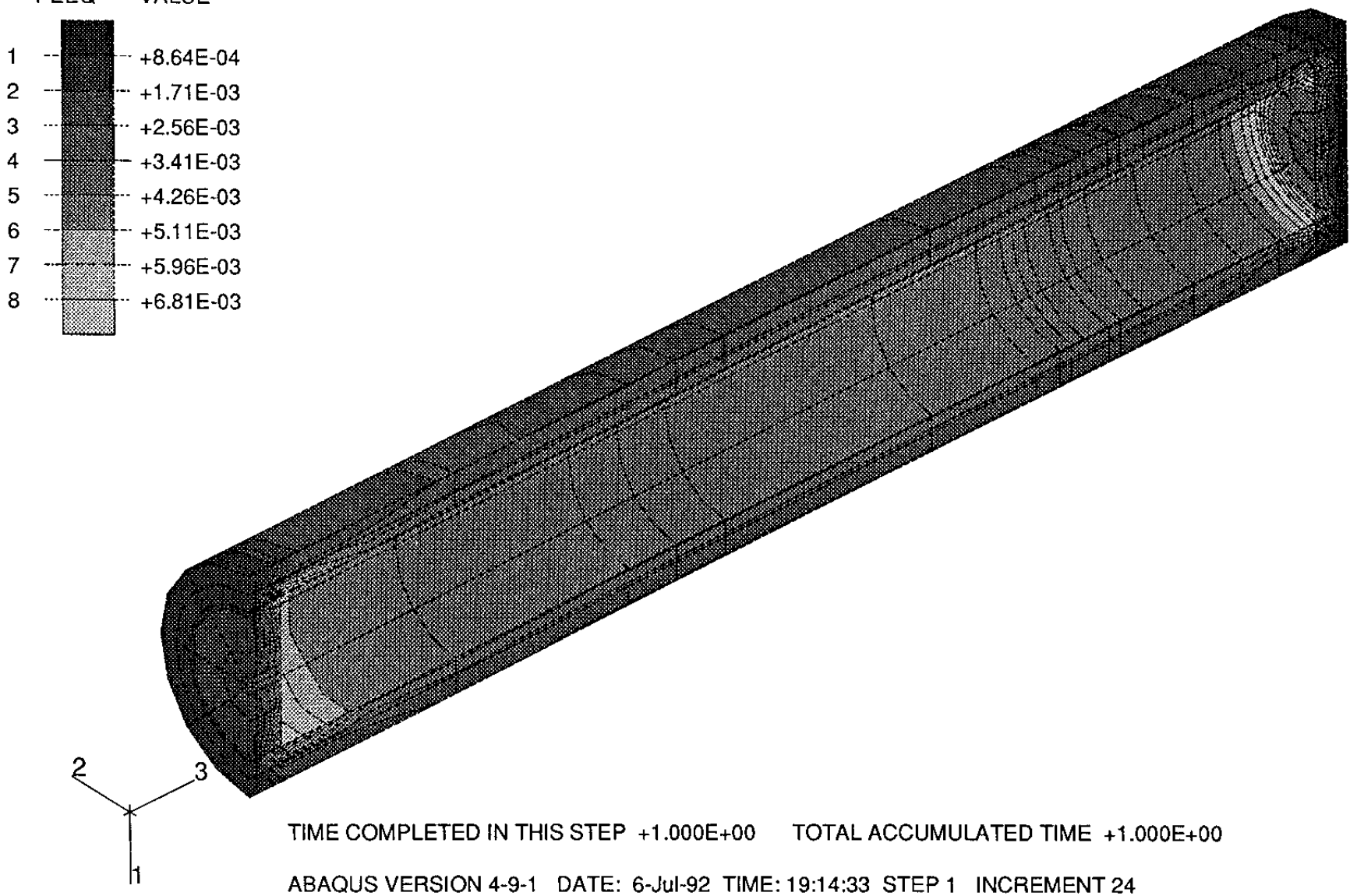

TIME COMPLETED IN THIS STEP +1.000E+00 TOTAL ACCUMULATED TIME +1.000E+00

ABAQUS VERSION 4-9-1 DATE: 6-Jul-92 TIME: 19:14:33 STEP 1 INCREMENT 24

ABAQUS

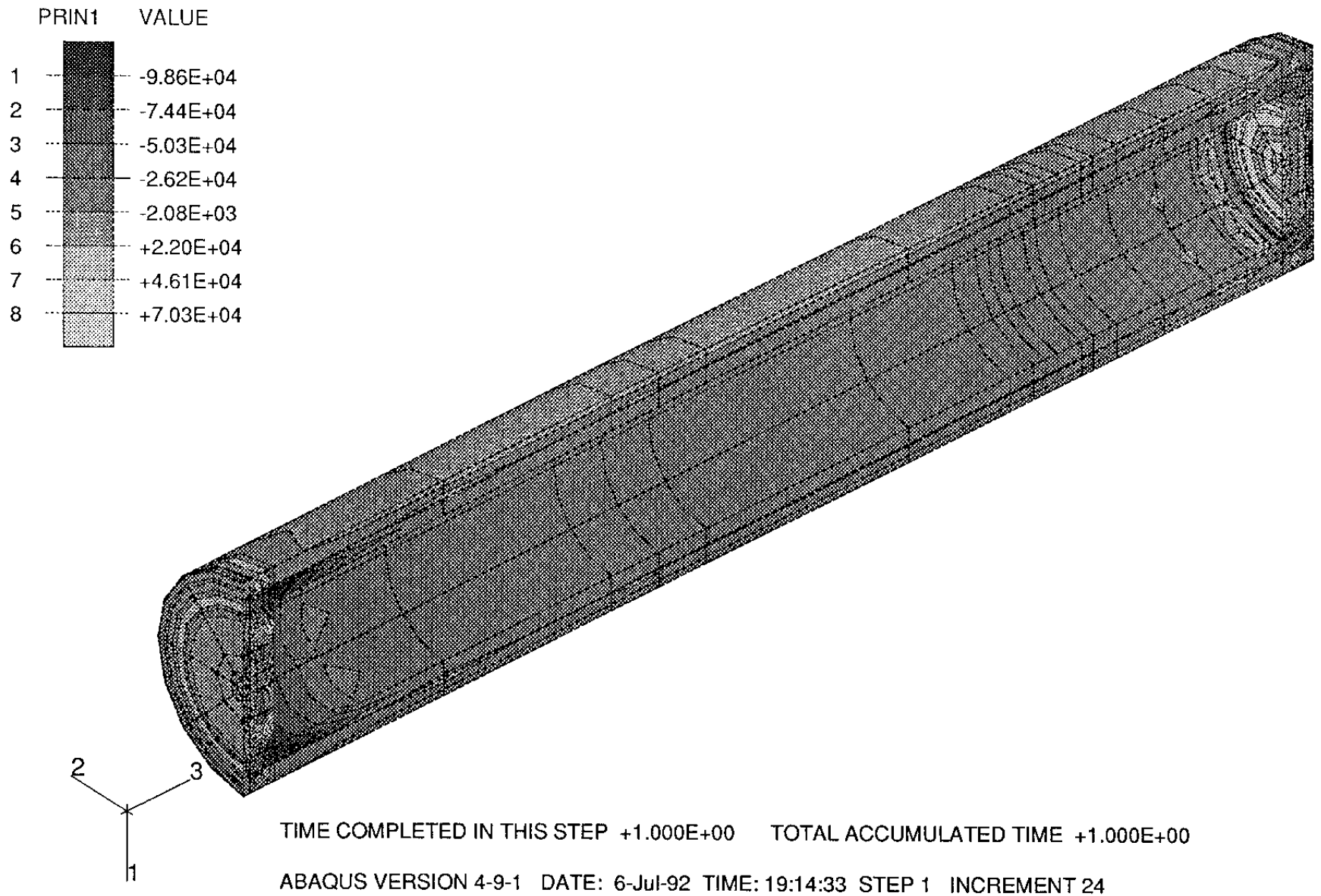

TIME COMPLETED IN THIS STEP +1.000E+00 TOTAL ACCUMULATED TIME +1.000E+00

ABAQUS VERSION 4-9-1 DATE: 6-Jul-92 TIME: 19:14:33 STEP 1 INCREMENT 24

ABAQUS

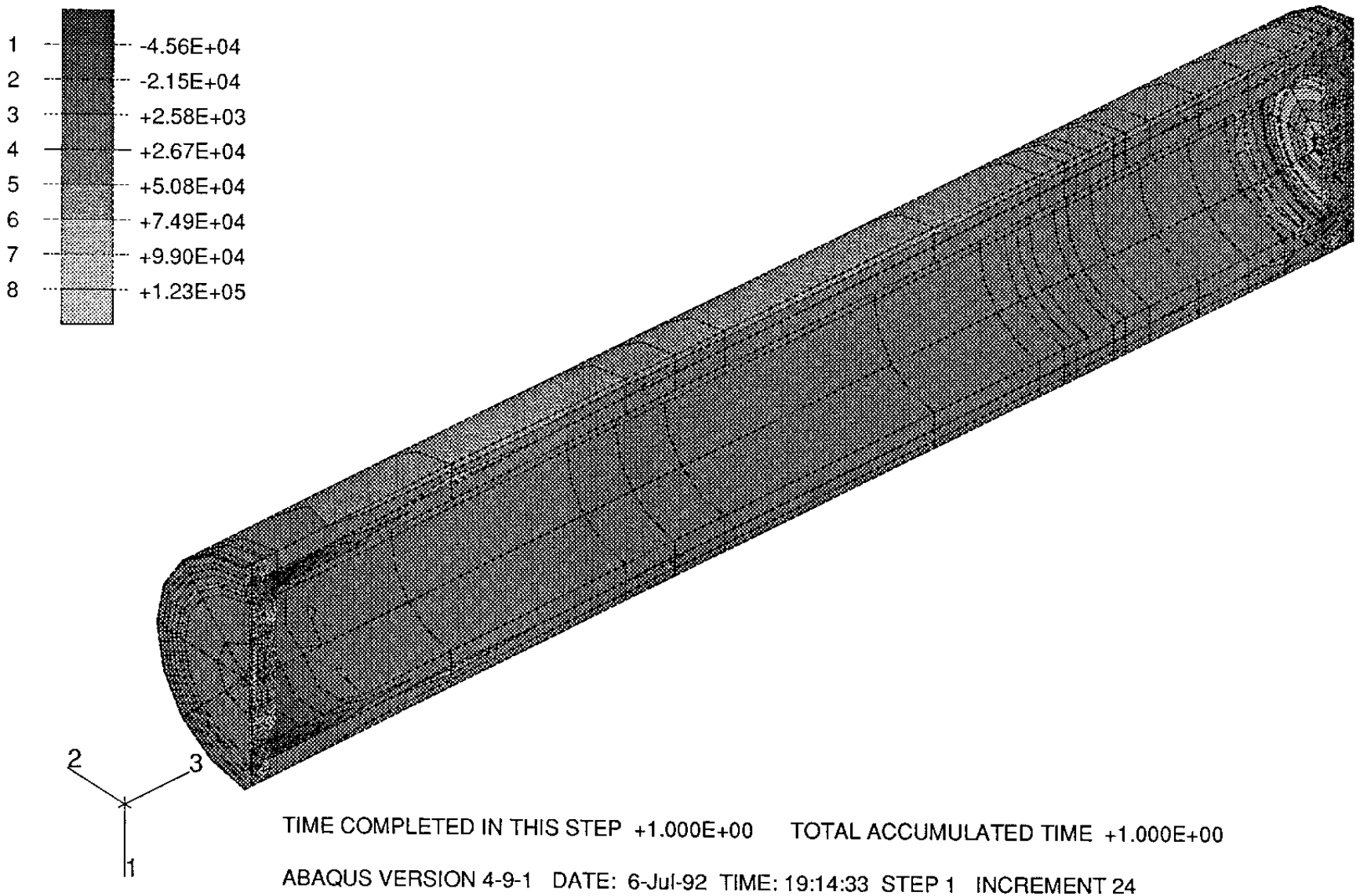

TIME COMPLETED IN THIS STEP +1.000E+00 TOTAL ACCUMULATED TIME +1.000E+00

ABAQUS VERSION 4-9-1 DATE: 6-Jul-92 TIME: 19:14:33 STEP 1 INCREMENT 24

ABAQUS

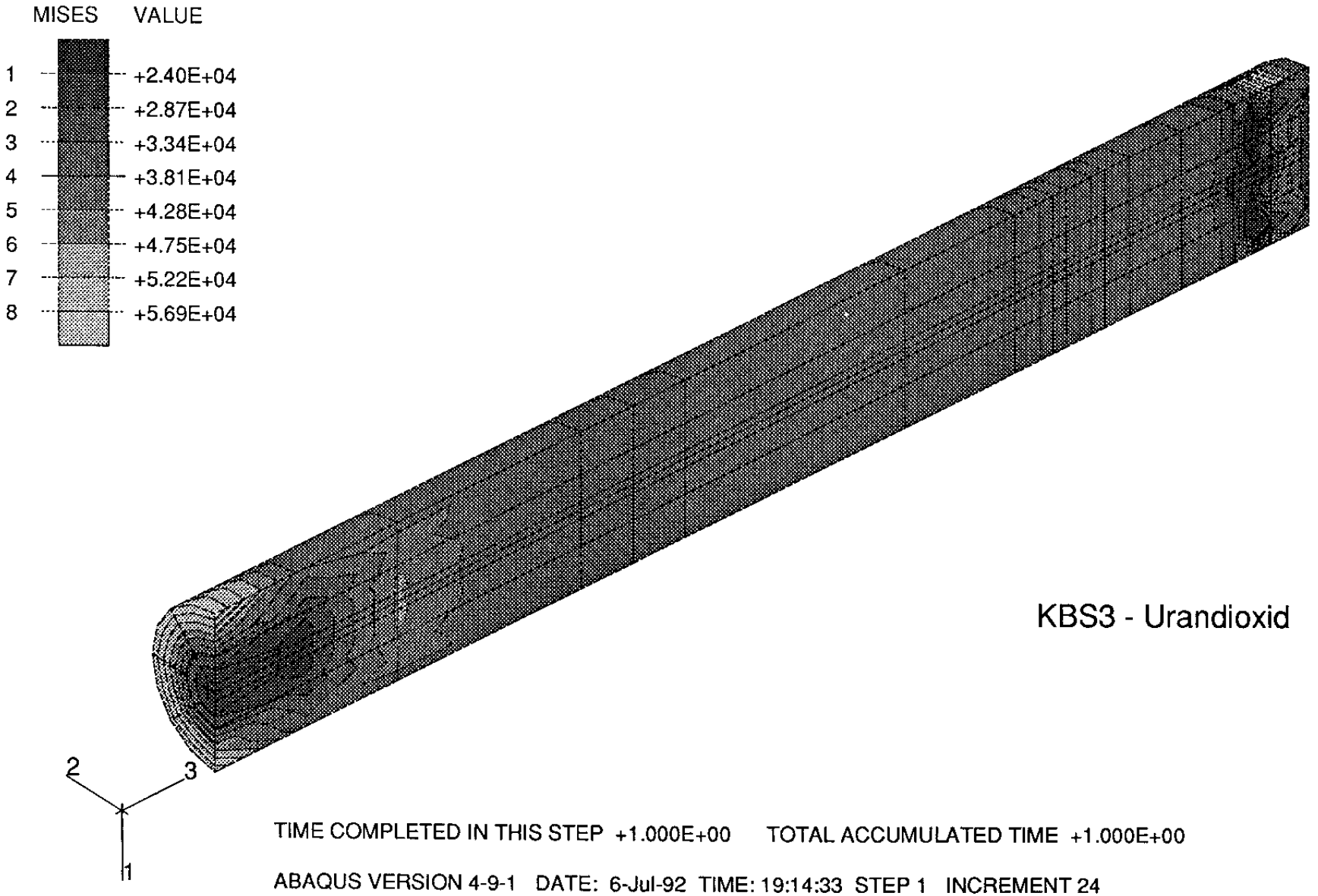

TIME COMPLETED IN THIS STEP +1.000E+00 TOTAL ACCUMULATED TIME +1.000E+00

ABAQUS VERSION 4-9-1 DATE: 6-Jul-92 TIME: 19:14:33 STEP 1 INCREMENT 24

ABAQUS

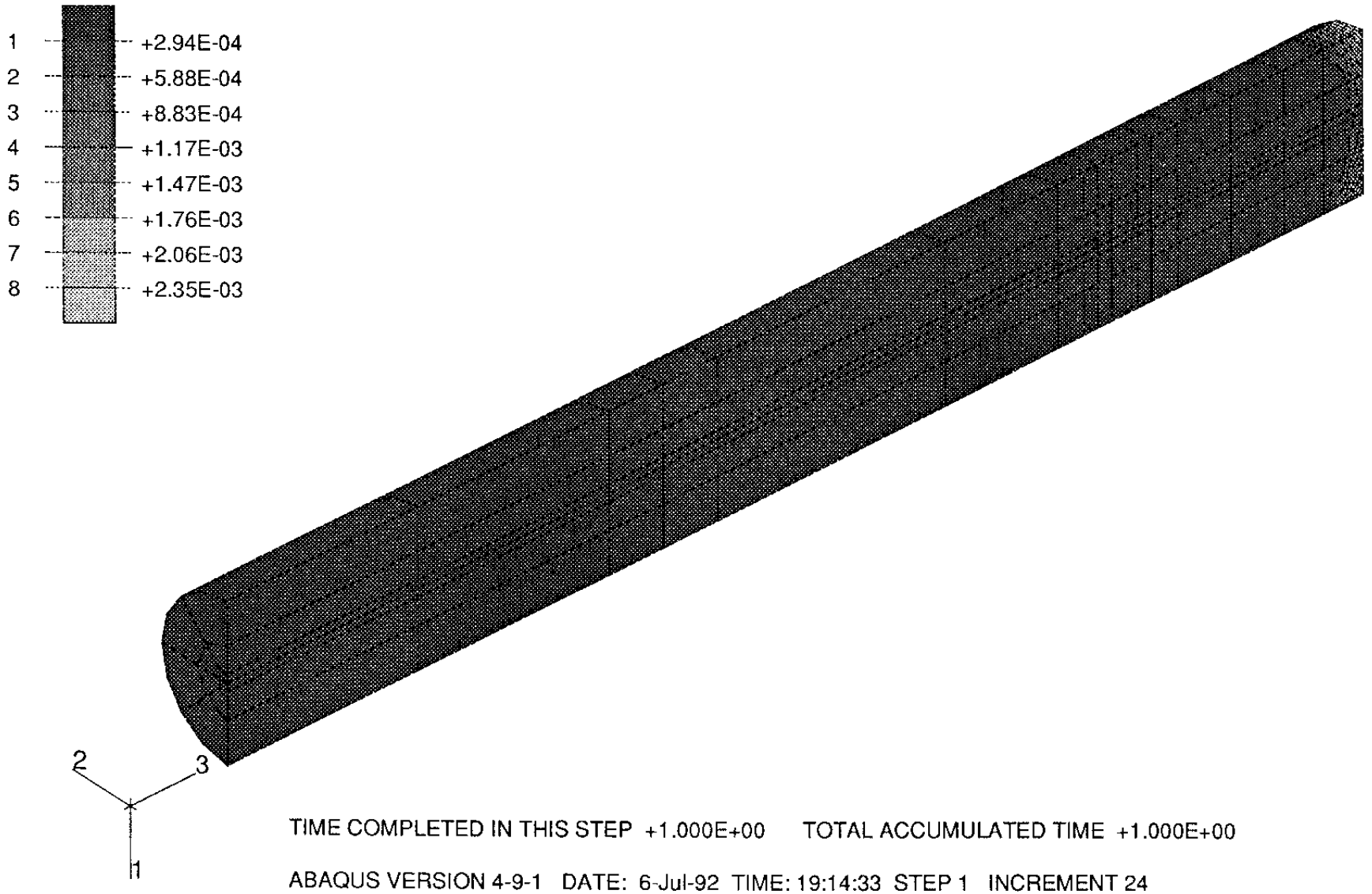

TIME COMPLETED IN THIS STEP +1.000E+00 TOTAL ACCUMULATED TIME +1.000E+00

ABAQUS VERSION 4-9-1 DATE: 6-Jul-92 TIME: 19:14:33 STEP 1 INCREMENT 24

ABAQUS

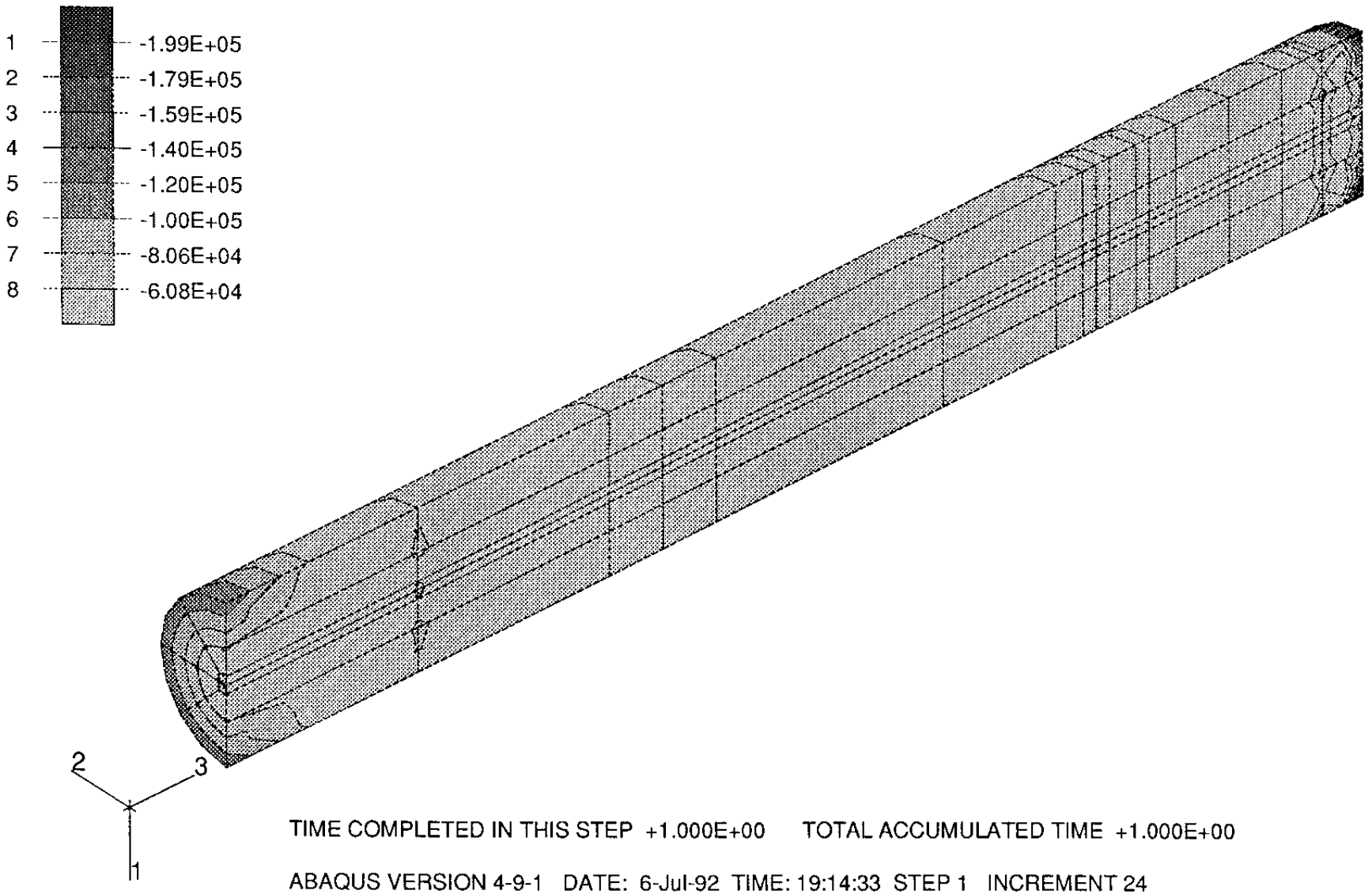

TIME COMPLETED IN THIS STEP +1.000E+00 TOTAL ACCUMULATED TIME +1.000E+00

ABAQUS VERSION 4-9-1 DATE: 6-Jul-92 TIME: 19:14:33 STEP 1 INCREMENT 24

ABAQUS

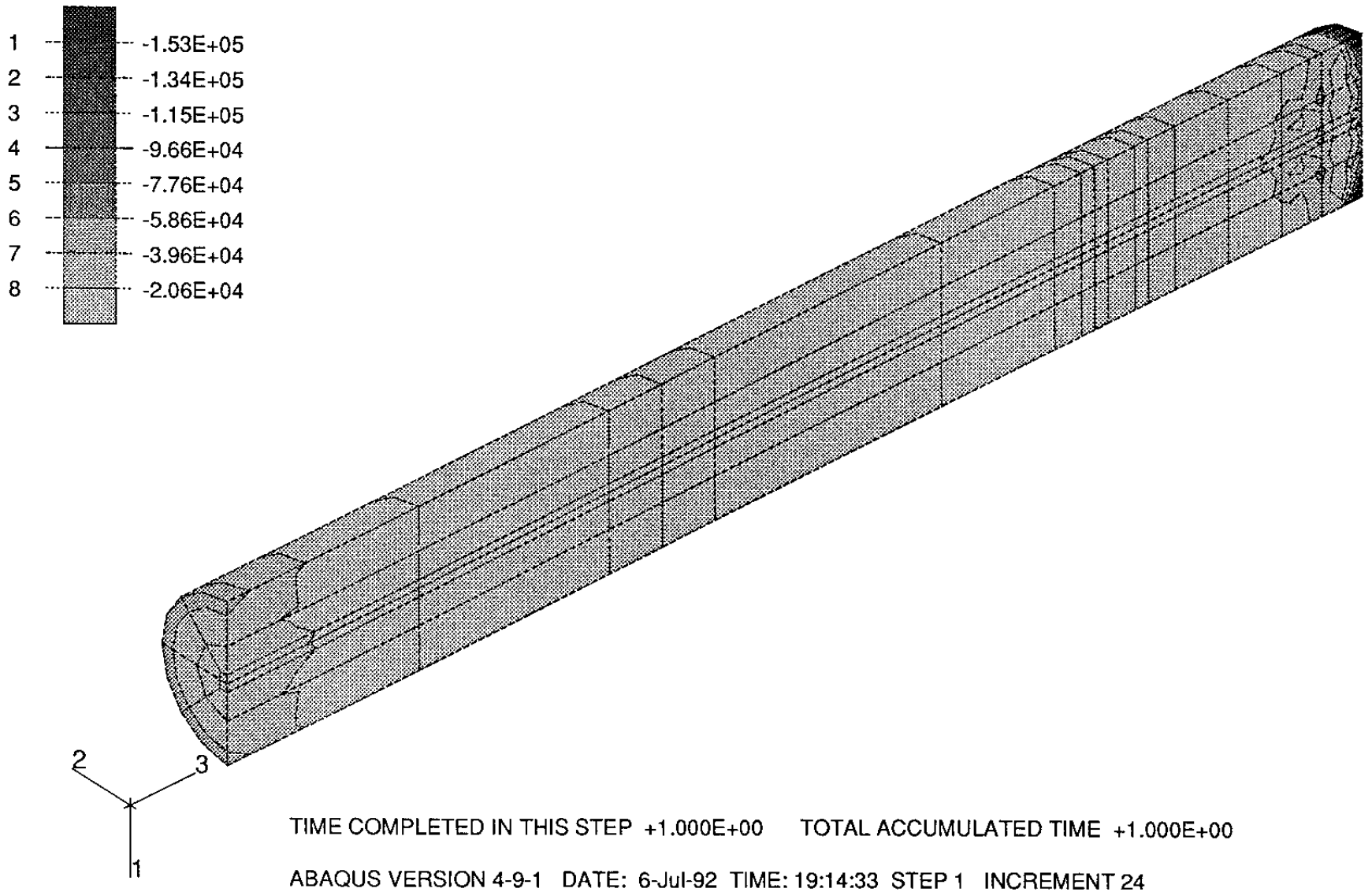

TIME COMPLETED IN THIS STEP +1.000E+00 TOTAL ACCUMULATED TIME +1.000E+00

ABAQUS VERSION 4-9-1 DATE: 6-Jul-92 TIME: 19:14:33 STEP 1 INCREMENT 24

APPENDIX Ib

Results from a rock shear calculation
KBS3 HIP canister with residual stresses

After 4 cm rock displacement

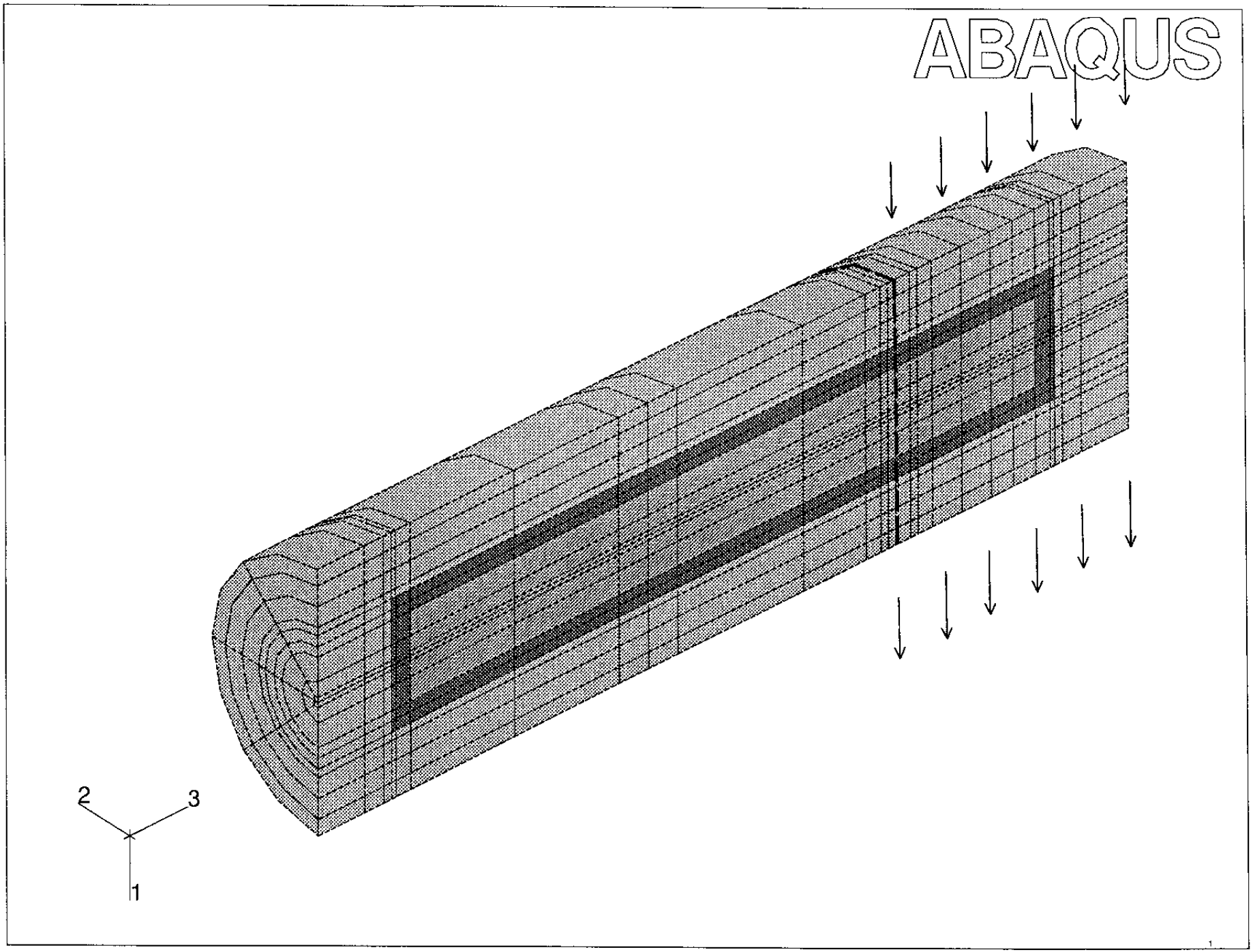
ABAQUS
2
3
1

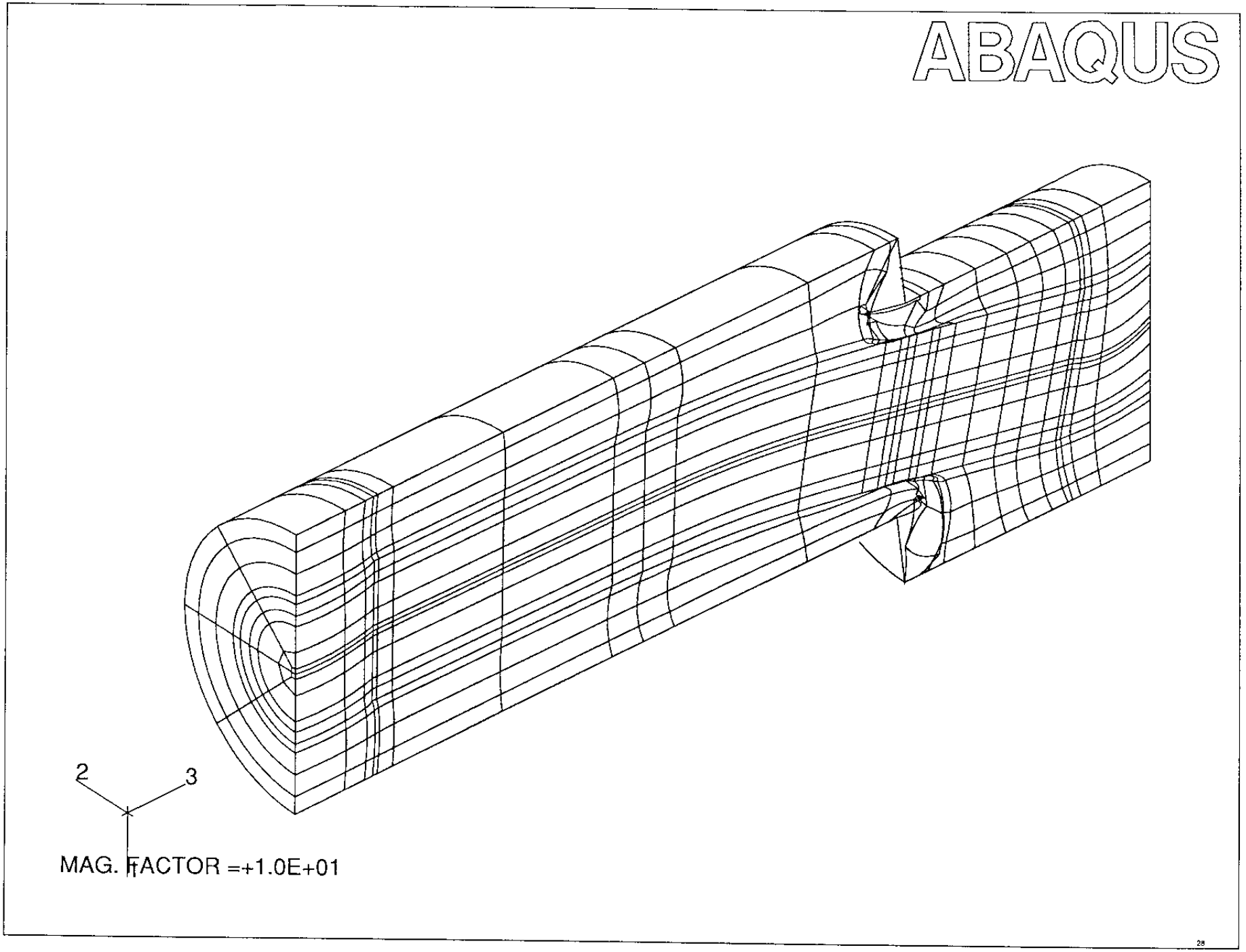
ABAQUS
2
3
MAG. FACTOR =+1.0E+01

ABAQUS

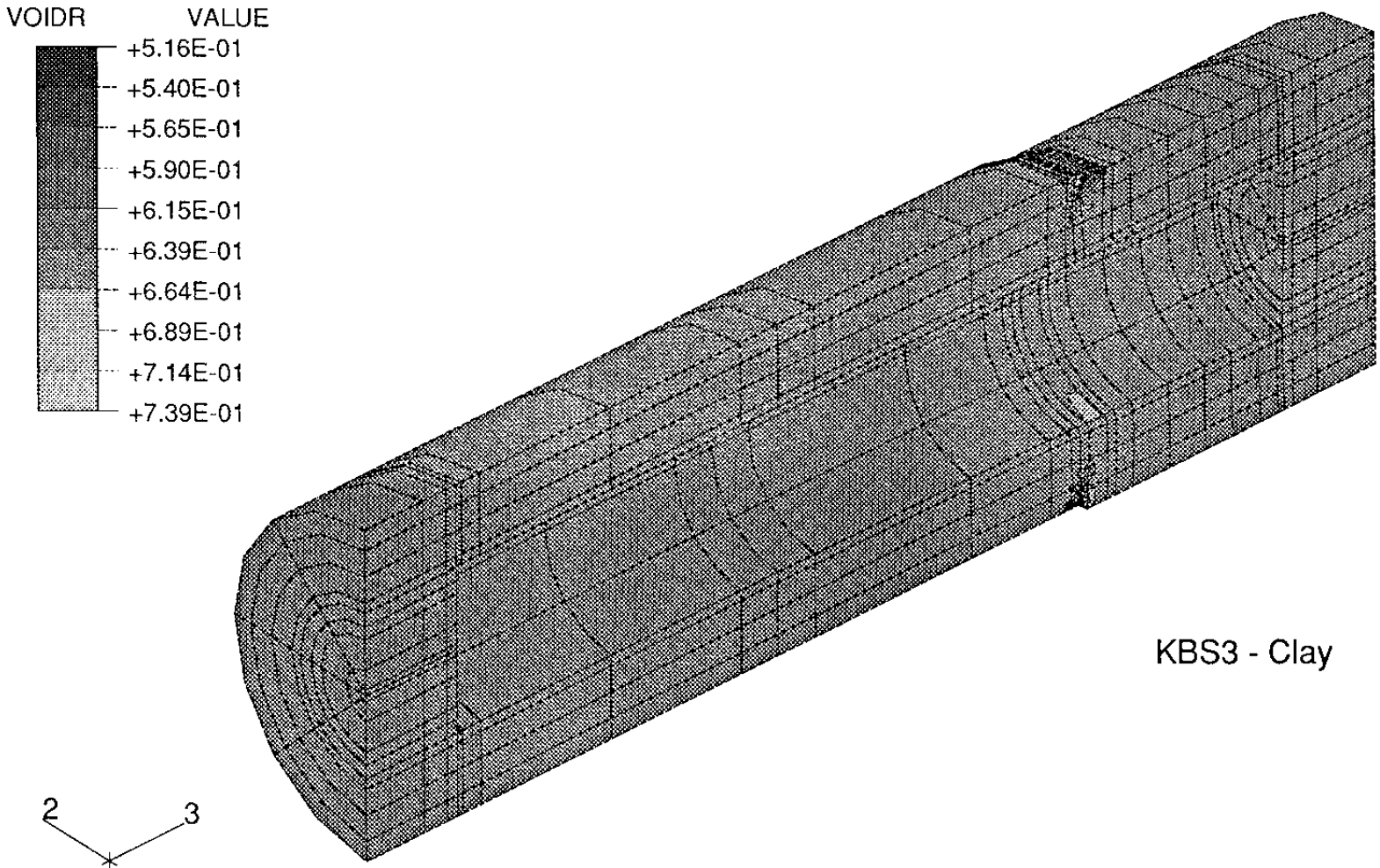

TIME COMPLETED IN THIS STEP +1.018E+06 TOTAL ACCUMULATED TIME +2.018E+06

ABAQUS VERSION 5.0-88 DATE: 24-Jun-92 TIME: 07:17:49 STEP 4 INCREMENT 30

ABAQUS

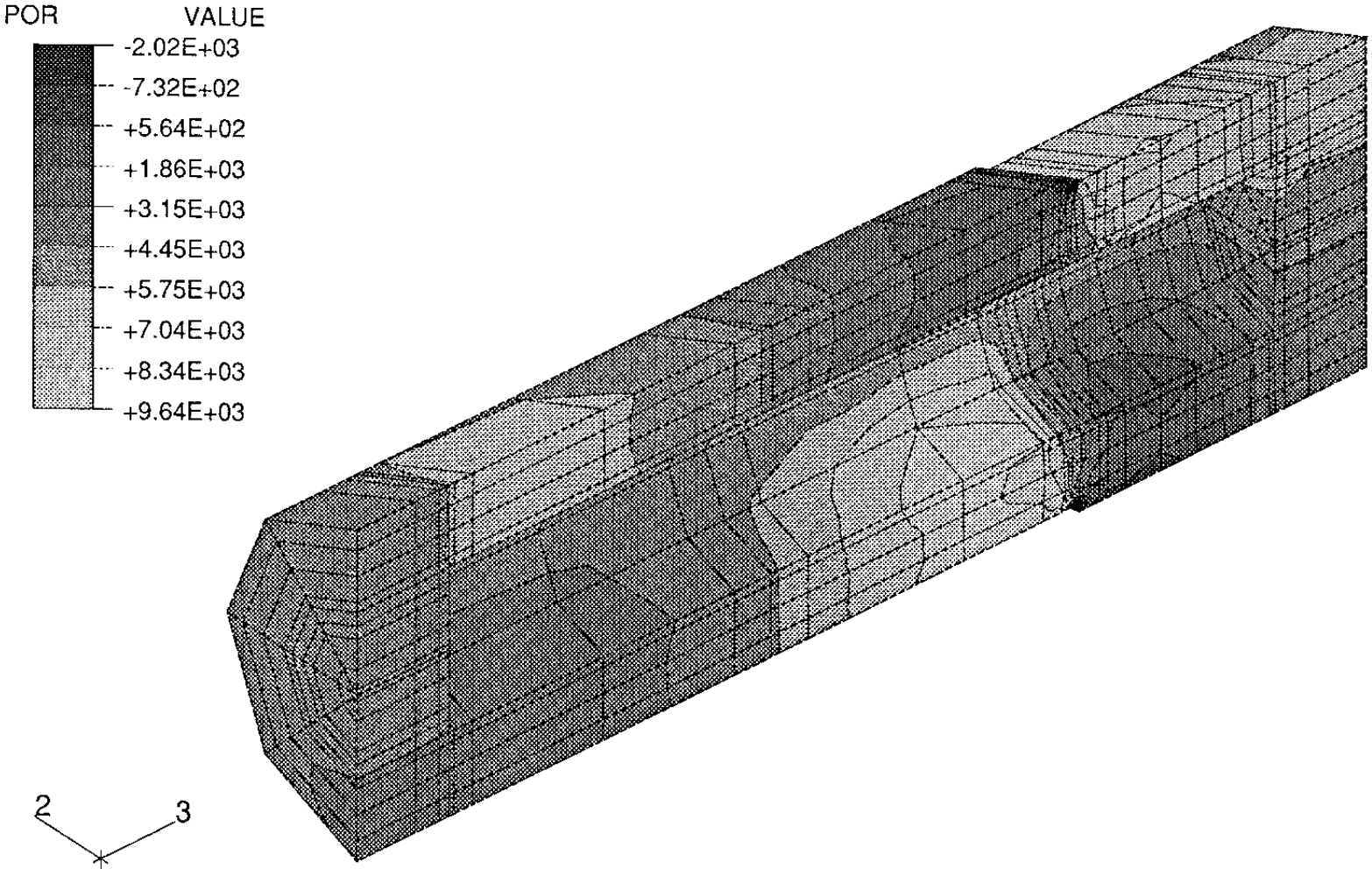

TIME COMPLETED IN THIS STEP +1.018E+06 TOTAL ACCUMULATED TIME +2.018E+06

ABAQUS VERSION 5.0-88 DATE: 24-Jun-92 TIME: 07:17:49 STEP 4 INCREMENT 30

ABAQUS

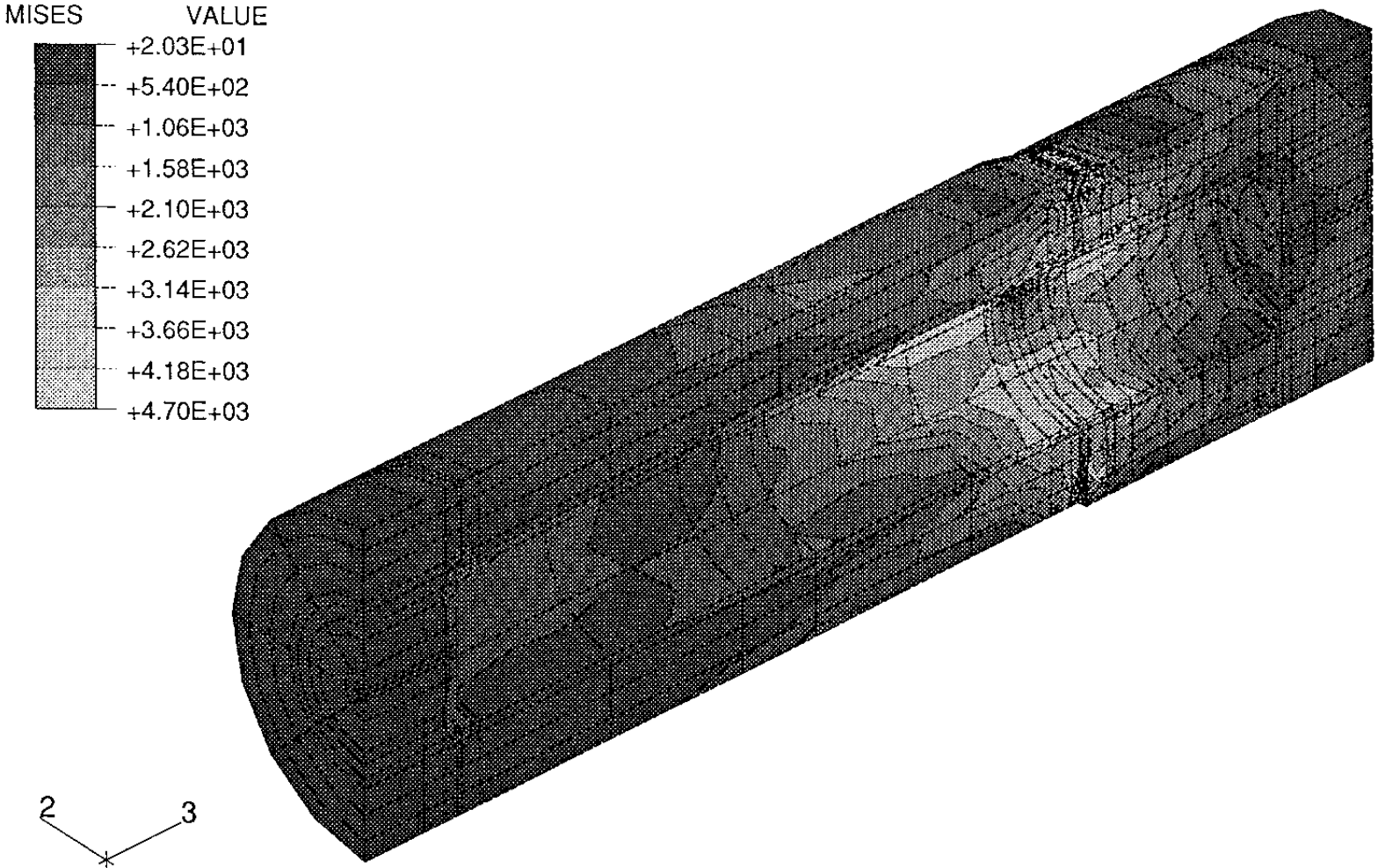

TIME COMPLETED IN THIS STEP +1.018E+06 TOTAL ACCUMULATED TIME +2.018E+06

ABAQUS VERSION 5.0-88 DATE: 24-Jun-92 TIME: 07:17:49 STEP 4 INCREMENT 30

ABAQUS

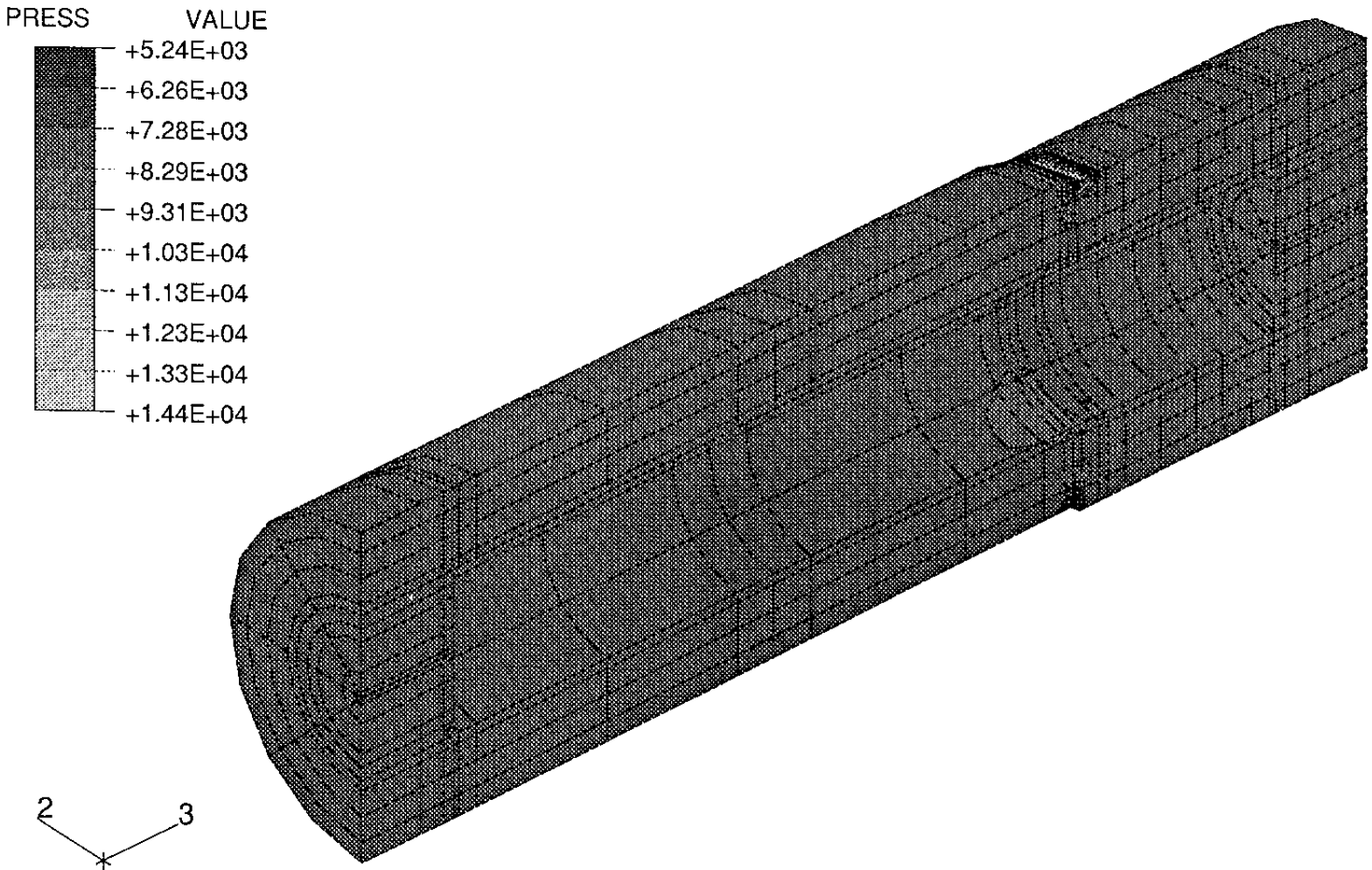

TIME COMPLETED IN THIS STEP +1.018E+06 TOTAL ACCUMULATED TIME +2.018E+06

ABAQUS VERSION 5.0-88 DATE: 24-Jun-92 TIME: 07:17:49 STEP 4 INCREMENT 30

ABAQUS

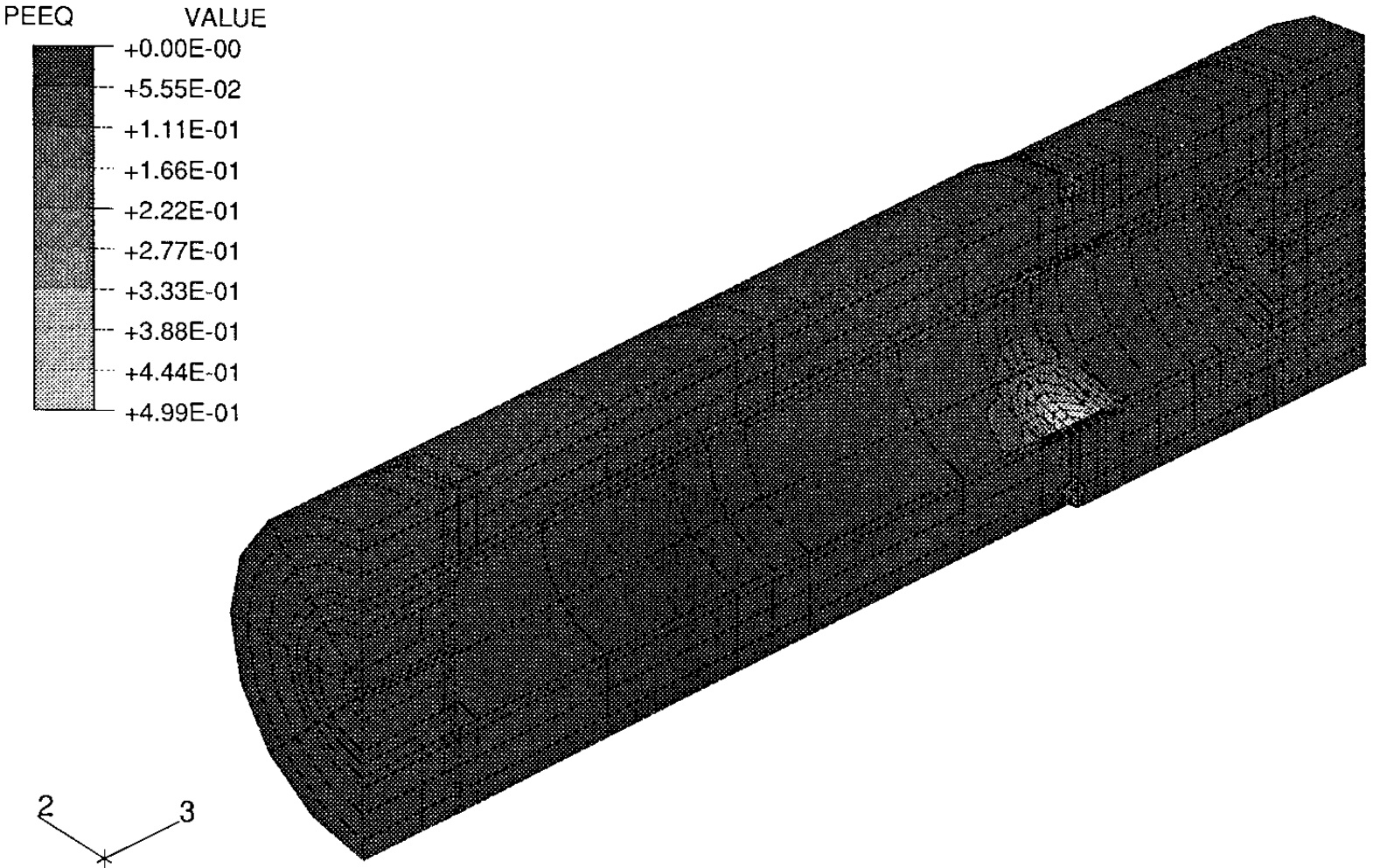

TIME COMPLETED IN THIS STEP +1.018E+06 TOTAL ACCUMULATED TIME +2.018E+06

ABAQUS VERSION 5.0-88 DATE: 24-Jun-92 TIME: 07:17:49 STEP 4 INCREMENT 30

ABAQUS

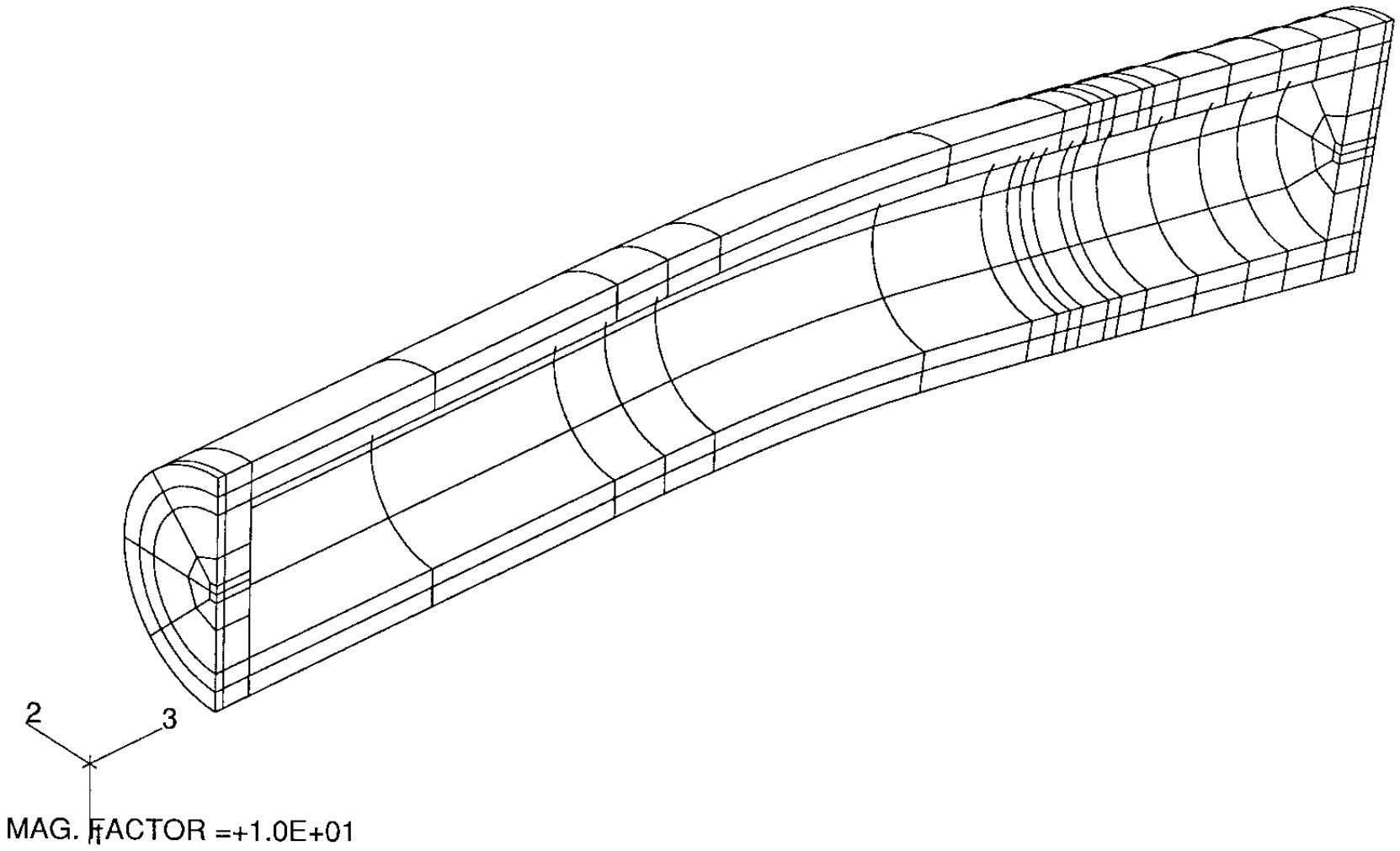

ABAQUS

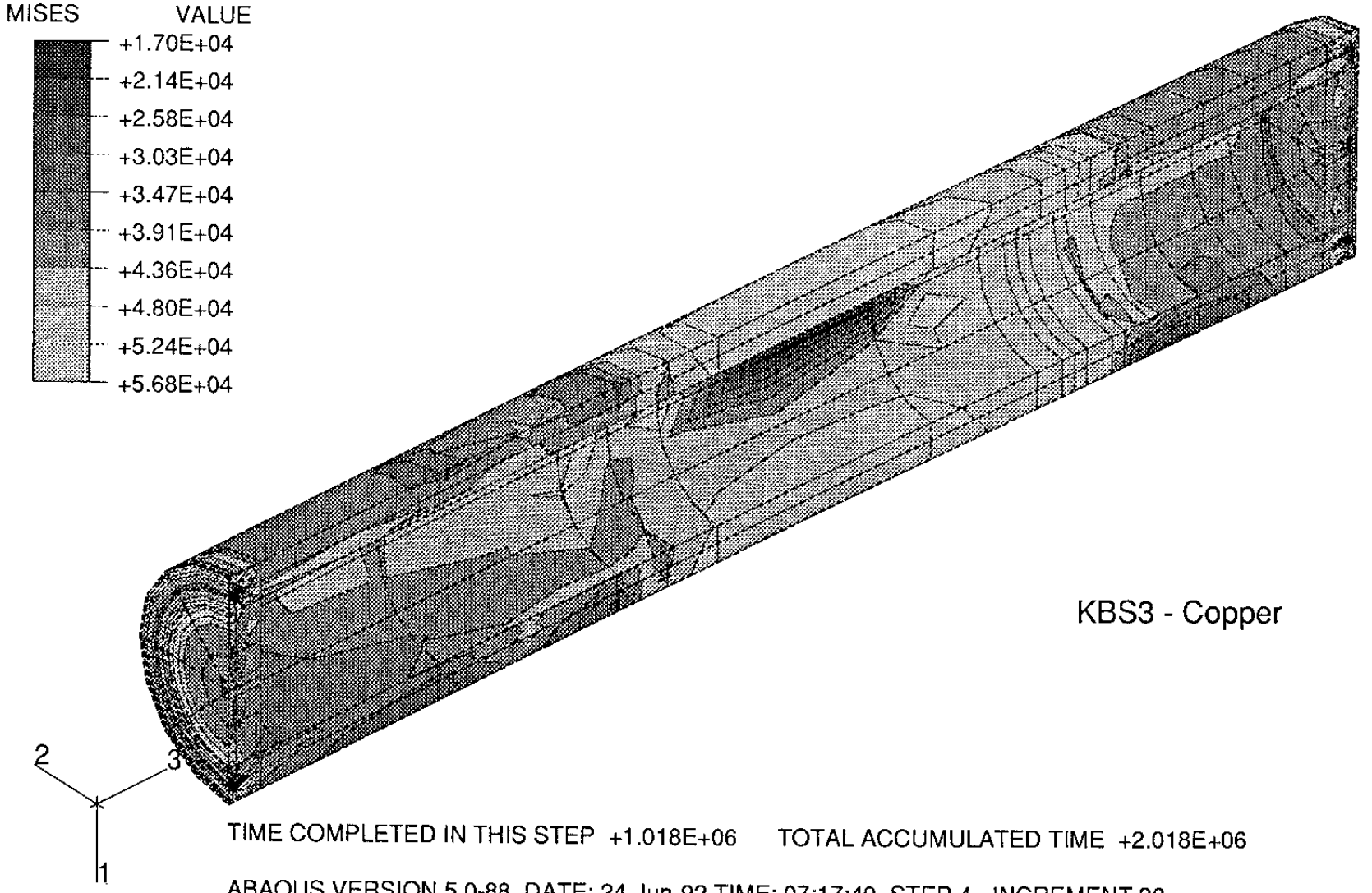

TIME COMPLETED IN THIS STEP +1.018E+06 TOTAL ACCUMULATED TIME +2.018E+06

ABAQUS VERSION 5.0-88 DATE: 24-Jun-92 TIME: 07:17:49 STEP 4 INCREMENT 30

ABAQUS

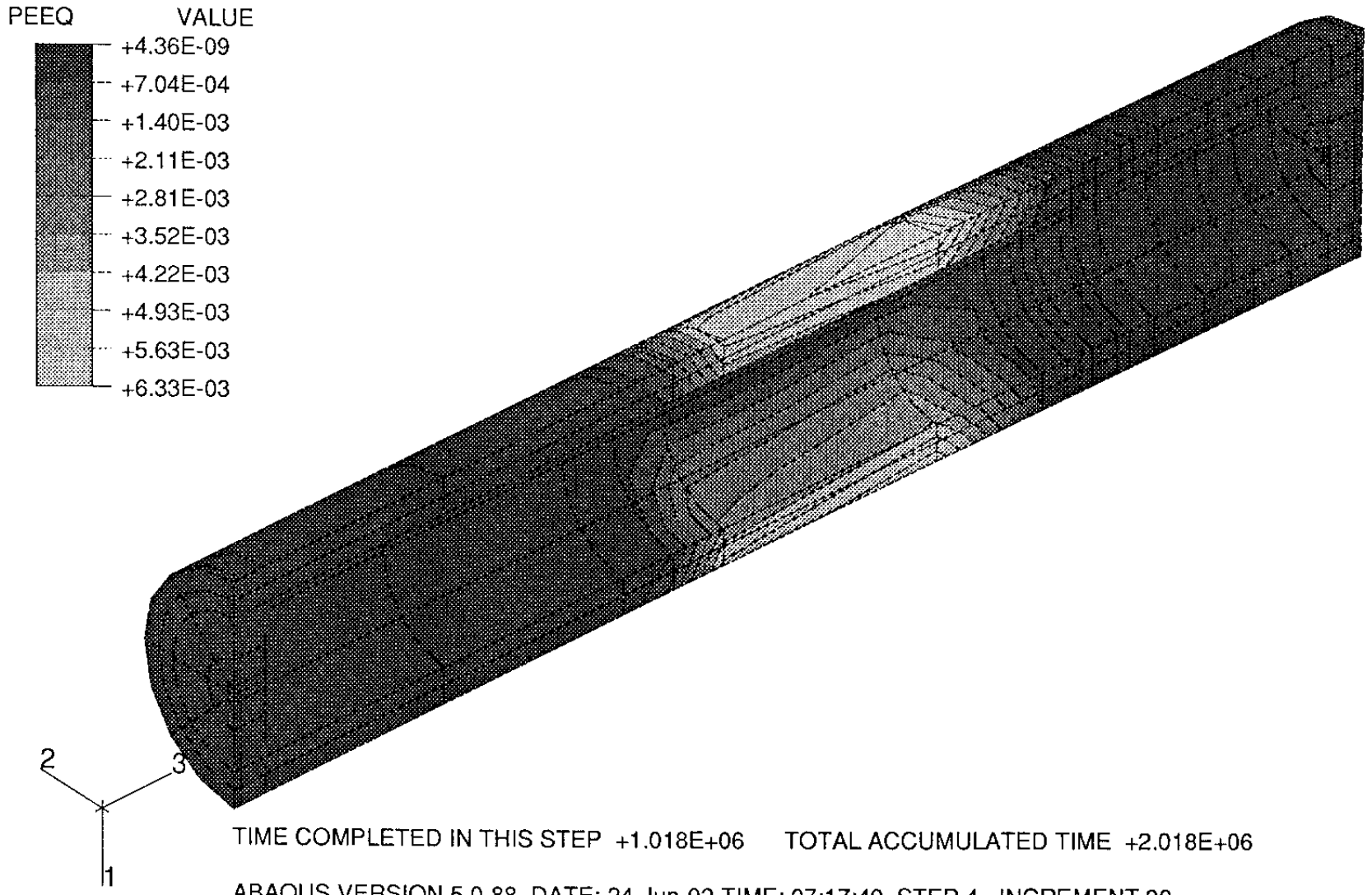

TIME COMPLETED IN THIS STEP +1.018E+06 TOTAL ACCUMULATED TIME +2.018E+06

ABAQUS VERSION 5.0-88 DATE: 24-Jun-92 TIME: 07:17:49 STEP 4 INCREMENT 30

ABAQUS

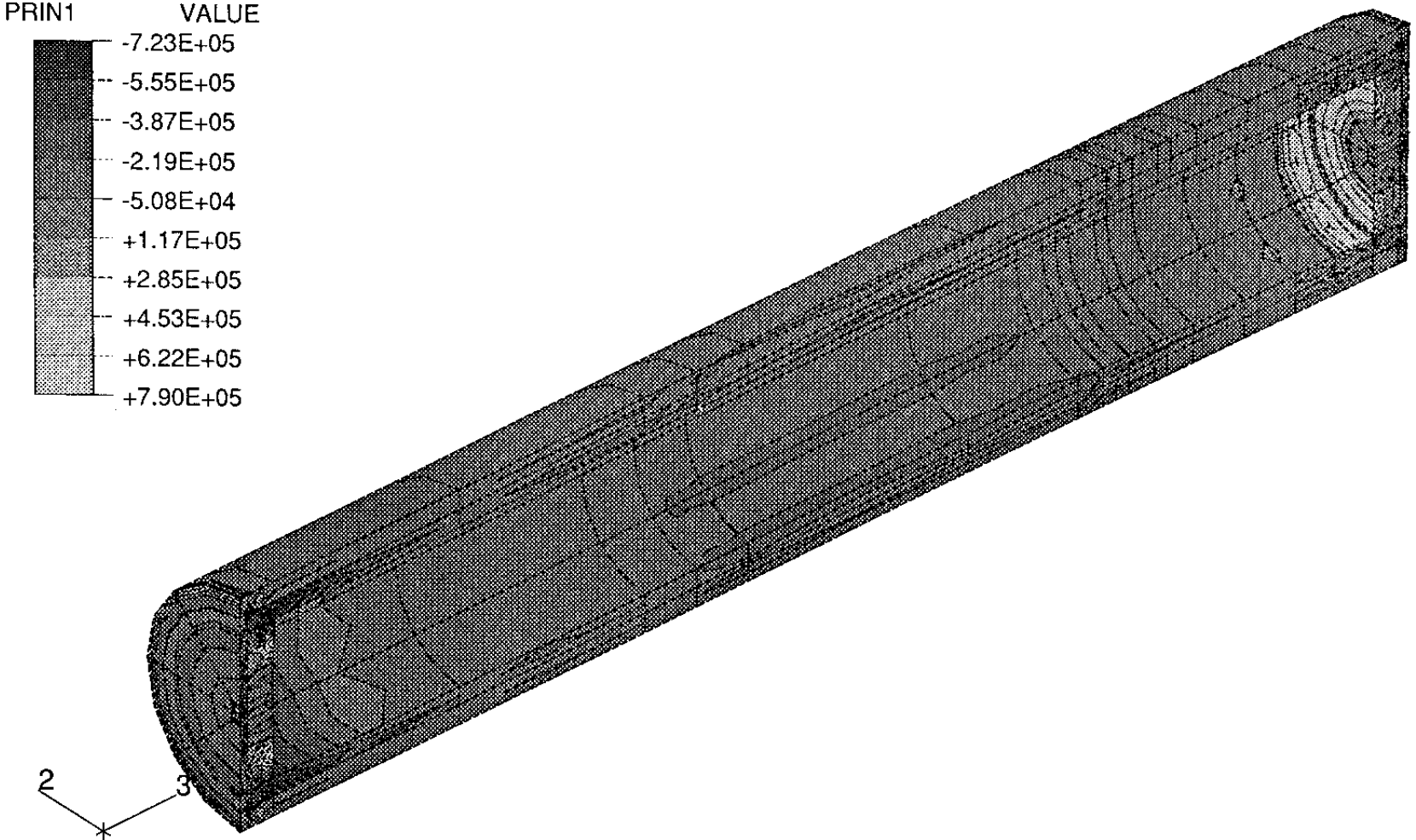

TIME COMPLETED IN THIS STEP +1.018E+06 TOTAL ACCUMULATED TIME +2.018E+06

ABAQUS VERSION 5.0-88 DATE: 24-Jun-92 TIME: 07:17:49 STEP 4 INCREMENT 30

ABAQUS

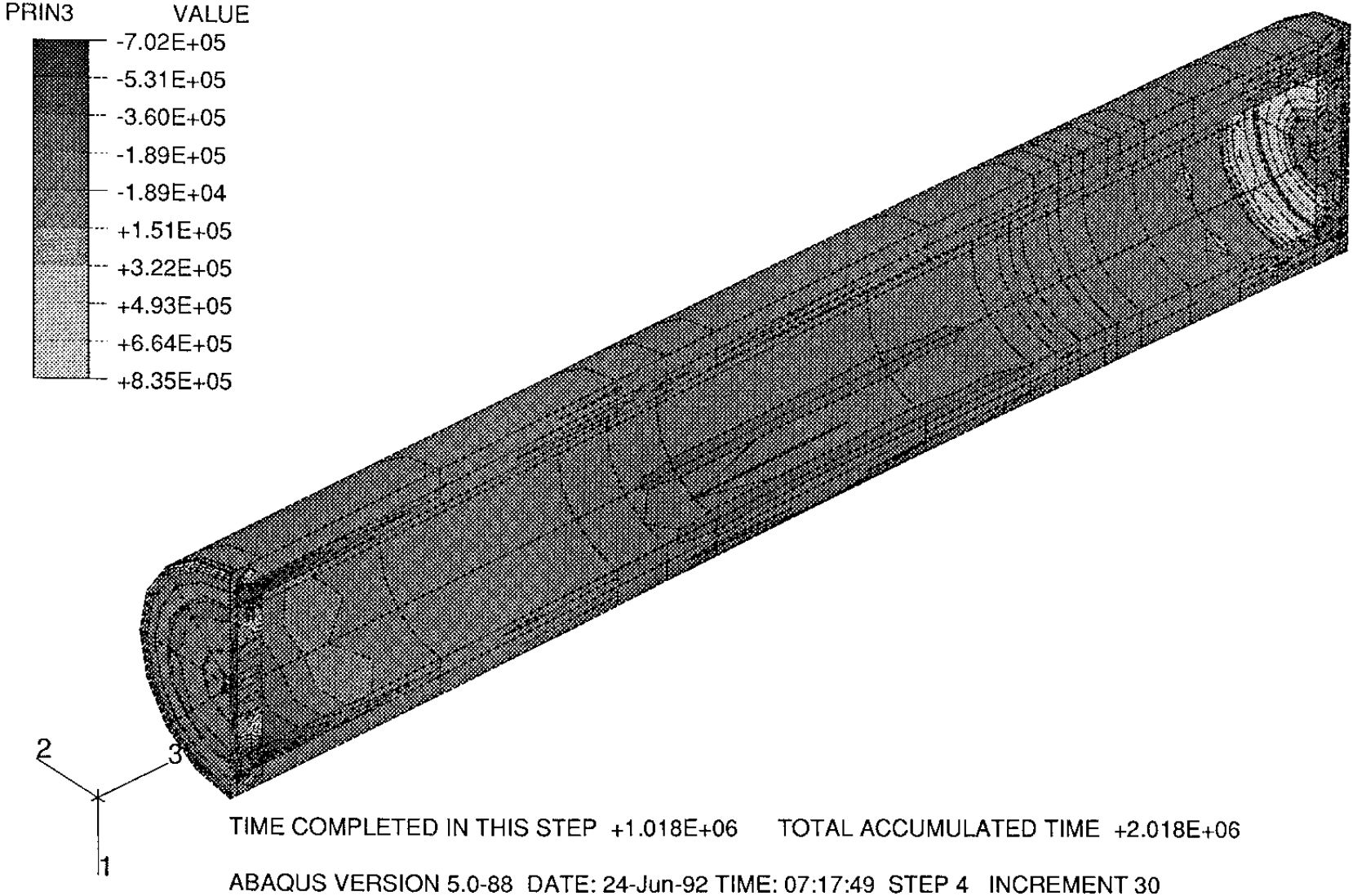

TIME COMPLETED IN THIS STEP +1.018E+06 TOTAL ACCUMULATED TIME +2.018E+06

ABAQUS VERSION 5.0-88 DATE: 24-Jun-92 TIME: 07:17:49 STEP 4 INCREMENT 30

ABAQUS

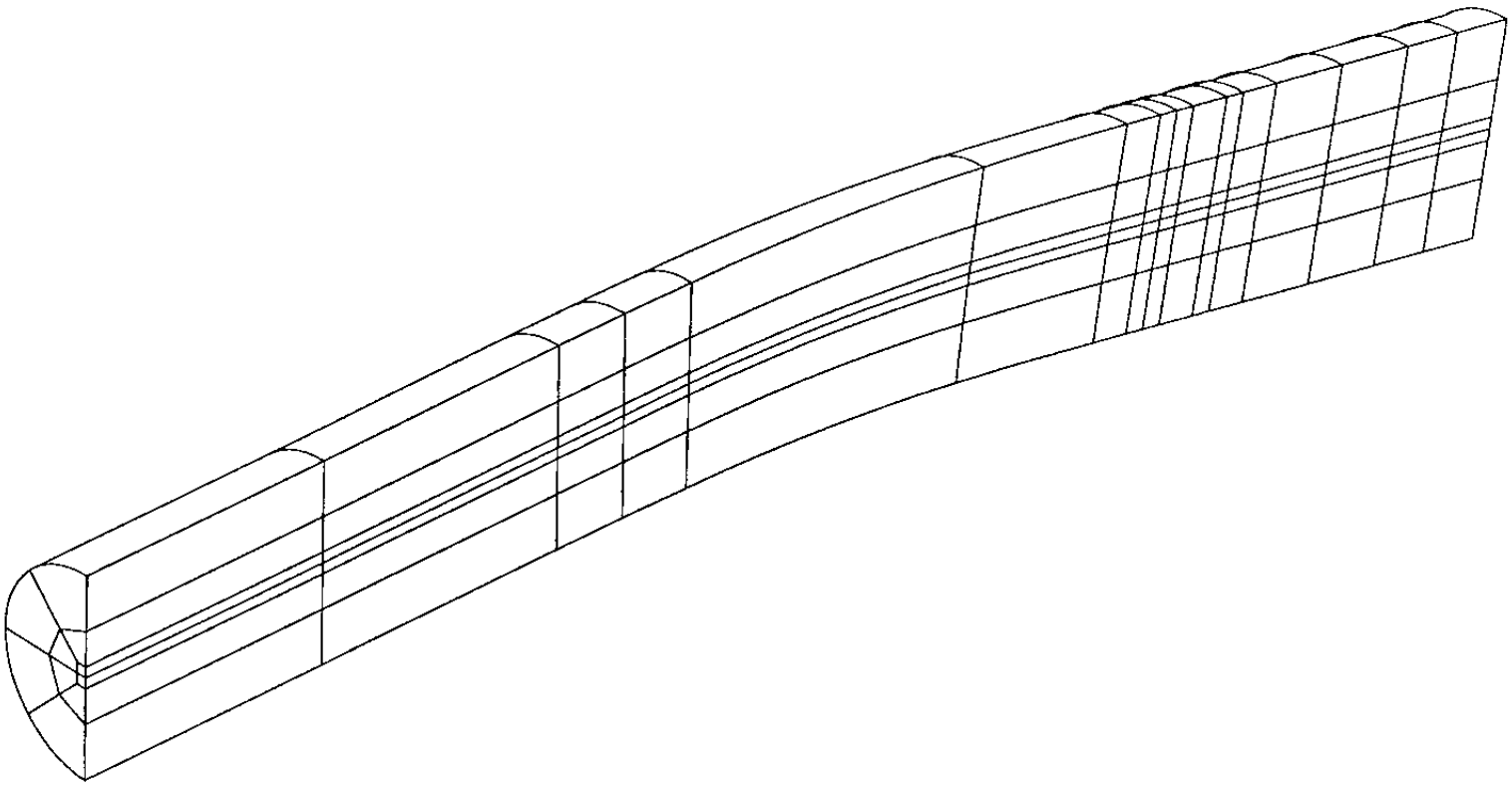

ABAQUS

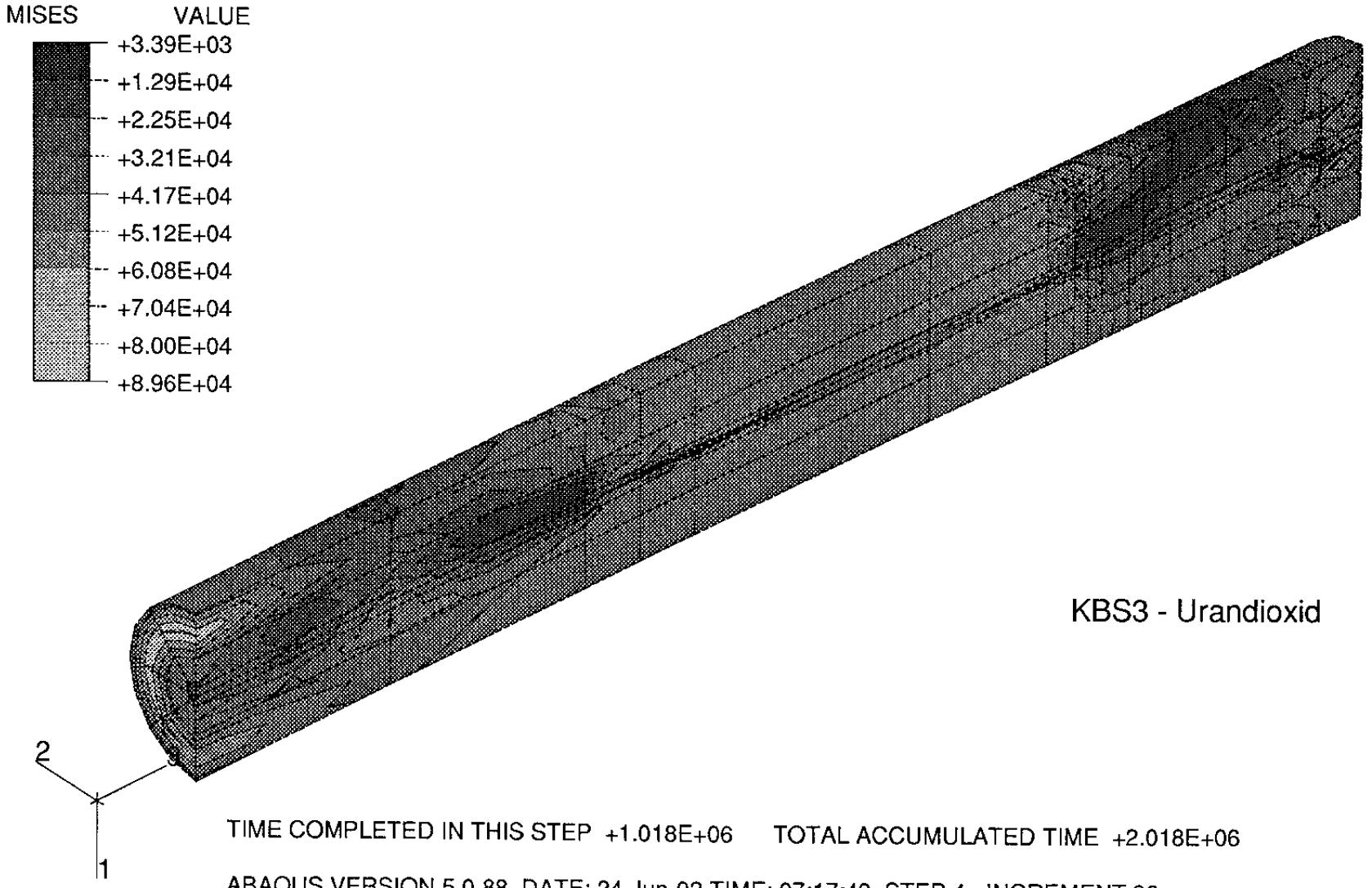

KBS3 - Urandioxid

TIME COMPLETED IN THIS STEP +1.018E+06 TOTAL ACCUMULATED TIME +2.018E+06

ABAQUS VERSION 5.0-88 DATE: 24-Jun-92 TIME: 07:17:49 STEP 4 INCREMENT 30

ABAQUS

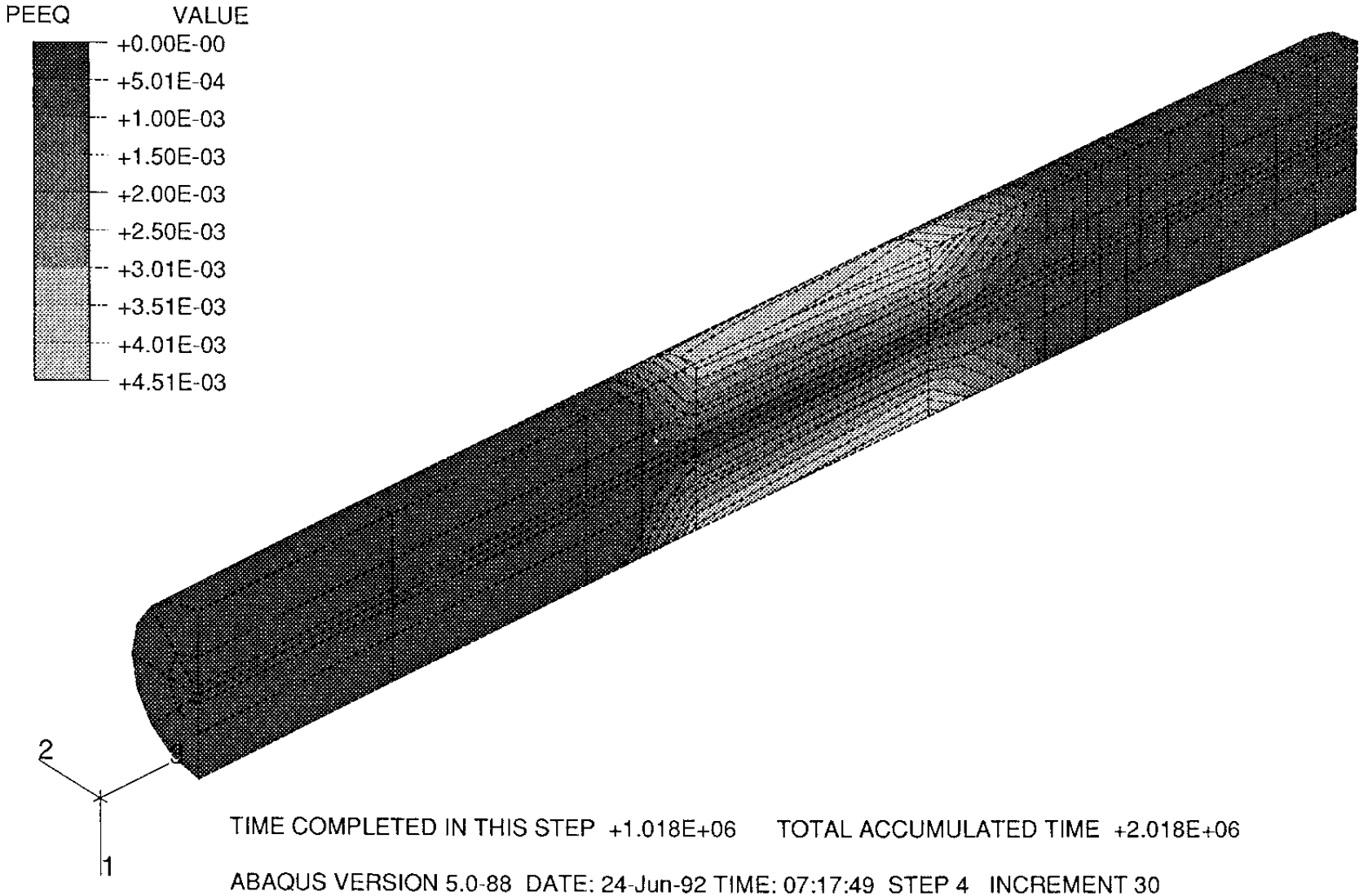

TIME COMPLETED IN THIS STEP +1.018E+06 TOTAL ACCUMULATED TIME +2.018E+06

ABAQUS VERSION 5.0-88 DATE: 24-Jun-92 TIME: 07:17:49 STEP 4 INCREMENT 30

APPENDIX II

Results from a swelling pressure calculation
KBS3 copper/steel canister

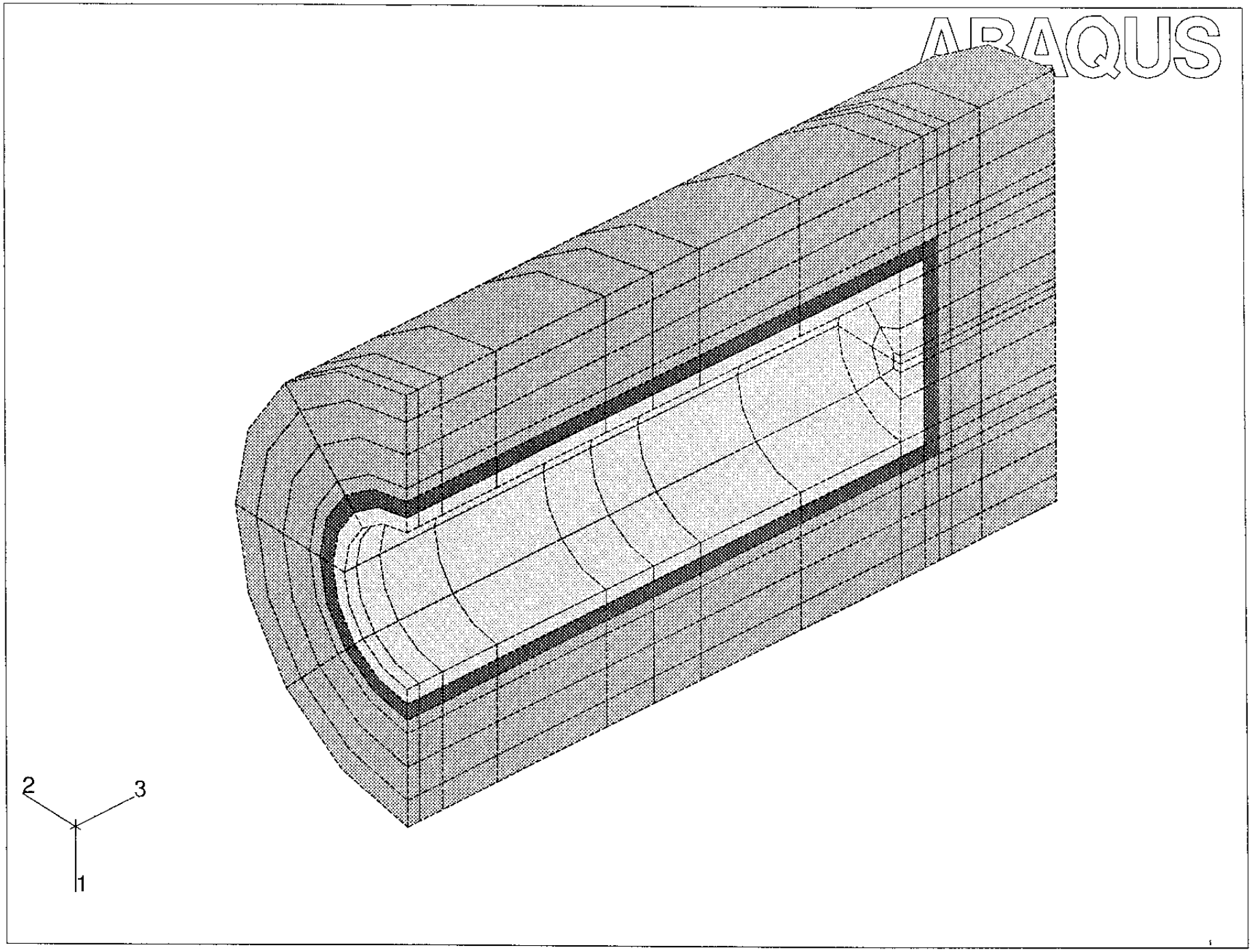
ABAQUS
2
3
1

ABAQUS

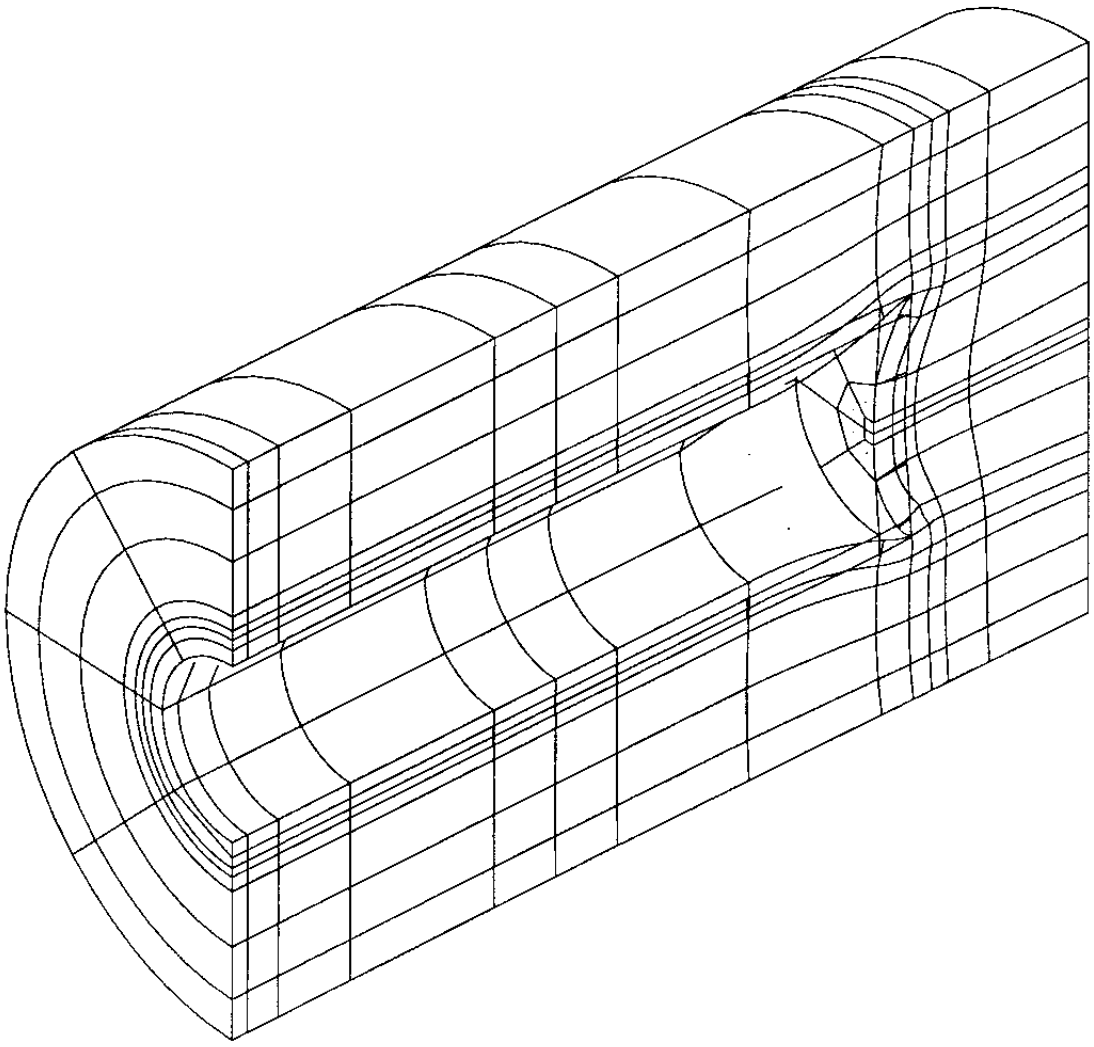

2
3
1

MAG. FACTOR =+1.0E+02

ABAQUS

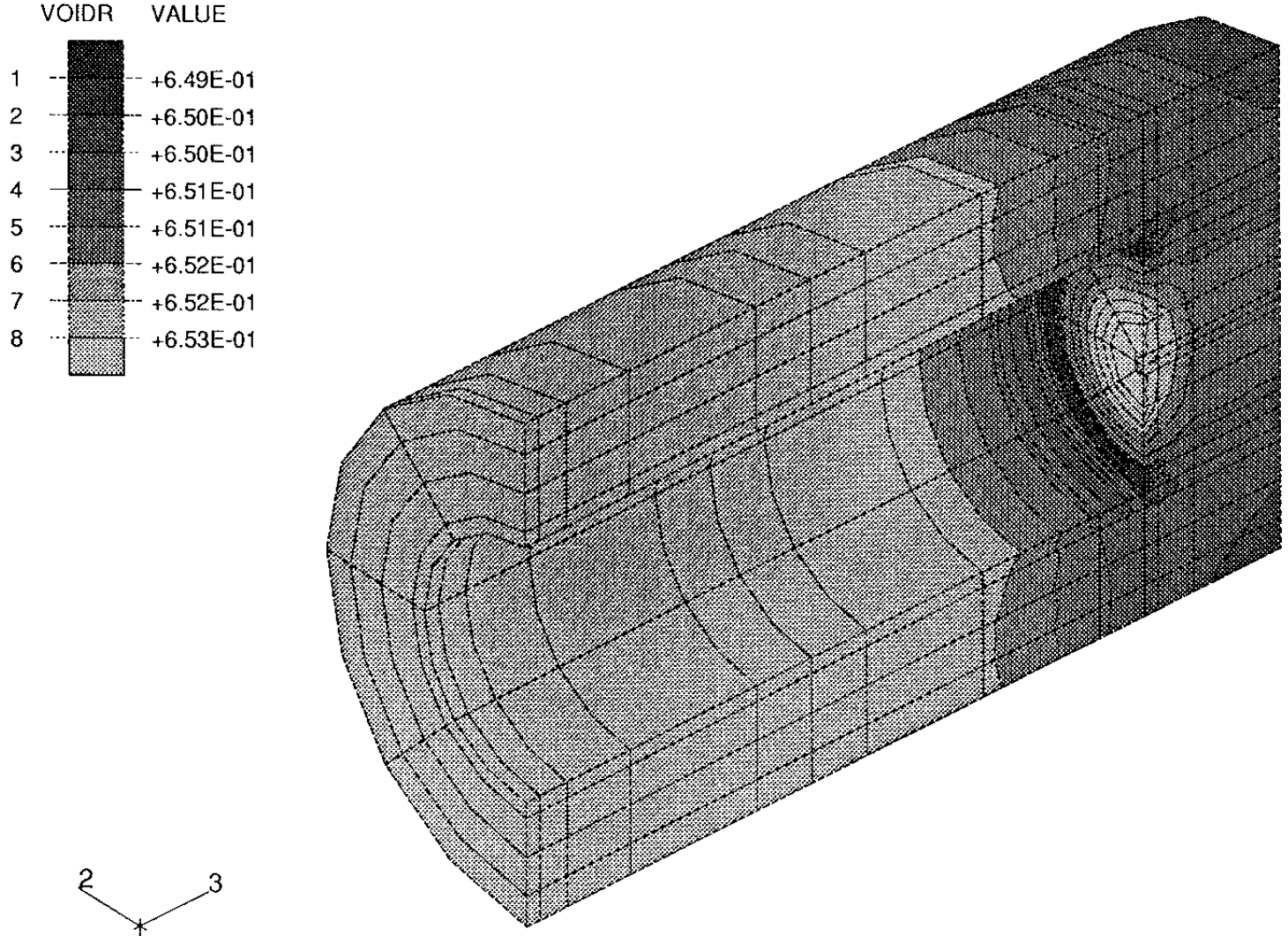

VLH - Clay

TIME COMPLETED IN THIS STEP +1.000E-03 TOTAL ACCUMULATED TIME +1.002E+00

ABAQUS VERSION 4-9-1 DATE: 18-Nov-91 TIME: 21:40:56 STEP 4 INCREMENT 1

ABAQUS

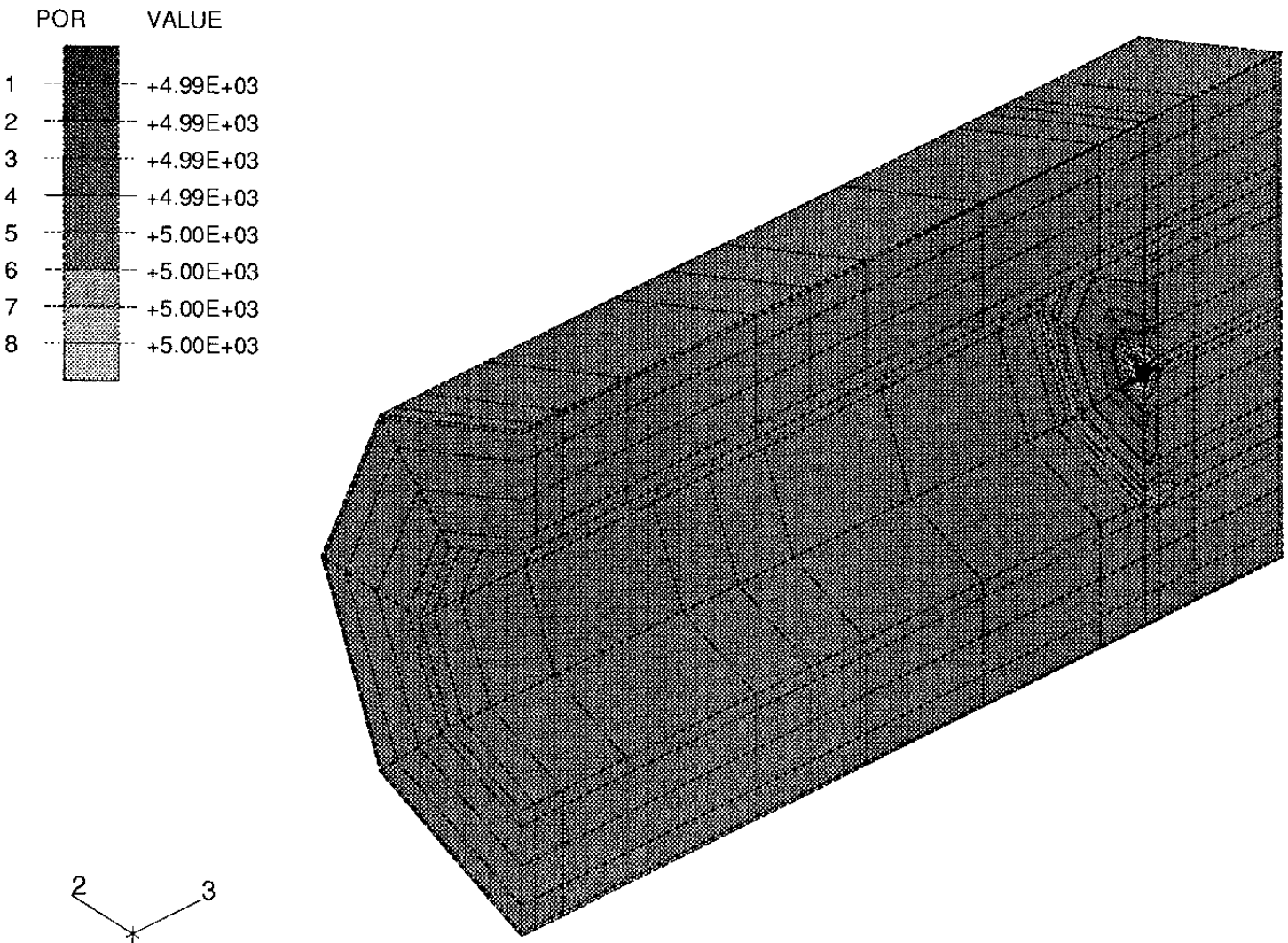

TIME COMPLETED IN THIS STEP +1.000E-03 TOTAL ACCUMULATED TIME +1.002E+00

ABAQUS VERSION 4-9-1 DATE: 18-Nov-91 TIME: 21:40:56 STEP 4 INCREMENT 1

ABAQUS

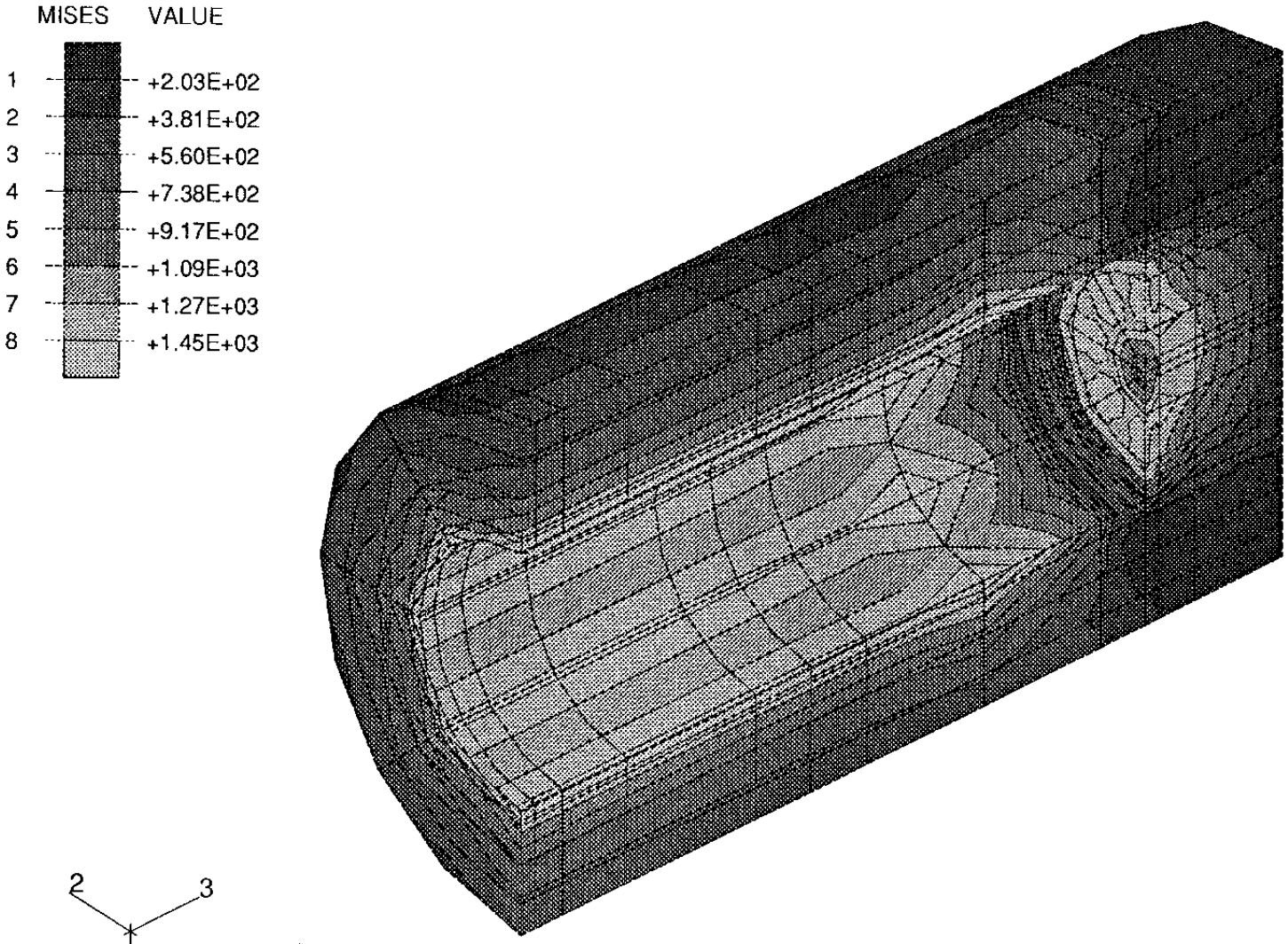

TIME COMPLETED IN THIS STEP +1.000E-03 TOTAL ACCUMULATED TIME +1.002E+00

ABAQUS VERSION 4-9-1 DATE: 18-Nov-91 TIME: 21:40:56 STEP 4 INCREMENT 1

ABAQUS

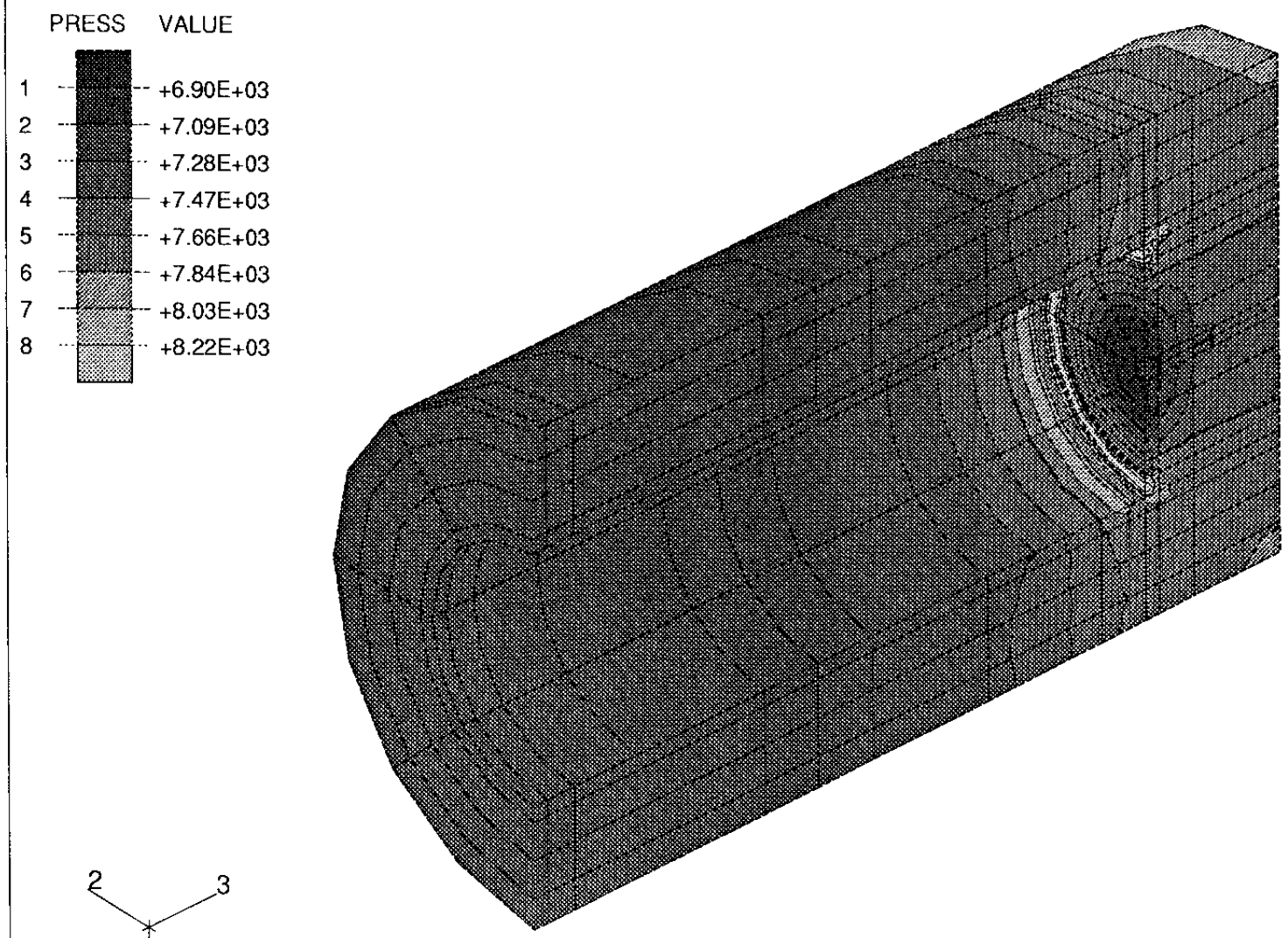

TIME COMPLETED IN THIS STEP +1.000E-03 TOTAL ACCUMULATED TIME +1.002E+00

ABAQUS VERSION 4-9-1 DATE: 18-Nov-91 TIME: 21:40:56 STEP 4 INCREMENT 1

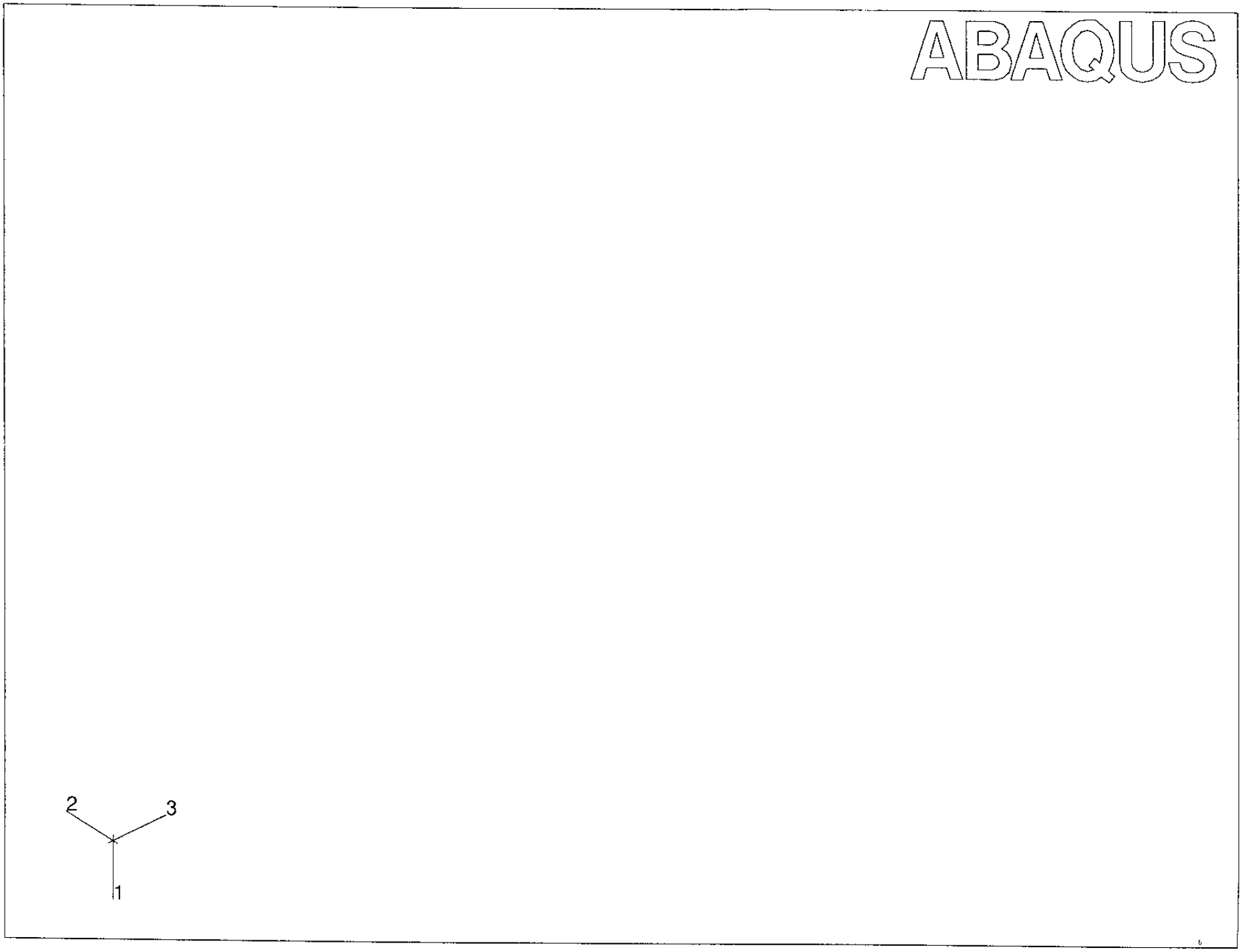
ABAQUS
2
3
1

ABAQUS

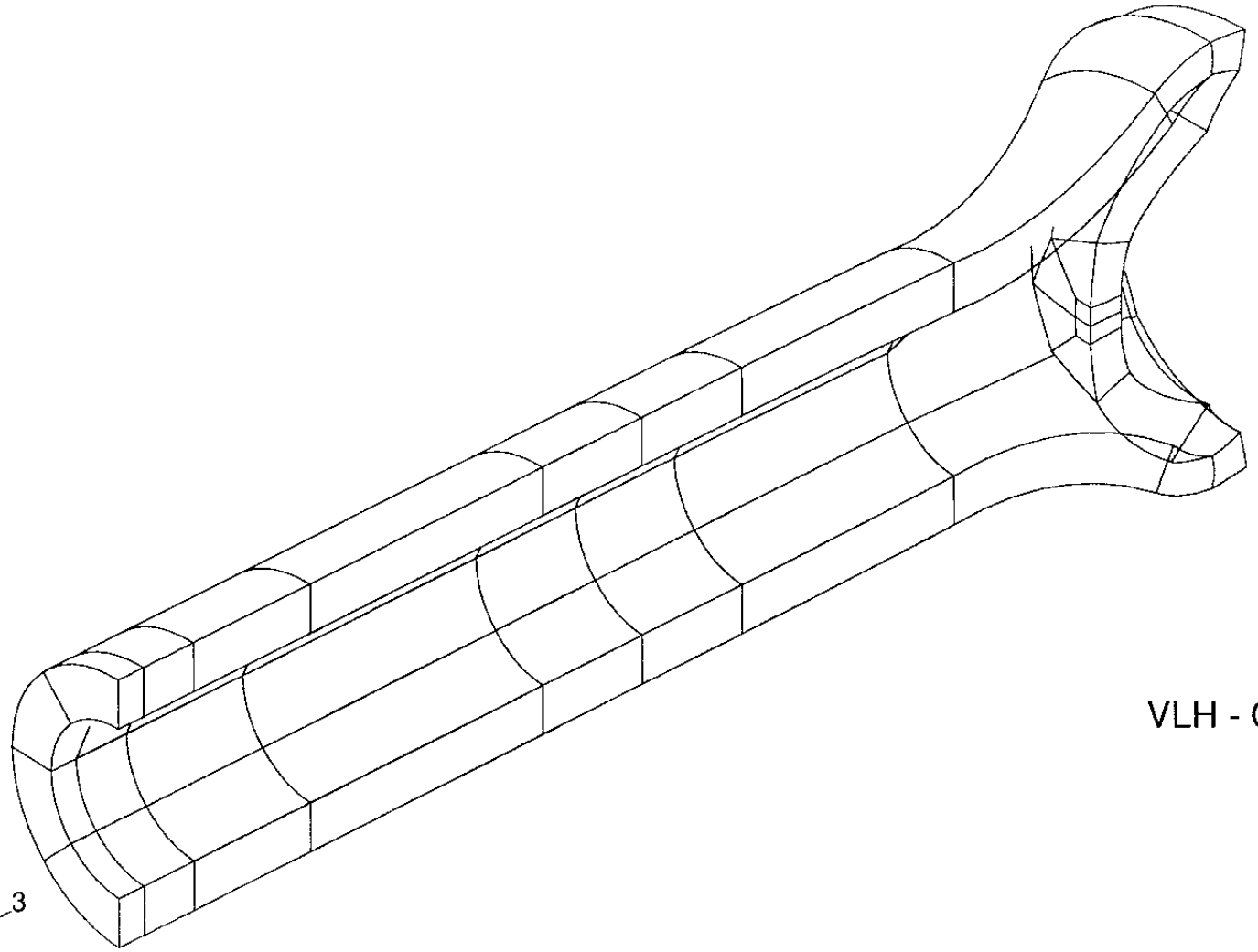

VLH - Copper

2
3
1

MAG. FACTOR =+2.0E+02

ABAQUS

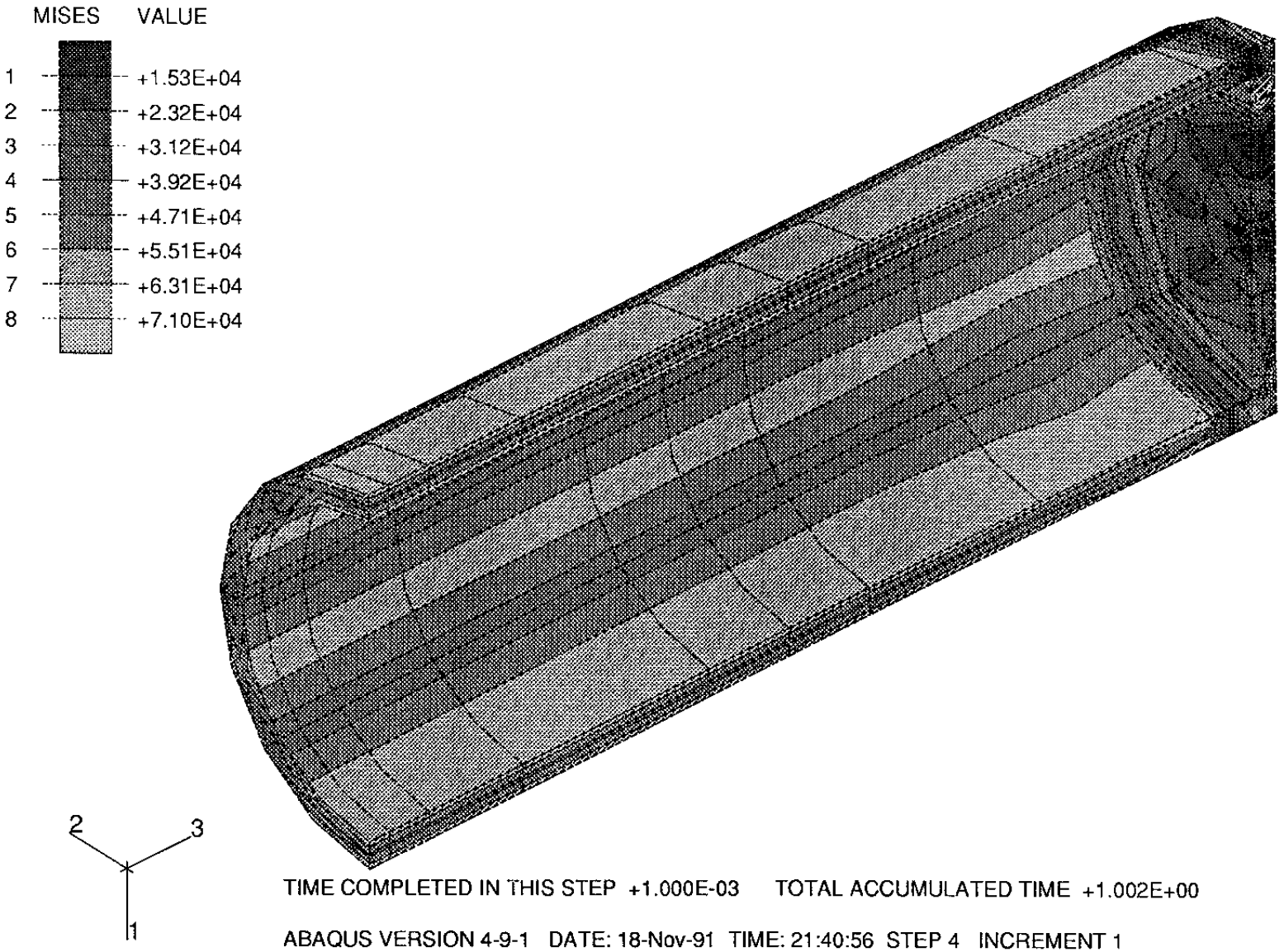

TIME COMPLETED IN THIS STEP +1.000E-03 TOTAL ACCUMULATED TIME +1.002E+00

ABAQUS VERSION 4-9-1 DATE: 18-Nov-91 TIME: 21:40:56 STEP 4 INCREMENT 1

ABAQUS

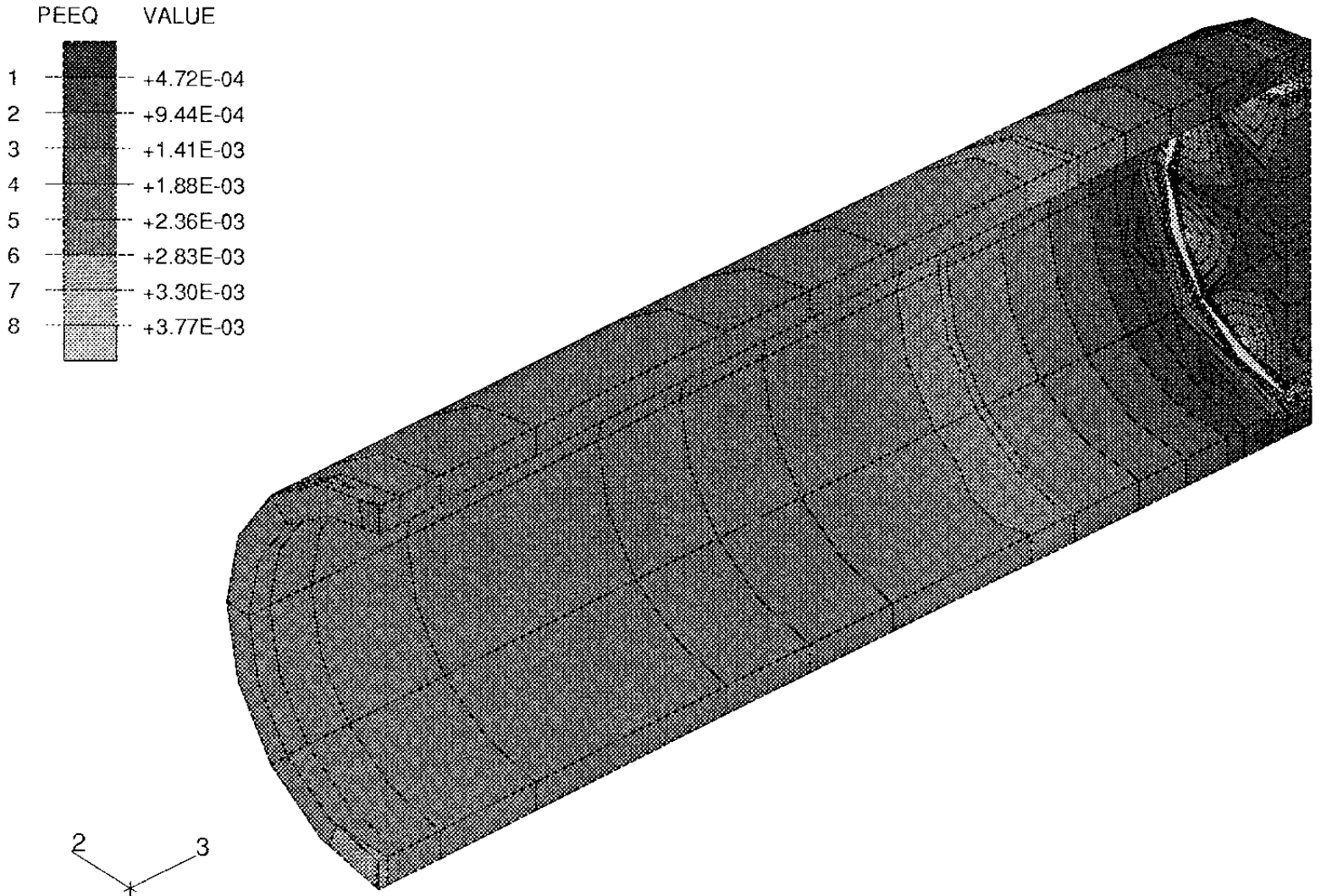

TIME COMPLETED IN THIS STEP +1.000E-03 TOTAL ACCUMULATED TIME +1.002E+00

ABAQUS VERSION 4-9-1 DATE: 18-Nov-91 TIME: 21:40:56 STEP 4 INCREMENT 1

ABAQUS

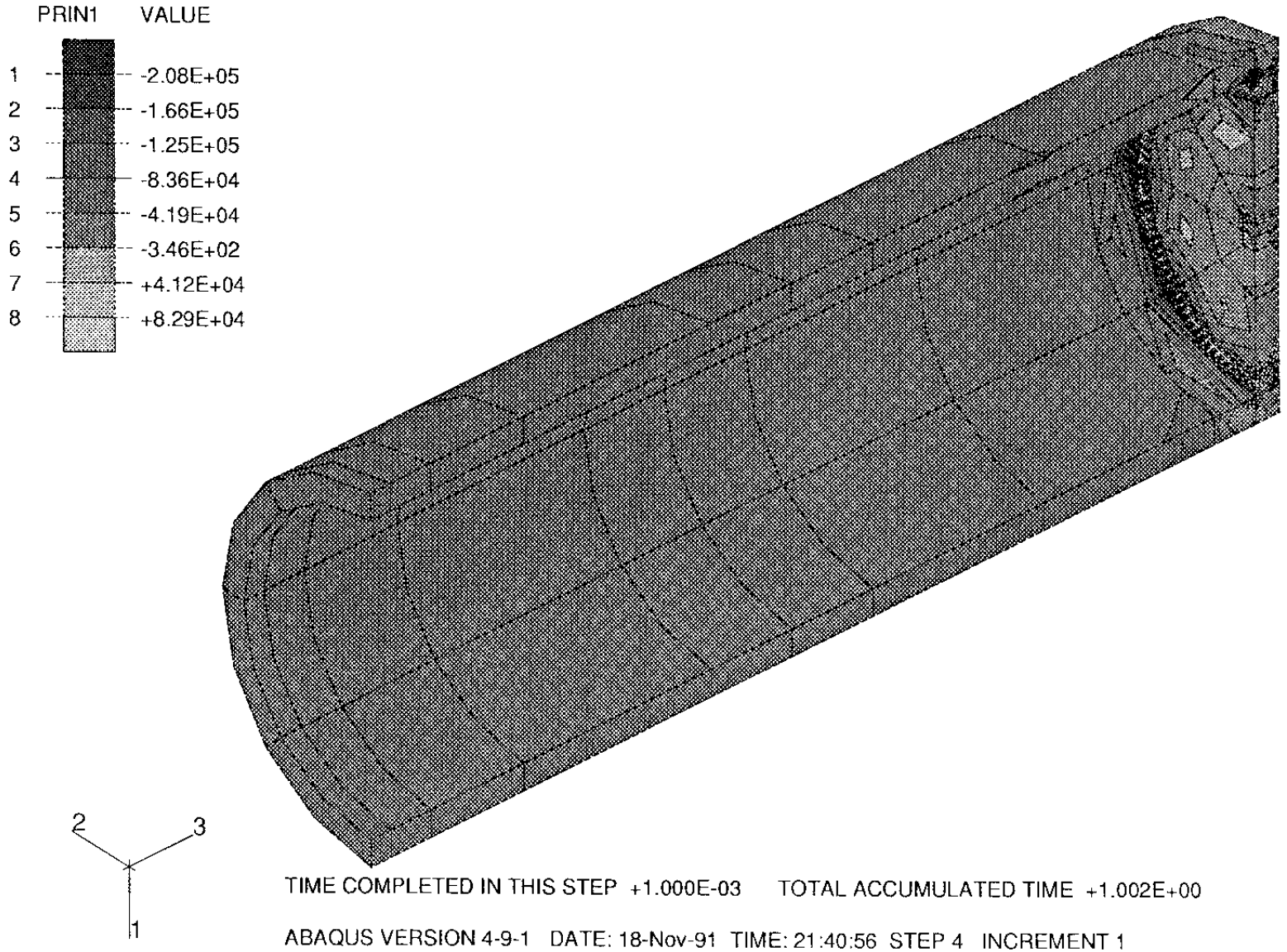

TIME COMPLETED IN THIS STEP +1.000E-03 TOTAL ACCUMULATED TIME +1.002E+00

ABAQUS VERSION 4-9-1 DATE: 18-Nov-91 TIME: 21:40:56 STEP 4 INCREMENT 1

ABAQUS

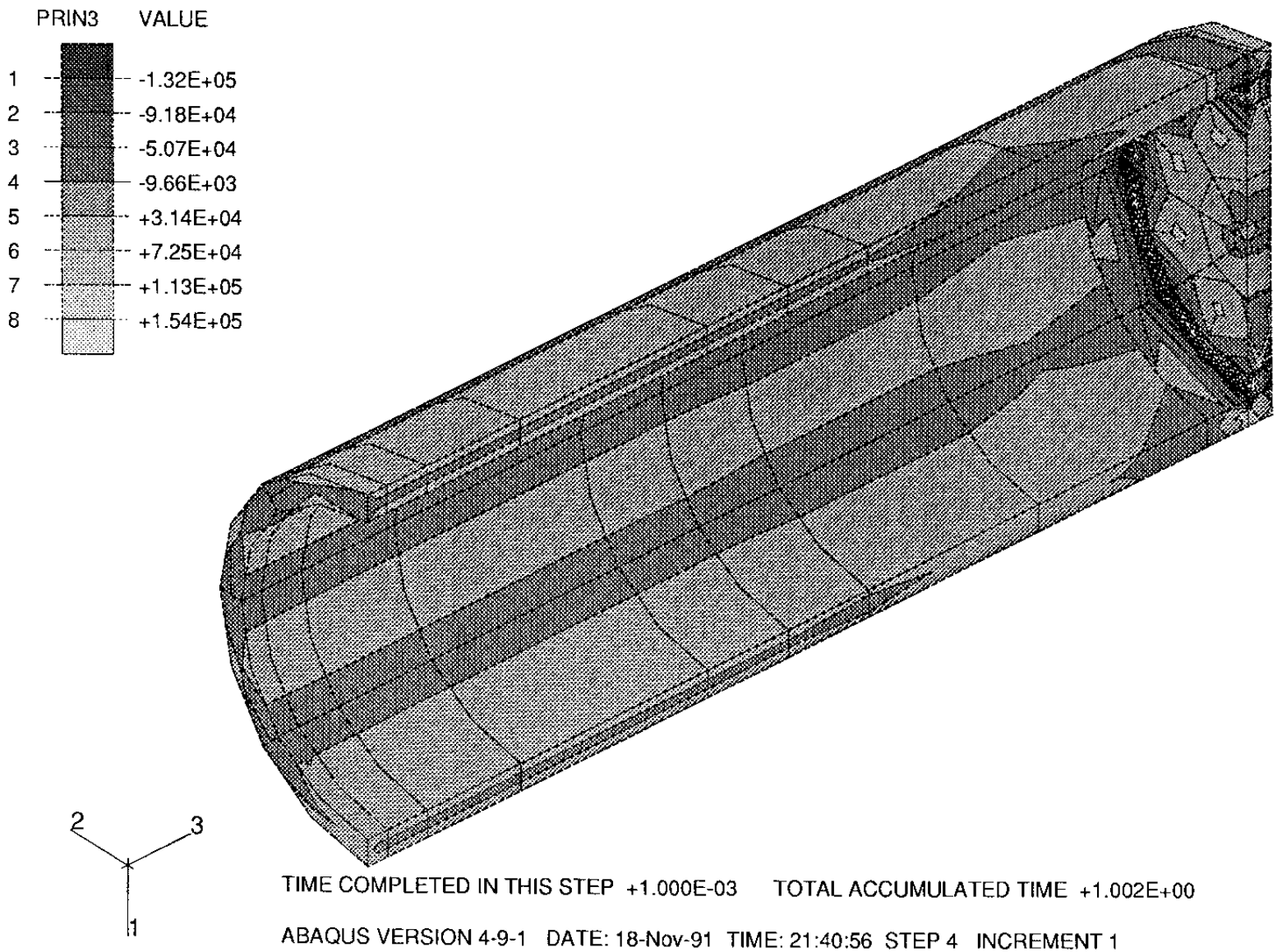

TIME COMPLETED IN THIS STEP +1.000E-03 TOTAL ACCUMULATED TIME +1.002E+00

ABAQUS VERSION 4-9-1 DATE: 18-Nov-91 TIME: 21:40:56 STEP 4 INCREMENT 1

ABAQUS

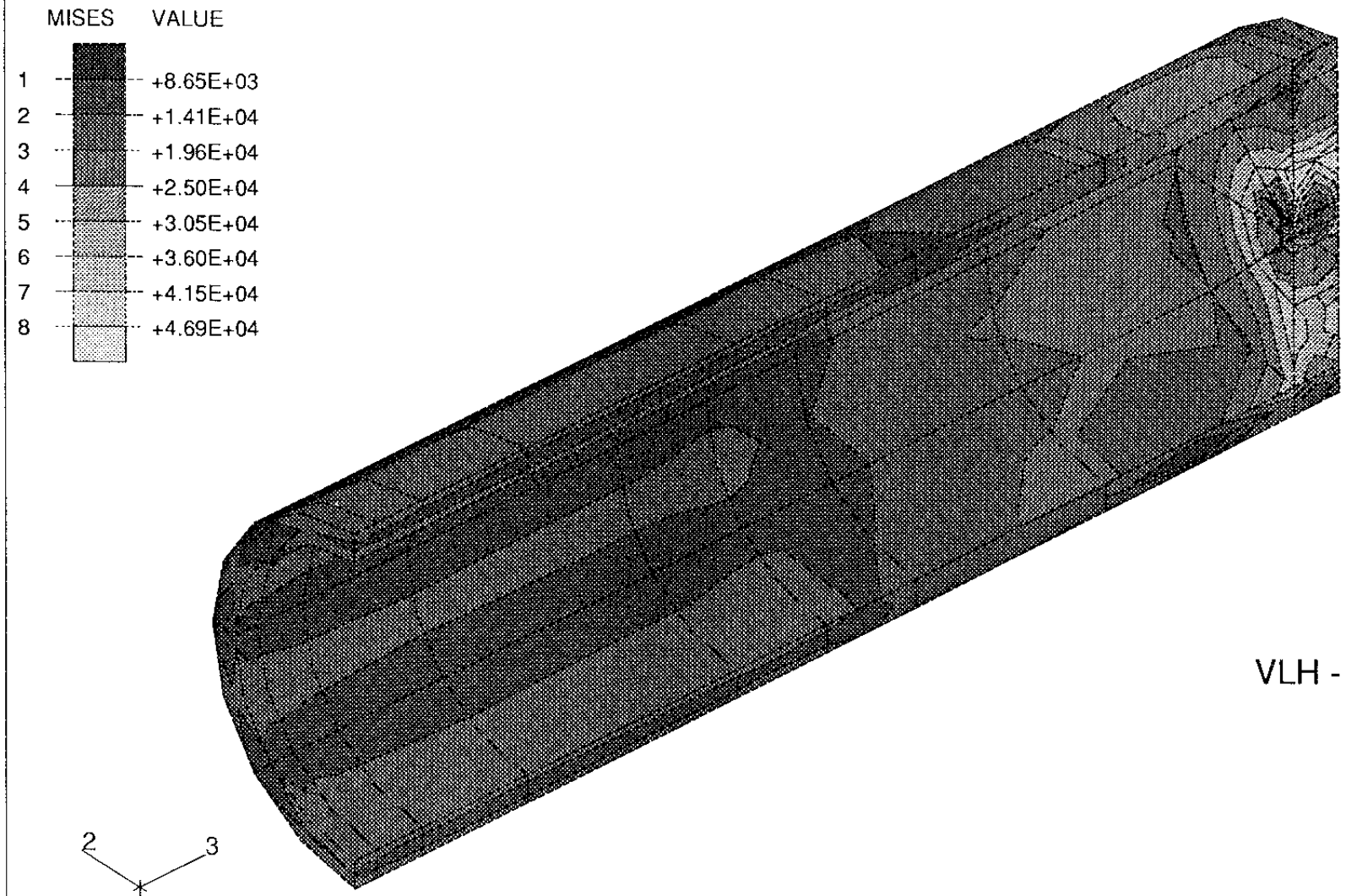

VLH - Steel

TIME COMPLETED IN THIS STEP +1.000E-03 TOTAL ACCUMULATED TIME +1.002E+00

ABAQUS VERSION 4-9-1 DATE: 18-Nov-91 TIME: 21:40:56 STEP 4 INCREMENT 1

ABAQUS

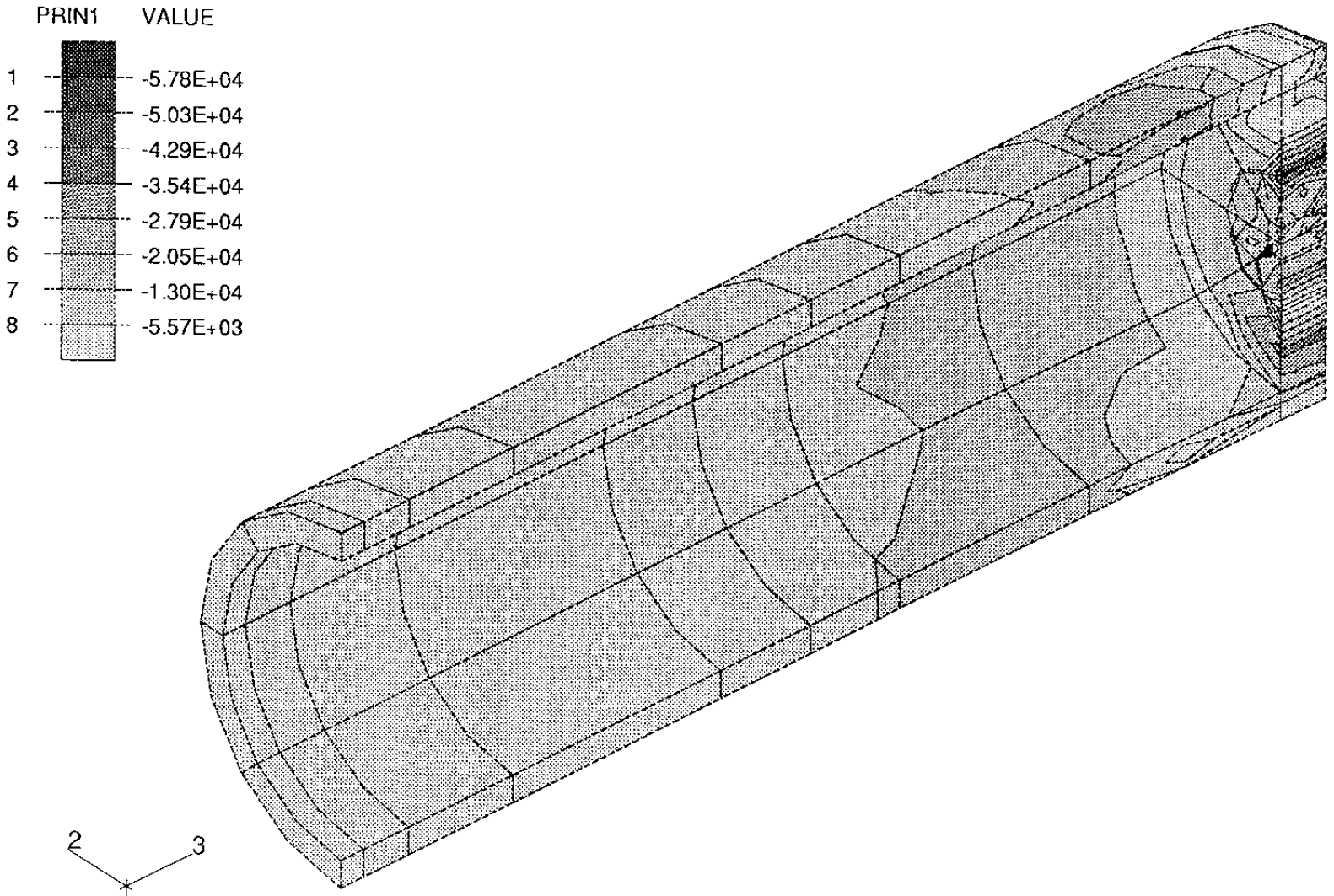

TIME COMPLETED IN THIS STEP +1.000E-03 TOTAL ACCUMULATED TIME +1.002E+00

ABAQUS VERSION 4-9-1 DATE: 18-Nov-91 TIME: 21:40:56 STEP 4 INCREMENT 1

ABAQUS

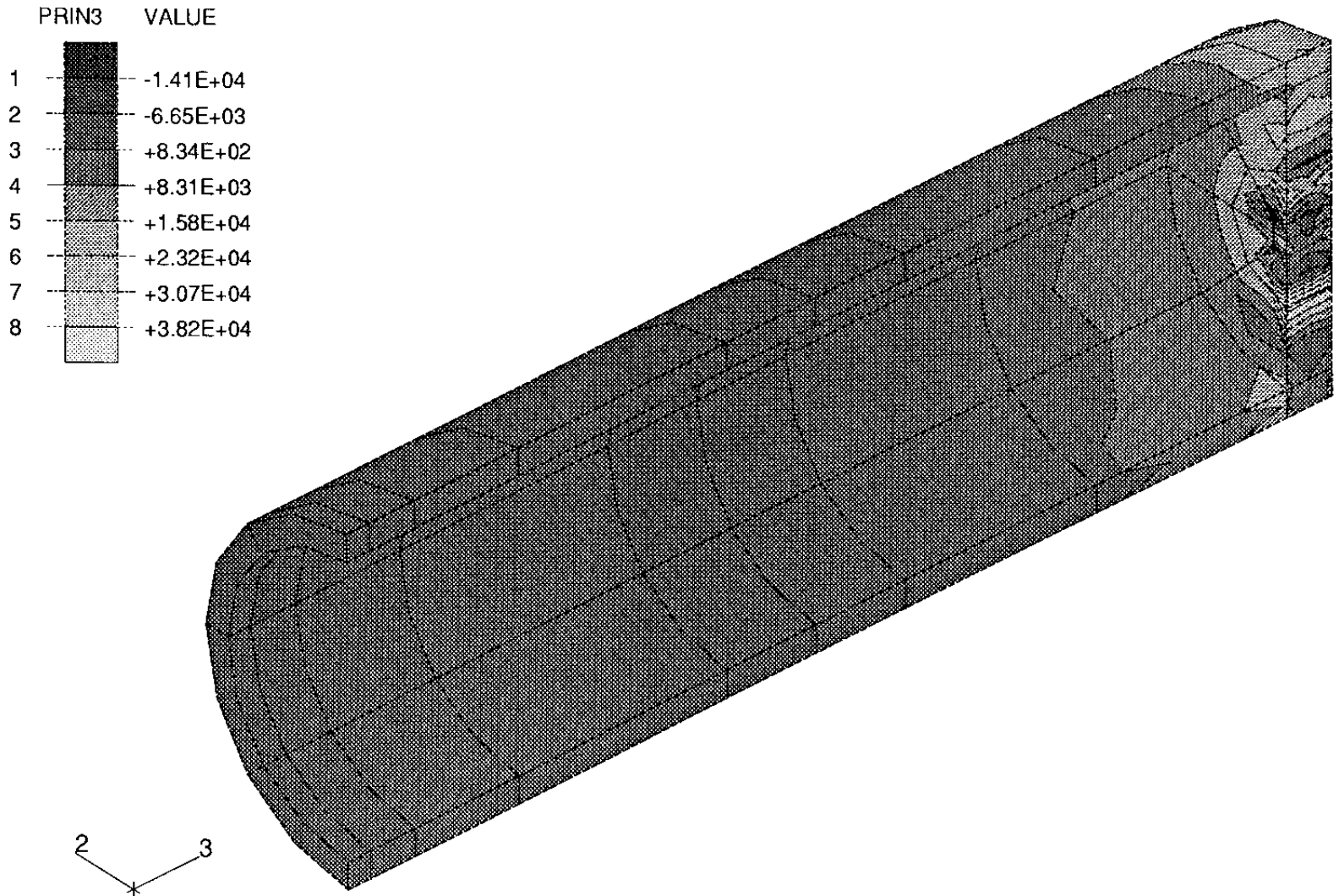

TIME COMPLETED IN THIS STEP +1.000E-03 TOTAL ACCUMULATED TIME +1.002E+00

ABAQUS VERSION 4-9-1 DATE: 18-Nov-91 TIME: 21:40:56 STEP 4 INCREMENT 1

ABAQUS

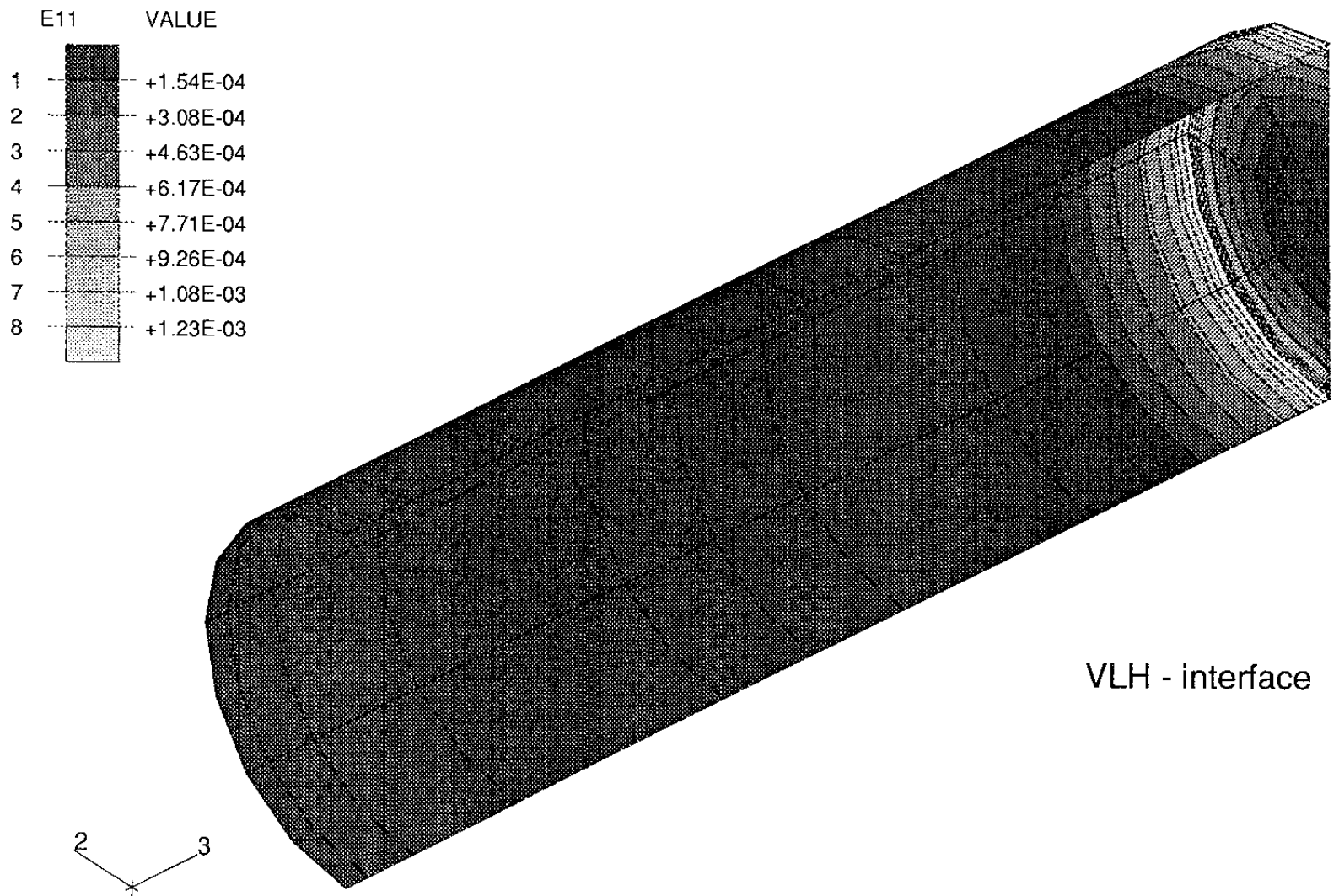

TIME COMPLETED IN THIS STEP +1.000E-03 TOTAL ACCUMULATED TIME +1.002E+00

ABAQUS VERSION 4-9-1 DATE: 18-Nov-91 TIME: 21:40:56 STEP 4 INCREMENT 1

ABAQUS

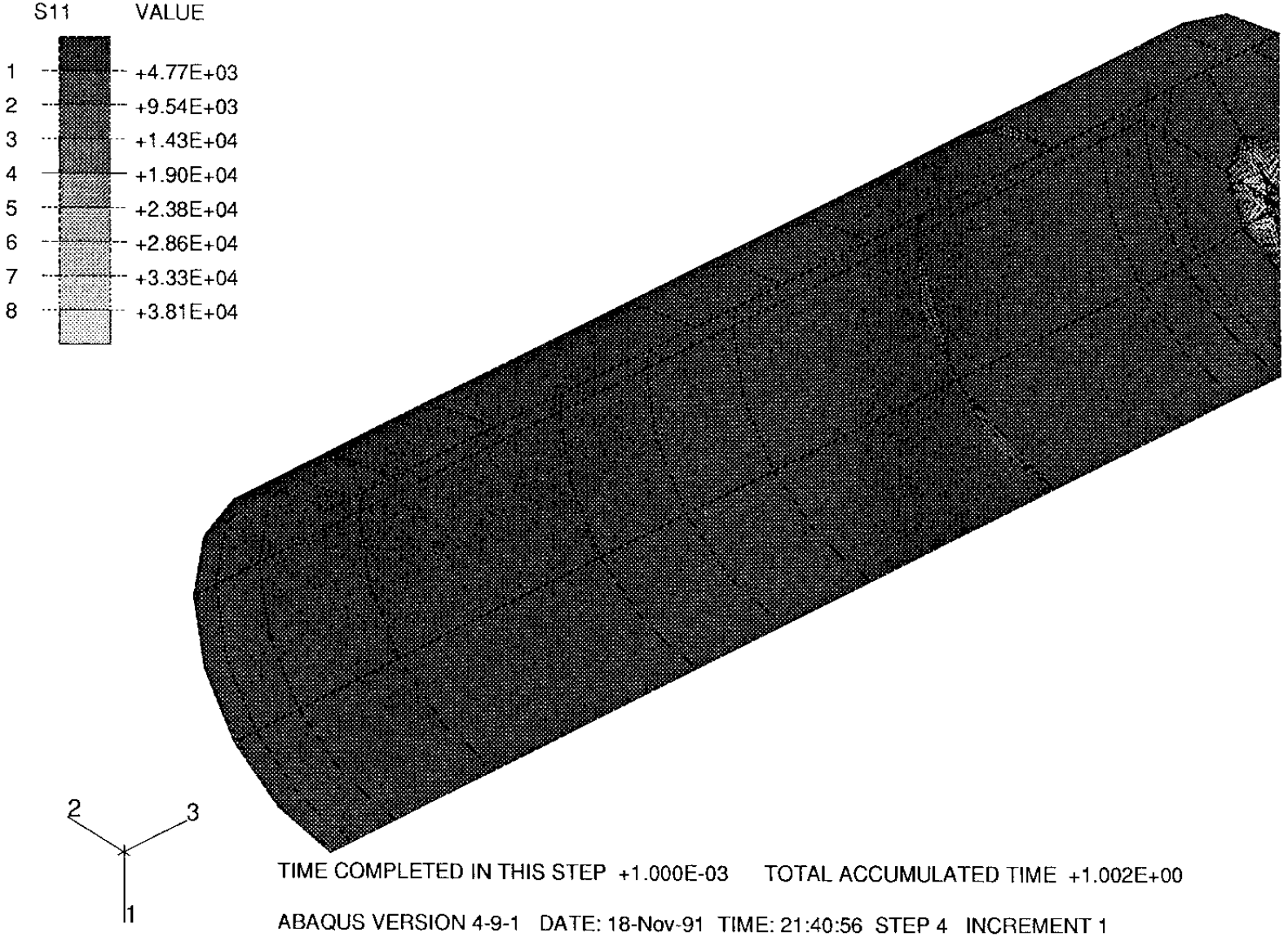

TIME COMPLETED IN THIS STEP +1.000E-03 TOTAL ACCUMULATED TIME +1.002E+00

ABAQUS VERSION 4-9-1 DATE: 18-Nov-91 TIME: 21:40:56 STEP 4 INCREMENT 1

APPENDIX III

Results from a rock shear calculation
Symmetric shear
KBS3 copper/steel canister

ABAQUS

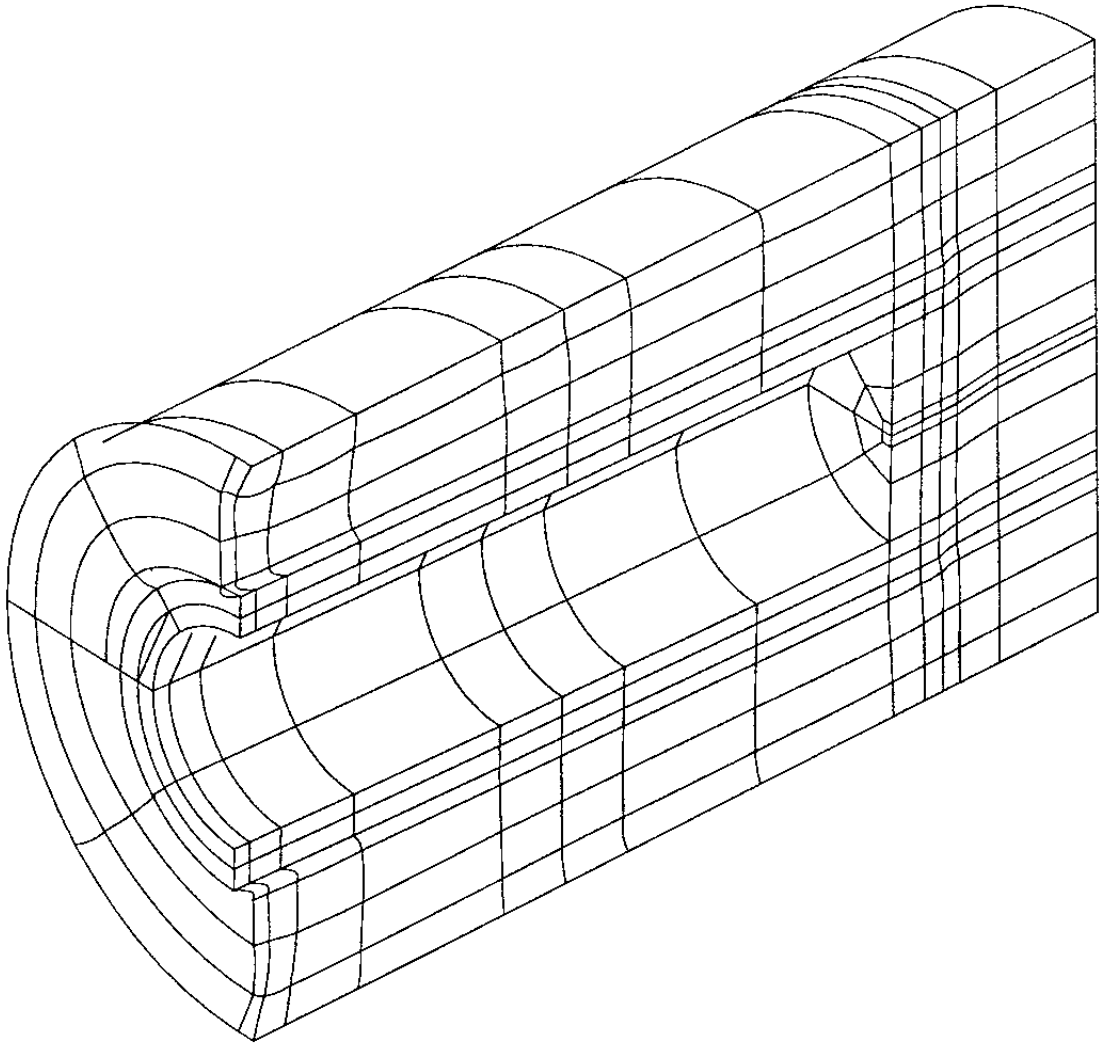

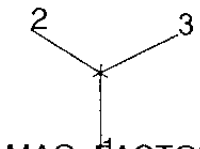

MAG. FACTOR =+1.0E+00

ABAQUS

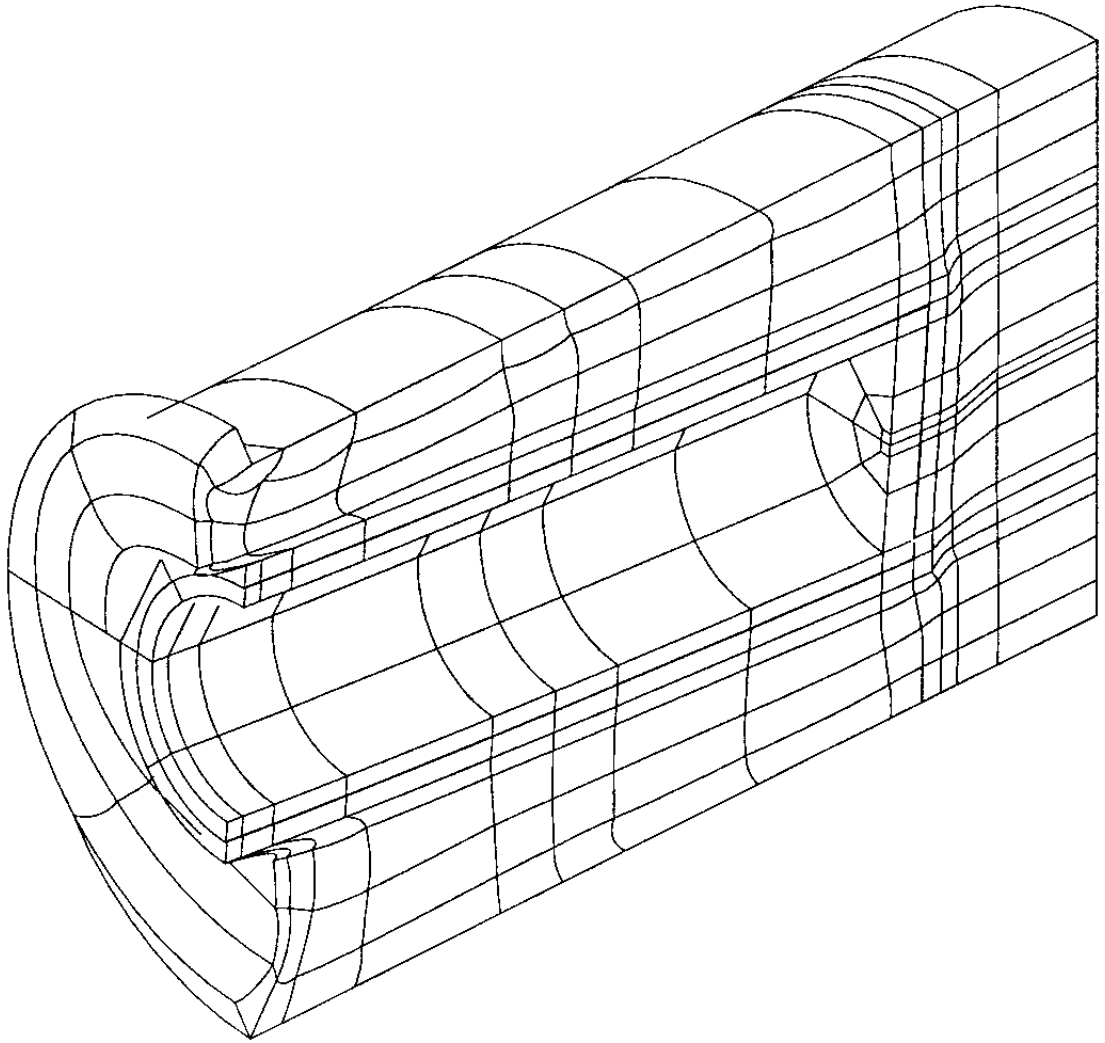

2
3
1

MAG. FACTOR =+2.5E+00

ABAQUS

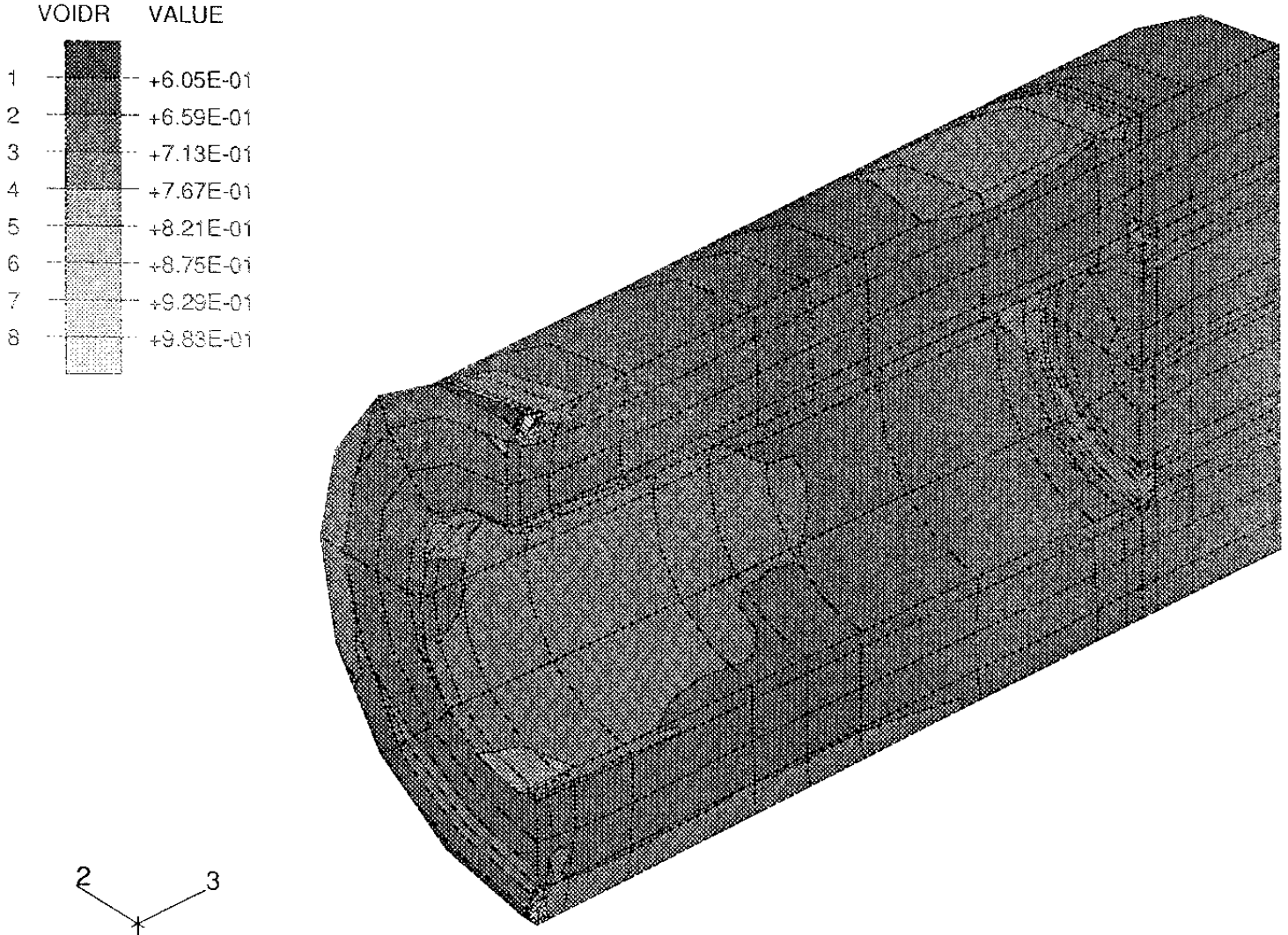

KBS3 - Clay

TIME COMPLETED IN THIS STEP +2.592E+06 TOTAL ACCUMULATED TIME +2.592E+06

ABAQUS VERSION 4-9-1 DATE: 21-Nov-91 TIME: 16:08:42 STEP 5 INCREMENT 153

ABAQUS

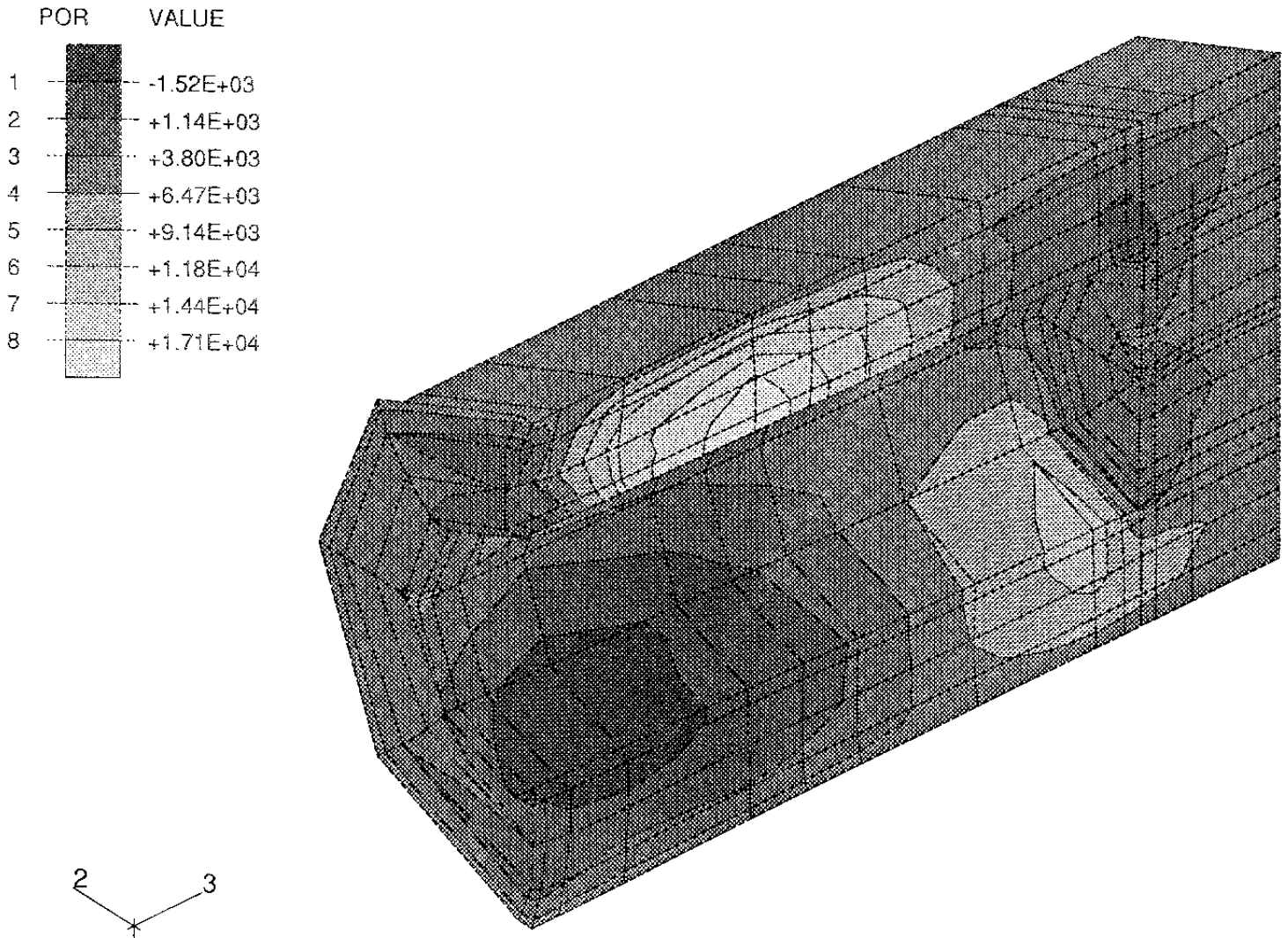

TIME COMPLETED IN THIS STEP +2.592E+06 TOTAL ACCUMULATED TIME +2.592E+06

ABAQUS VERSION 4-9-1 DATE: 21-Nov-91 TIME: 16:08:42 STEP 5 INCREMENT 153

ABAQUS

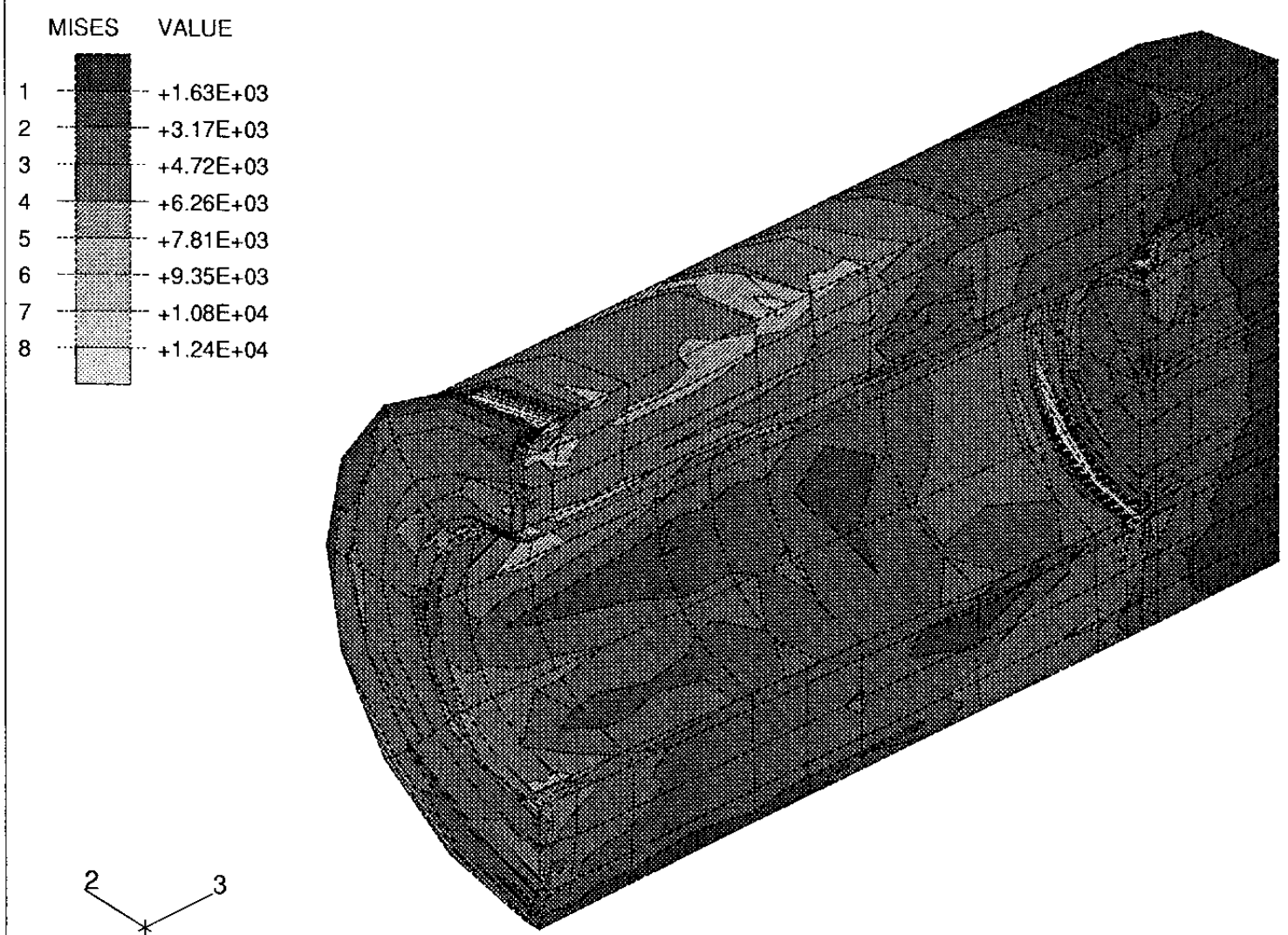

TIME COMPLETED IN THIS STEP +2.592E+06 TOTAL ACCUMULATED TIME +2.592E+06

ABAQUS VERSION 4-9-1 DATE: 21-Nov-91 TIME: 16:08:42 STEP 5 INCREMENT 153

ABAQUS

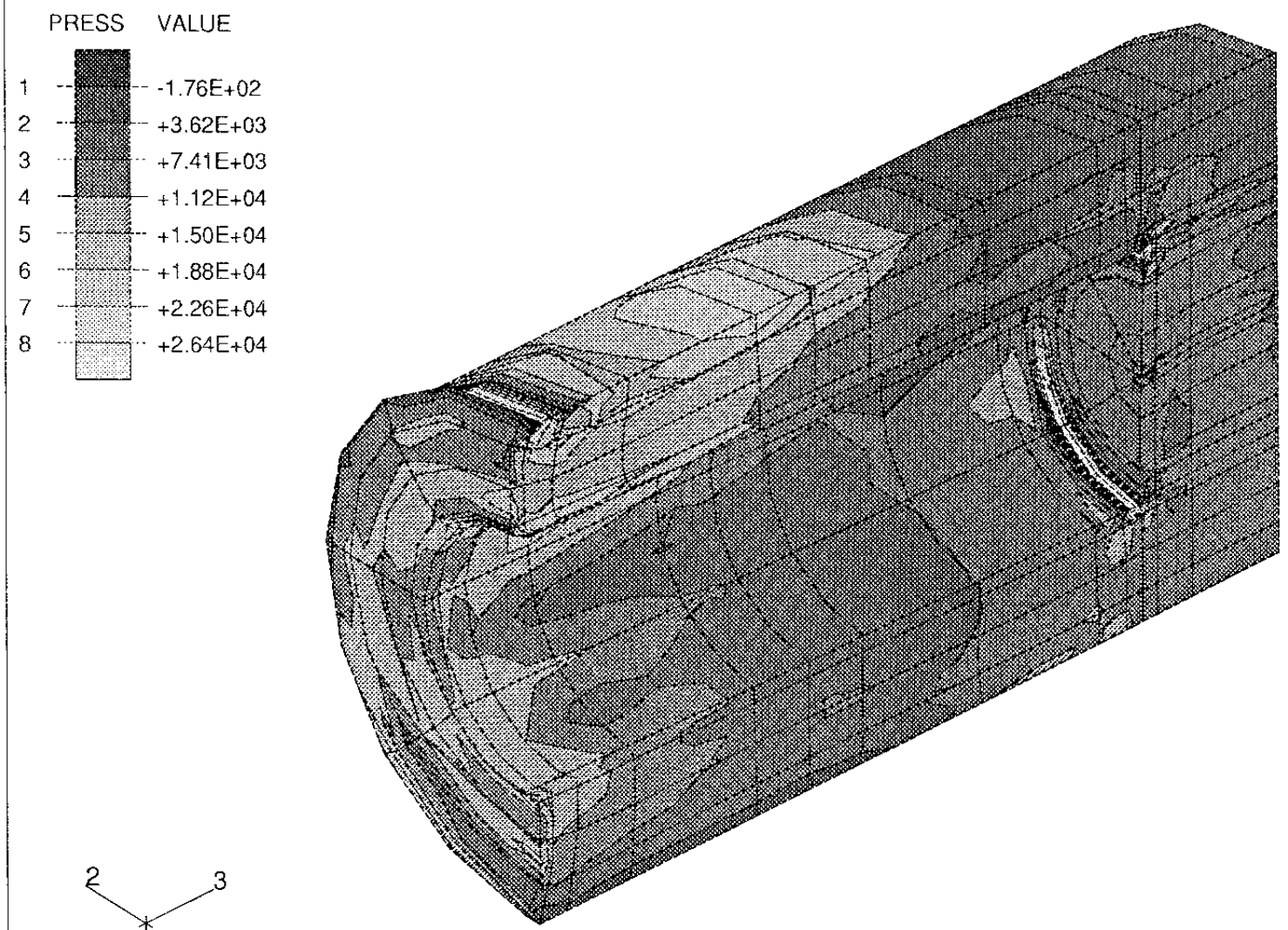

TIME COMPLETED IN THIS STEP +2.592E+06 TOTAL ACCUMULATED TIME +2.592E+06

ABAQUS VERSION 4-9-1 DATE: 21-Nov-91 TIME: 16:08:42 STEP 5 INCREMENT 153

ABAQUS

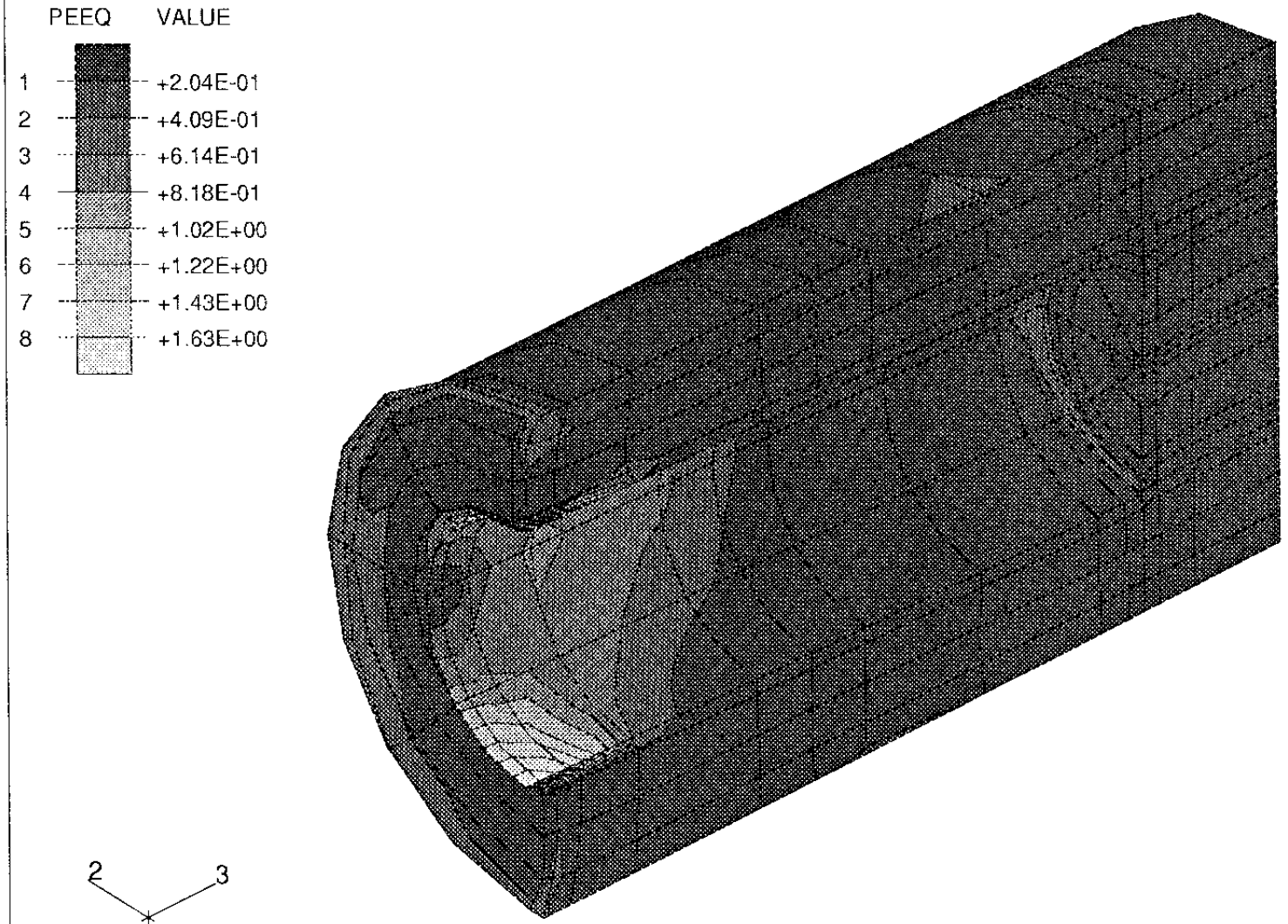

TIME COMPLETED IN THIS STEP +2.592E+06 TOTAL ACCUMULATED TIME +2.592E+06

ABAQUS VERSION 4-9-1 DATE: 21-Nov-91 TIME: 16:08:42 STEP 5 INCREMENT 153

ABAQUS

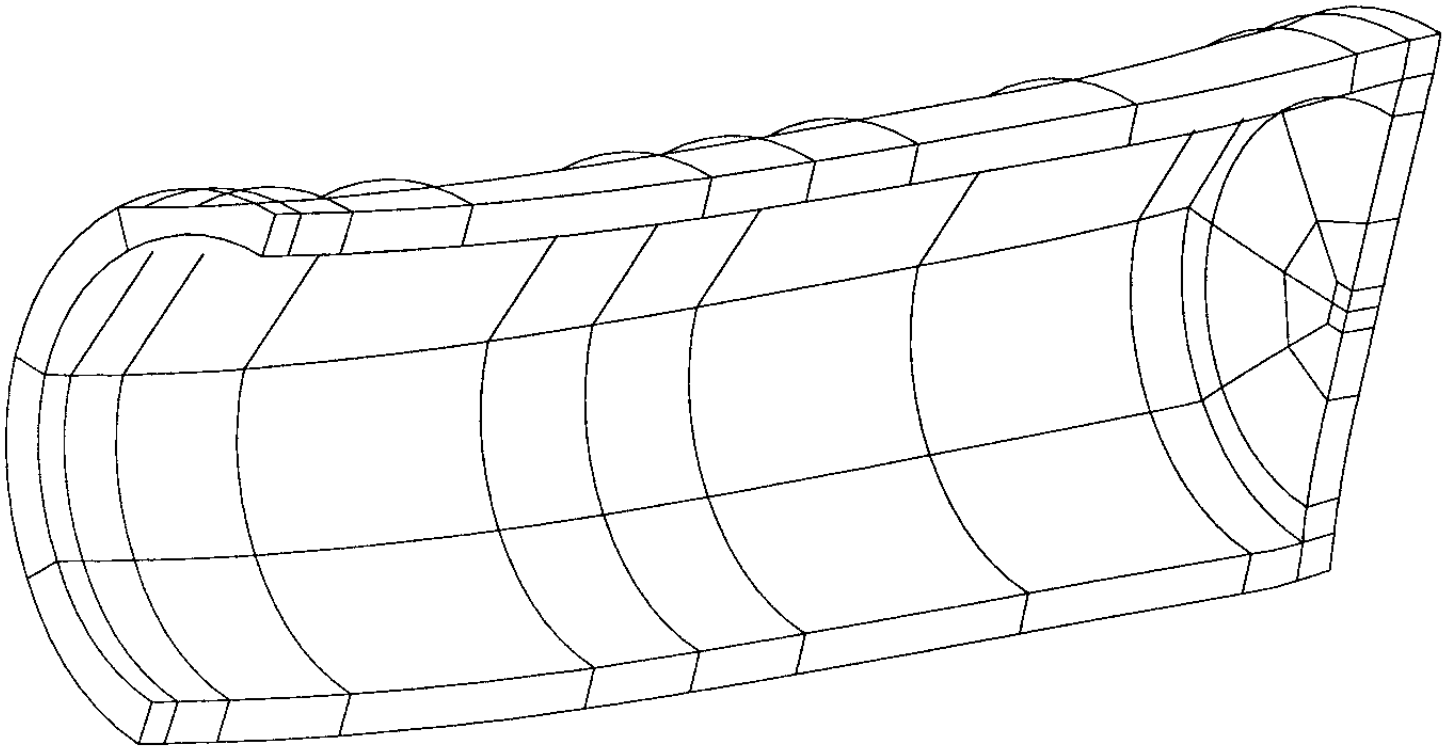

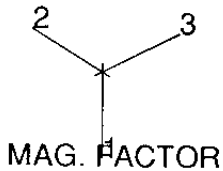

MAG. FACTOR =+1.0E+01

ABAQUS

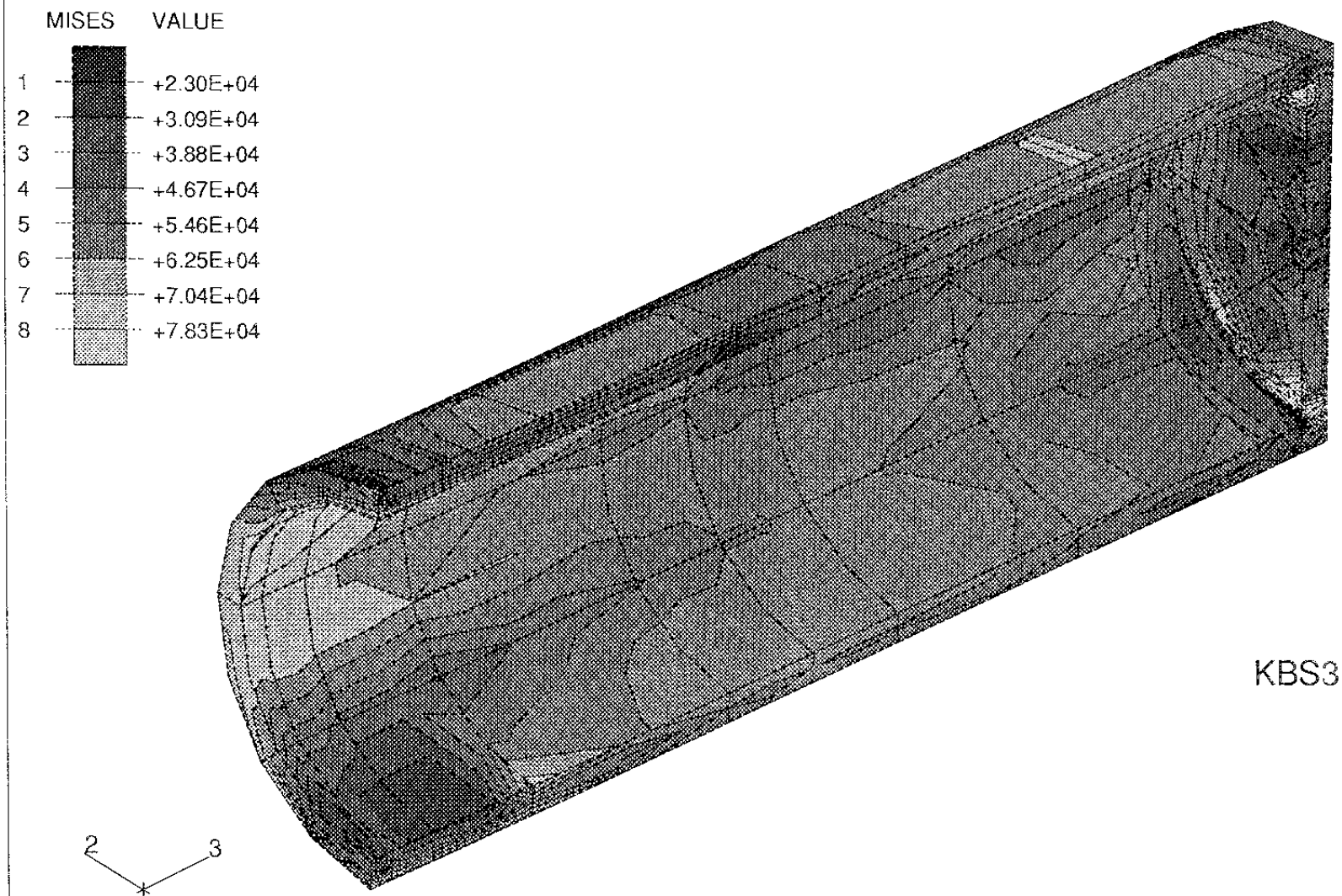

KBS3 - Copper

TIME COMPLETED IN THIS STEP +2.592E+06 TOTAL ACCUMULATED TIME +2.592E+06

ABAQUS VERSION 4-9-1 DATE: 21-Nov-91 TIME: 16:08:42 STEP 5 INCREMENT 153

ABAQUS

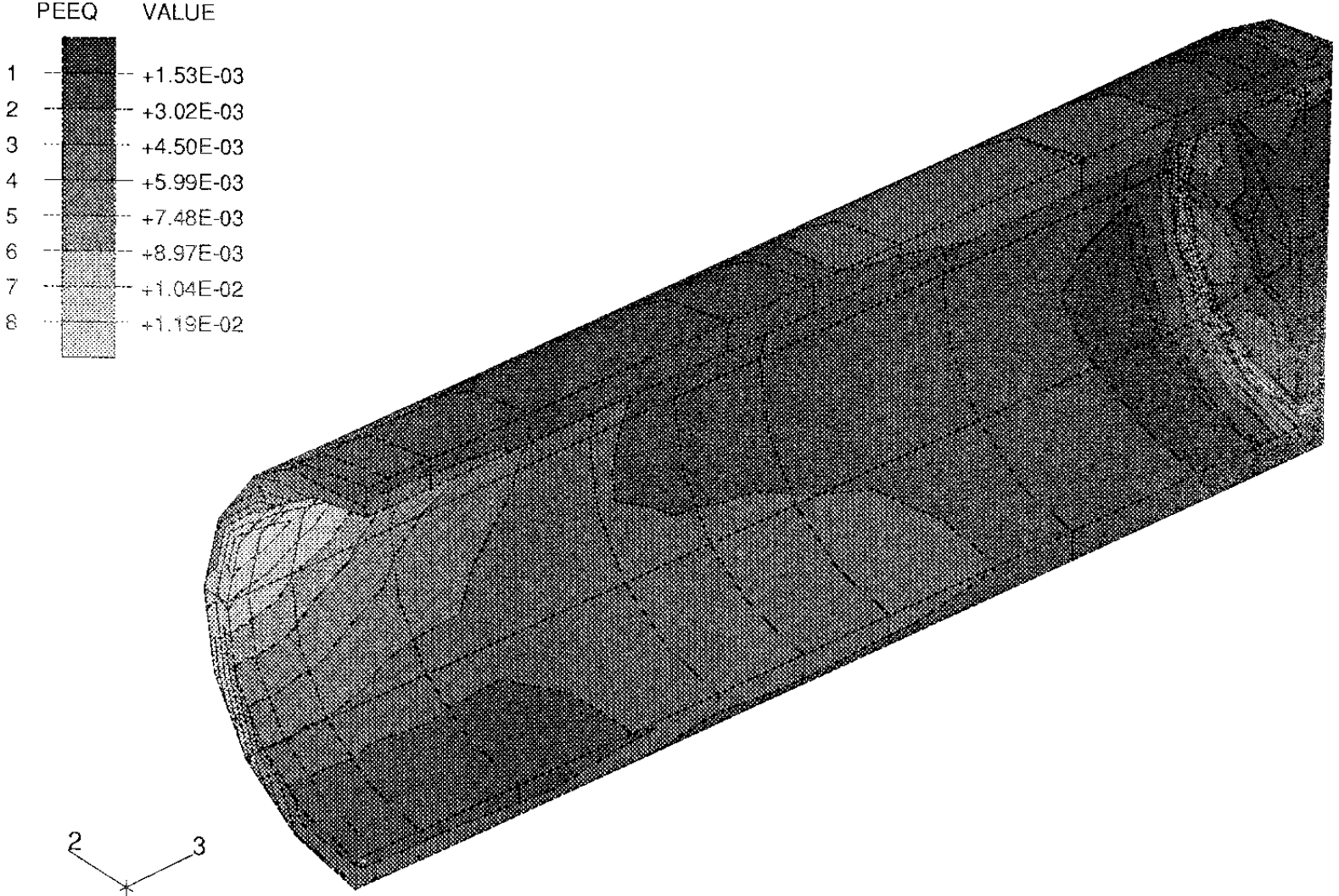

TIME COMPLETED IN THIS STEP +2.592E+06 TOTAL ACCUMULATED TIME +2.592E+06

ABAQUS VERSION 4-9-1 DATE: 21-Nov-91 TIME: 16:08:42 STEP 5 INCREMENT 153

ABAQUS

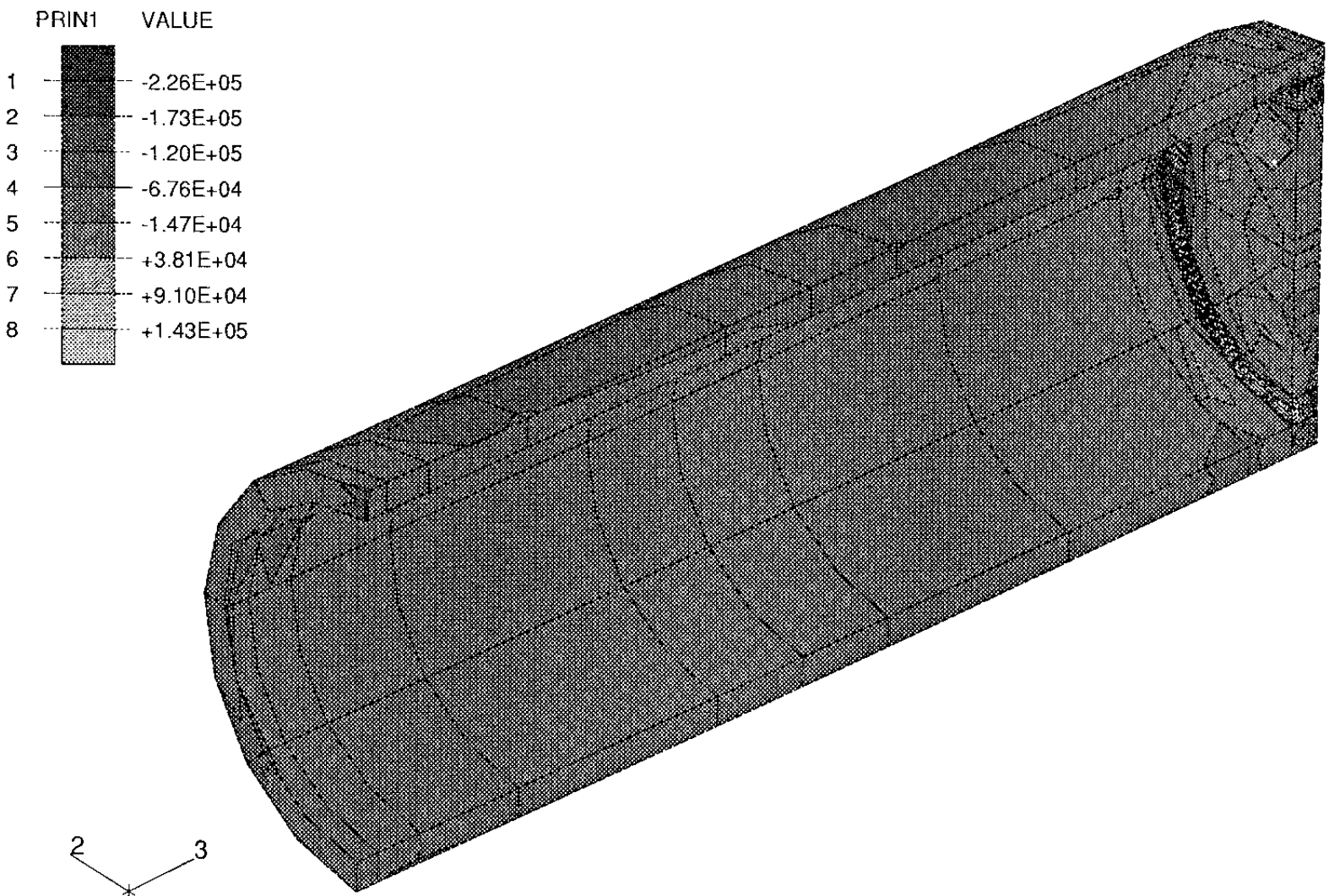

TIME COMPLETED IN THIS STEP +2.592E+06 TOTAL ACCUMULATED TIME +2.592E+06

ABAQUS VERSION 4-9-1 DATE: 21-Nov-91 TIME: 16:08:42 STEP 5 INCREMENT 153

ABAQUS

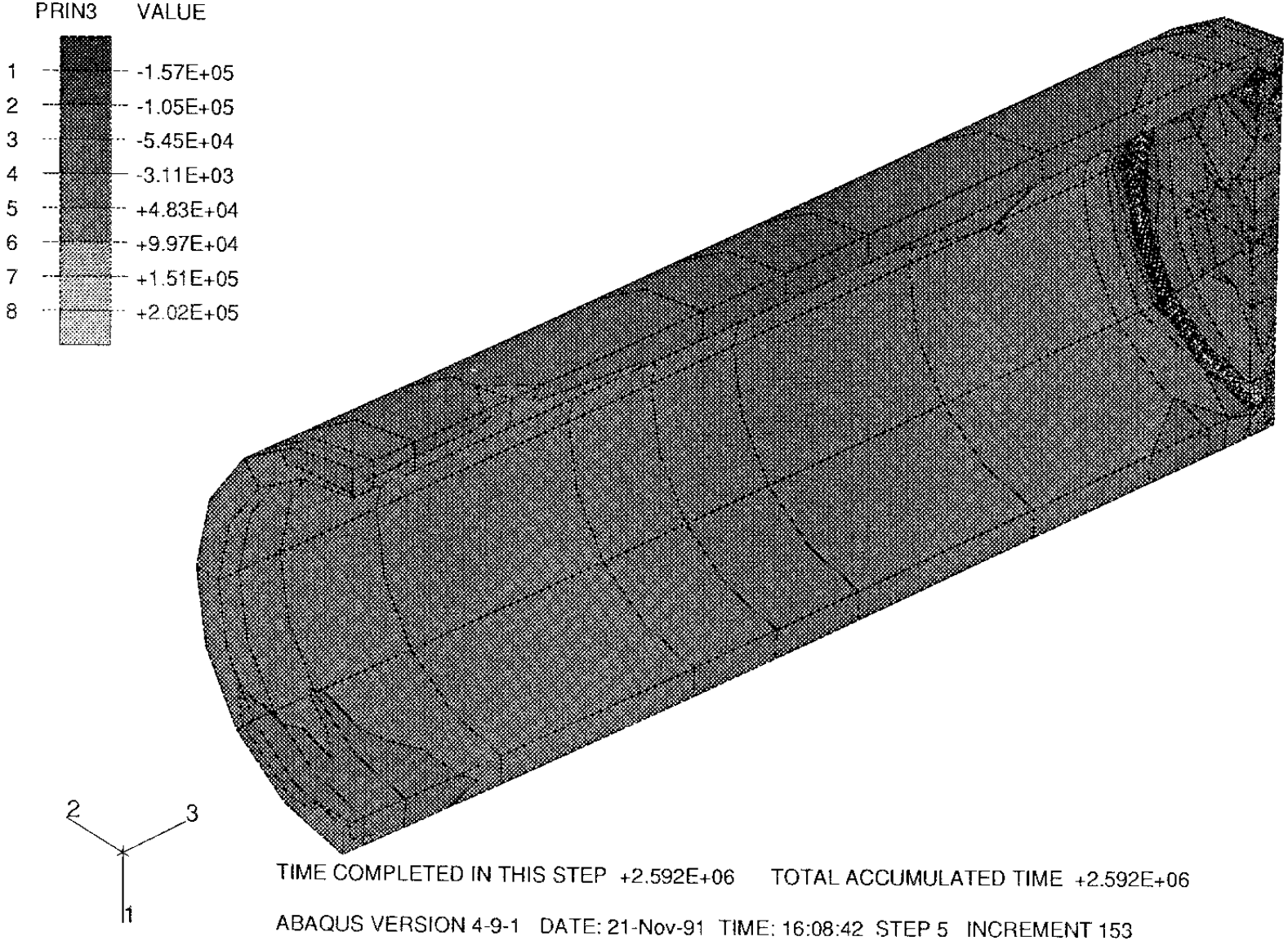

TIME COMPLETED IN THIS STEP +2.592E+06 TOTAL ACCUMULATED TIME +2.592E+06

ABAQUS VERSION 4-9-1 DATE: 21-Nov-91 TIME: 16:08:42 STEP 5 INCREMENT 153

ABAQUS

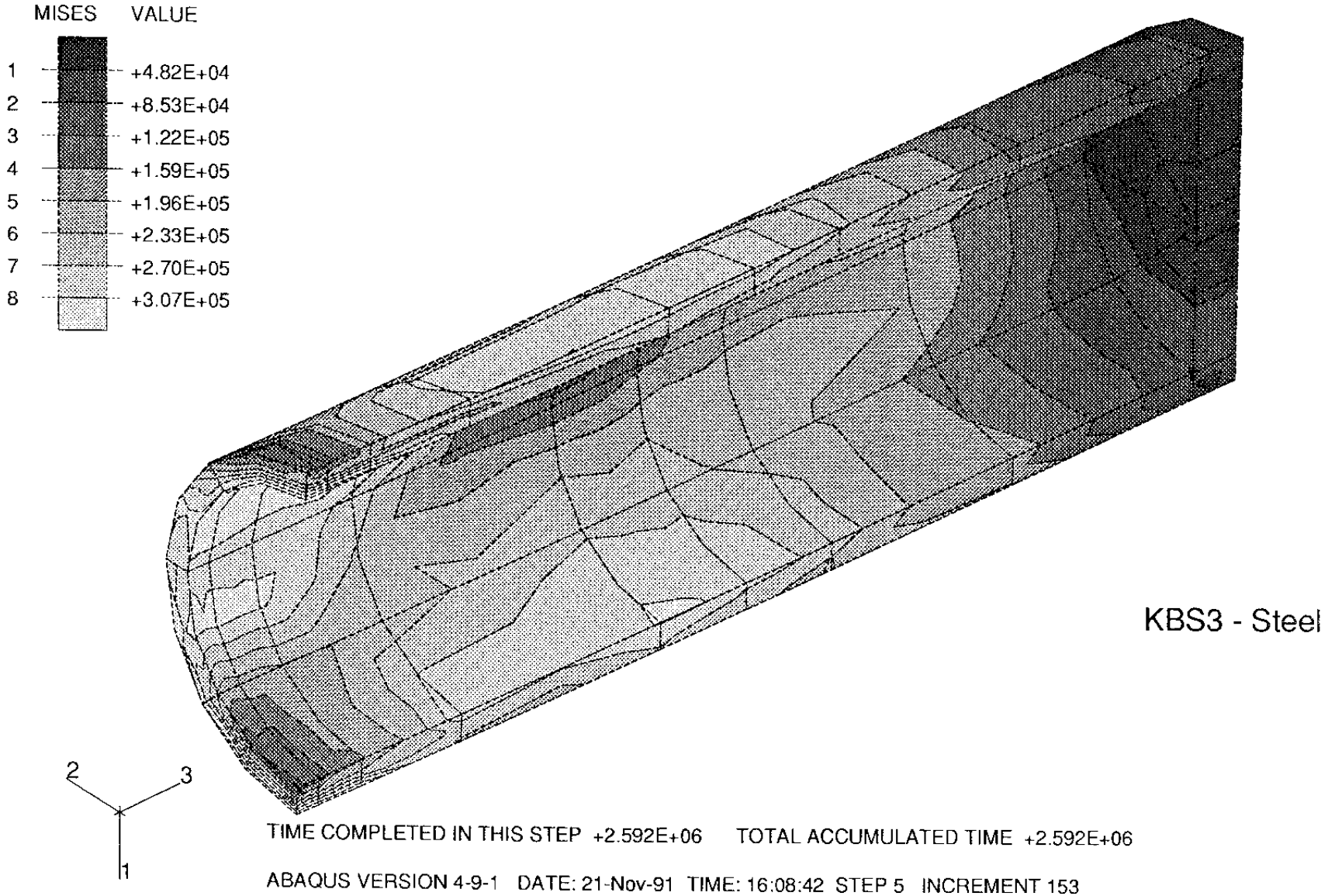

TIME COMPLETED IN THIS STEP +2.592E+06 TOTAL ACCUMULATED TIME +2.592E+06

ABAQUS VERSION 4-9-1 DATE: 21-Nov-91 TIME: 16:08:42 STEP 5 INCREMENT 153

ABAQUS

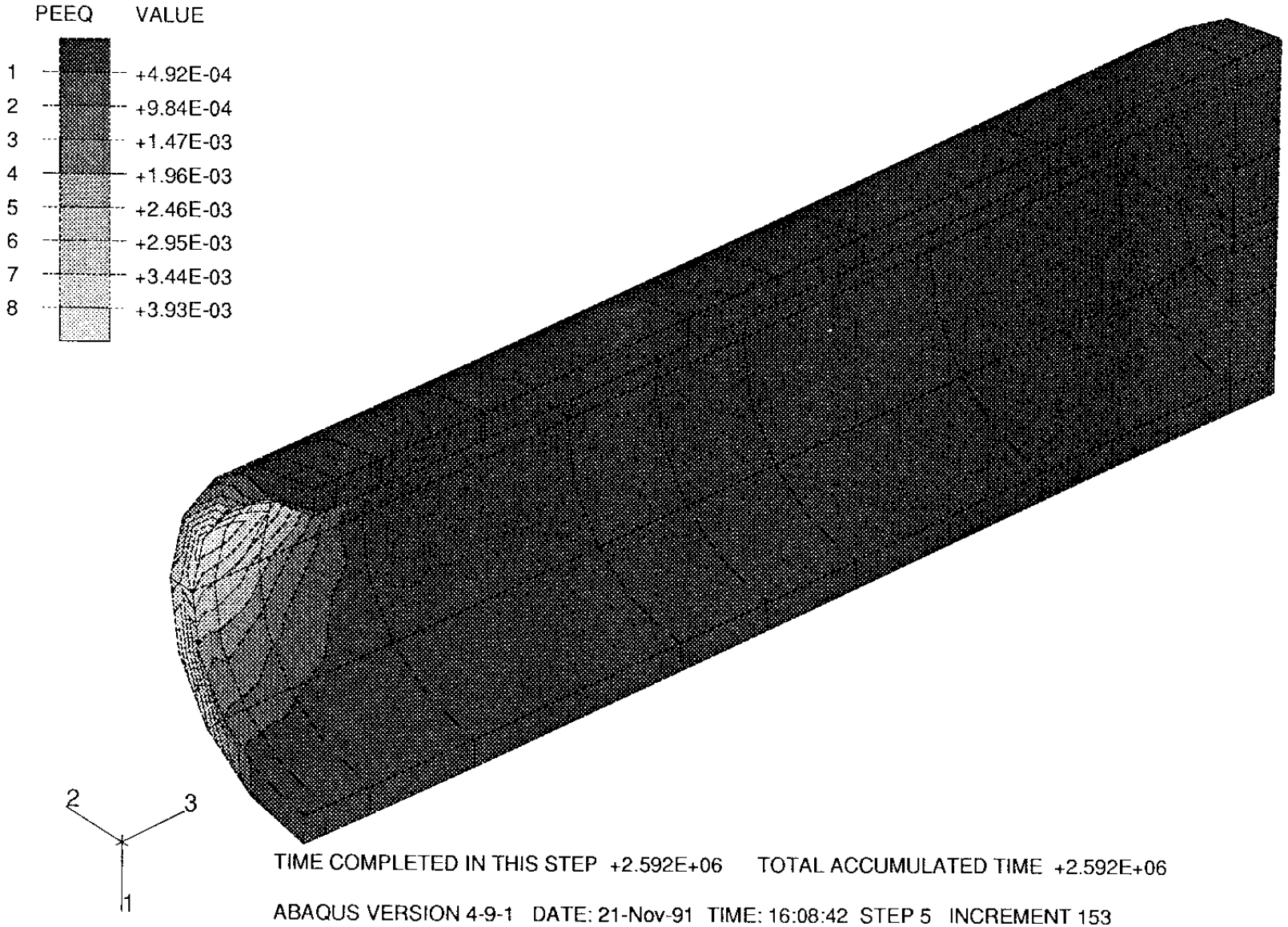

TIME COMPLETED IN THIS STEP +2.592E+06 TOTAL ACCUMULATED TIME +2.592E+06

ABAQUS VERSION 4-9-1 DATE: 21-Nov-91 TIME: 16:08:42 STEP 5 INCREMENT 153

ABAQUS

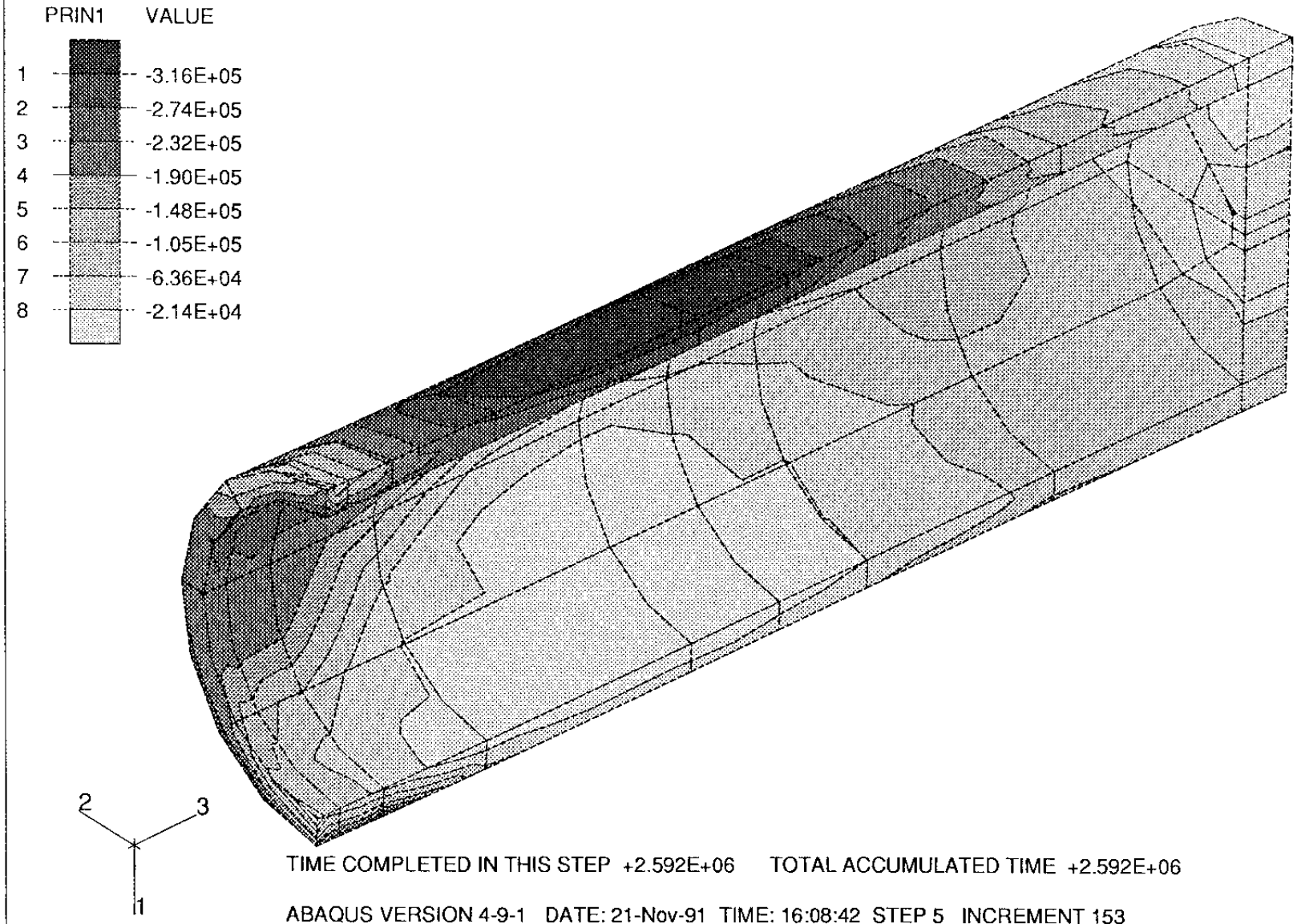

TIME COMPLETED IN THIS STEP +2.592E+06 TOTAL ACCUMULATED TIME +2.592E+06

ABAQUS VERSION 4-9-1 DATE: 21-Nov-91 TIME: 16:08:42 STEP 5 INCREMENT 153

ABAQUS

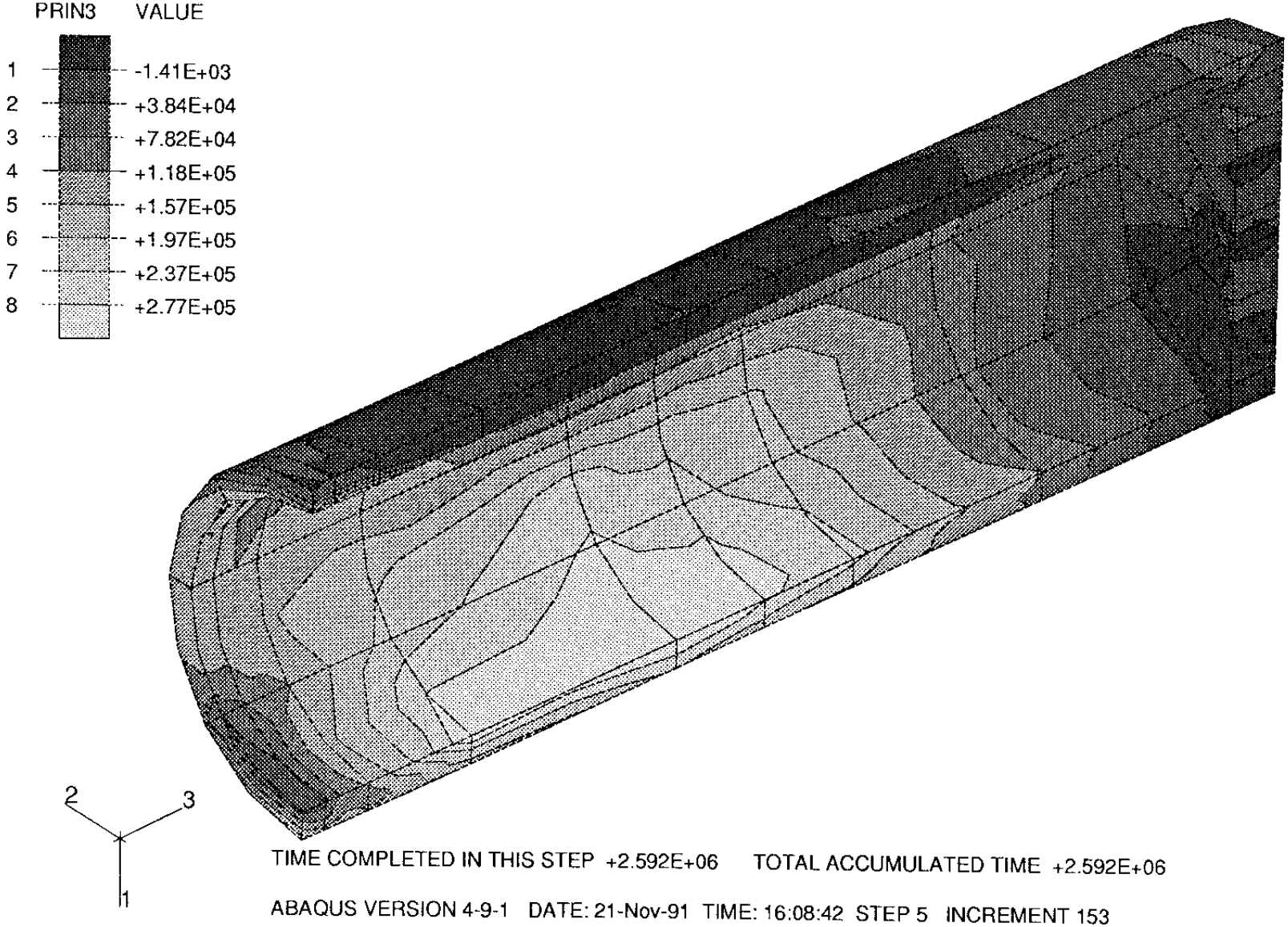

TIME COMPLETED IN THIS STEP +2.592E+06 TOTAL ACCUMULATED TIME +2.592E+06

ABAQUS VERSION 4-9-1 DATE: 21-Nov-91 TIME: 16:08:42 STEP 5 INCREMENT 153

ABAQUS

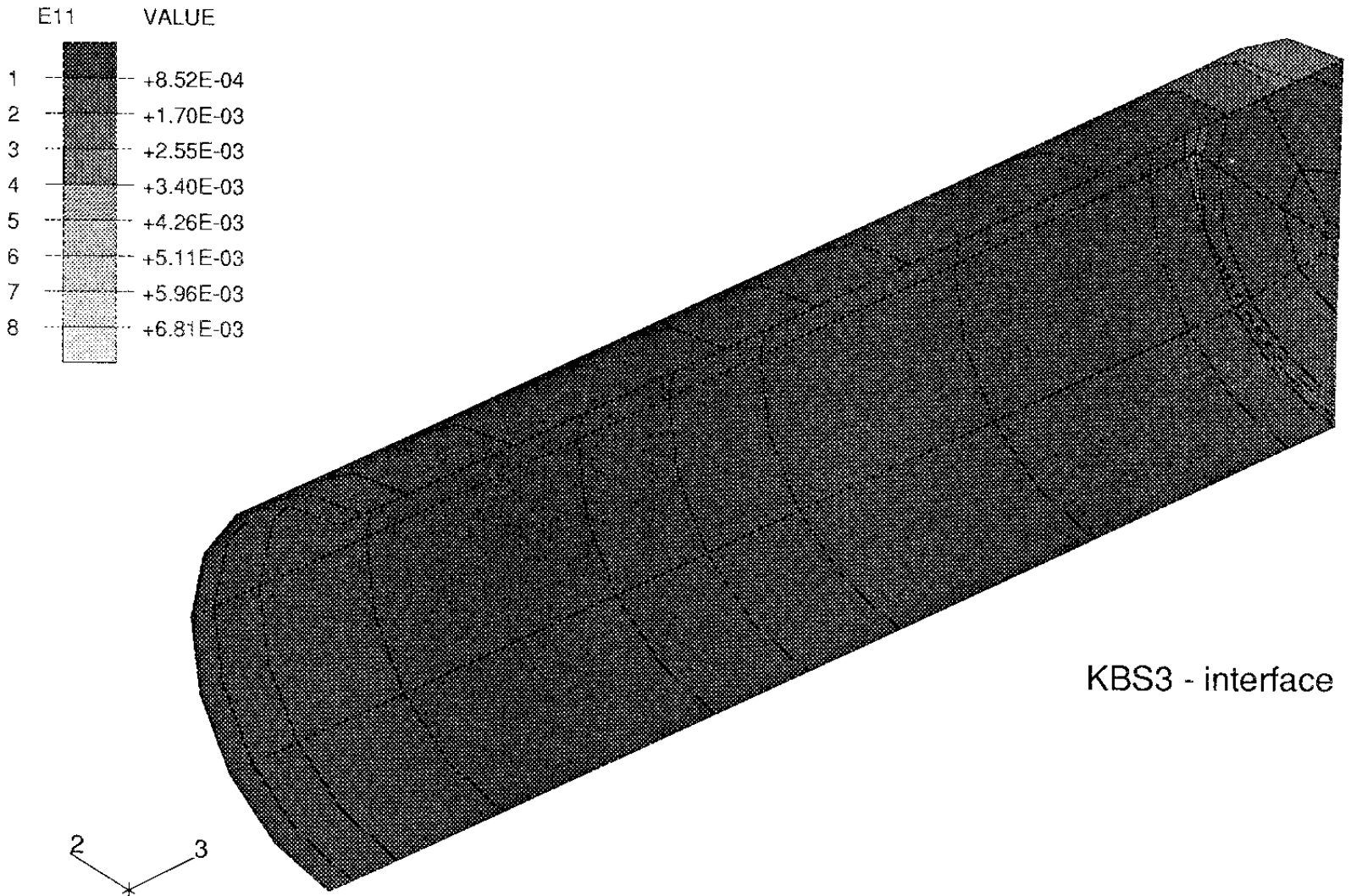

TIME COMPLETED IN THIS STEP +2.592E+06 TOTAL ACCUMULATED TIME +2.592E+06

ABAQUS VERSION 4-9-1 DATE: 21-Nov-91 TIME: 16:08:42 STEP 5 INCREMENT 153

ABAQUS

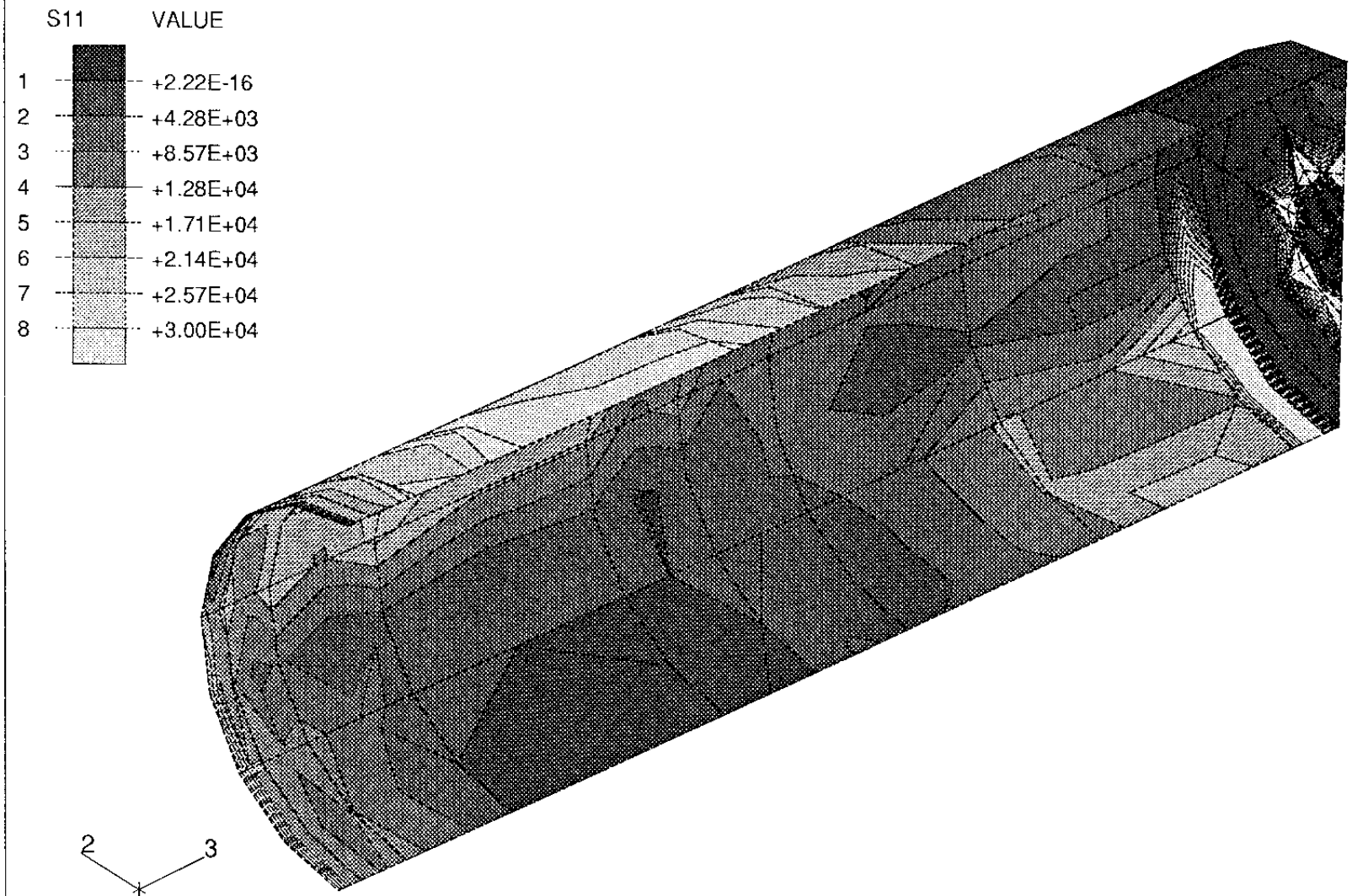

TIME COMPLETED IN THIS STEP +2.592E+06 TOTAL ACCUMULATED TIME +2.592E+06

ABAQUS VERSION 4-9-1 DATE: 21-Nov-91 TIME: 16:08:42 STEP 5 INCREMENT 153

APPENDIX IV

Results from a rock shear calculation
Symmetric shear
KBS3 copper/steel canister

Deformations (U) and strains (E) in the copper canister
just after shear

ABAQUS

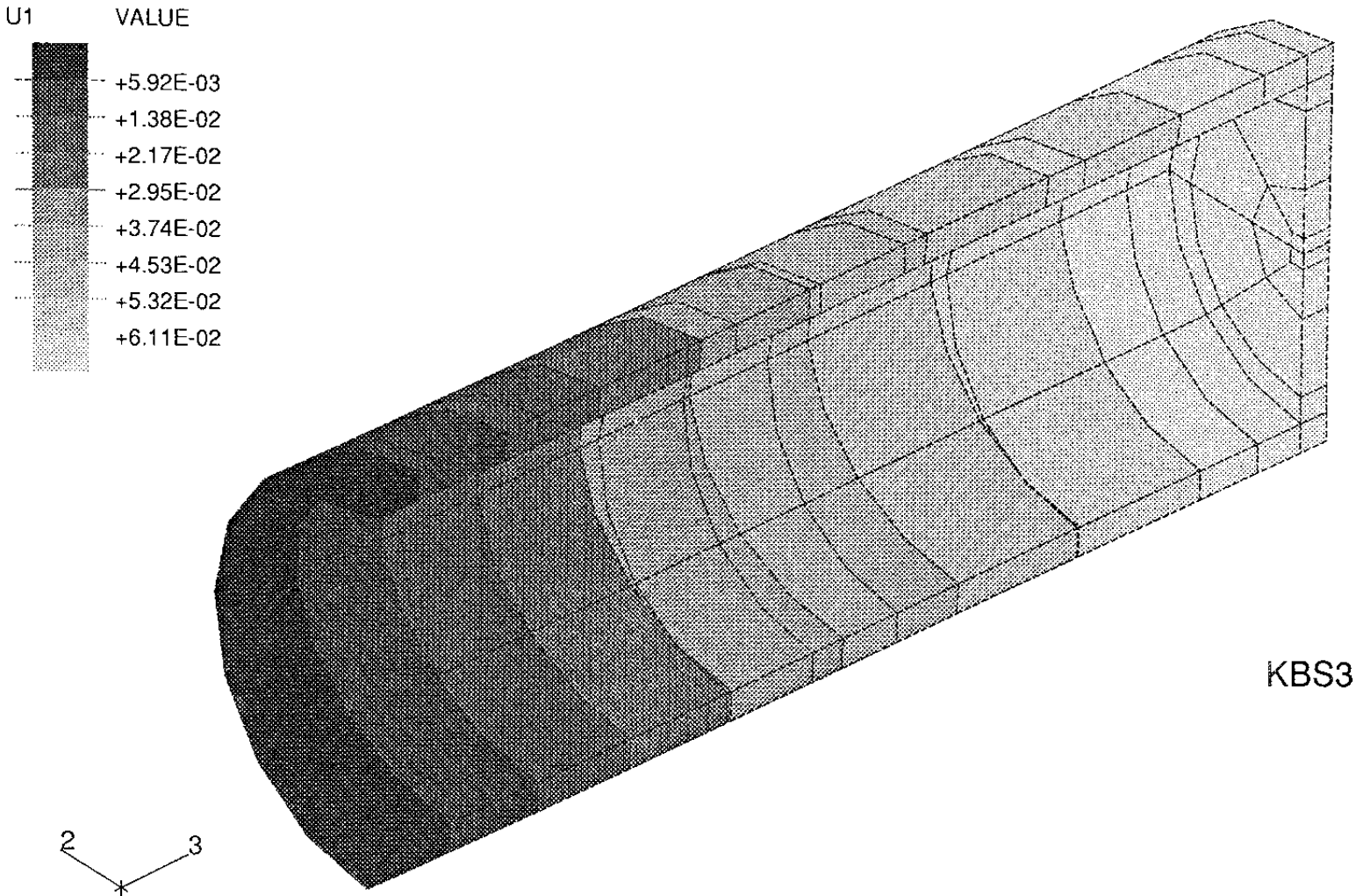

KBS3 - Copper

TIME COMPLETED IN THIS STEP +2.592E+06 TOTAL ACCUMULATED TIME +2.592E+06

ABAQUS VERSION 4-9-1 DATE: 21-Nov-91 TIME: 16:08:42 STEP 5 INCREMENT 153

ABAQUS

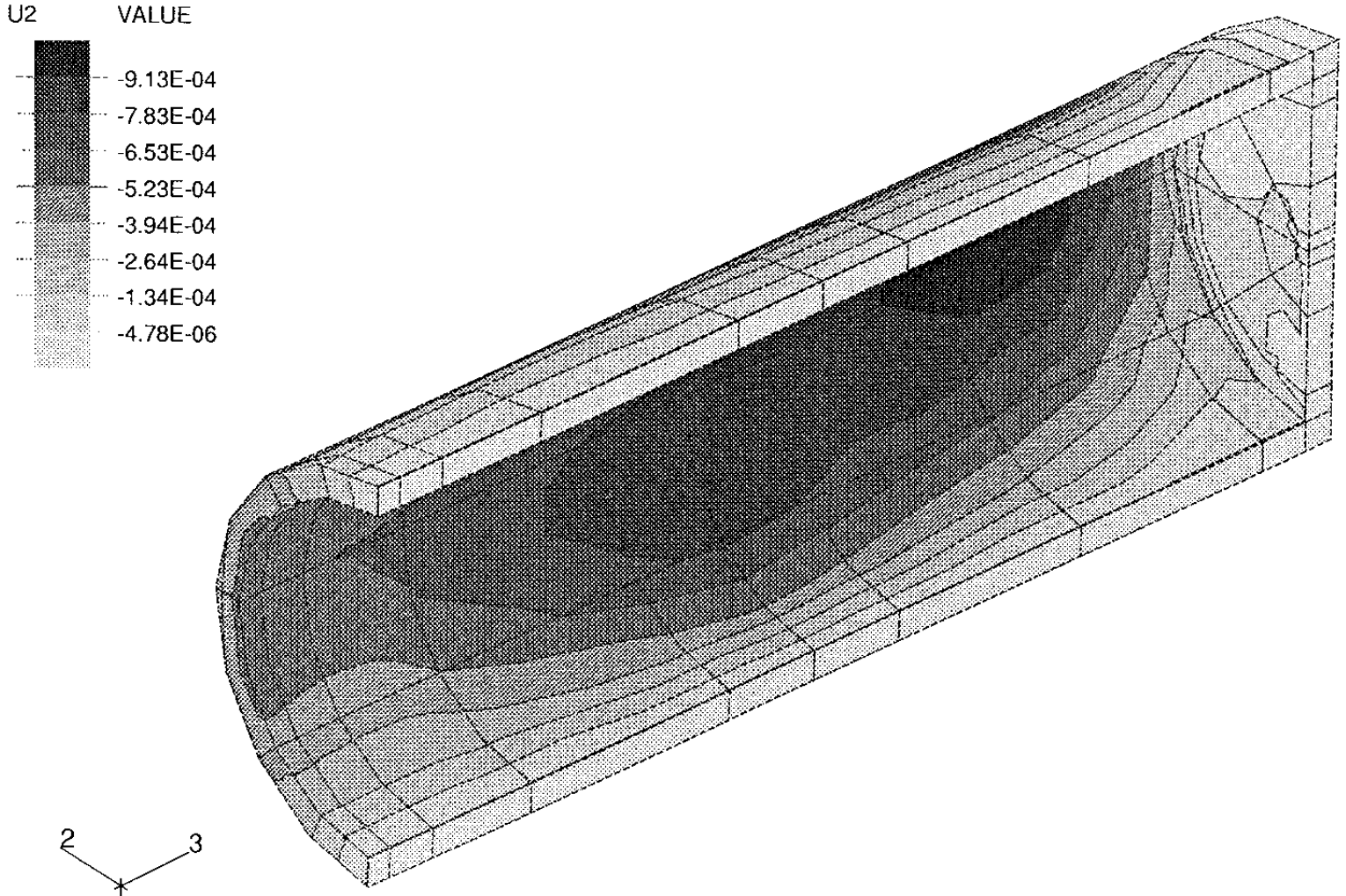

TIME COMPLETED IN THIS STEP +2.592E+06 TOTAL ACCUMULATED TIME +2.592E+06

ABAQUS VERSION 4-9-1 DATE: 21-Nov-91 TIME: 16:08:42 STEP 5 INCREMENT 153

ABAQUS

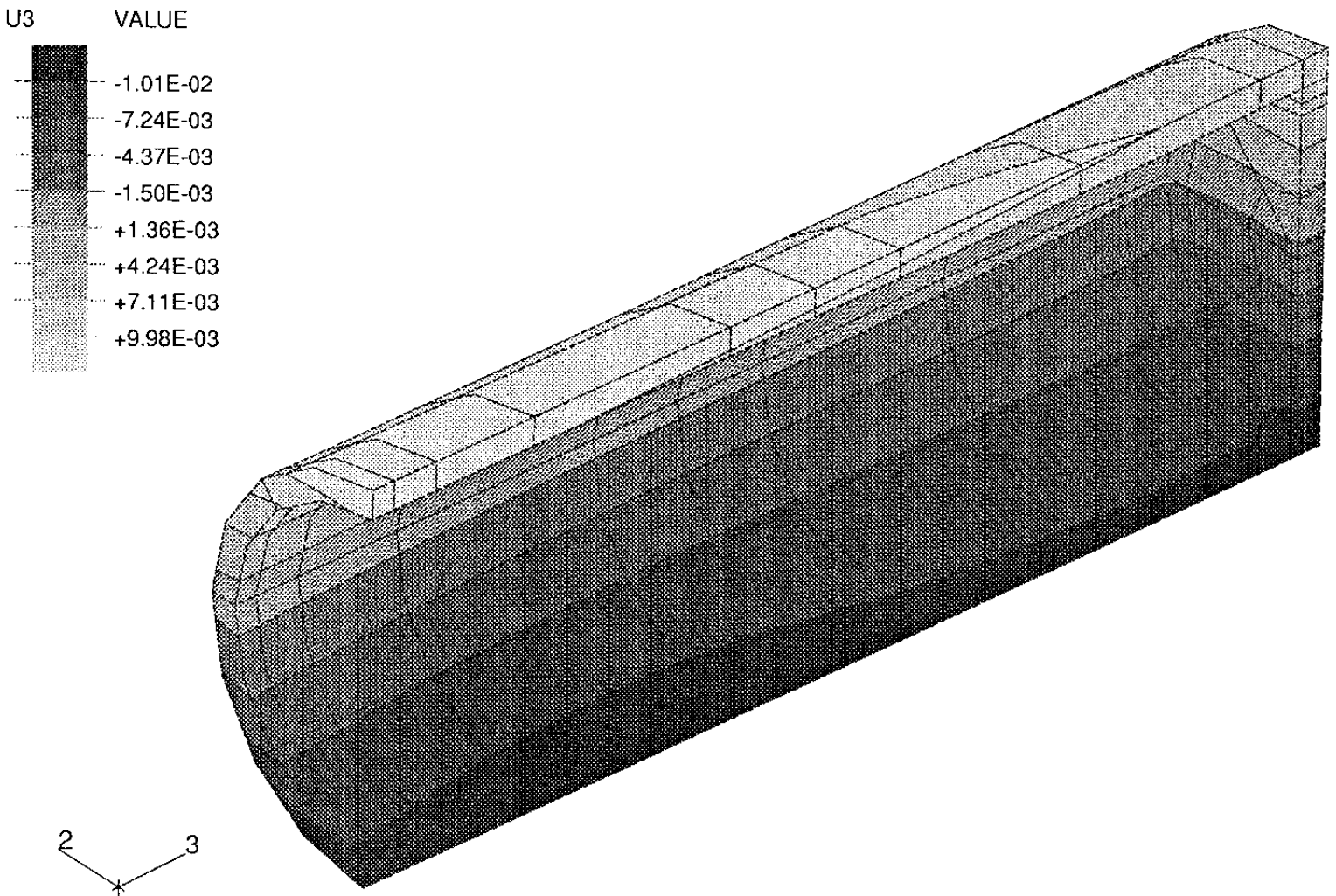

TIME COMPLETED IN THIS STEP +2.592E+06 TOTAL ACCUMULATED TIME +2.592E+06

ABAQUS VERSION 4-9-1 DATE: 21-Nov-91 TIME: 16:08:42 STEP 5 INCREMENT 153

ABAQUS

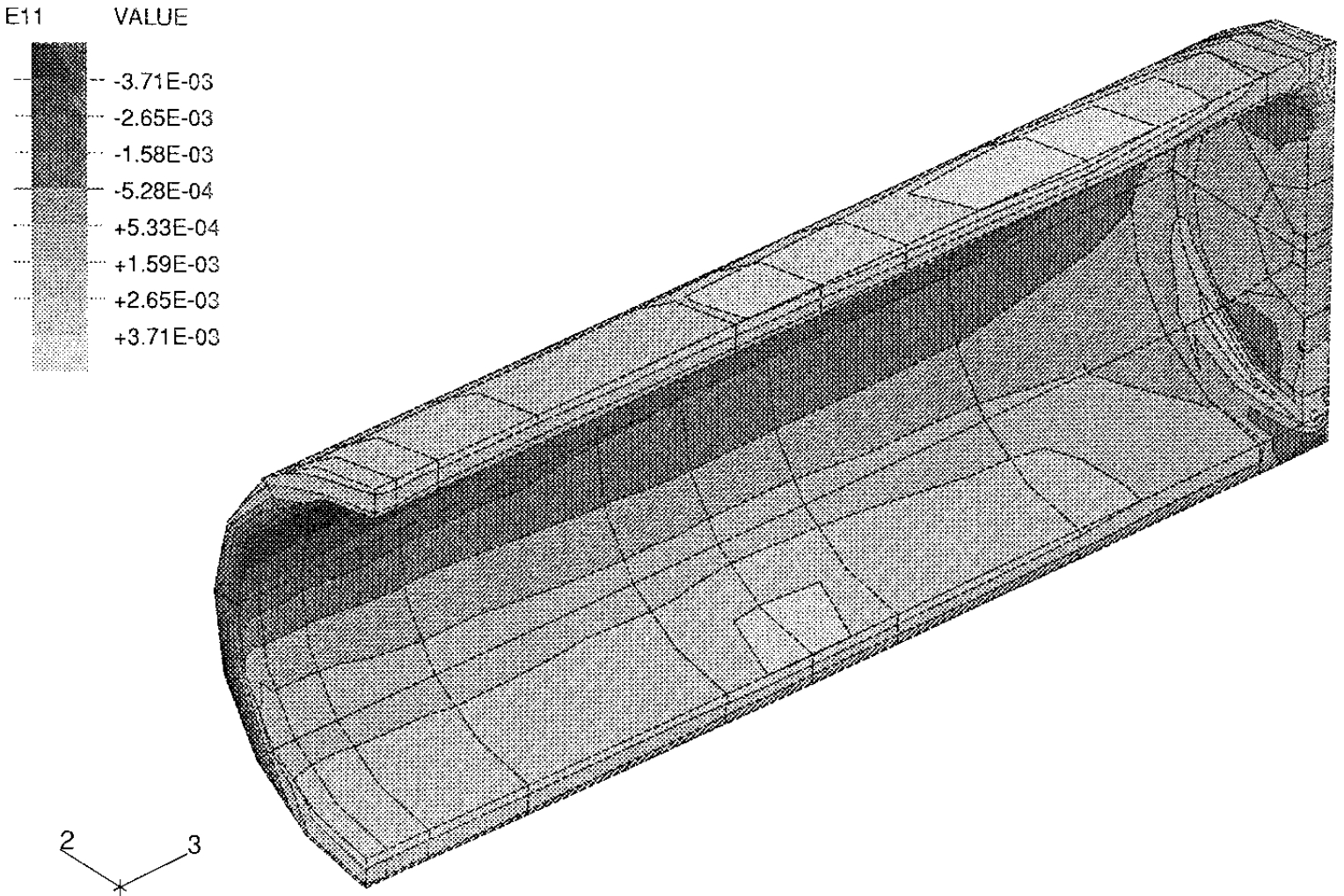

TIME COMPLETED IN THIS STEP +2.592E+06 TOTAL ACCUMULATED TIME +2.592E+06

ABAQUS VERSION 4-9-1 DATE: 21-Nov-91 TIME: 16:08:42 STEP 5 INCREMENT 153

ABAQUS

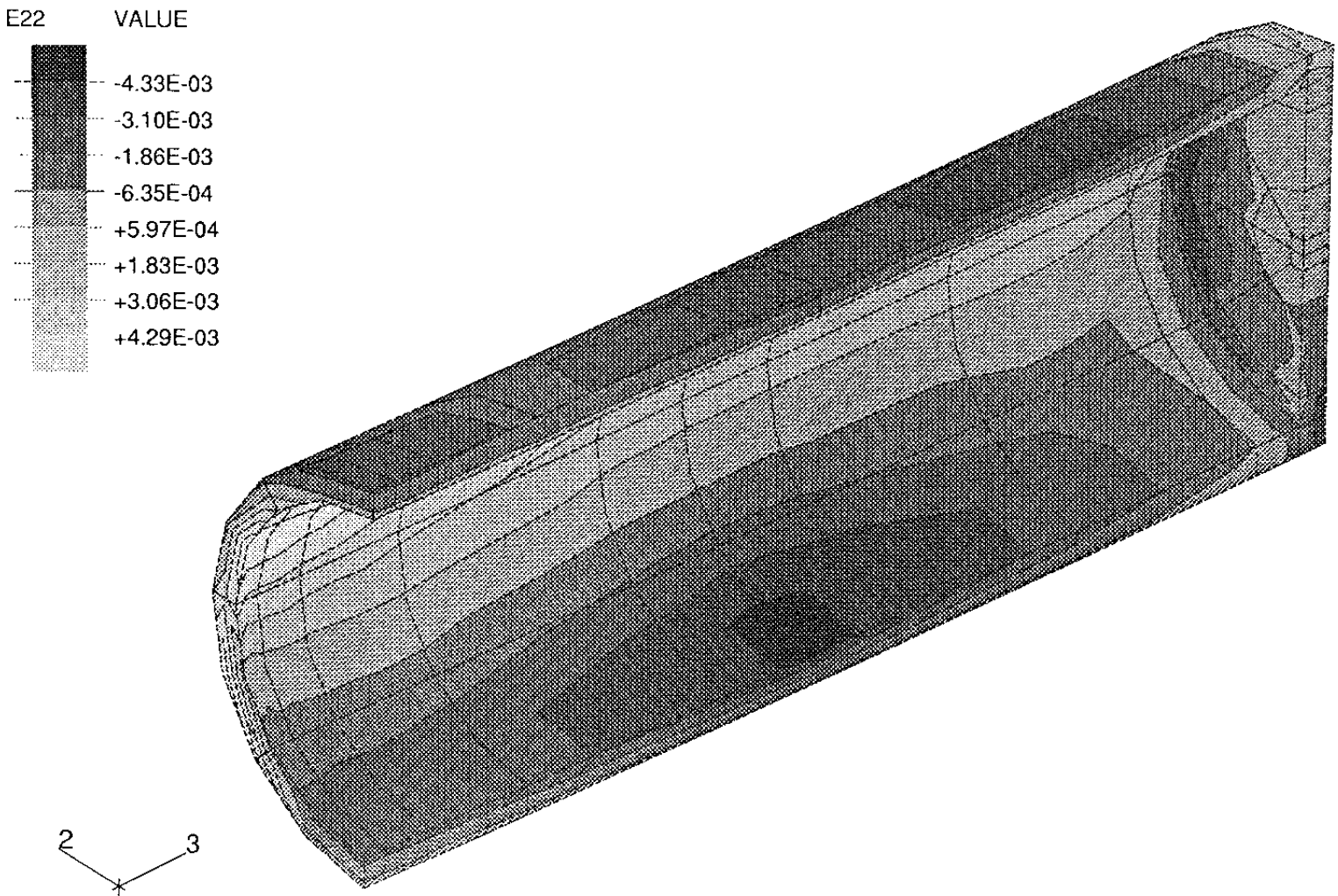

TIME COMPLETED IN THIS STEP +2.592E+06 TOTAL ACCUMULATED TIME +2.592E+06

ABAQUS VERSION 4-9-1 DATE: 21-Nov-91 TIME: 16:08:42 STEP 5 INCREMENT 153

ABAQUS

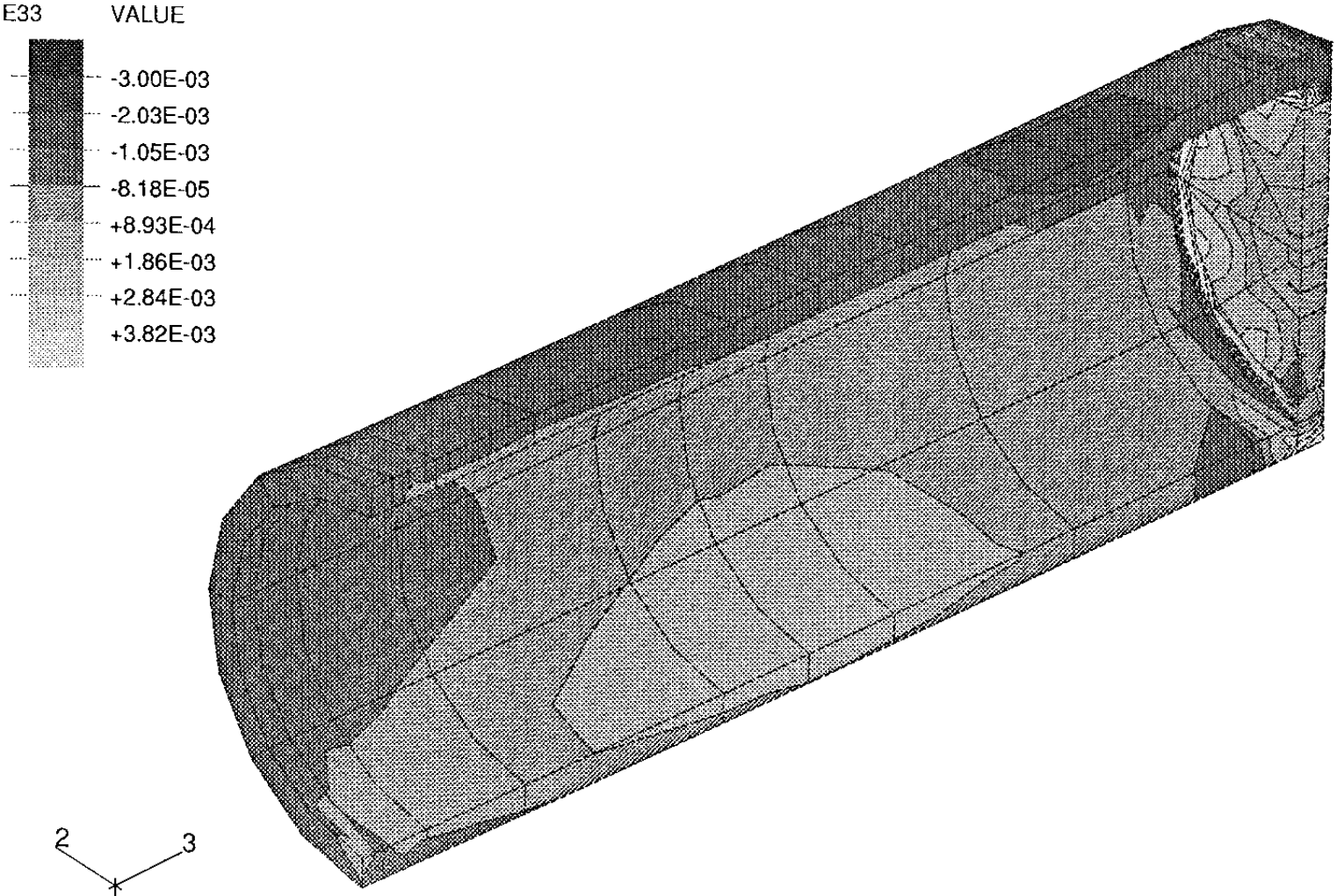

TIME COMPLETED IN THIS STEP +2.592E+06 TOTAL ACCUMULATED TIME +2.592E+06

ABAQUS VERSION 4-9-1 DATE: 21-Nov-91 TIME: 16:08:42 STEP 5 INCREMENT 153

ABAQUS

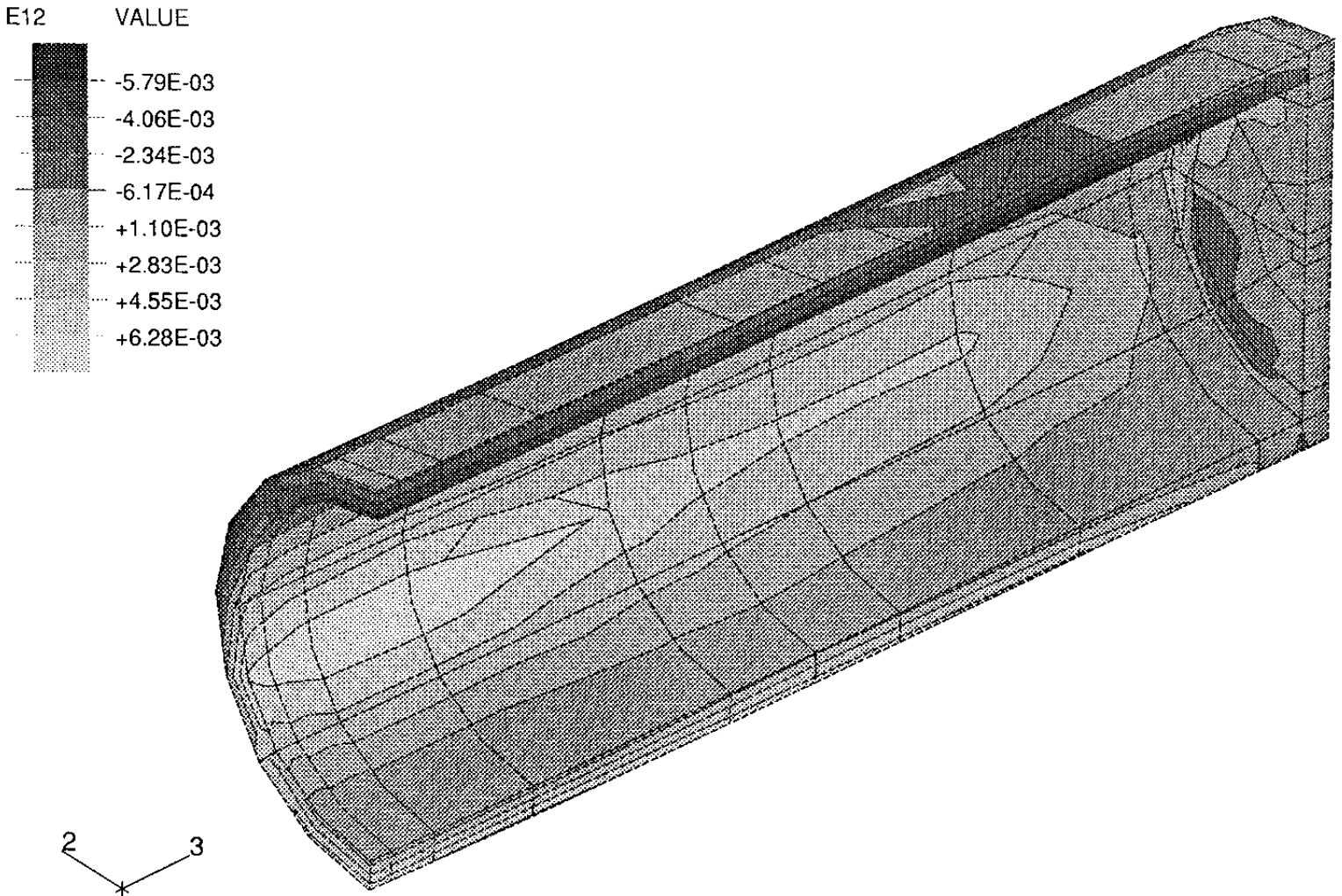

TIME COMPLETED IN THIS STEP +2.592E+06 TOTAL ACCUMULATED TIME +2.592E+06

ABAQUS VERSION 4-9-1 DATE: 21-Nov-91 TIME: 16:08:42 STEP 5 INCREMENT 153

ABAQUS

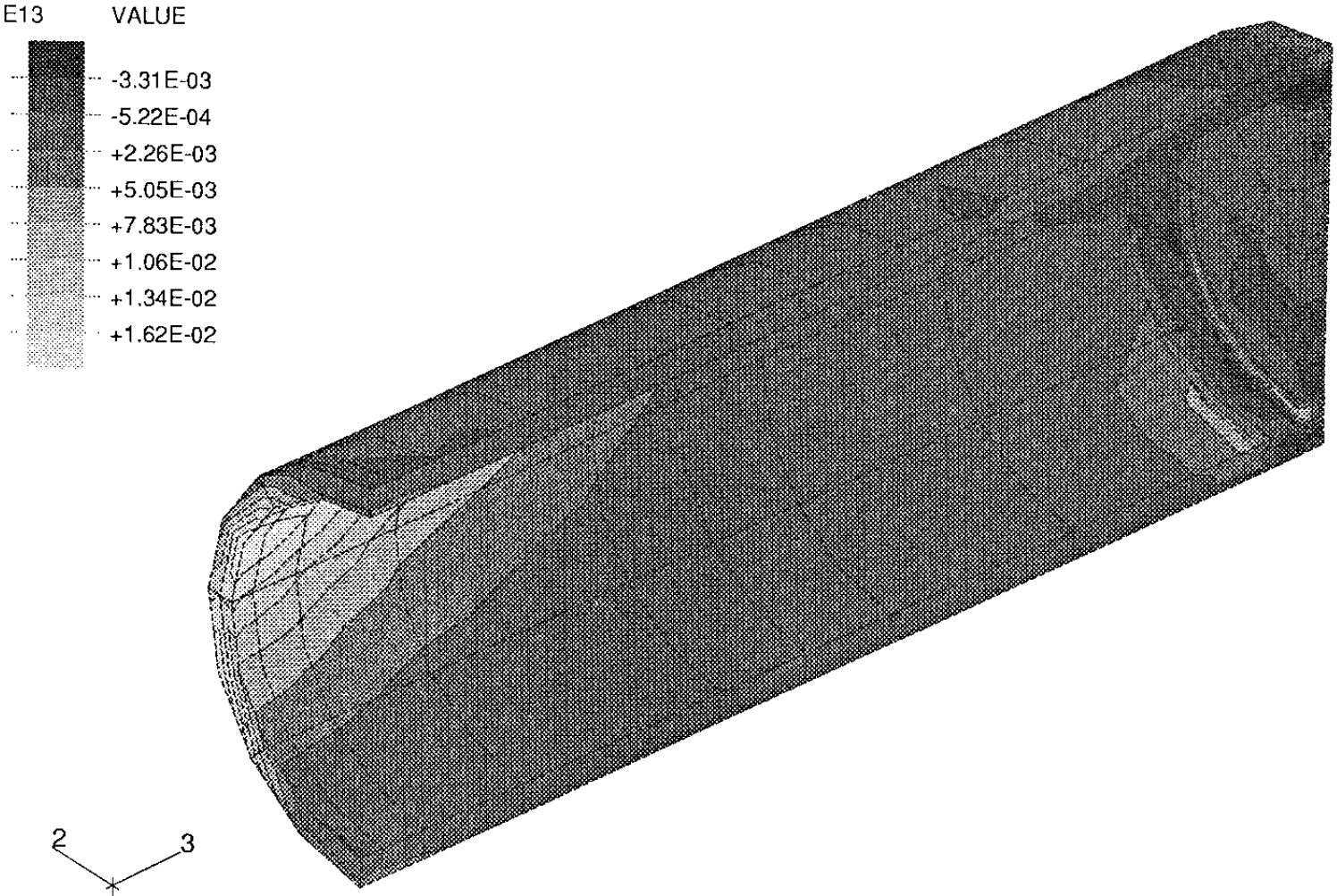

TIME COMPLETED IN THIS STEP +1.000E+09 TOTAL ACCUMULATED TIME +1.002E+09

ABAQUS VERSION 4-9-1 DATE: 22-Nov-91 TIME: 07:58:53 STEP 6 INCREMENT 175

ABAQUS

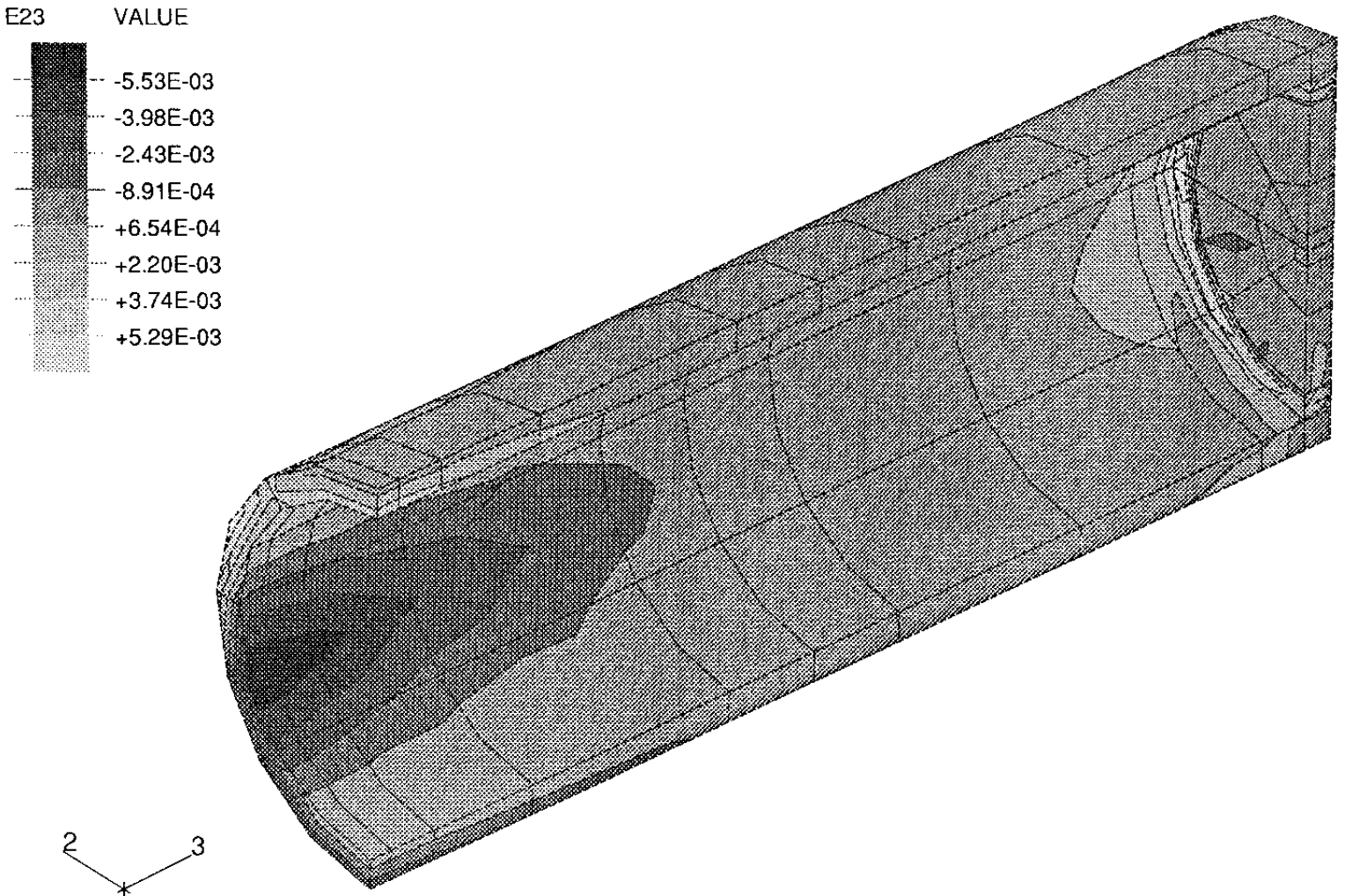

TIME COMPLETED IN THIS STEP +2.592E+06 TOTAL ACCUMULATED TIME +2.592E+06

ABAQUS VERSION 4-9-1 DATE: 21-Nov-91 TIME: 16:08:42 STEP 5 INCREMENT 153

APPENDIX V

Results from a rock shear calculation
Symmetric shear
KBS3 copper/steel canister

Deformations (U) and strains (E) in the copper canister after 10^9 sec. creep in the copper and consolidation in the clay

ABAQUS

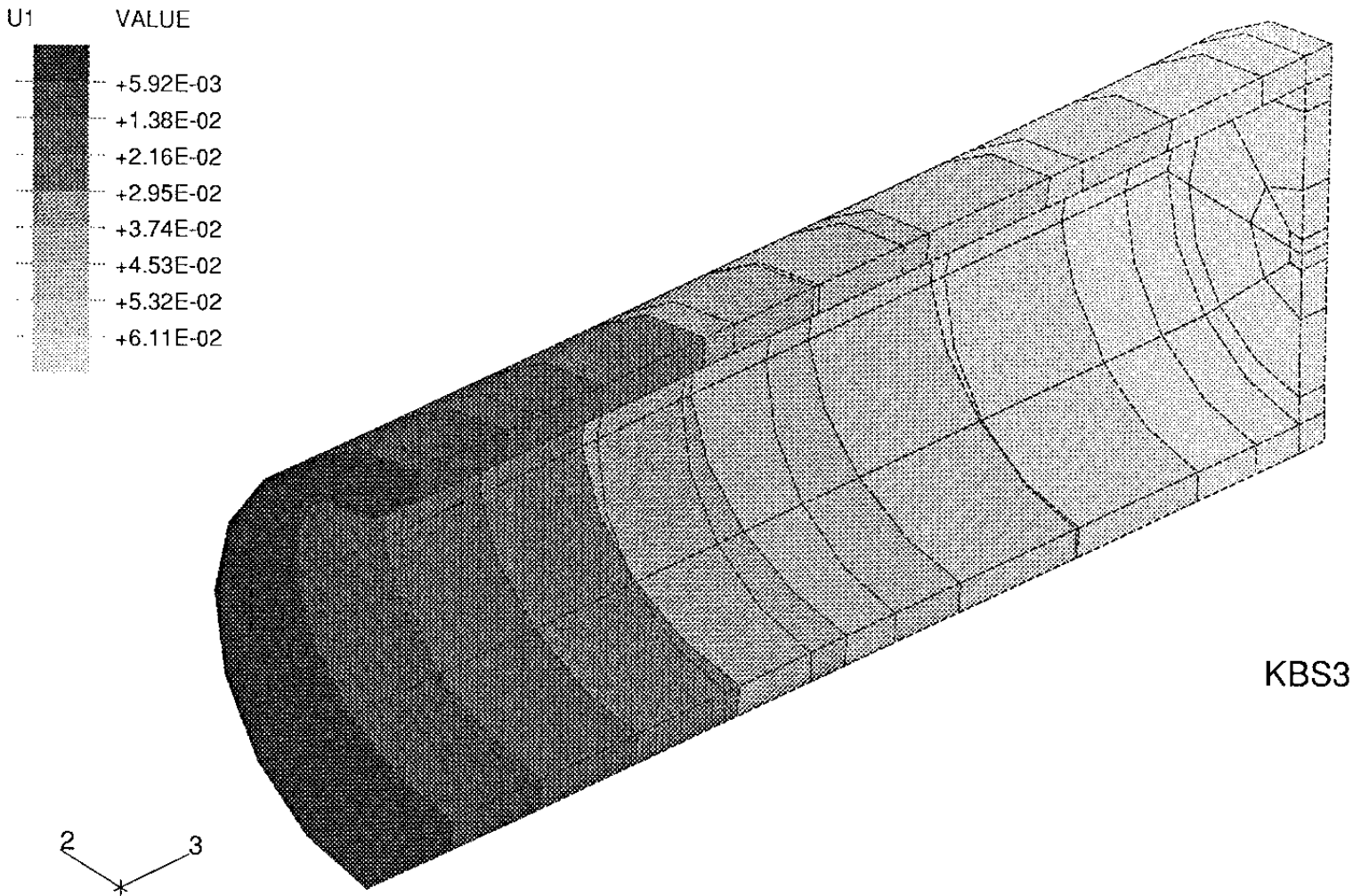

KBS3 - Copper

TIME COMPLETED IN THIS STEP +1.000E+09 TOTAL ACCUMULATED TIME +1.002E+09

ABAQUS VERSION 4-9-1 DATE: 22-Nov-91 TIME: 07:58:53 STEP 6 INCREMENT 175

ABAQUS

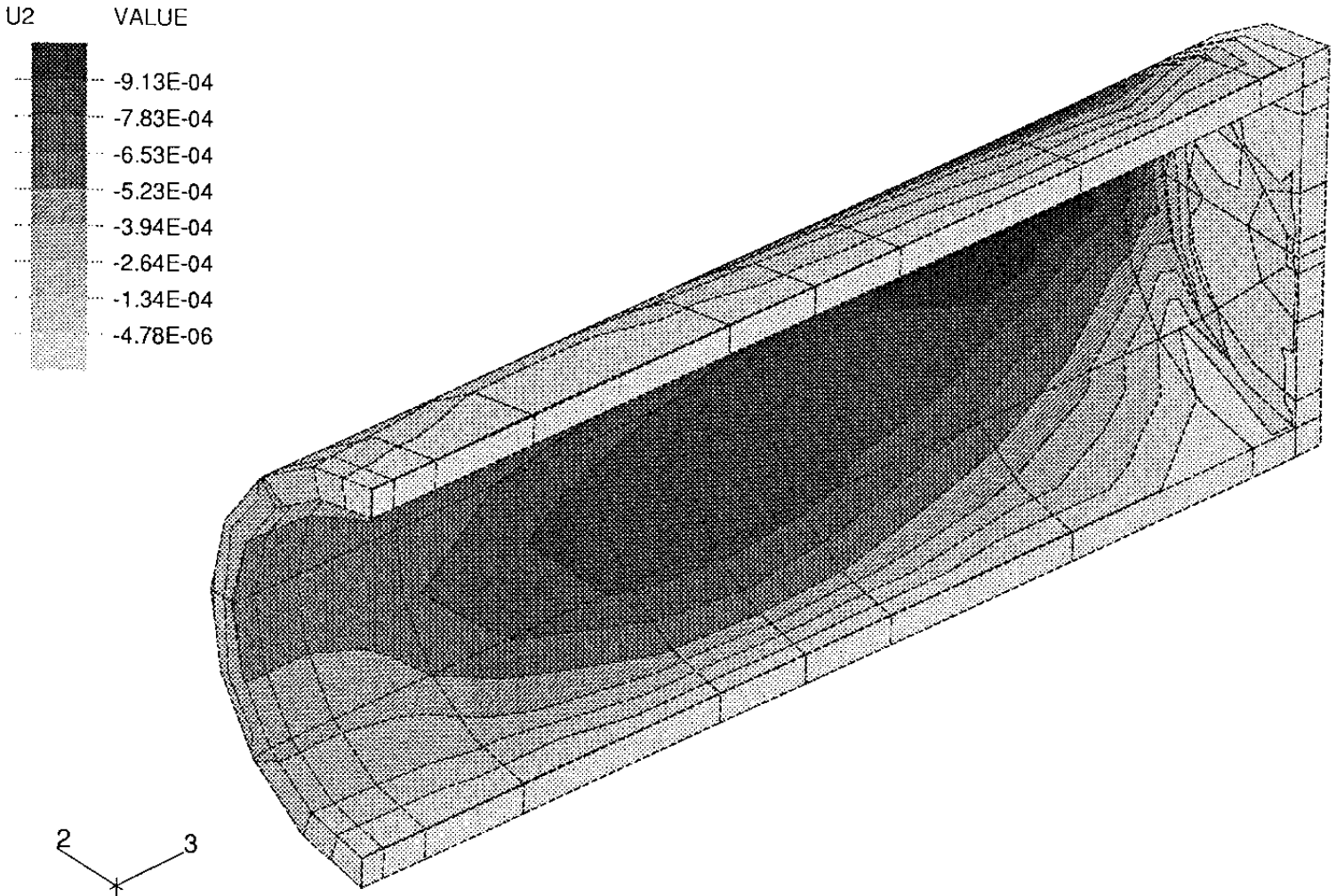

TIME COMPLETED IN THIS STEP +1.000E+09 TOTAL ACCUMULATED TIME +1.002E+09

ABAQUS VERSION 4-9-1 DATE: 22-Nov-91 TIME: 07:58:53 STEP 6 INCREMENT 175

ABAQUS

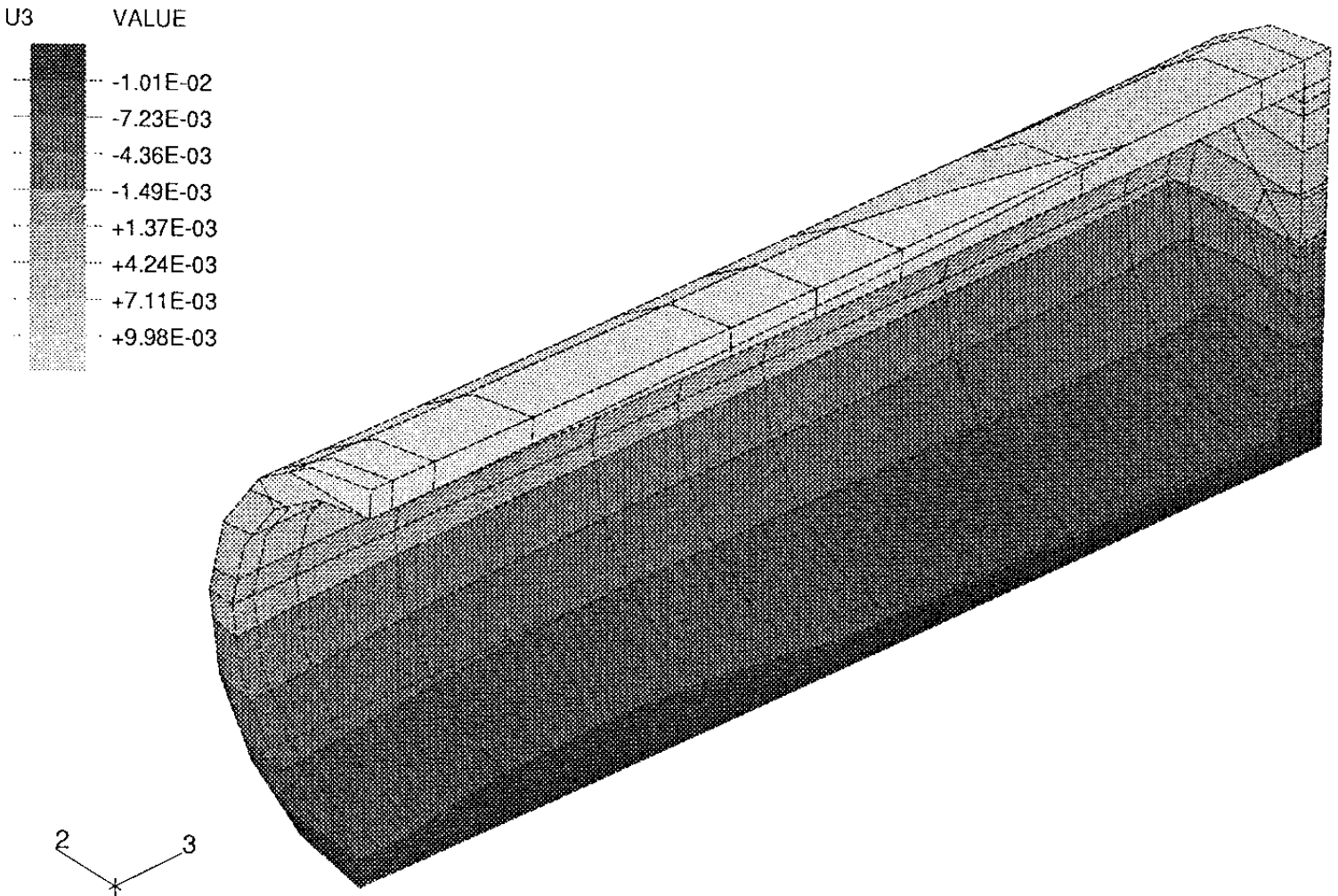

TIME COMPLETED IN THIS STEP +1.000E+09 TOTAL ACCUMULATED TIME +1.002E+09

ABAQUS VERSION 4-9-1 DATE: 22-Nov-91 TIME: 07:58:53 STEP 6 INCREMENT 175

ABAQUS

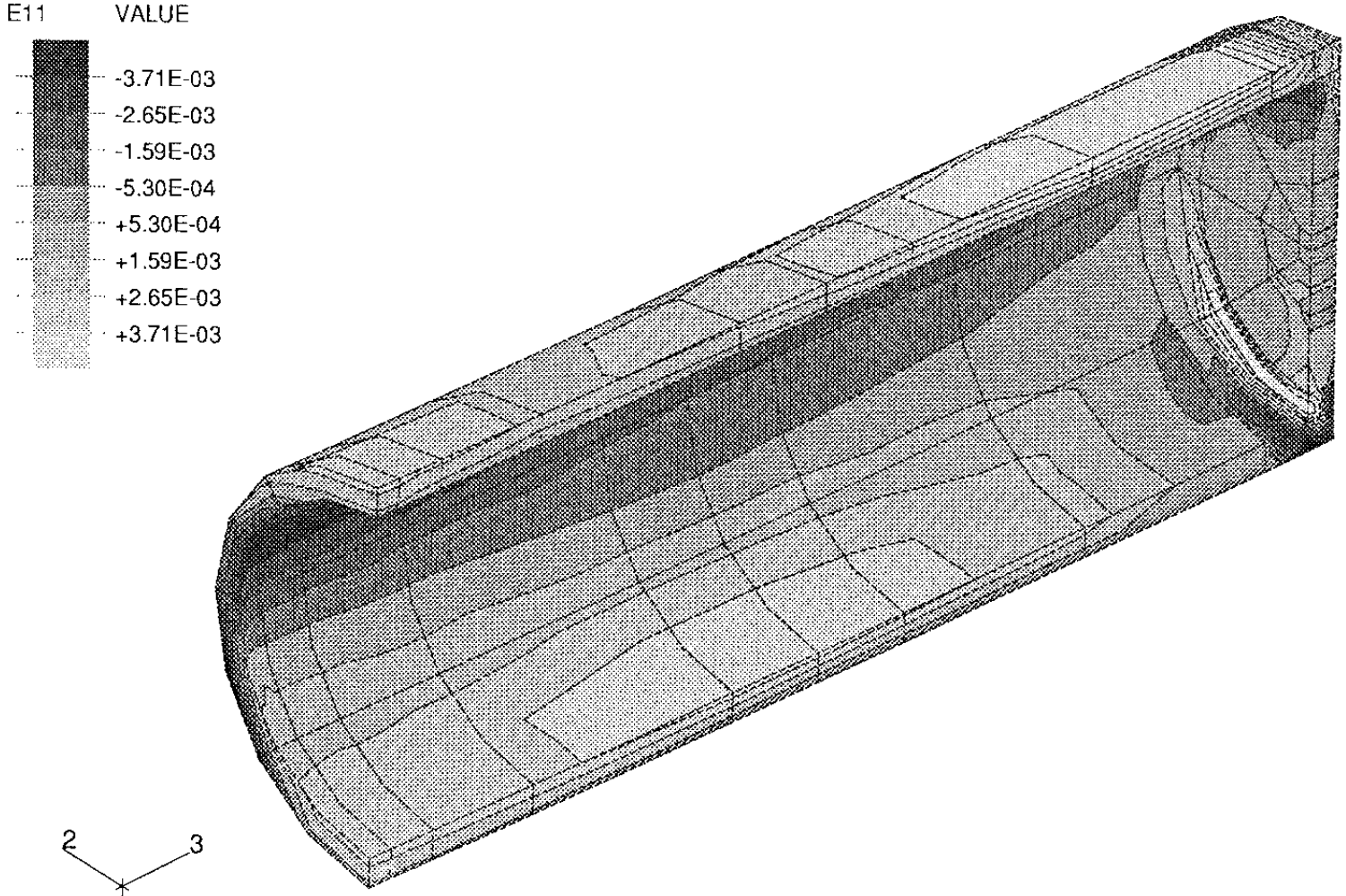

TIME COMPLETED IN THIS STEP +1.000E+09 TOTAL ACCUMULATED TIME +1.002E+09

ABAQUS VERSION 4-9-1 DATE: 22-Nov-91 TIME: 07:58:53 STEP 6 INCREMENT 175

ABAQUS

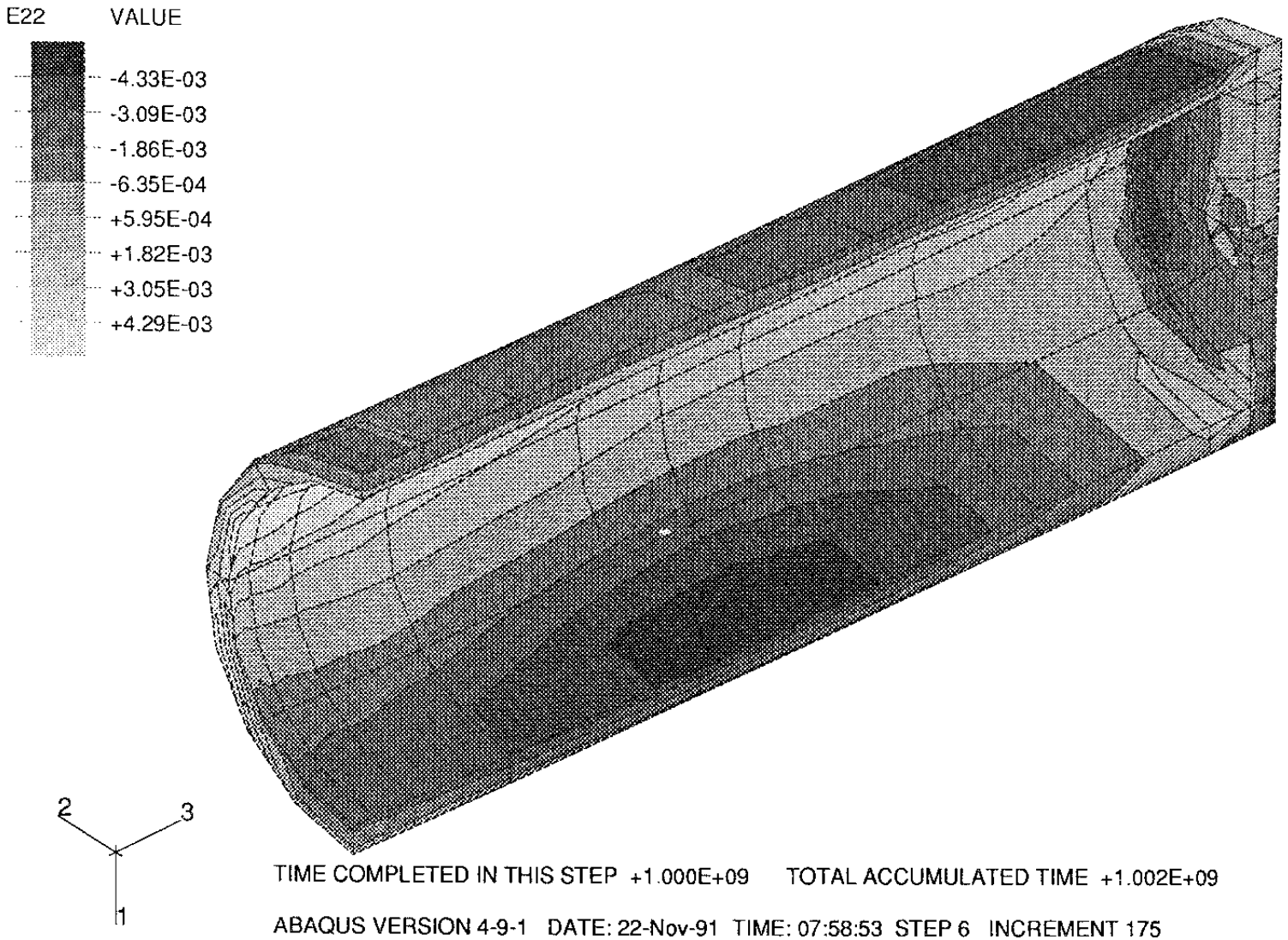

TIME COMPLETED IN THIS STEP +1.000E+09 TOTAL ACCUMULATED TIME +1.002E+09

ABAQUS VERSION 4-9-1 DATE: 22-Nov-91 TIME: 07:58:53 STEP 6 INCREMENT 175

ABAQUS

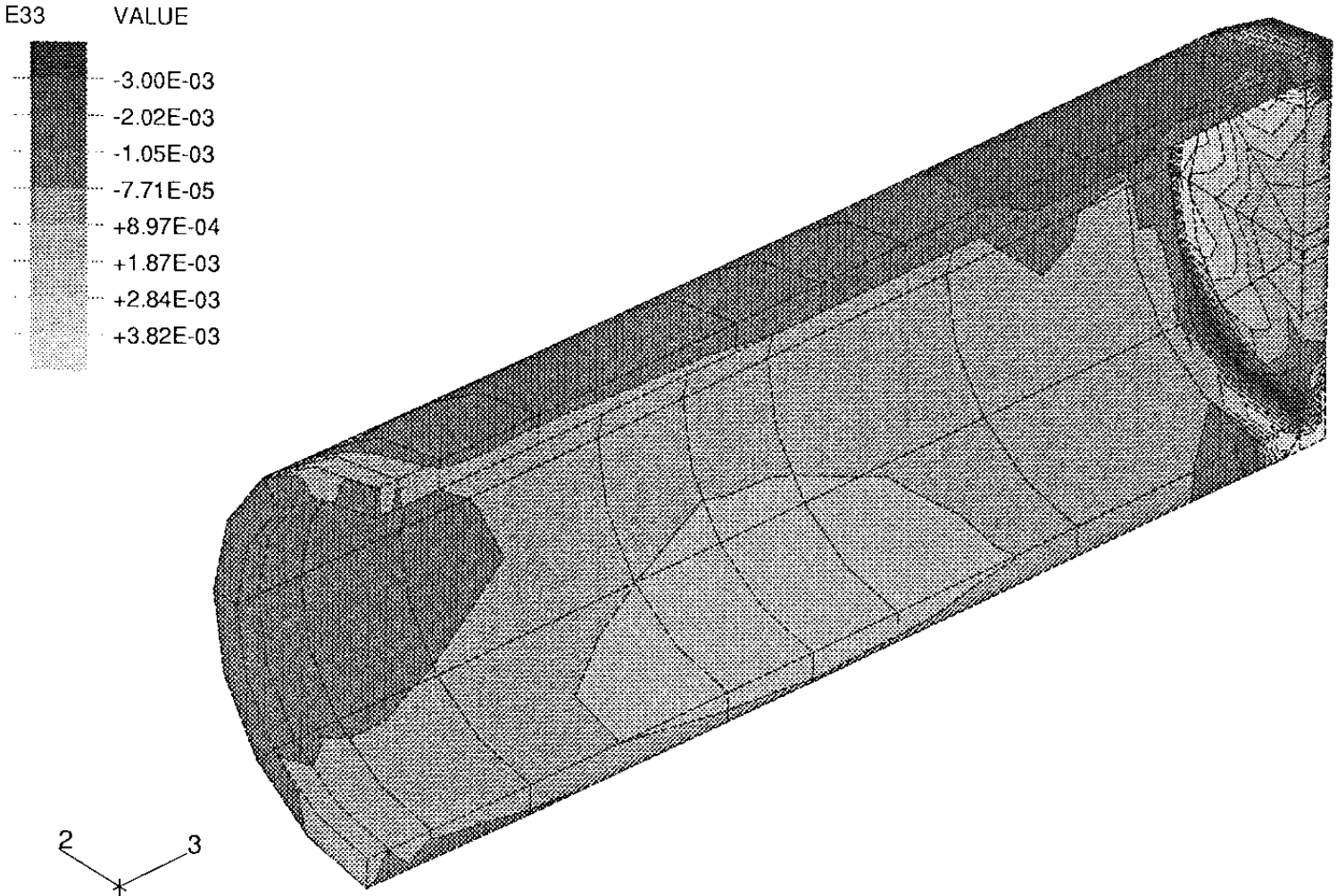

TIME COMPLETED IN THIS STEP +1.000E+09 TOTAL ACCUMULATED TIME +1.002E+09

ABAQUS VERSION 4-9-1 DATE: 22-Nov-91 TIME: 07:58:53 STEP 6 INCREMENT 175

ABAQUS

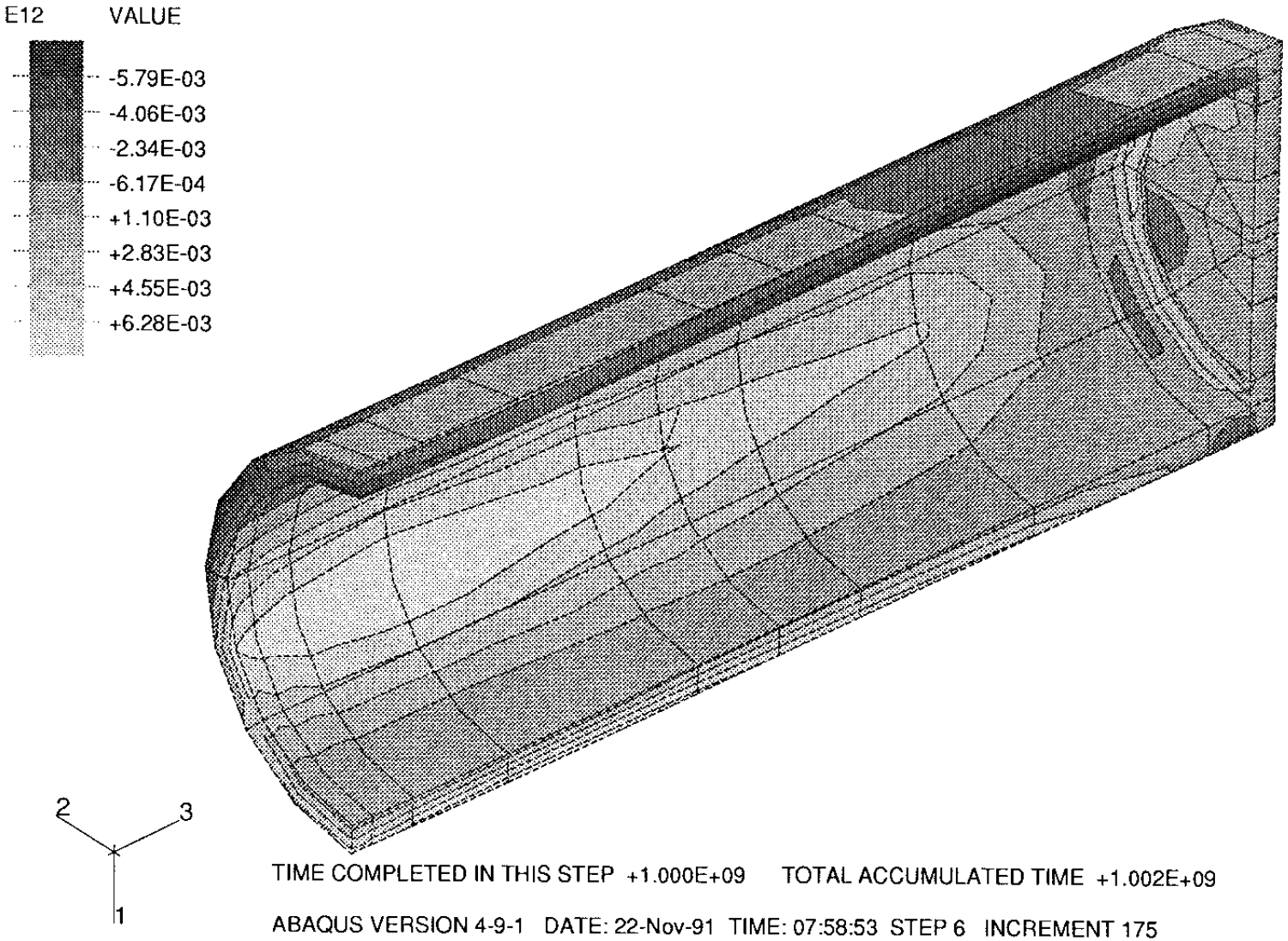

TIME COMPLETED IN THIS STEP +1.000E+09 TOTAL ACCUMULATED TIME +1.002E+09

ABAQUS VERSION 4-9-1 DATE: 22-Nov-91 TIME: 07:58:53 STEP 6 INCREMENT 175

ABAQUS

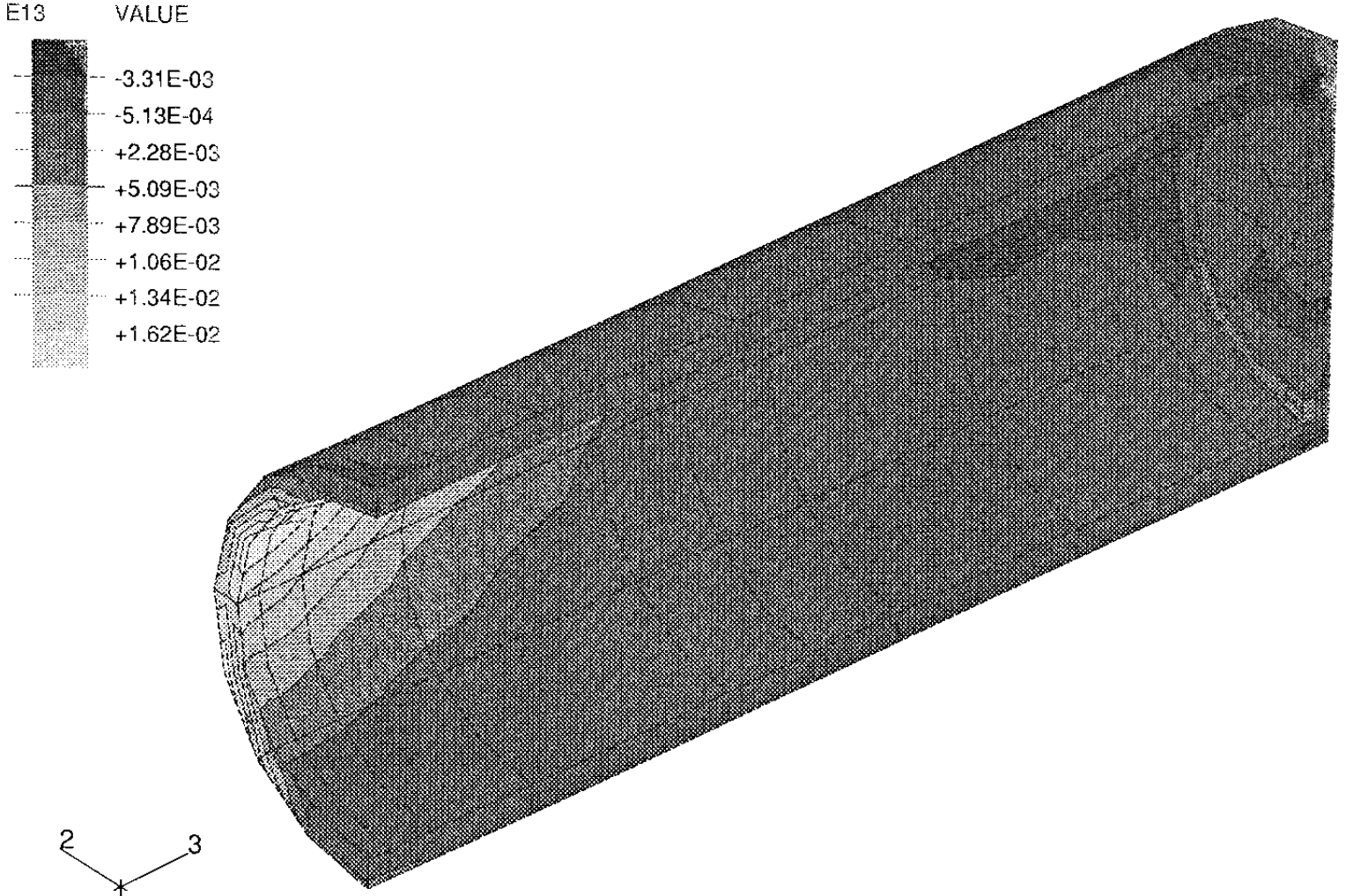

TIME COMPLETED IN THIS STEP +2.592E+06 TOTAL ACCUMULATED TIME +2.592E+06

ABAQUS VERSION 4-9-1 DATE: 21-Nov-91 TIME: 16:08:42 STEP 5 INCREMENT 153

ABAQUS

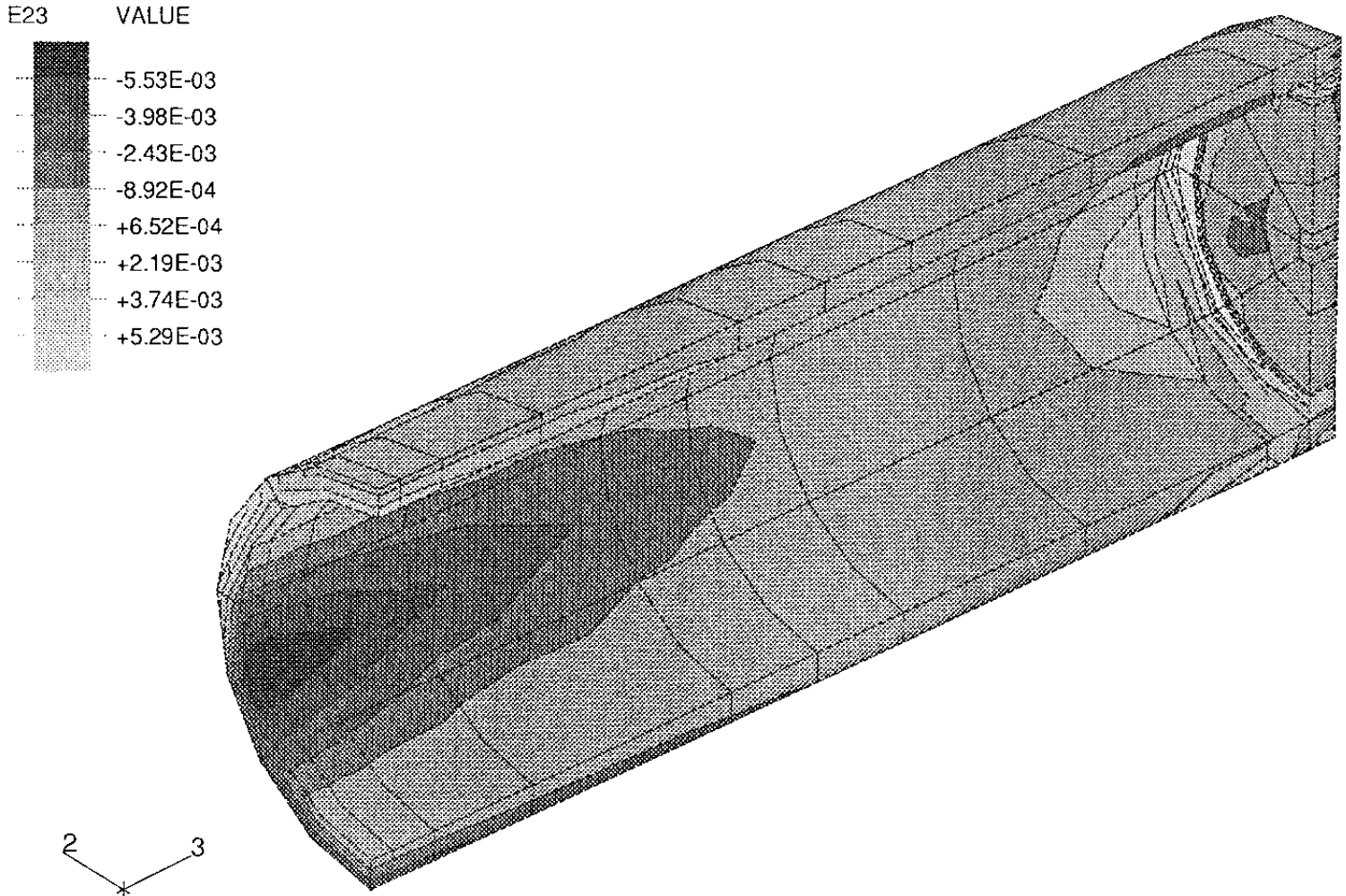

TIME COMPLETED IN THIS STEP +1.000E+09 TOTAL ACCUMULATED TIME +1.002E+09

ABAQUS VERSION 4-9-1 DATE: 22-Nov-91 TIME: 07:58:53 STEP 6 INCREMENT 175

APPENDIX VI

Results from a rock shear calculation
Symmetric shear
KBS3 copper/steel canister

Deformations (U) and strains (E) in the copper canister after 10^9 sec. consolidation in the clay

ABAQUS

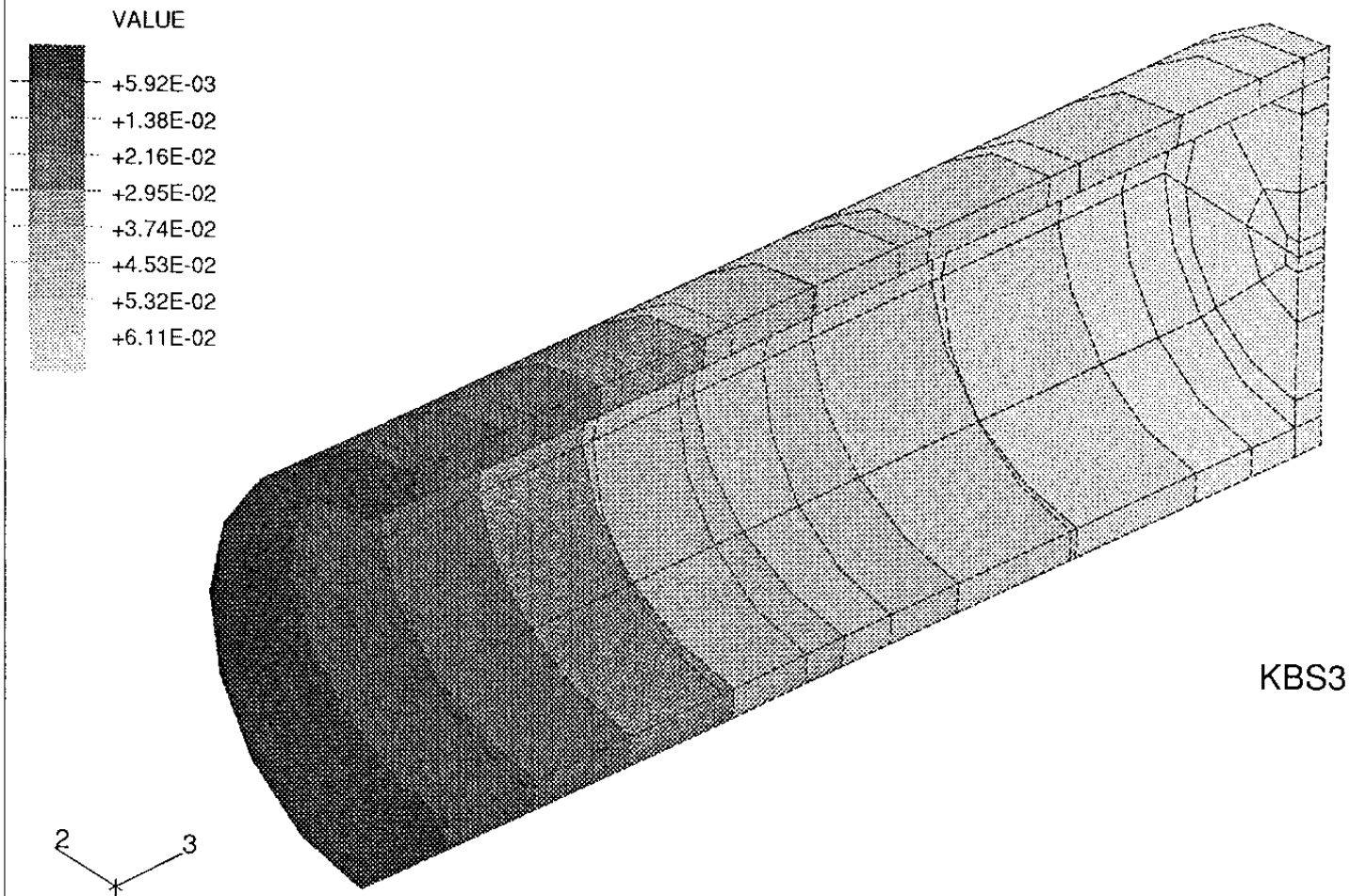

KBS3 - Copper No creep

TIME COMPLETED IN THIS STEP +1.000E+09 TOTAL ACCUMULATED TIME +1.002E+09

ABAQUS VERSION 4-9-1 DATE: 4-Dec-91 TIME: 08:21:02 STEP 6 INCREMENT 48

ABAQUS

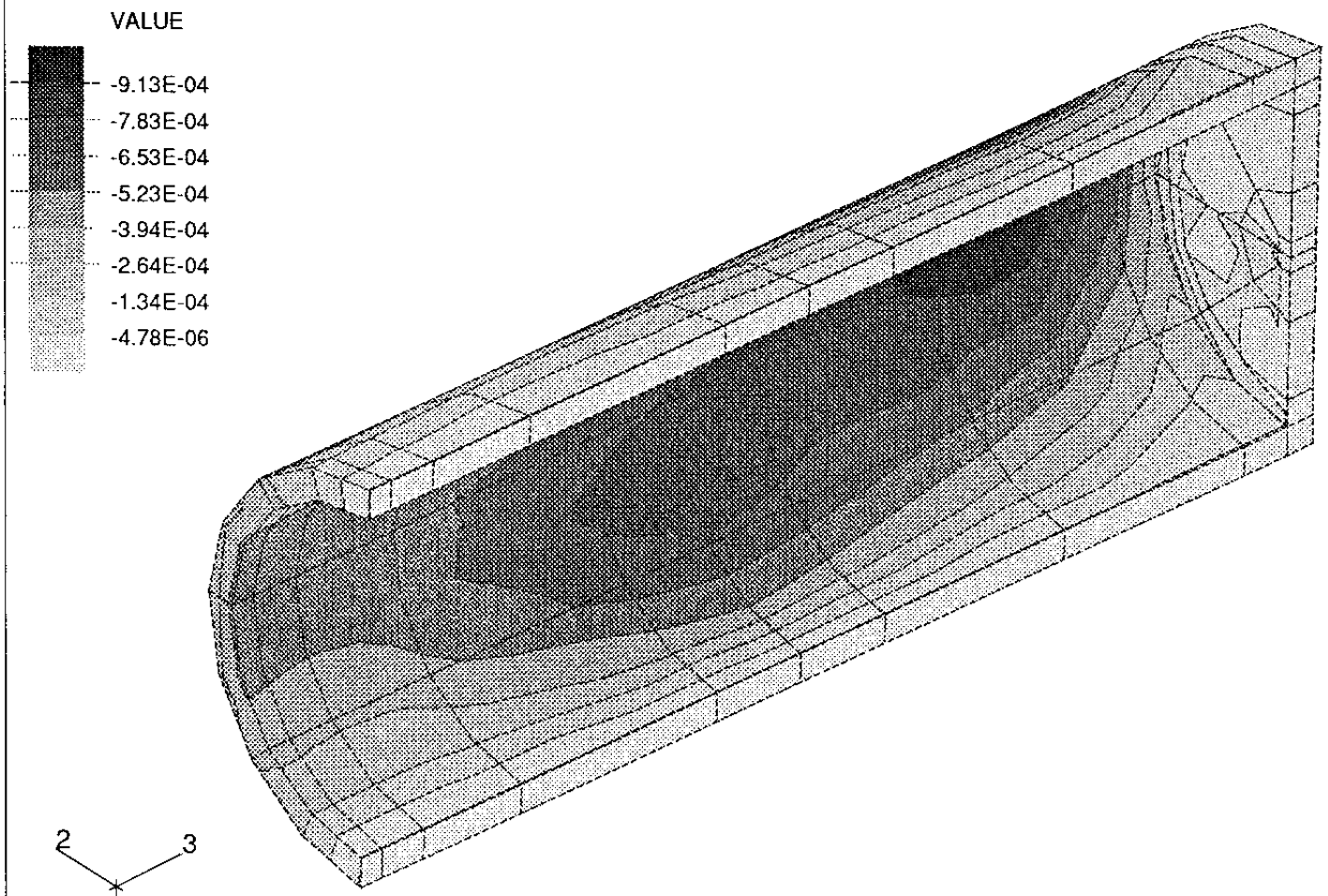

TIME COMPLETED IN THIS STEP +1.000E+09 TOTAL ACCUMULATED TIME +1.002E+09

ABAQUS VERSION 4-9-1 DATE: 4-Dec-91 TIME: 08:21:02 STEP 6 INCREMENT 48

ABAQUS

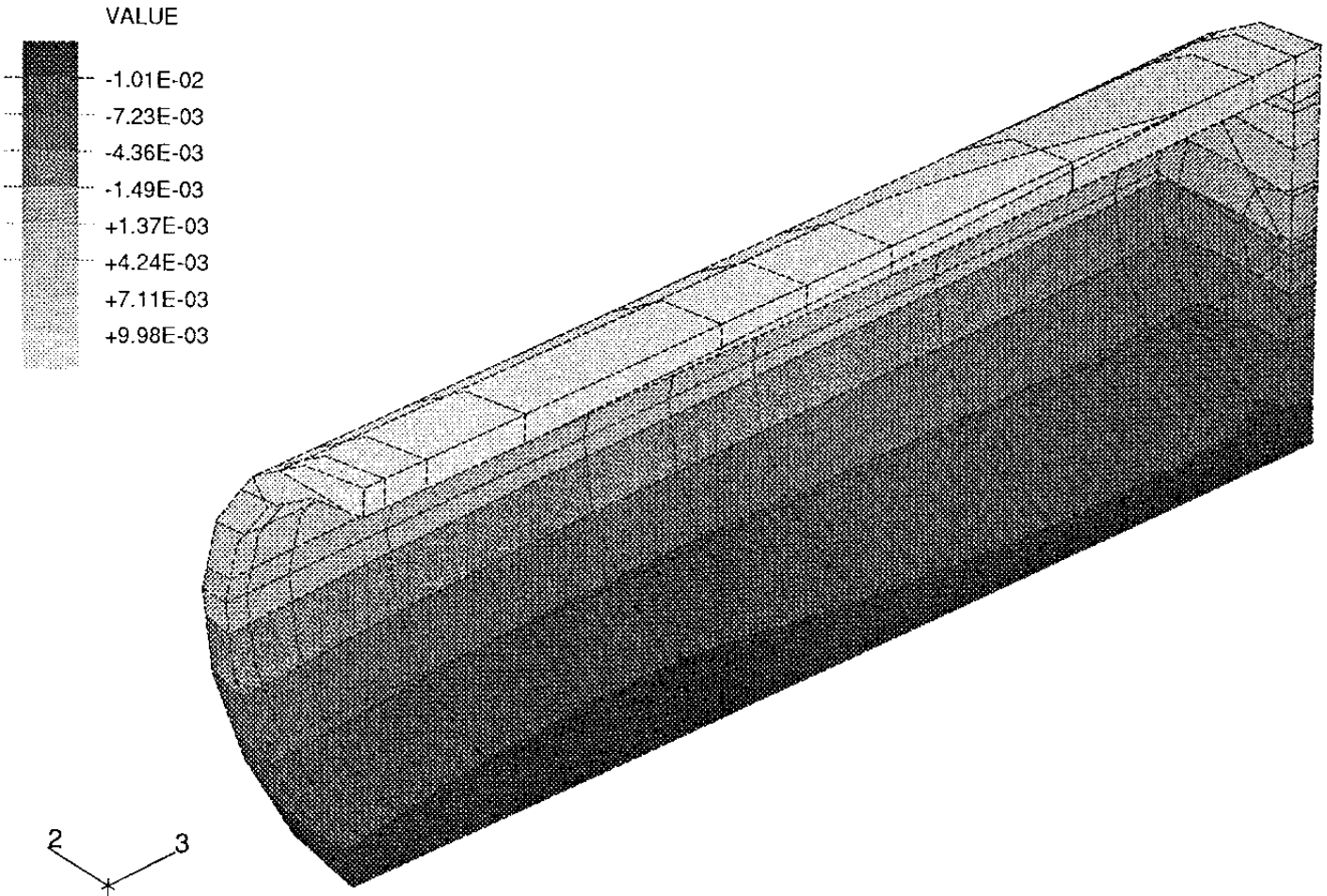

TIME COMPLETED IN THIS STEP +1.000E+09 TOTAL ACCUMULATED TIME +1.002E+09

ABAQUS VERSION 4-9-1 DATE: 4-Dec-91 TIME: 08:21:02 STEP 6 INCREMENT 48

ABAQUS

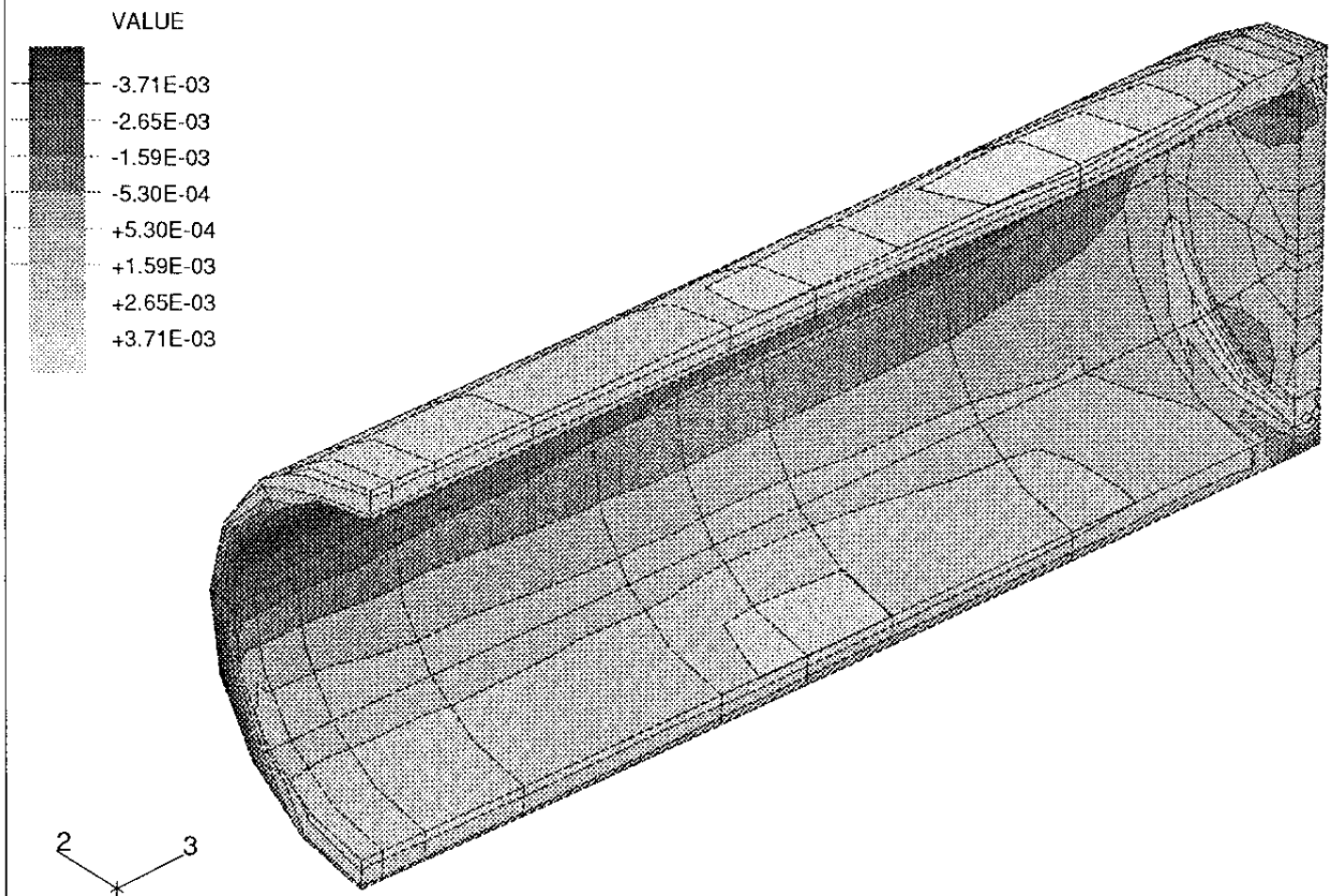

TIME COMPLETED IN THIS STEP +1.000E+09 TOTAL ACCUMULATED TIME +1.002E+09

ABAQUS VERSION 4-9-1 DATE: 4-Dec-91 TIME: 08:21:02 STEP 6 INCREMENT 48

ABAQUS

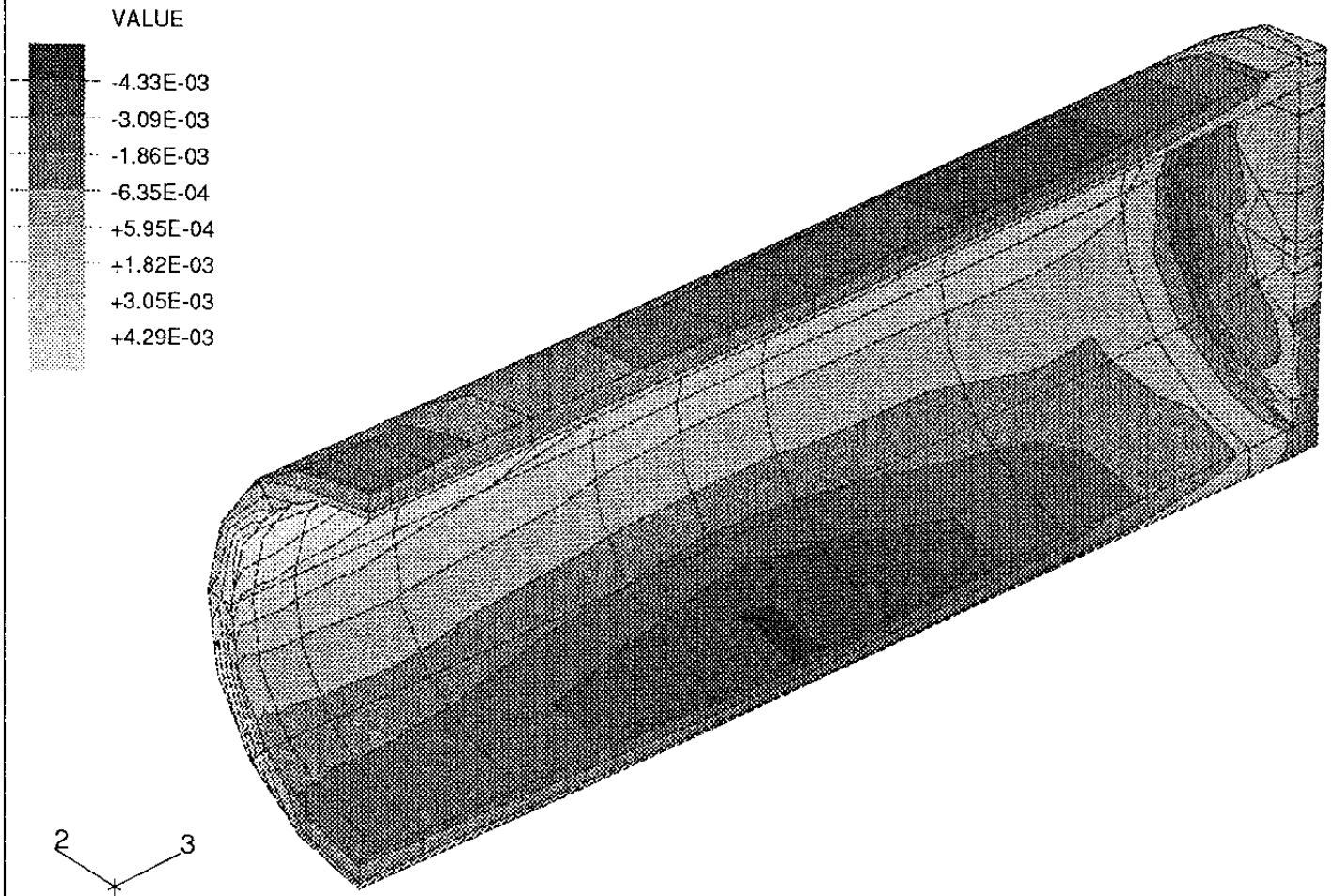

TIME COMPLETED IN THIS STEP +1.000E+09 TOTAL ACCUMULATED TIME +1.002E+09

ABAQUS VERSION 4-9-1 DATE: 4-Dec-91 TIME: 08:21:02 STEP 6 INCREMENT 48

ABAQUS

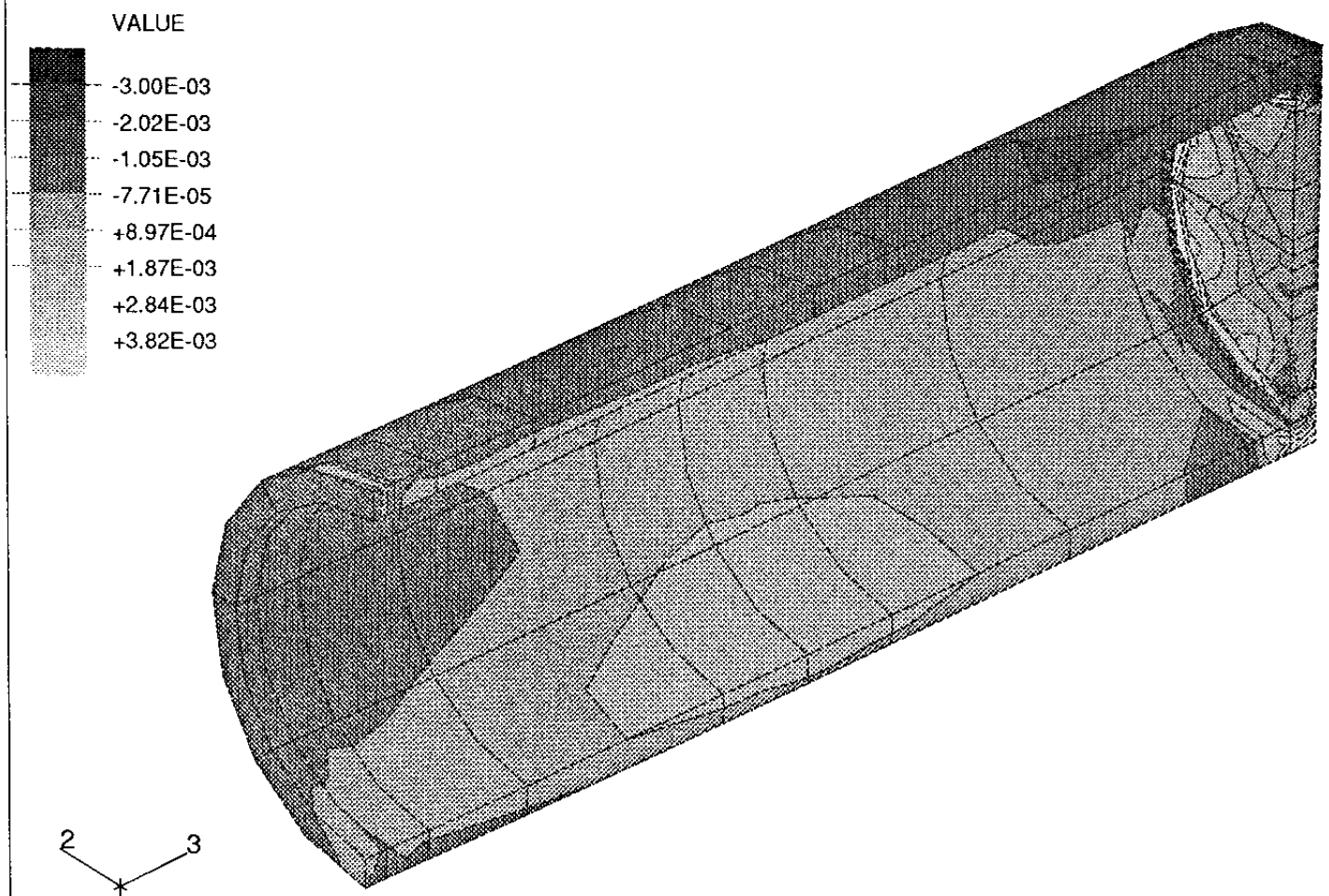

TIME COMPLETED IN THIS STEP +1.000E+09 TOTAL ACCUMULATED TIME +1.002E+09

ABAQUS VERSION 4-9-1 DATE: 4-Dec-91 TIME: 08:21:02 STEP 6 INCREMENT 48

ABAQUS

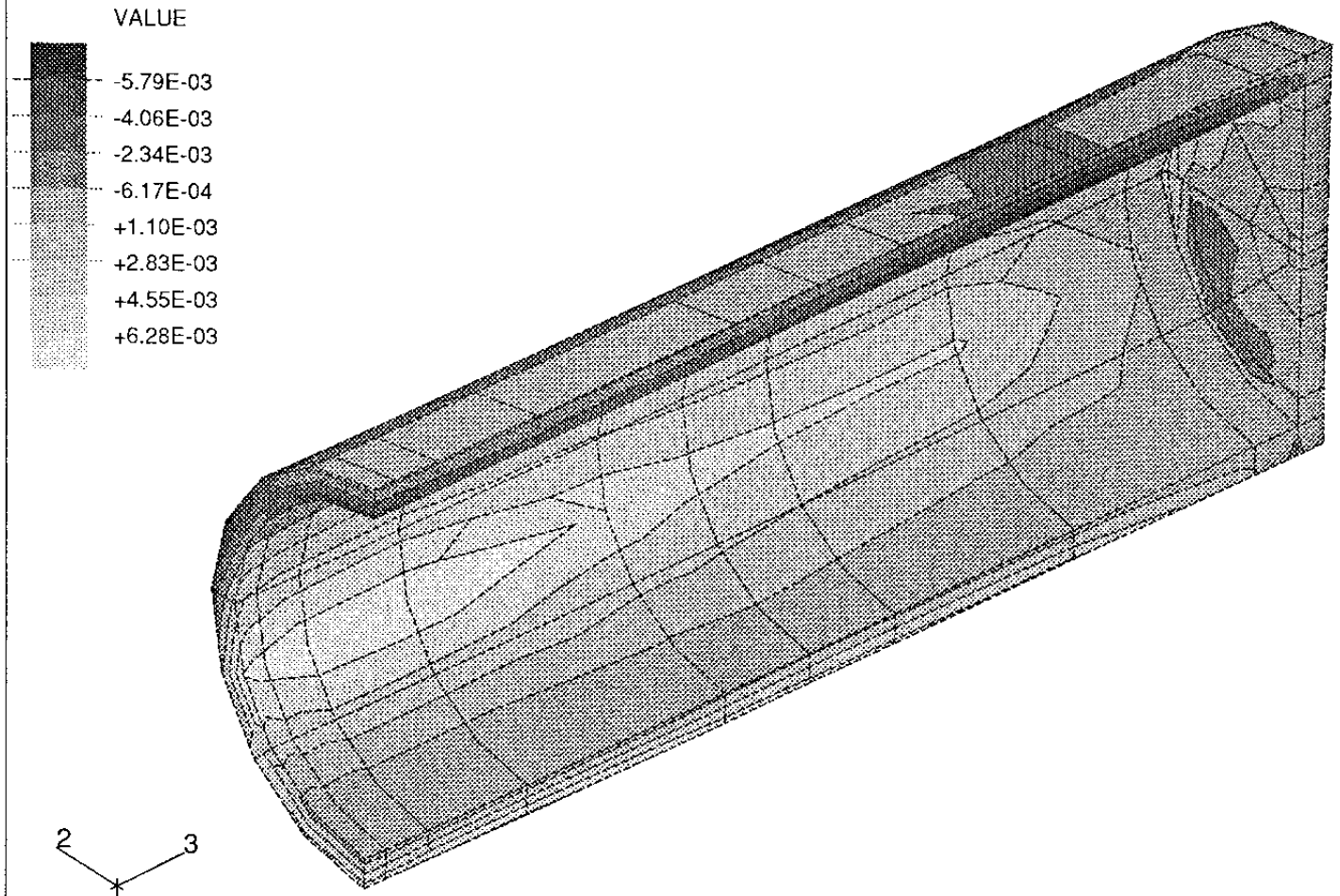

TIME COMPLETED IN THIS STEP +1.000E+09 TOTAL ACCUMULATED TIME +1.002E+09

ABAQUS VERSION 4-9-1 DATE: 4-Dec-91 TIME: 08:21:02 STEP 6 INCREMENT 48

ABAQUS

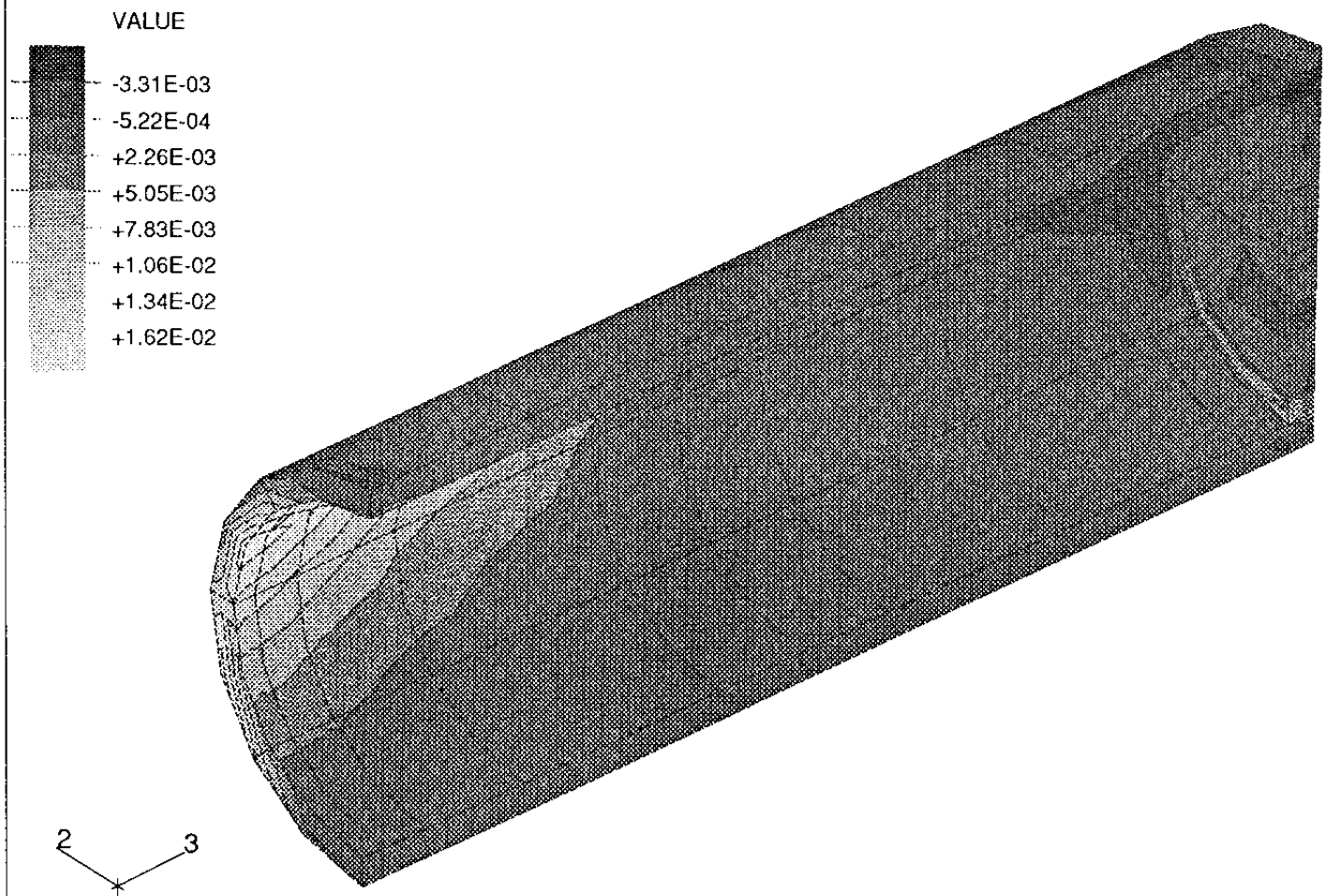

TIME COMPLETED IN THIS STEP +1.000E+09 TOTAL ACCUMULATED TIME +1.002E+09

ABAQUS VERSION 4-9-1 DATE: 4-Dec-91 TIME: 08:21:02 STEP 6 INCREMENT 48

ABAQUS

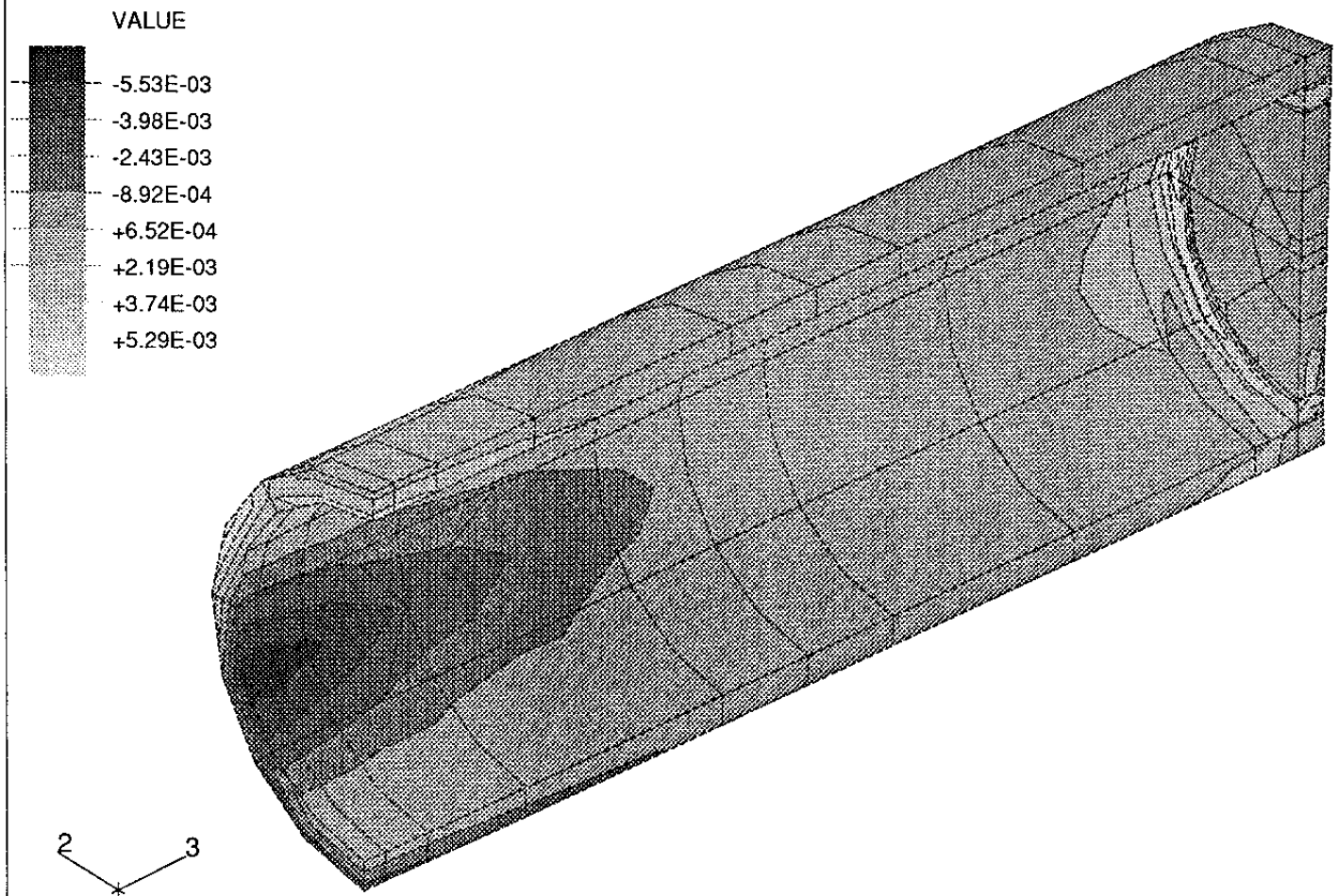

TIME COMPLETED IN THIS STEP +1.000E+09 TOTAL ACCUMULATED TIME +1.002E+09

ABAQUS VERSION 4-9-1 DATE: 4-Dec-91 TIME: 08:21:02 STEP 6 INCREMENT 48

APPENDIX VIIa

Results from a rock shear calculation
Asymmetric shear
KBS3 copper/steel canister

After 5 cm rock displacement

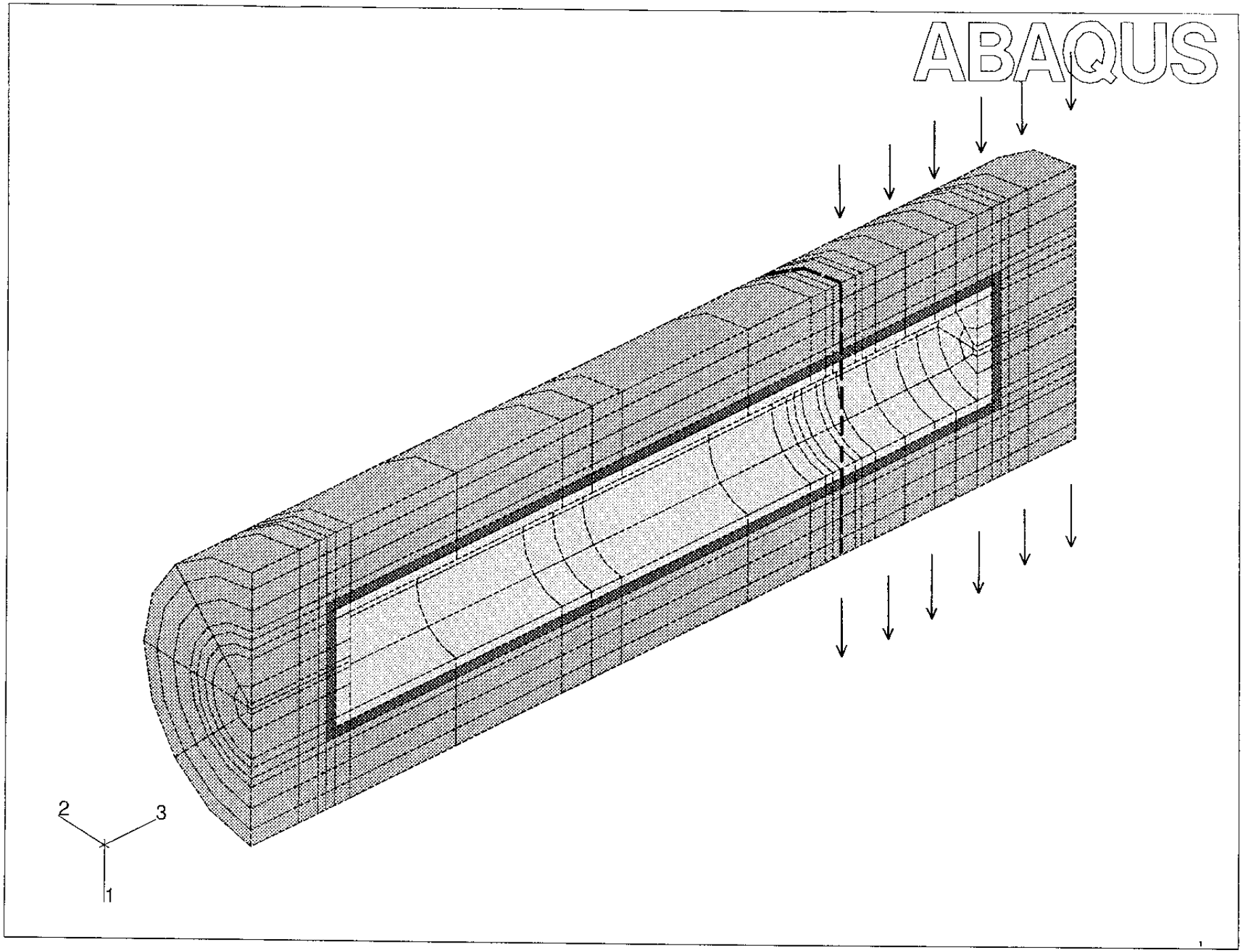
ABAQUS
2
3
1

ABAQUS

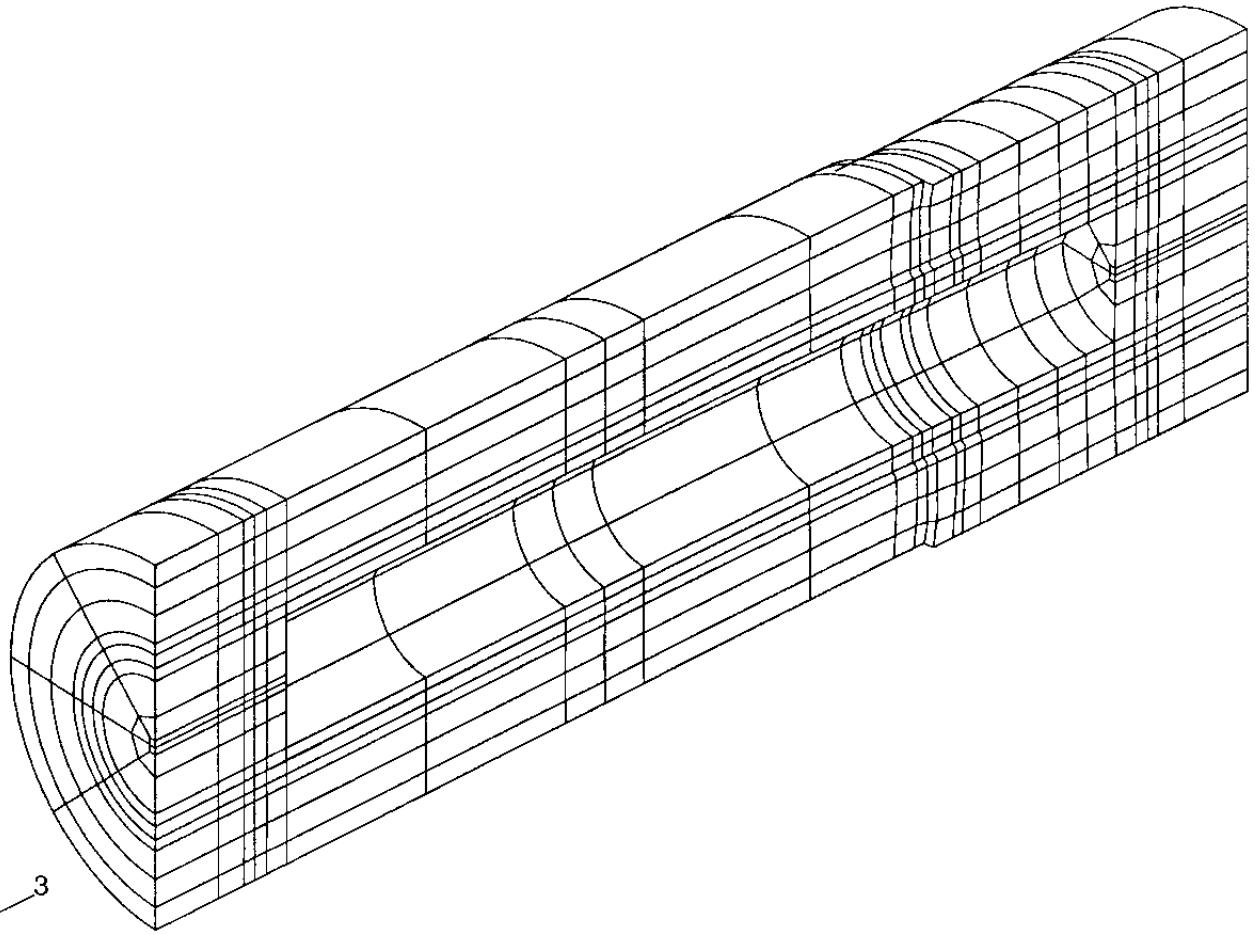

MAG. FACTOR =+1.0E+00

ABAQUS

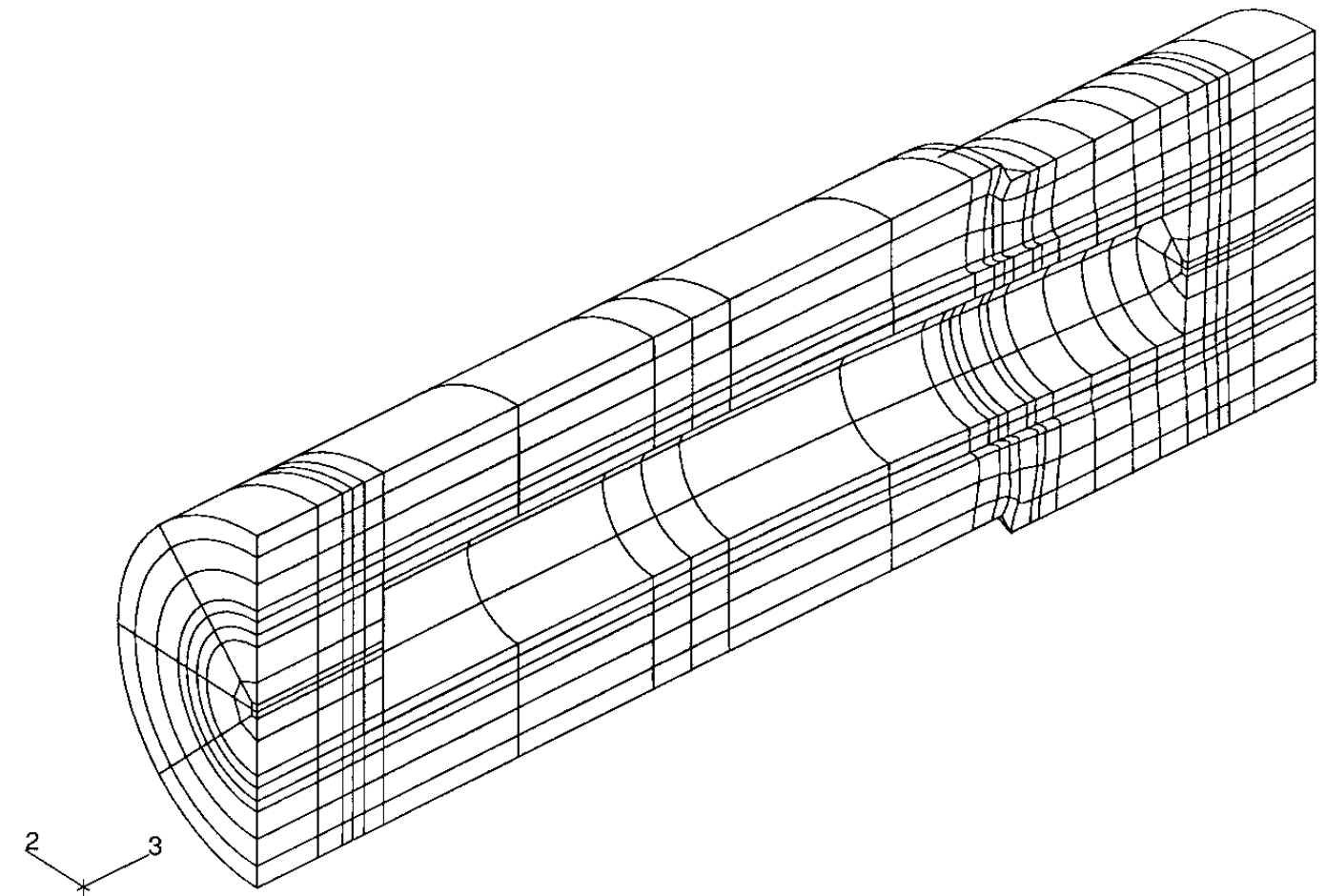

MAG. FACTOR =+2.5E+00

ABAQUS

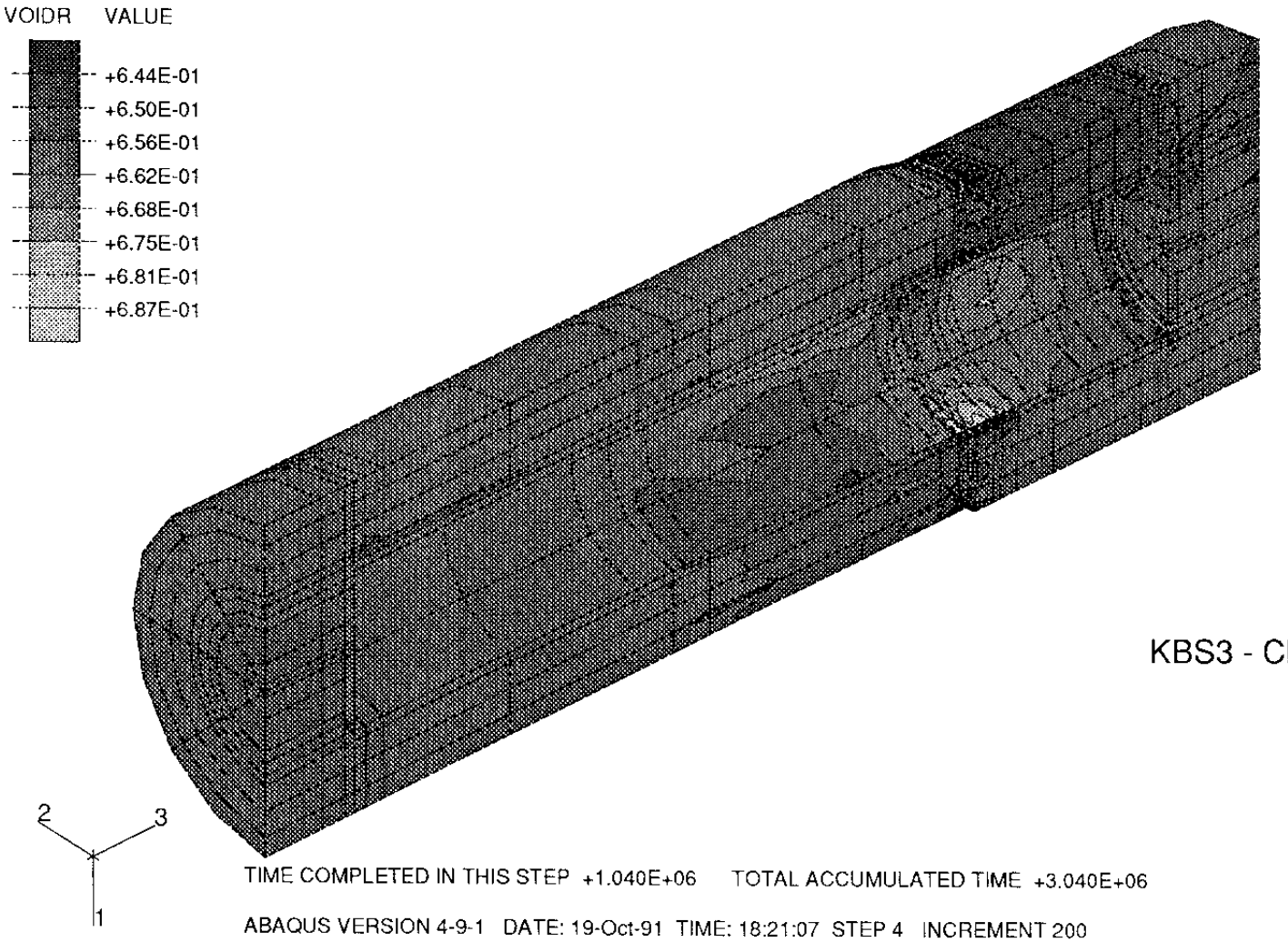

KBS3 - Clay

TIME COMPLETED IN THIS STEP +1.040E+06 TOTAL ACCUMULATED TIME +3.040E+06

ABAQUS VERSION 4-9-1 DATE: 19-Oct-91 TIME: 18:21:07 STEP 4 INCREMENT 200

ABAQUS

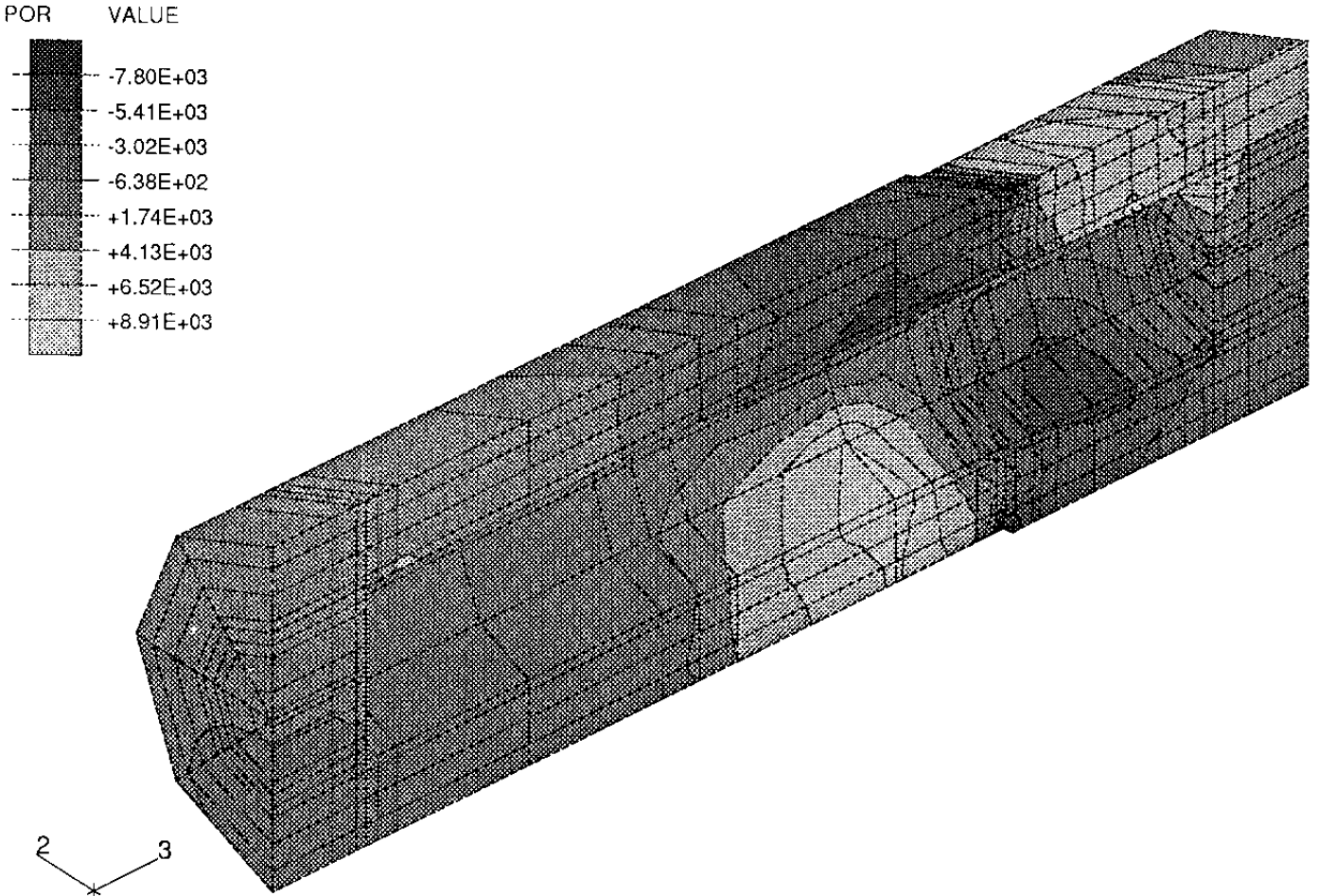

TIME COMPLETED IN THIS STEP +1.040E+06 TOTAL ACCUMULATED TIME +3.040E+06

ABAQUS VERSION 4-9-1 DATE: 19-Oct-91 TIME: 18:21:07 STEP 4 INCREMENT 200

ABAQUS

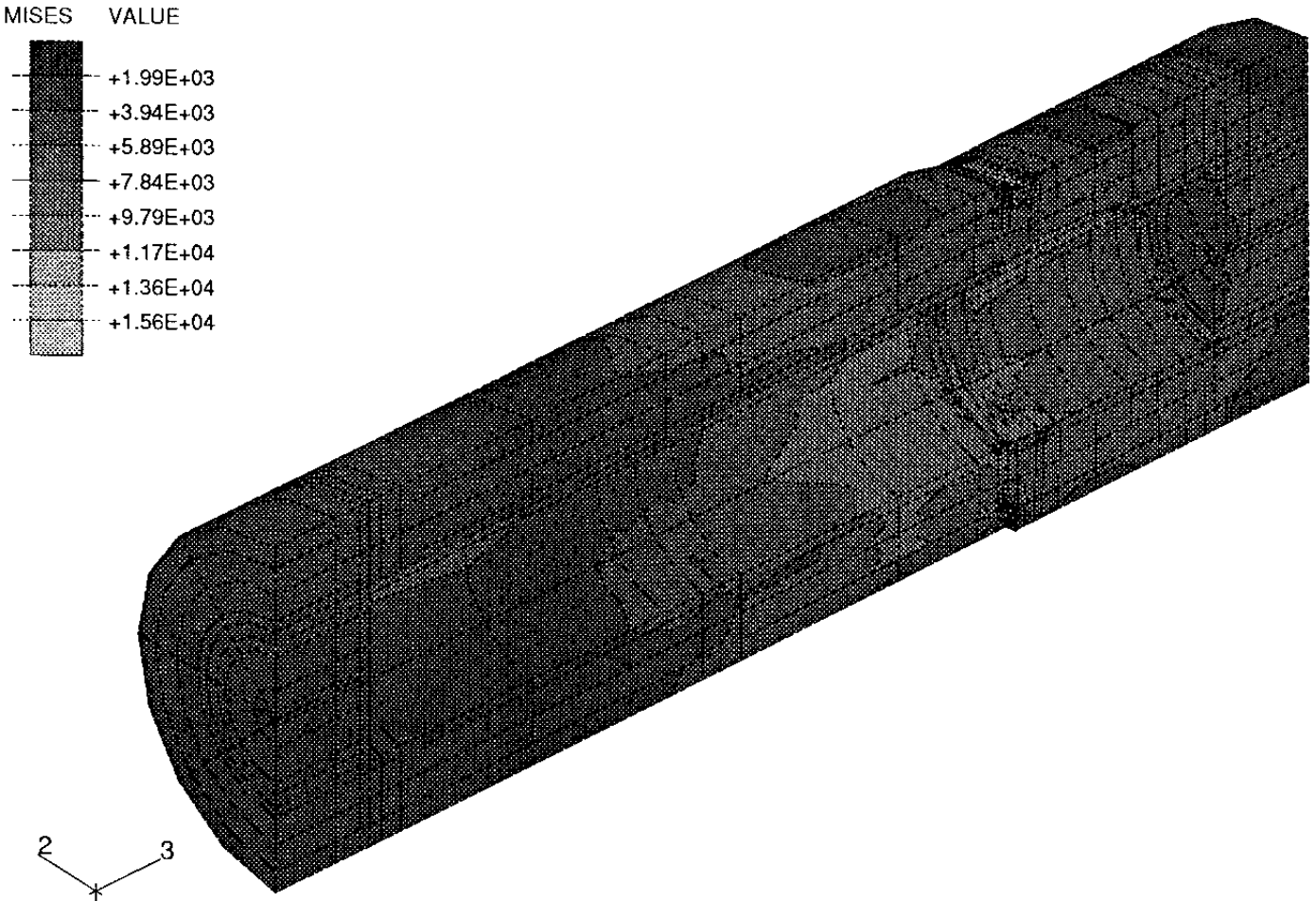

TIME COMPLETED IN THIS STEP +1.040E+06 TOTAL ACCUMULATED TIME +3.040E+06

ABAQUS VERSION 4-9-1 DATE: 19-Oct-91 TIME: 18:21:07 STEP 4 INCREMENT 200

ABAQUS

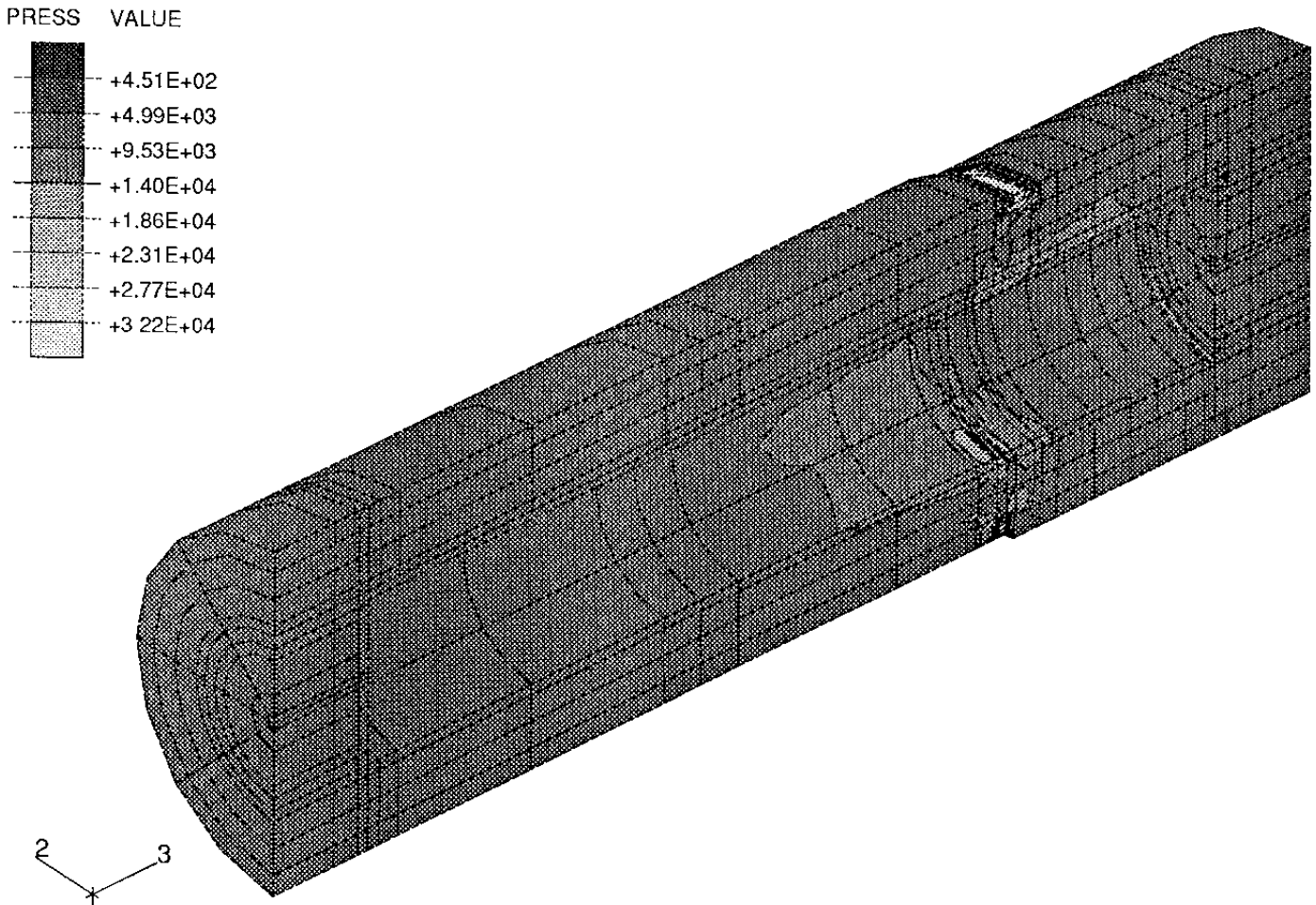

TIME COMPLETED IN THIS STEP +1.040E+06 TOTAL ACCUMULATED TIME +3.040E+06

ABAQUS VERSION 4-9-1 DATE: 19-Oct-91 TIME: 18:21:07 STEP 4 INCREMENT 200

ABAQUS

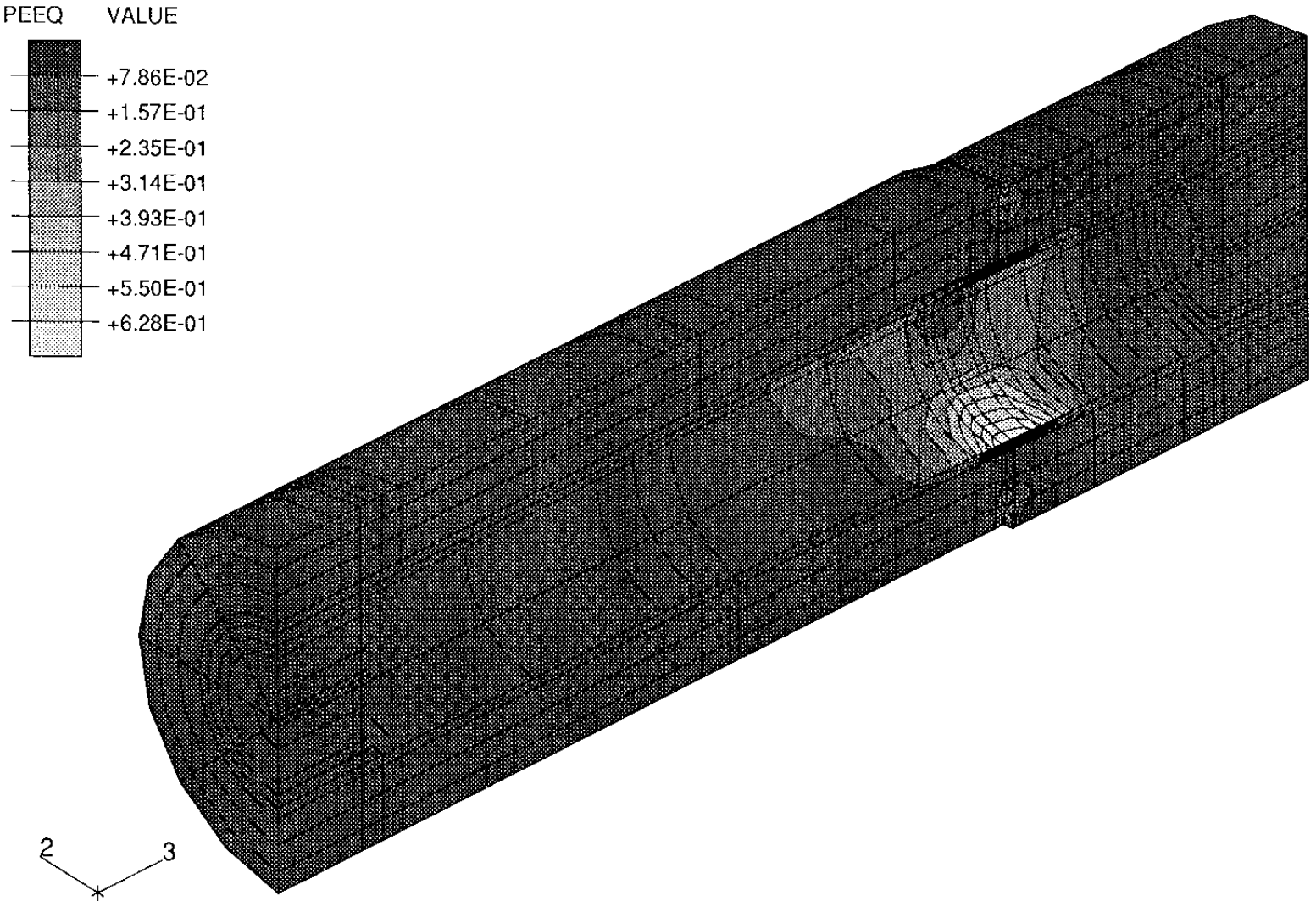

TIME COMPLETED IN THIS STEP +1.040E+06 TOTAL ACCUMULATED TIME +3.040E+06

ABAQUS VERSION 4-9-1 DATE: 19-Oct-91 TIME: 18:21:07 STEP 4 INCREMENT 200

ABAQUS

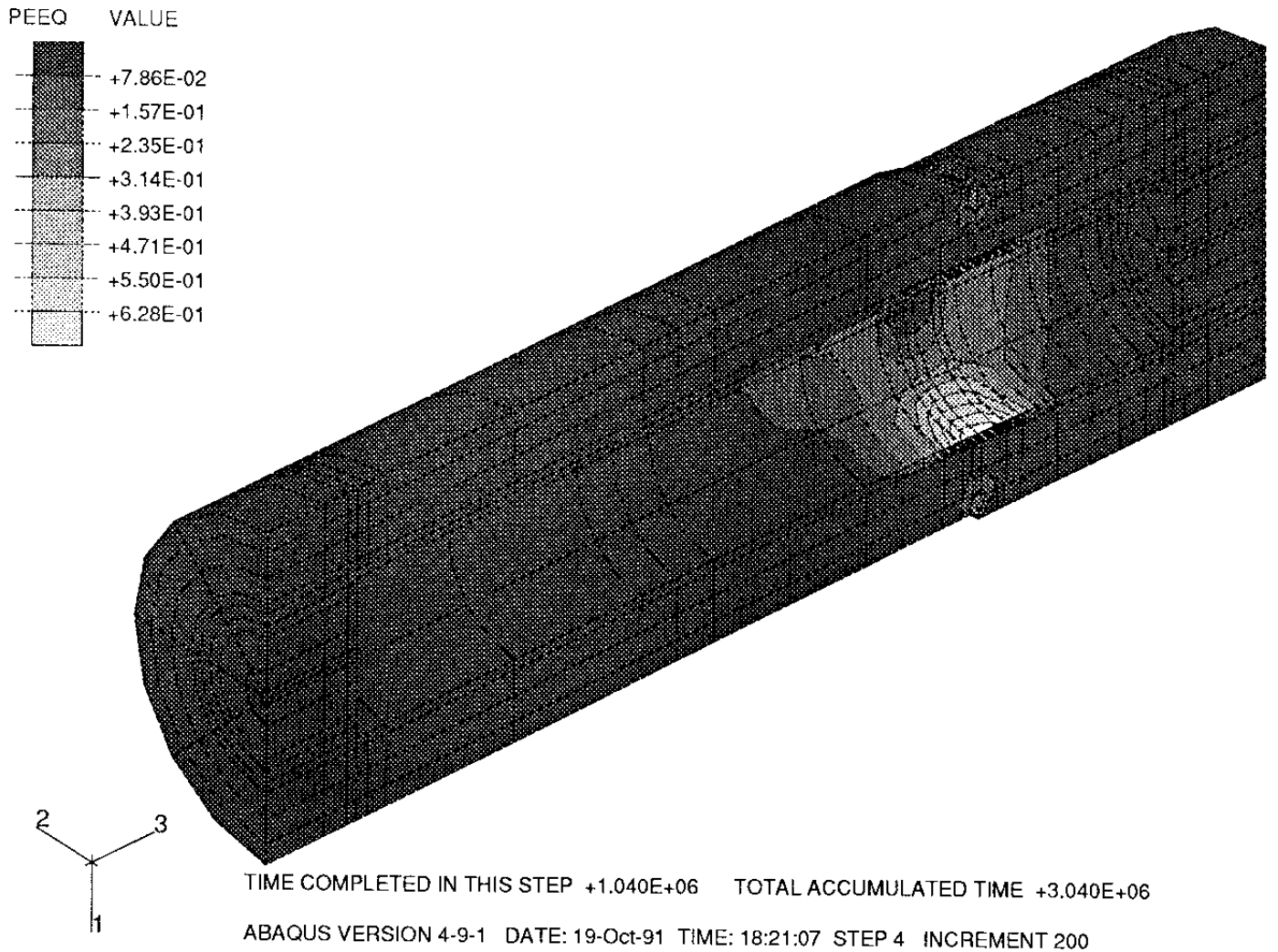

TIME COMPLETED IN THIS STEP +1.040E+06 TOTAL ACCUMULATED TIME +3.040E+06

ABAQUS VERSION 4-9-1 DATE: 19-Oct-91 TIME: 18:21:07 STEP 4 INCREMENT 200

ABAQUS

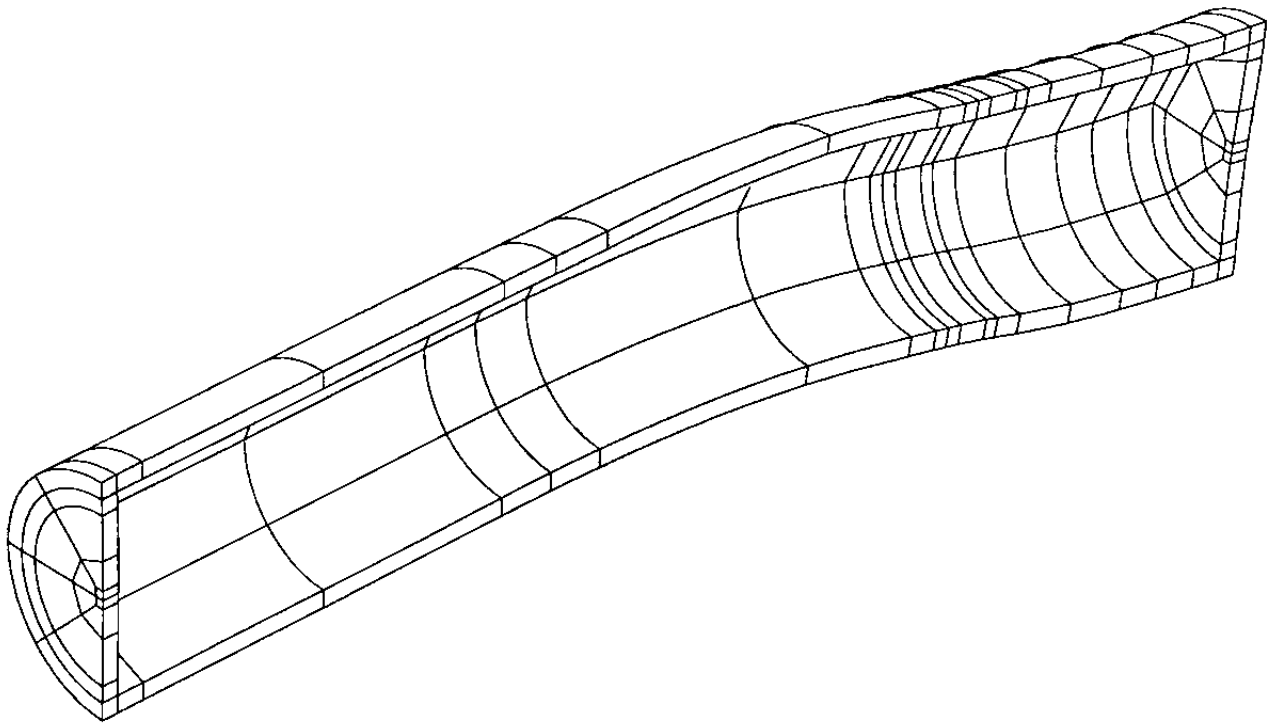

MAG. FACTOR =+1.0E+01

ABAQUS

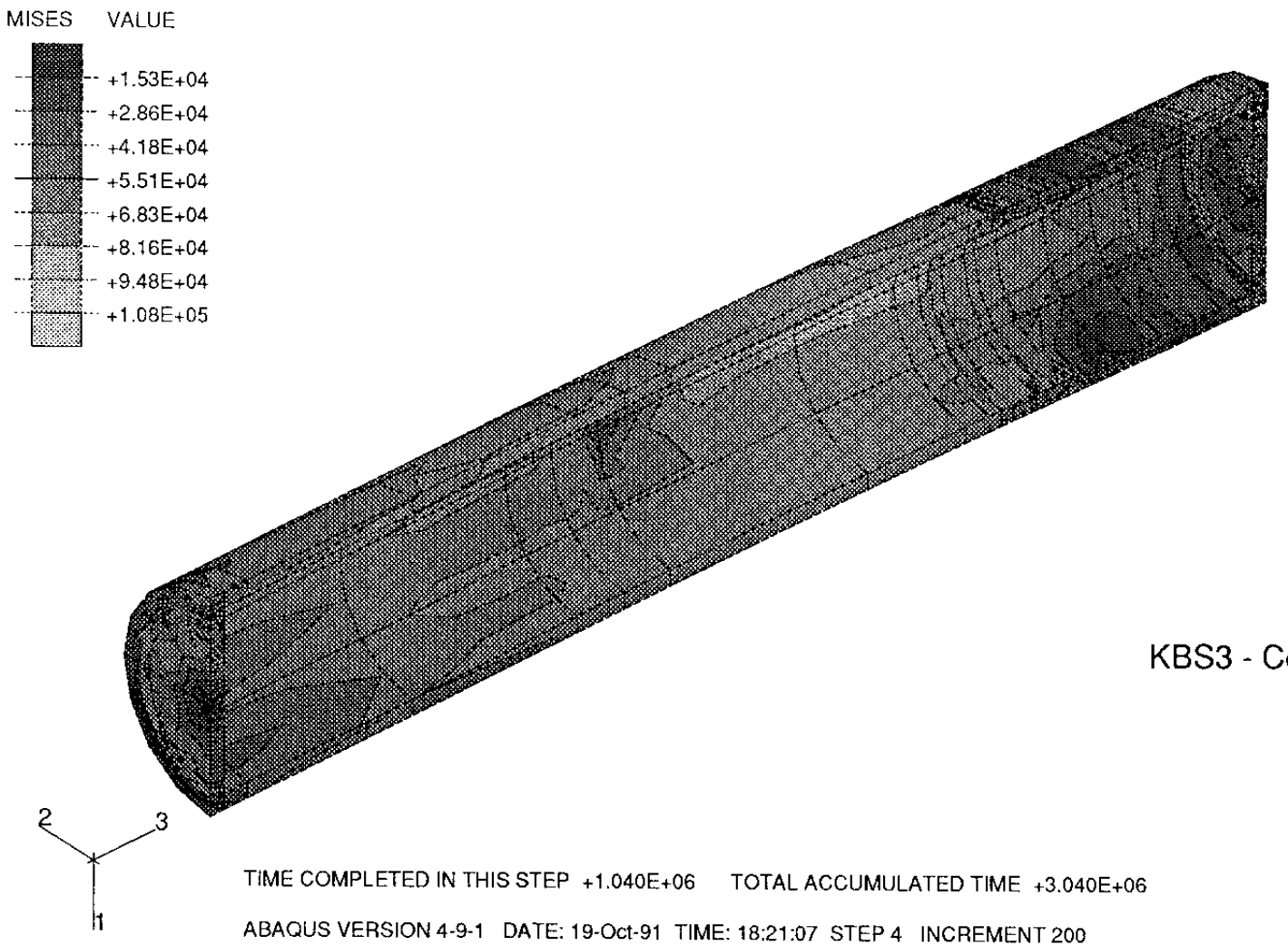

KBS3 - Copper

TIME COMPLETED IN THIS STEP +1.040E+06 TOTAL ACCUMULATED TIME +3.040E+06

ABAQUS VERSION 4-9-1 DATE: 19-Oct-91 TIME: 18:21:07 STEP 4 INCREMENT 200

ABAQUS

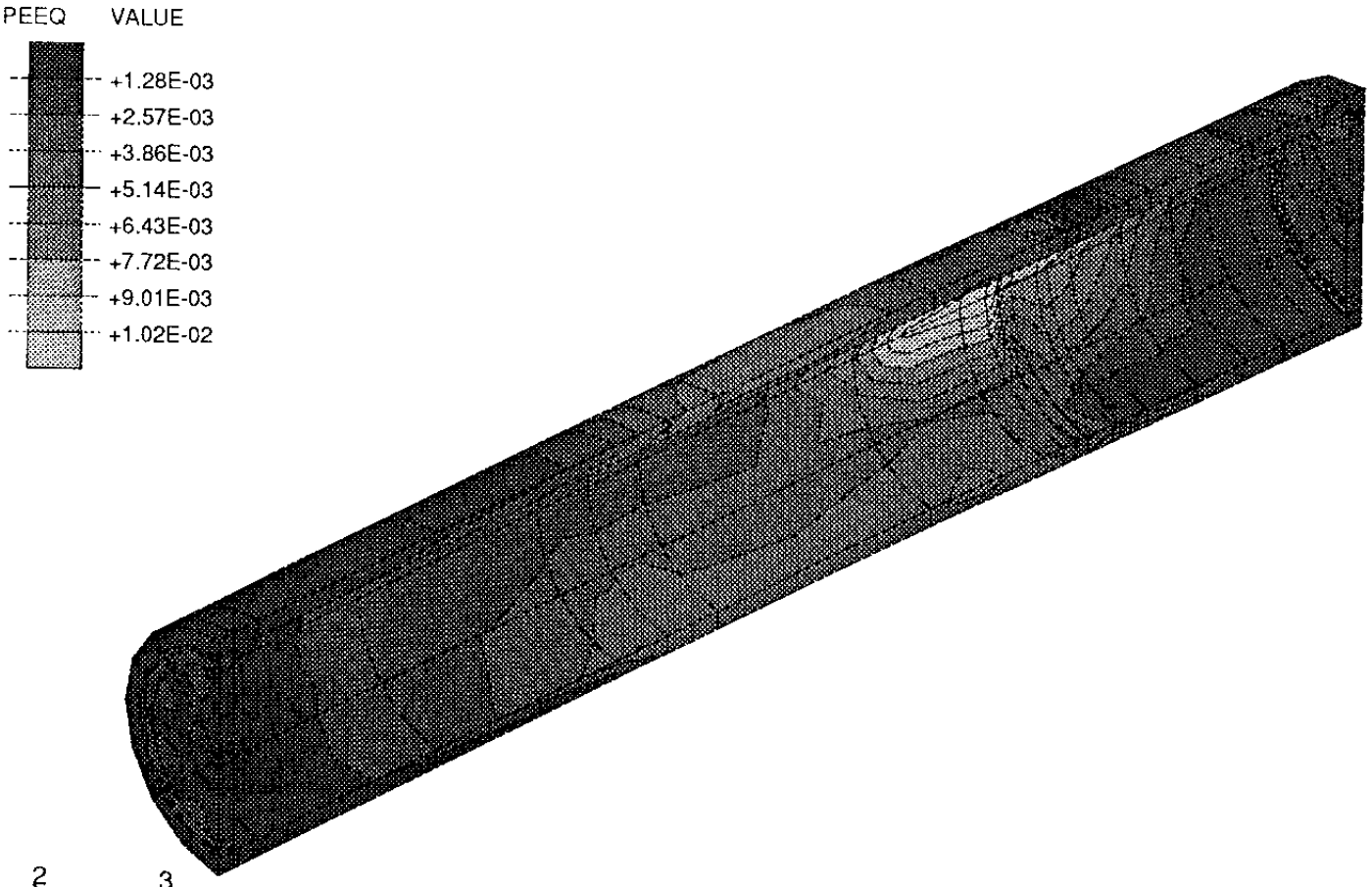

TIME COMPLETED IN THIS STEP +1.040E+06 TOTAL ACCUMULATED TIME +3.040E+06

ABAQUS VERSION 4-9-1 DATE: 19-Oct-91 TIME: 18:21:07 STEP 4 INCREMENT 200

ABAQUS

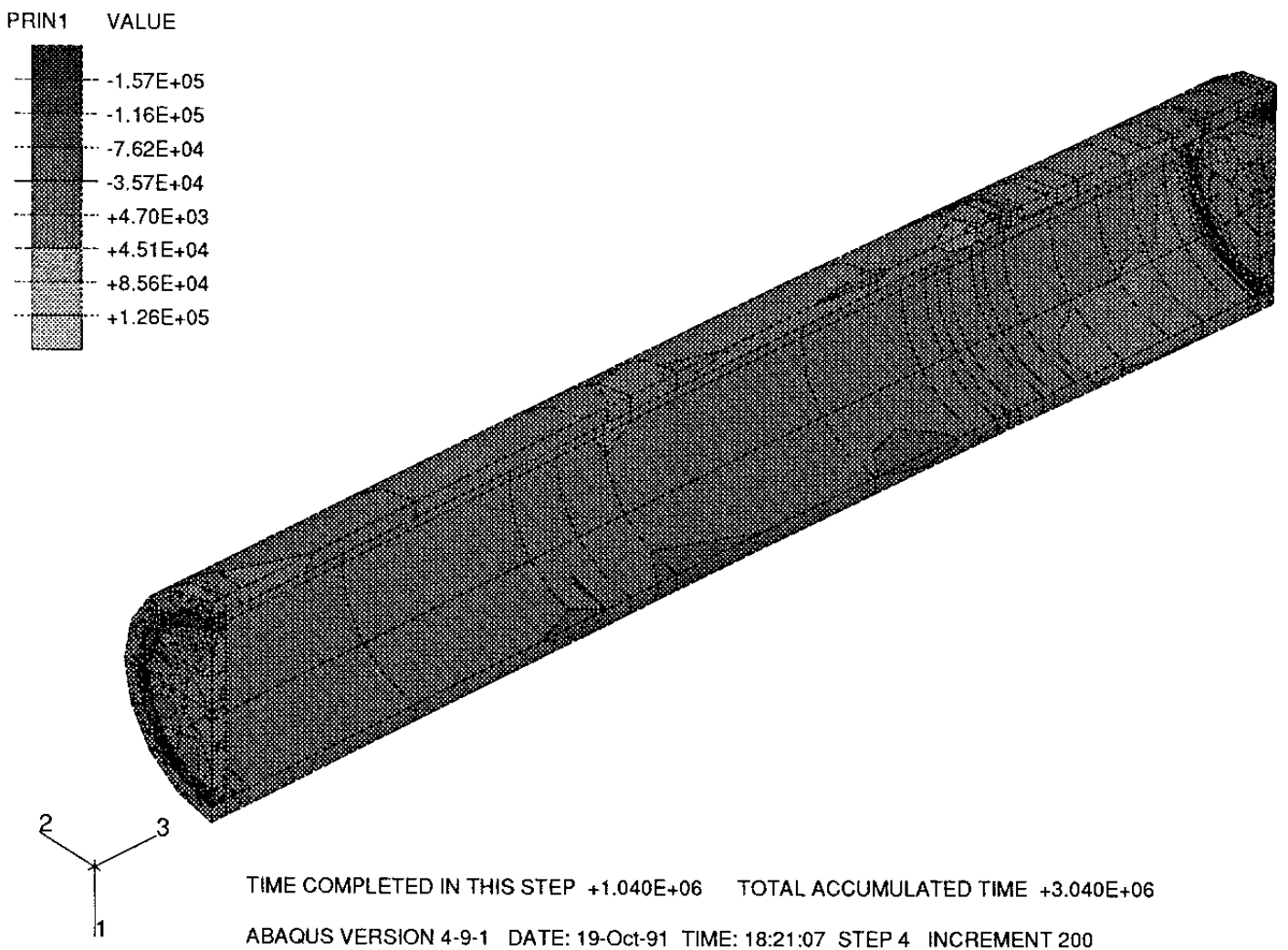

TIME COMPLETED IN THIS STEP +1.040E+06 TOTAL ACCUMULATED TIME +3.040E+06

ABAQUS VERSION 4-9-1 DATE: 19-Oct-91 TIME: 18:21:07 STEP 4 INCREMENT 200

ABAQUS

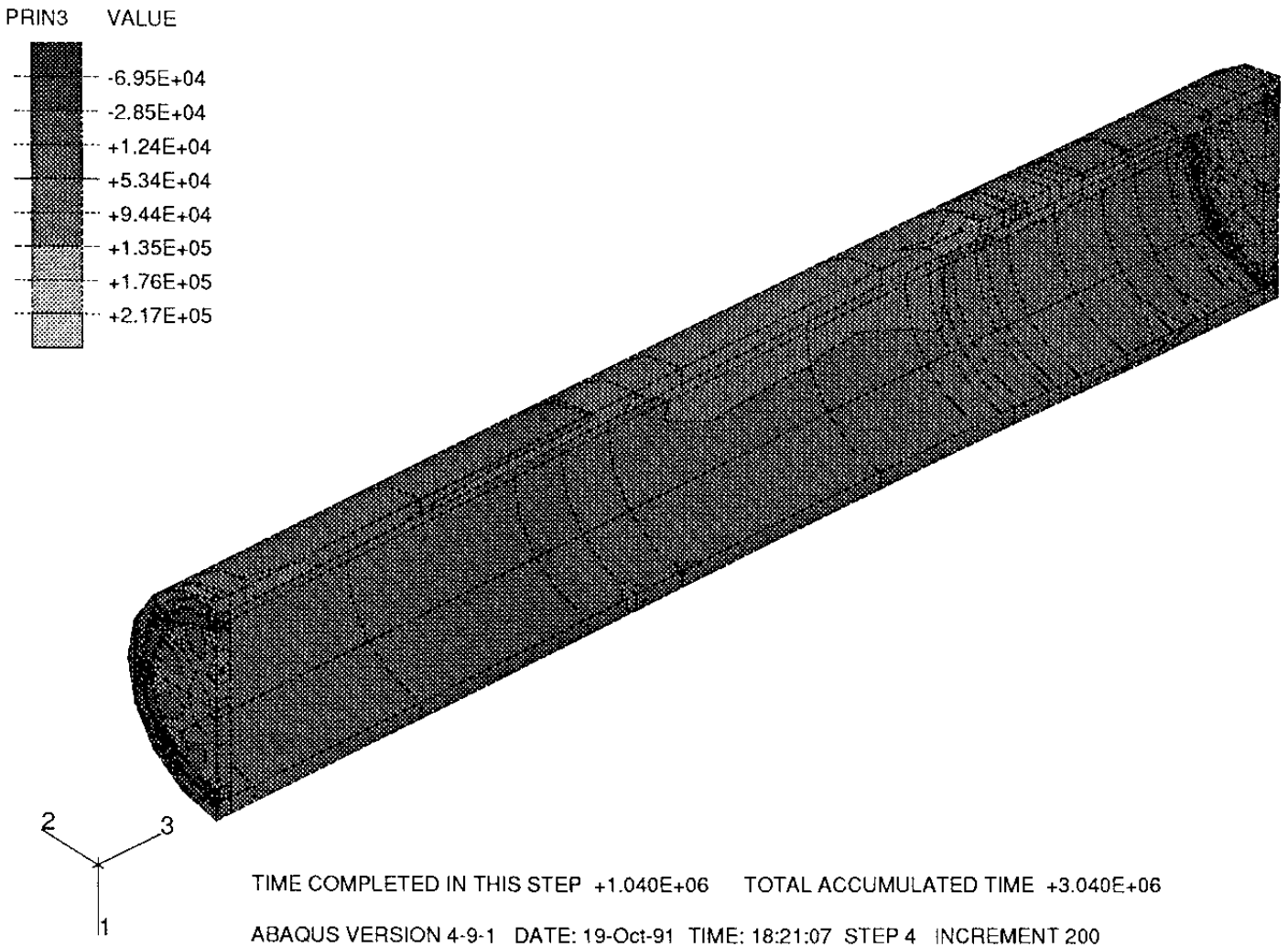

TIME COMPLETED IN THIS STEP +1.040E+06 TOTAL ACCUMULATED TIME +3.040E+06

ABAQUS VERSION 4-9-1 DATE: 19-Oct-91 TIME: 18:21:07 STEP 4 INCREMENT 200

ABAQUS

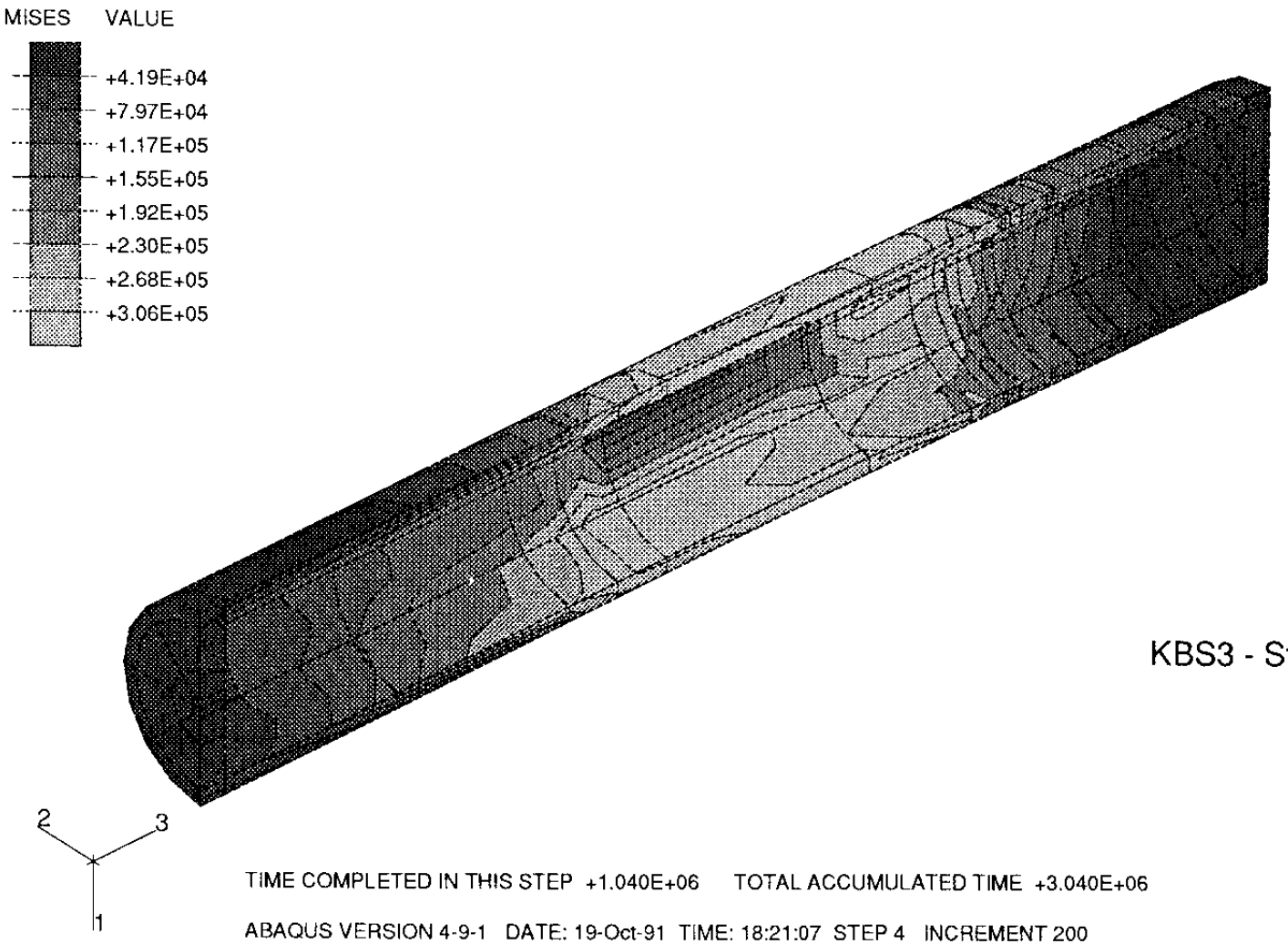

KBS3 - Steel

TIME COMPLETED IN THIS STEP +1.040E+06 TOTAL ACCUMULATED TIME +3.040E+06

ABAQUS VERSION 4-9-1 DATE: 19-Oct-91 TIME: 18:21:07 STEP 4 INCREMENT 200

ABAQUS

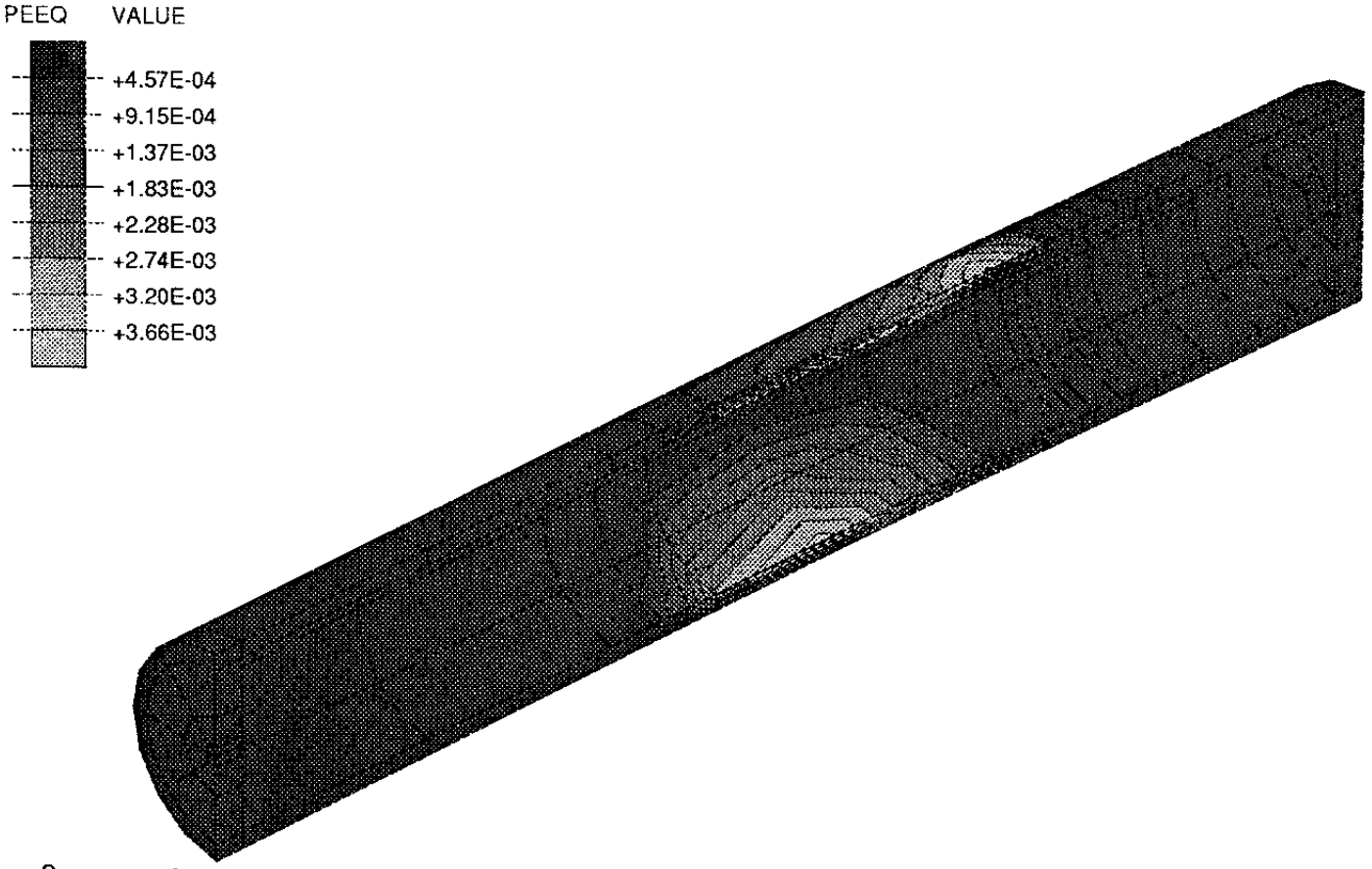

TIME COMPLETED IN THIS STEP +1.040E+06 TOTAL ACCUMULATED TIME +3.040E+06

ABAQUS VERSION 4-9-1 DATE: 19-Oct-91 TIME: 18:21:07 STEP 4 INCREMENT 200

ABAQUS

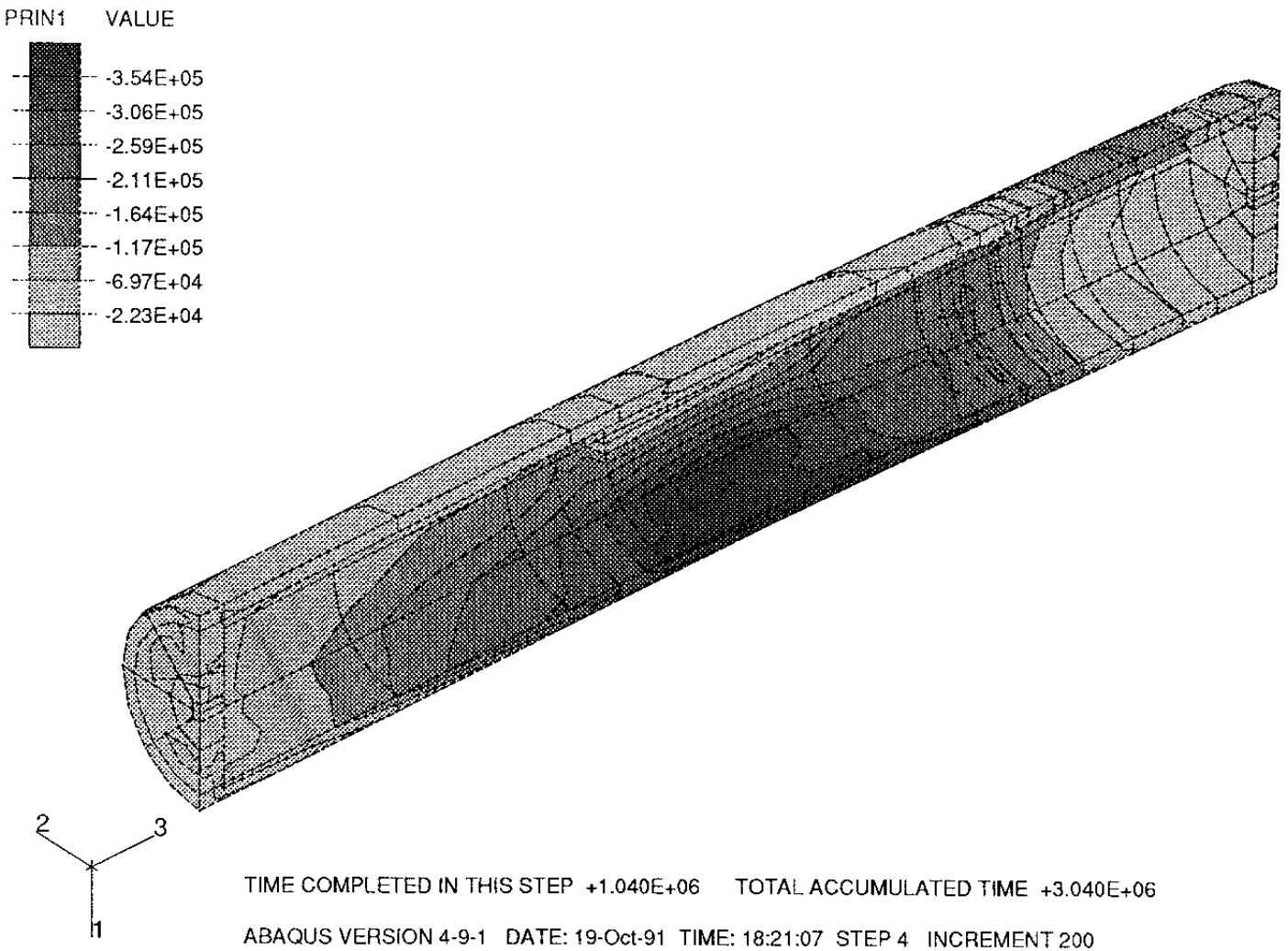

TIME COMPLETED IN THIS STEP +1.040E+06 TOTAL ACCUMULATED TIME +3.040E+06

ABAQUS VERSION 4-9-1 DATE: 19-Oct-91 TIME: 18:21:07 STEP 4 INCREMENT 200

ABAQUS

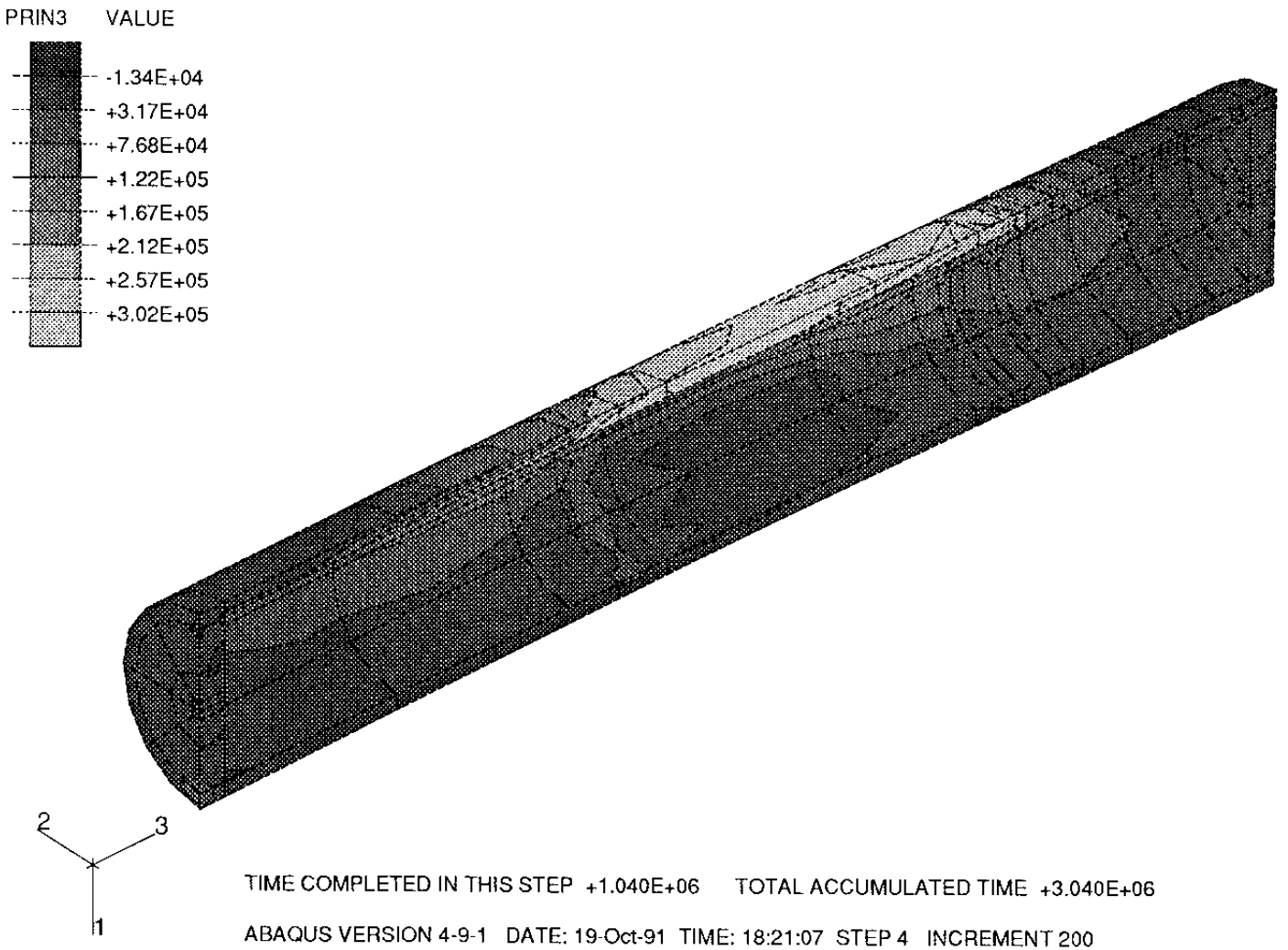

TIME COMPLETED IN THIS STEP +1.040E+06 TOTAL ACCUMULATED TIME +3.040E+06

ABAQUS VERSION 4-9-1 DATE: 19-Oct-91 TIME: 18:21:07 STEP 4 INCREMENT 200

ABAQUS

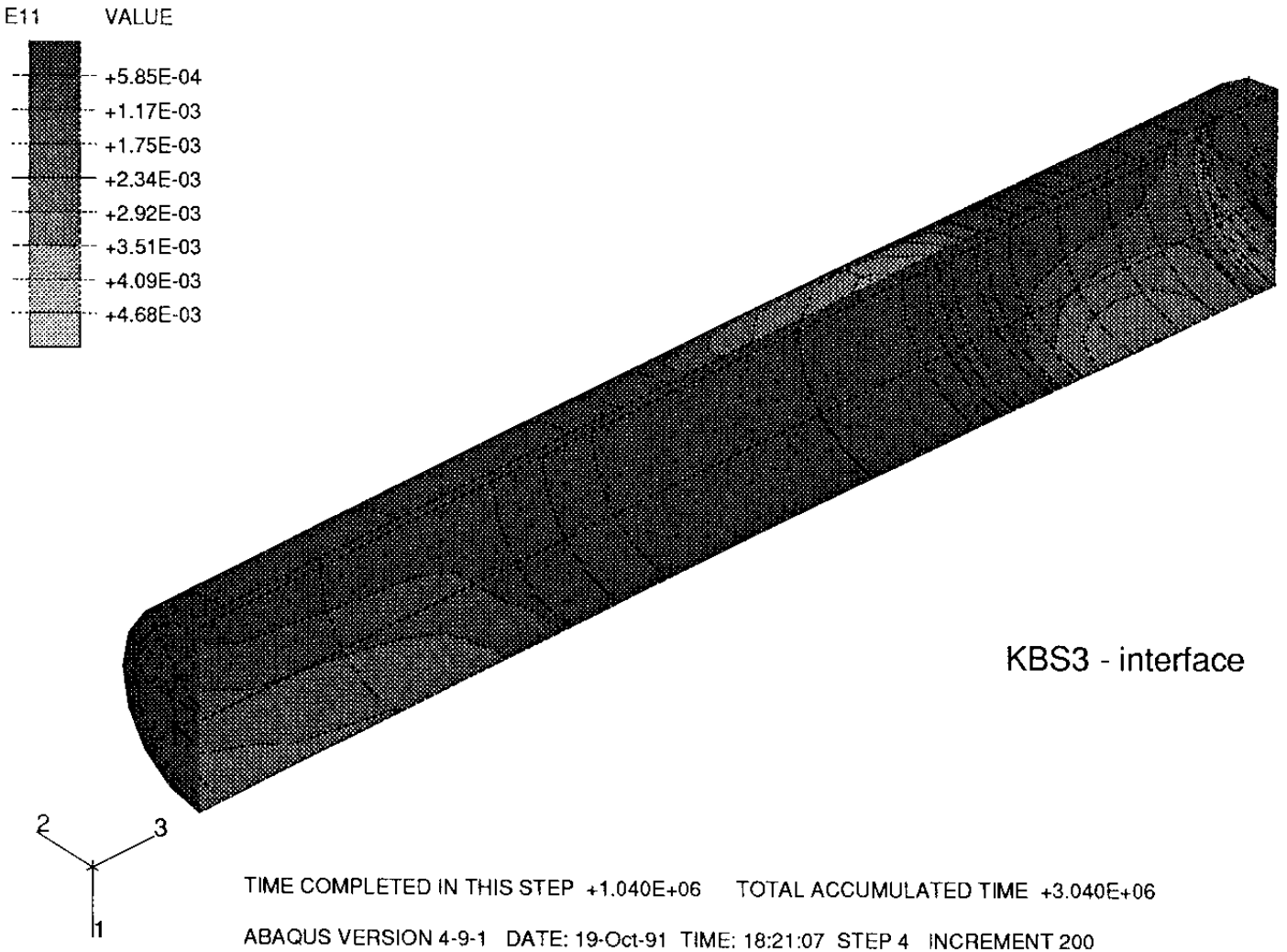

KBS3 - interface

TIME COMPLETED IN THIS STEP +1.040E+06 TOTAL ACCUMULATED TIME +3.040E+06

ABAQUS VERSION 4-9-1 DATE: 19-Oct-91 TIME: 18:21:07 STEP 4 INCREMENT 200

ABAQUS

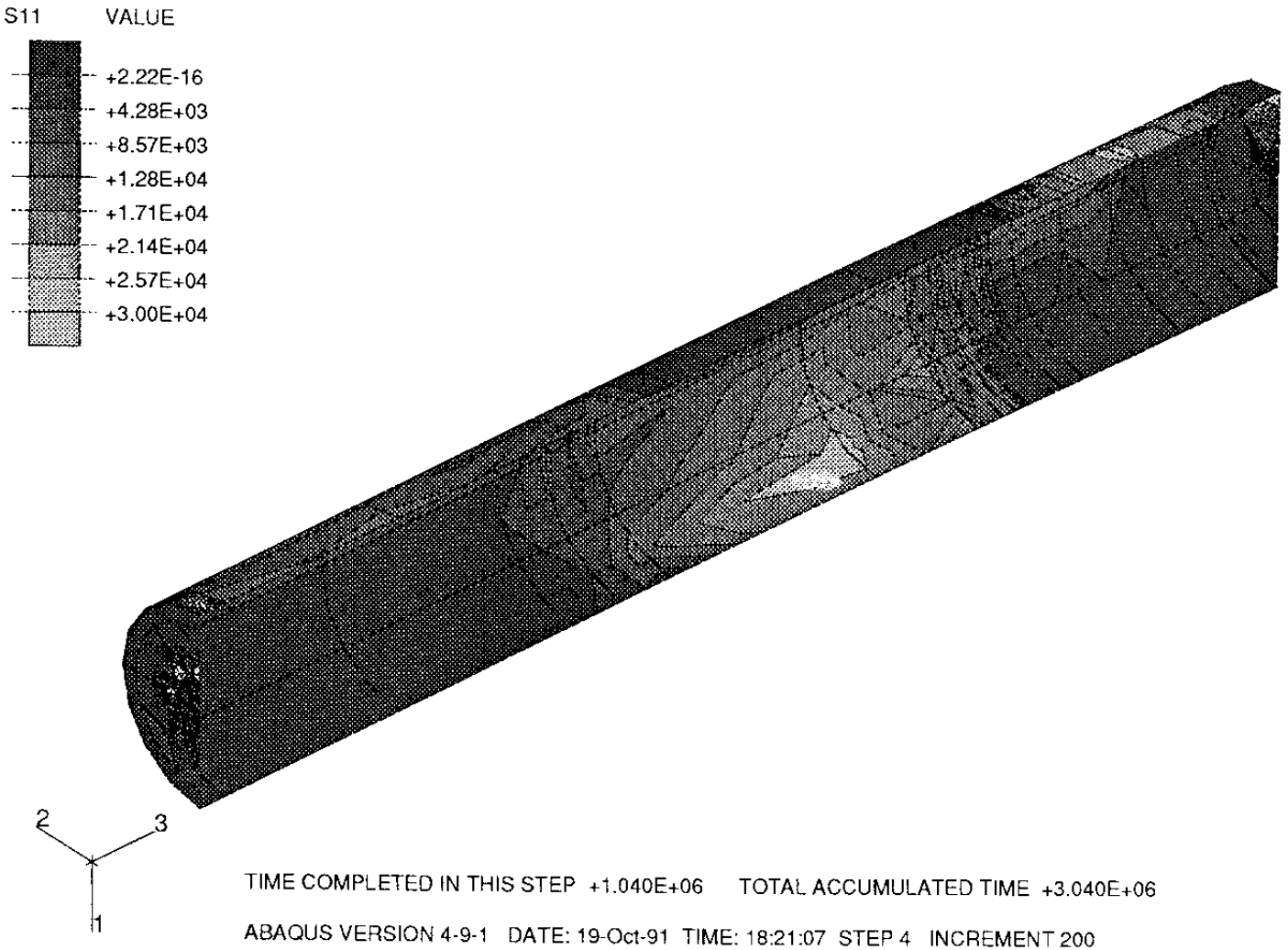

TIME COMPLETED IN THIS STEP +1.040E+06 TOTAL ACCUMULATED TIME +3.040E+06

ABAQUS VERSION 4-9-1 DATE: 19-Oct-91 TIME: 18:21:07 STEP 4 INCREMENT 200

APPENDIX VIIb

Results from a rock shear calculation
Asymmetric shear
KBS3 copper/steel canister

After 10 cm rock displacement

ABAQUS

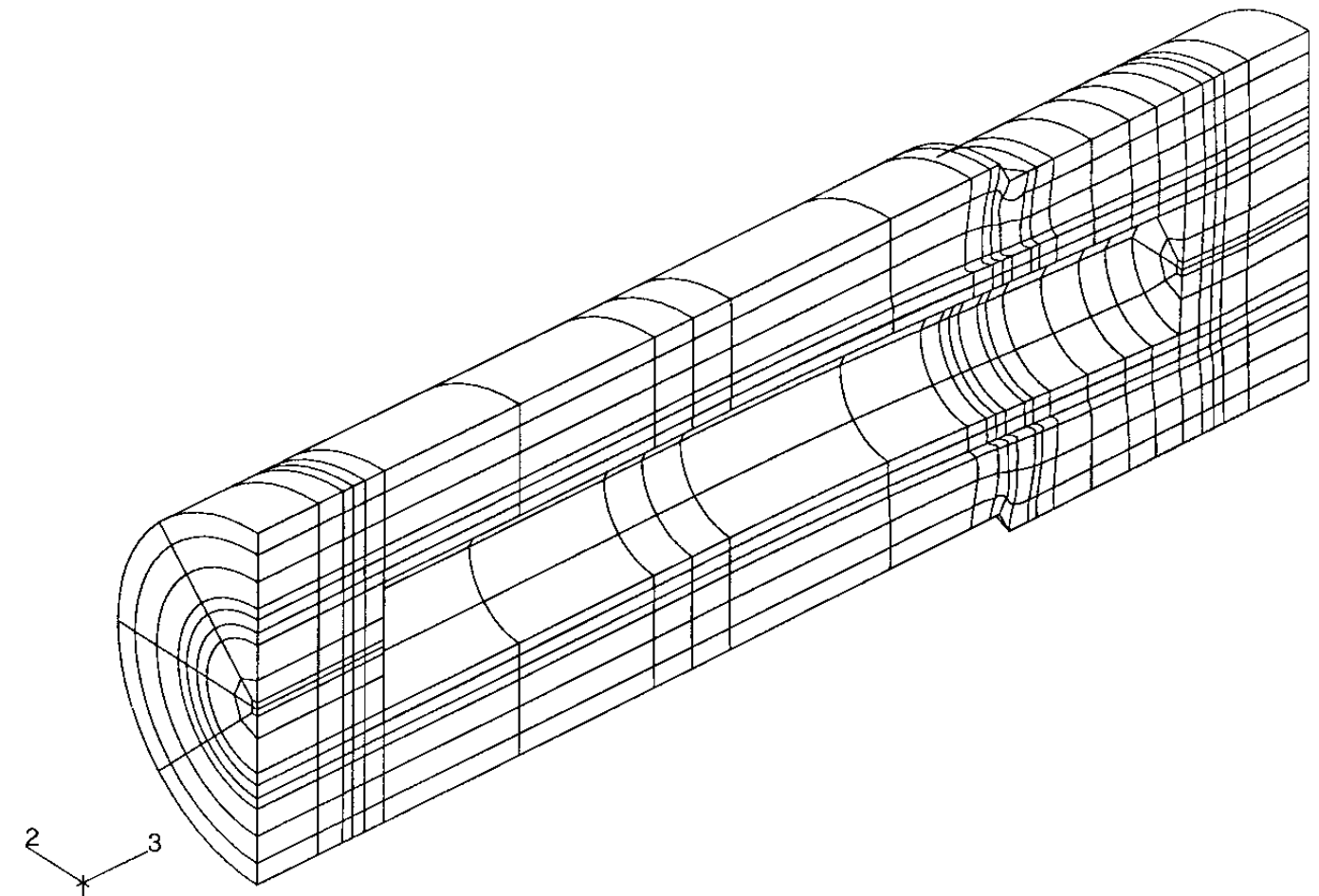

MAG. FACTOR =+1.0E+00

ABAQUS

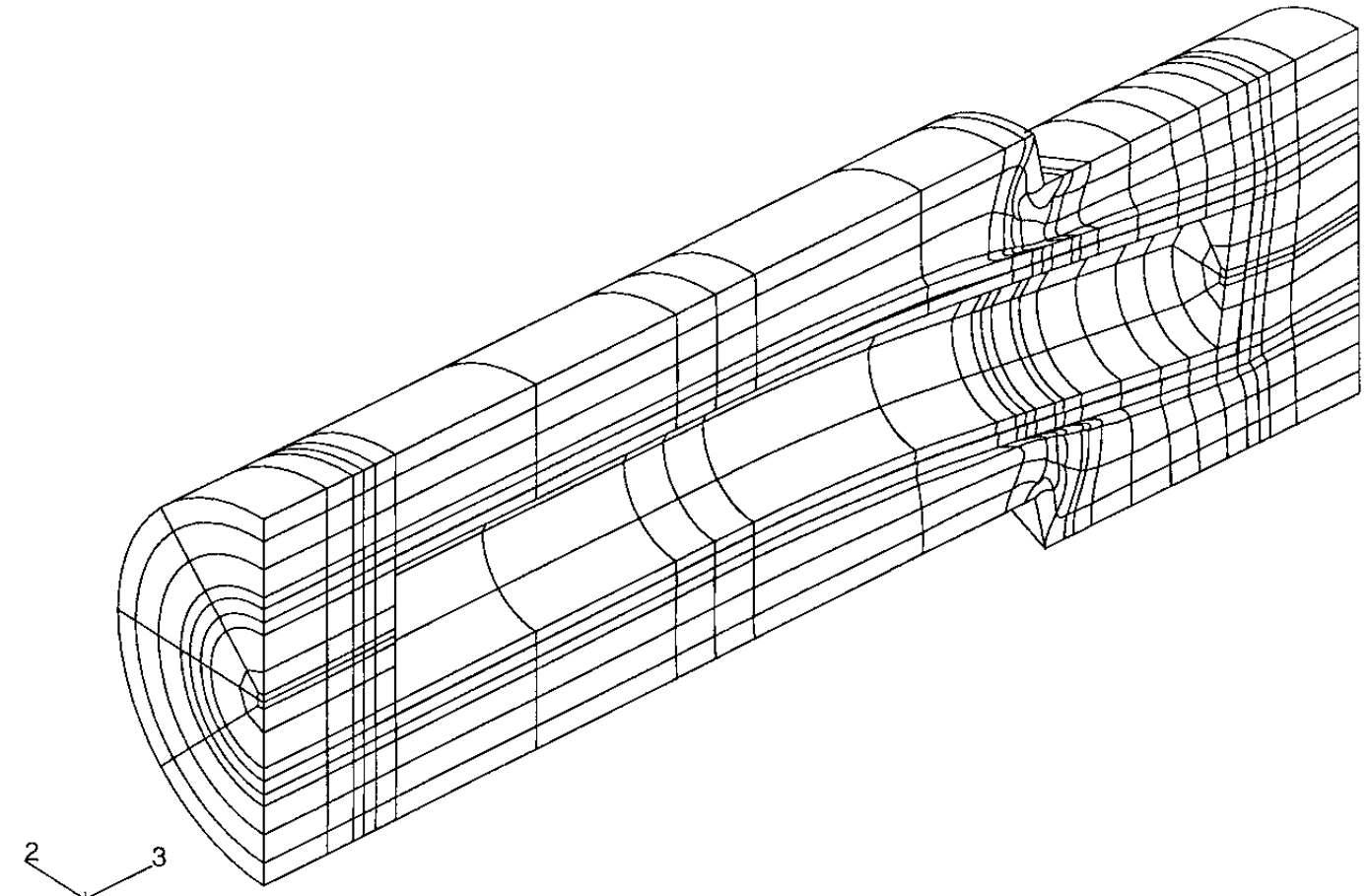

MAG. FACTOR =+2.5E+00

ABAQUS

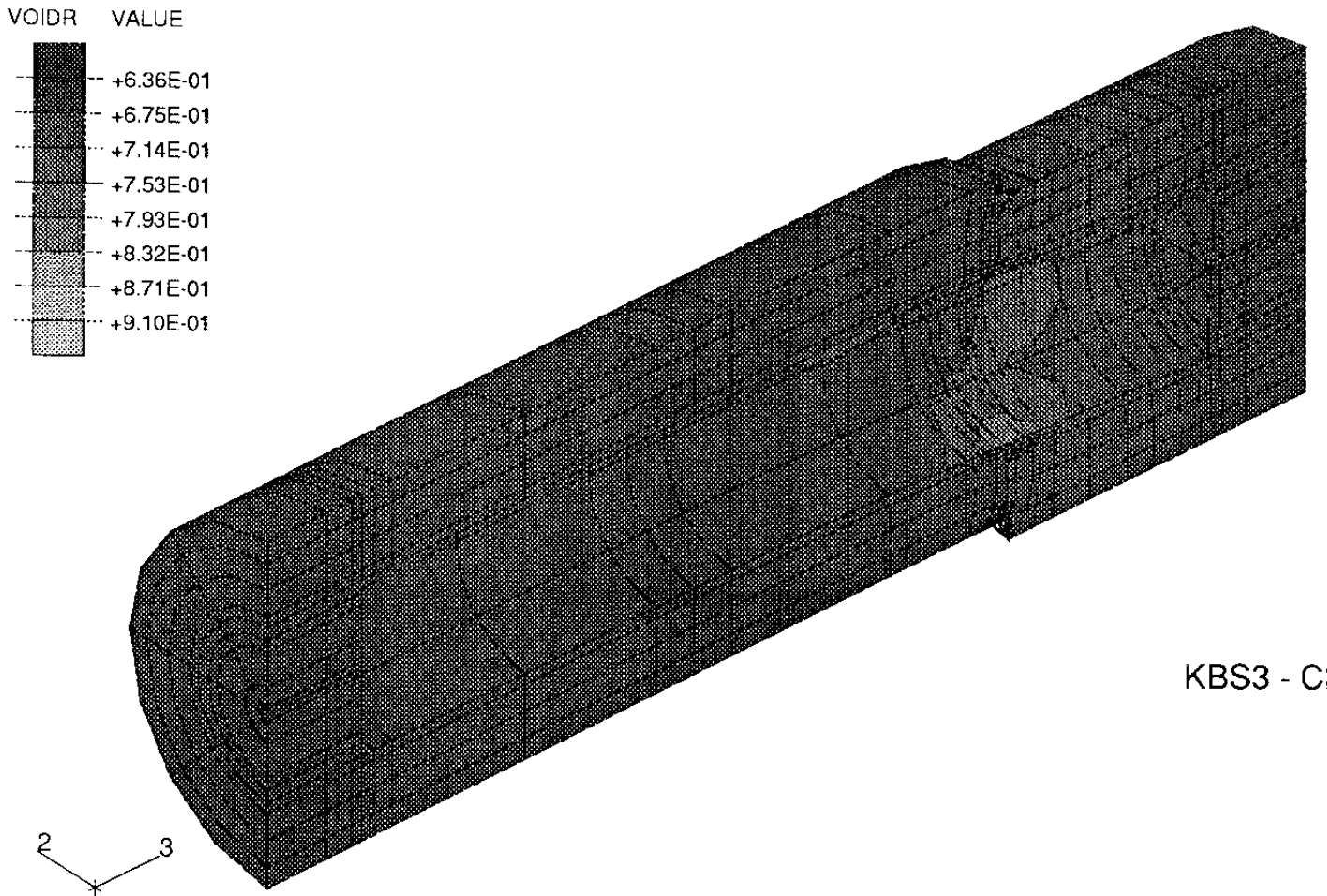

KBS3 - Clay

TIME COMPLETED IN THIS STEP +2.592E+06 TOTAL ACCUMULATED TIME +4.592E+06

ABAQUS VERSION 4-9-1 DATE: 19-Oct-91 TIME: 18:21:07 STEP 4 INCREMENT 360

ABAQUS

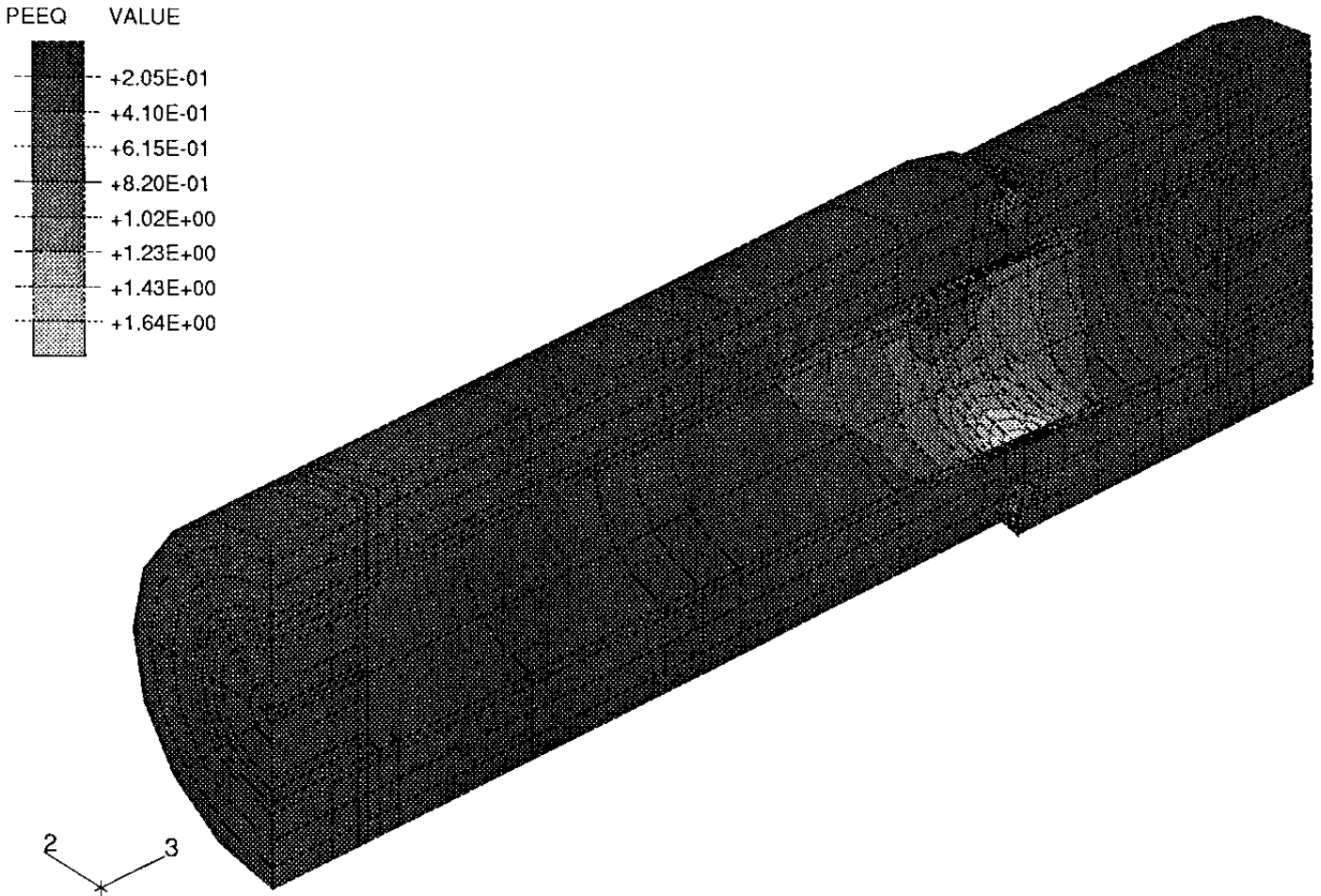

TIME COMPLETED IN THIS STEP +2.592E+06 TOTAL ACCUMULATED TIME +4.592E+06

ABAQUS VERSION 4-9-1 DATE: 19-Oct-91 TIME: 18:21:07 STEP 4 INCREMENT 360

ABAQUS

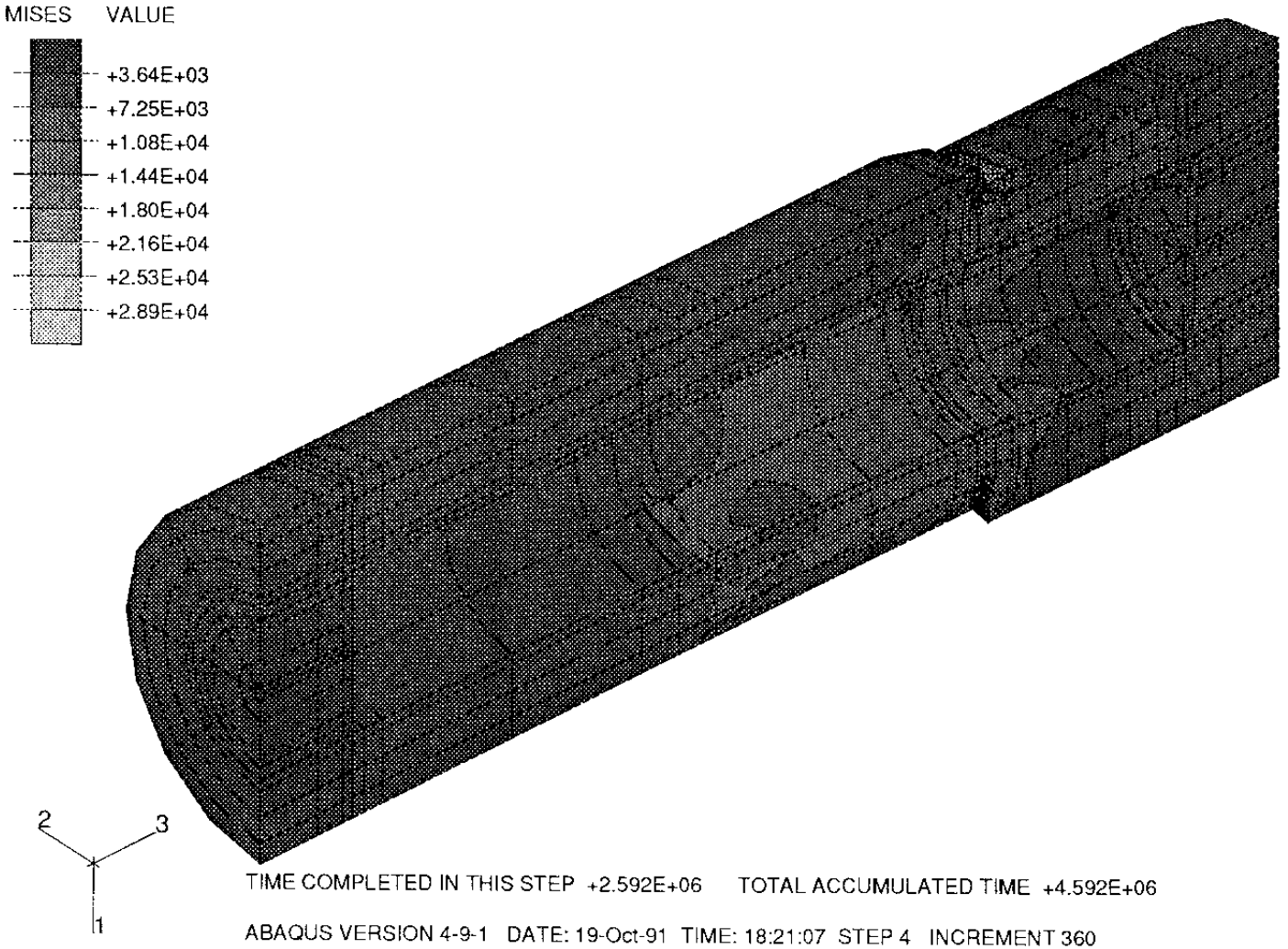

TIME COMPLETED IN THIS STEP +2.592E+06 TOTAL ACCUMULATED TIME +4.592E+06

ABAQUS VERSION 4-9-1 DATE: 19-Oct-91 TIME: 18:21:07 STEP 4 INCREMENT 360

ABAQUS

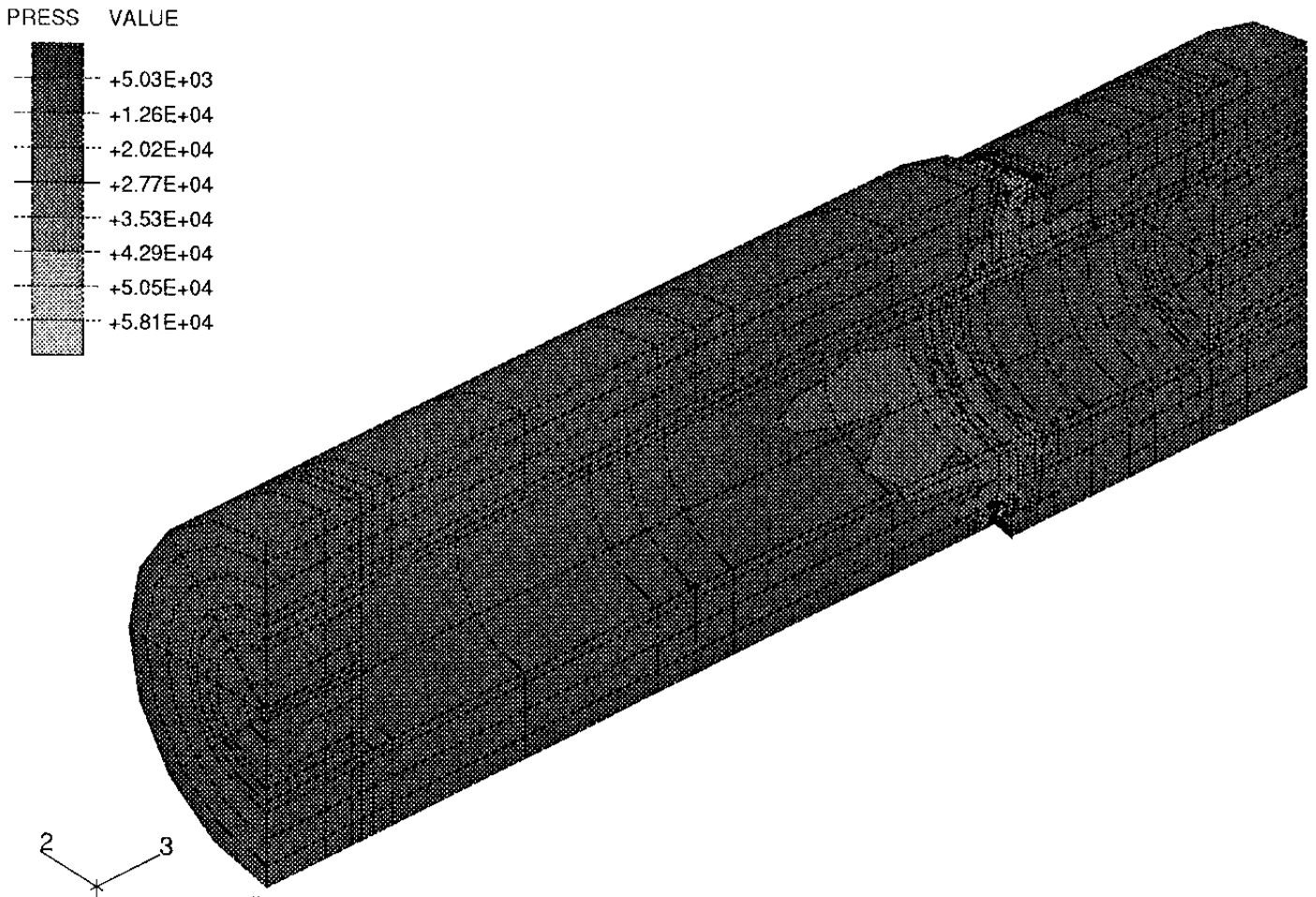

TIME COMPLETED IN THIS STEP +2.592E+06 TOTAL ACCUMULATED TIME +4.592E+06

ABAQUS VERSION 4-9-1 DATE: 19-Oct-91 TIME: 18:21:07 STEP 4 INCREMENT 360

ABAQUS

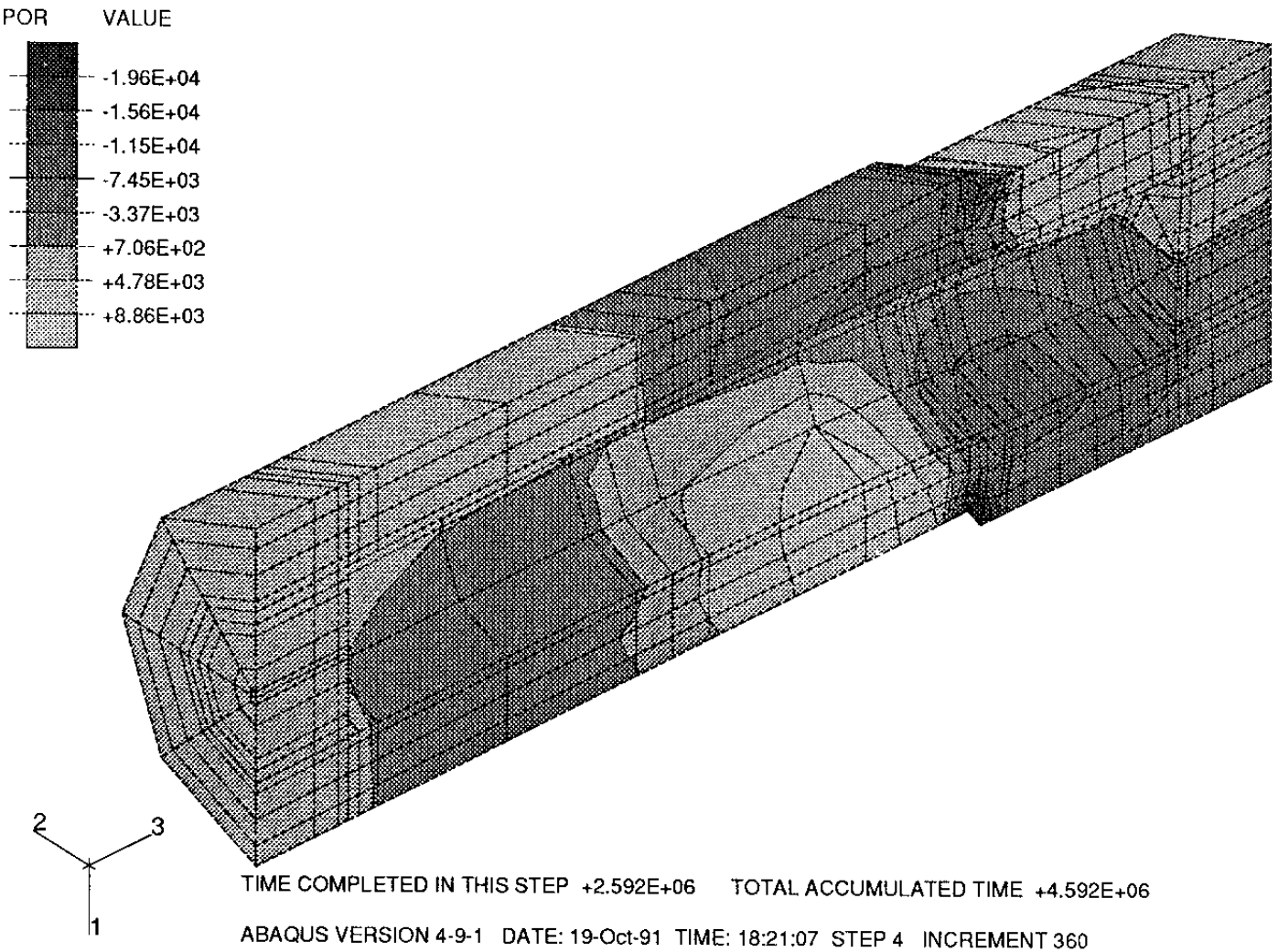

TIME COMPLETED IN THIS STEP +2.592E+06 TOTAL ACCUMULATED TIME +4.592E+06

ABAQUS VERSION 4-9-1 DATE: 19-Oct-91 TIME: 18:21:07 STEP 4 INCREMENT 360

ABAQUS

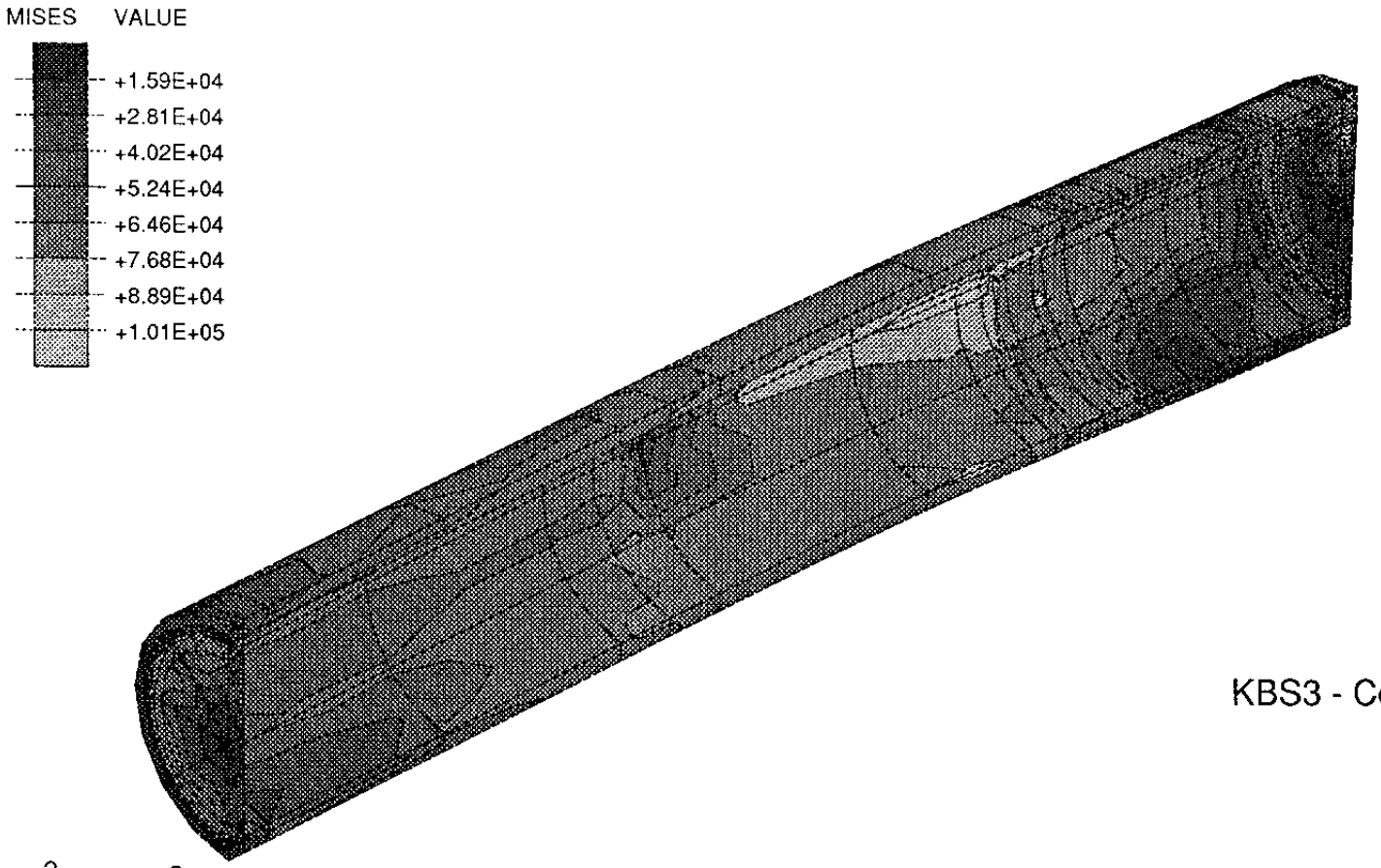

KBS3 - Copper

TIME COMPLETED IN THIS STEP +2.592E+06 TOTAL ACCUMULATED TIME +4.592E+06

ABAQUS VERSION 4-9-1 DATE: 19-Oct-91 TIME: 18:21:07 STEP 4 INCREMENT 360

ABAQUS

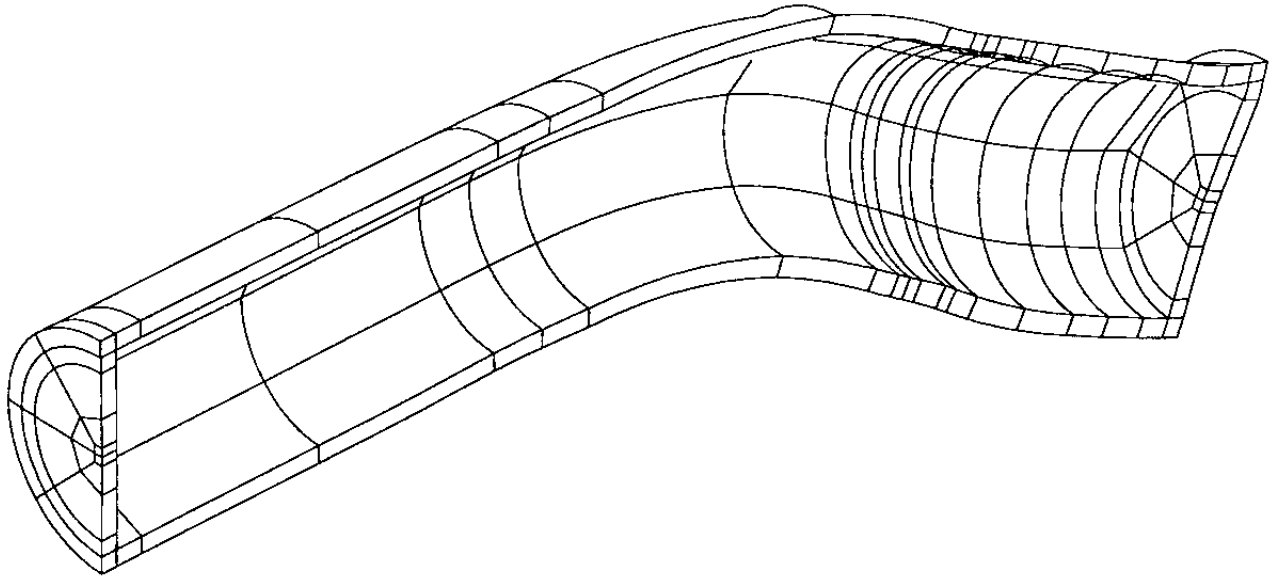

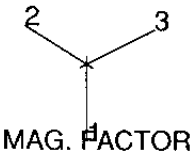

MAG. FACTOR =+1.0E+01

ABAQUS

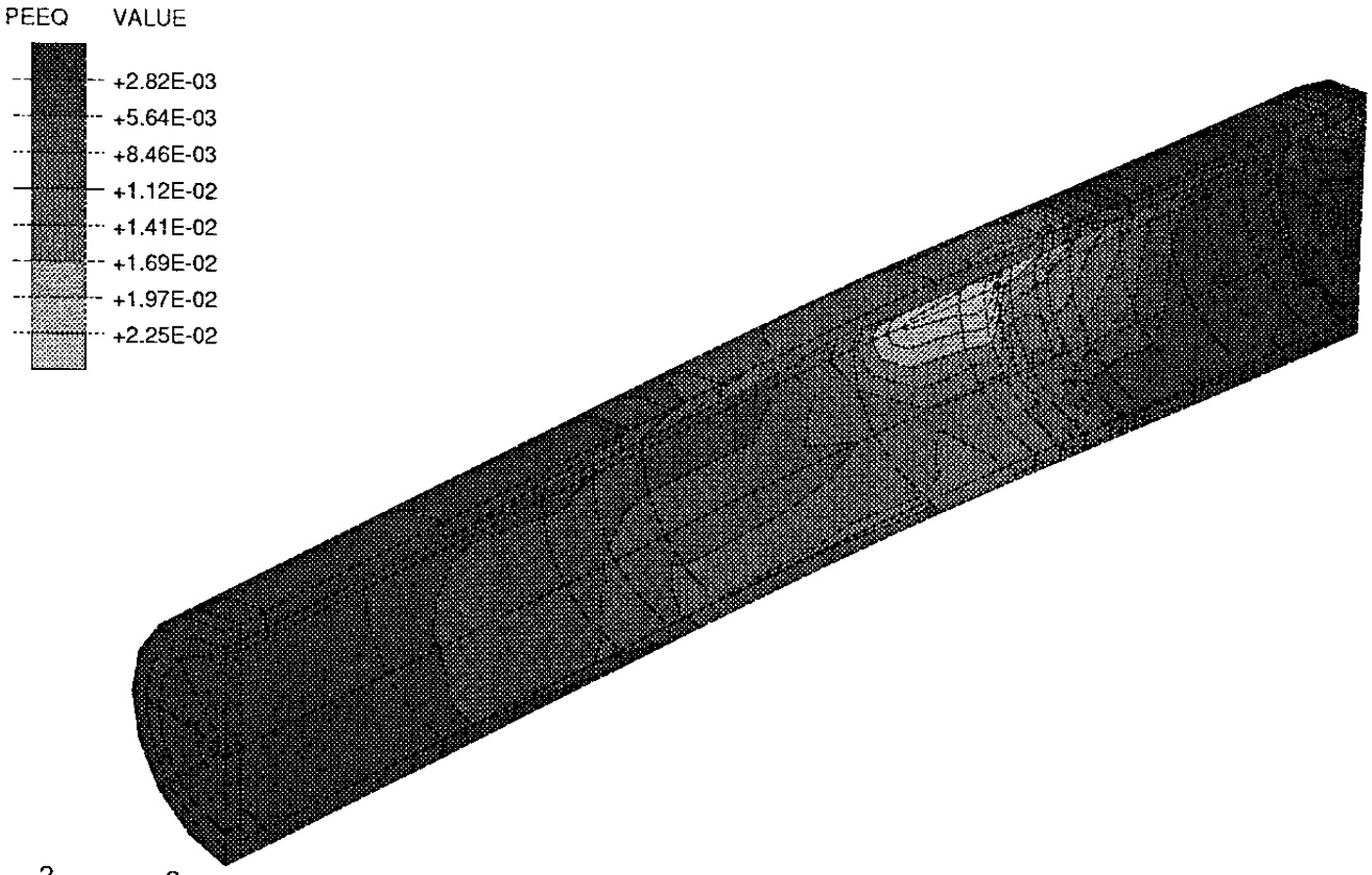

TIME COMPLETED IN THIS STEP +2.592E+06 TOTAL ACCUMULATED TIME +4.592E+06

ABAQUS VERSION 4-9-1 DATE: 19-Oct-91 TIME: 18:21:07 STEP 4 INCREMENT 360

ABAQUS

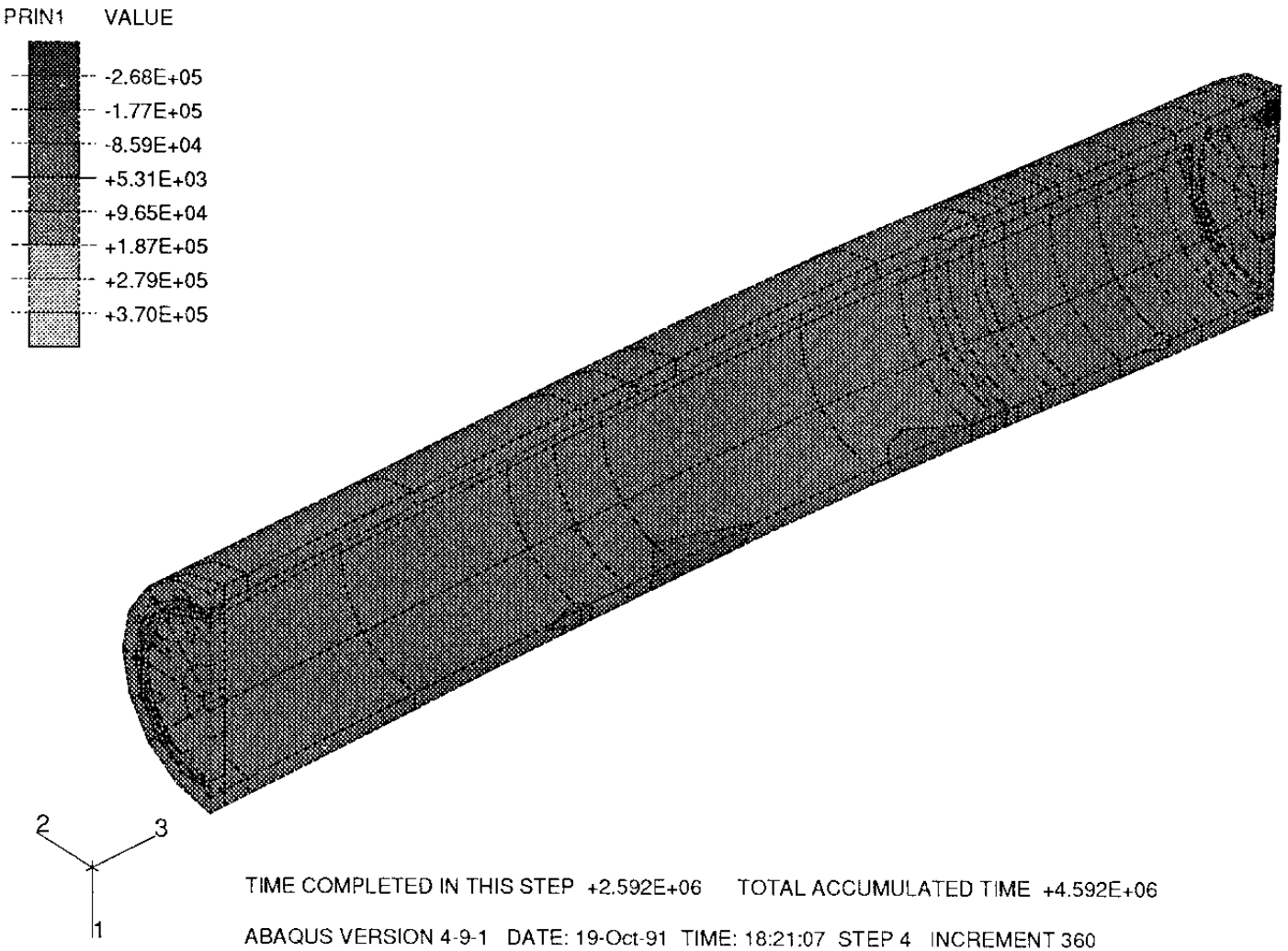

TIME COMPLETED IN THIS STEP +2.592E+06 TOTAL ACCUMULATED TIME +4.592E+06

ABAQUS VERSION 4-9-1 DATE: 19-Oct-91 TIME: 18:21:07 STEP 4 INCREMENT 360

ABAQUS

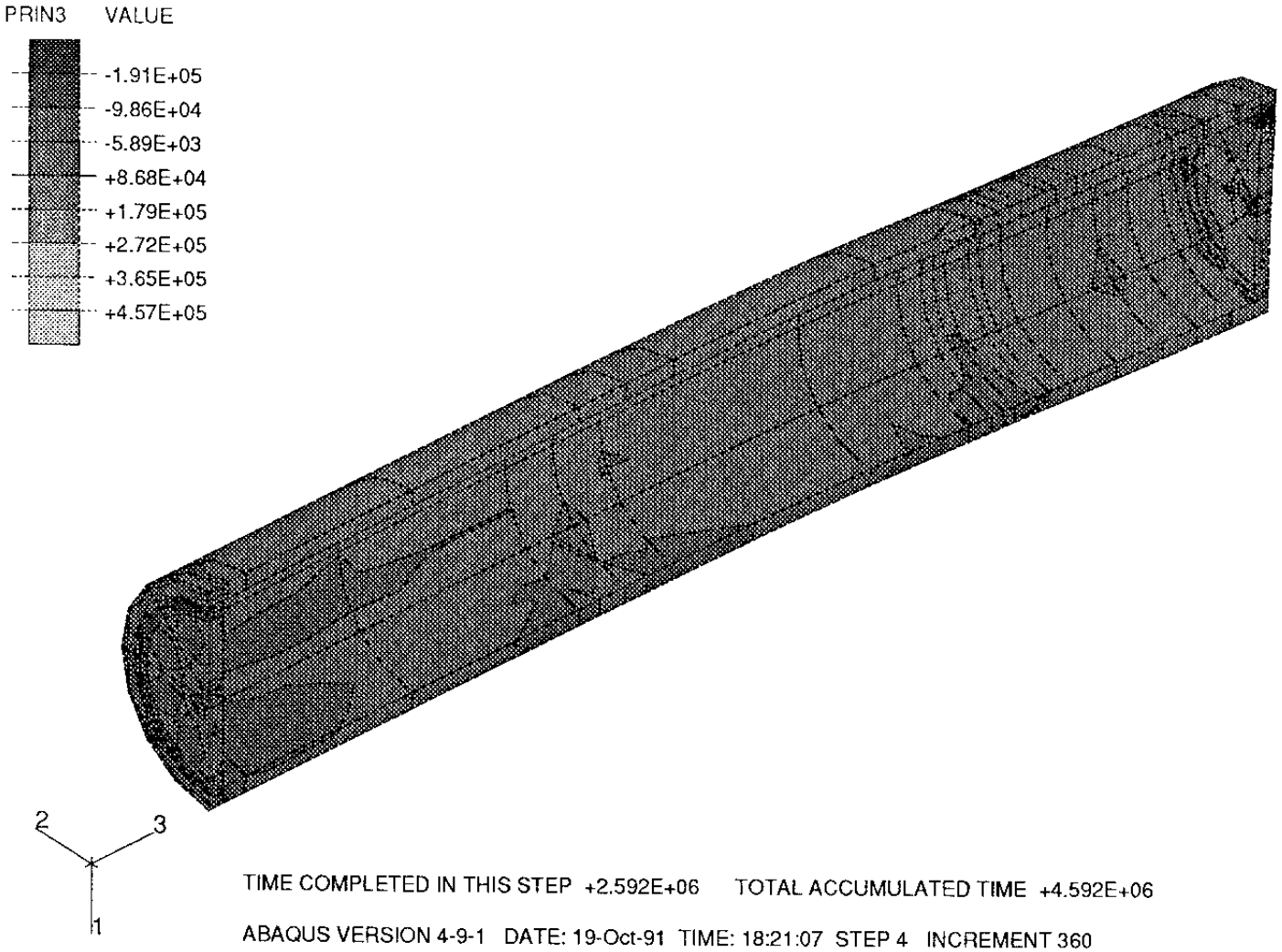

TIME COMPLETED IN THIS STEP +2.592E+06 TOTAL ACCUMULATED TIME +4.592E+06

ABAQUS VERSION 4-9-1 DATE: 19-Oct-91 TIME: 18:21:07 STEP 4 INCREMENT 360

ABAQUS

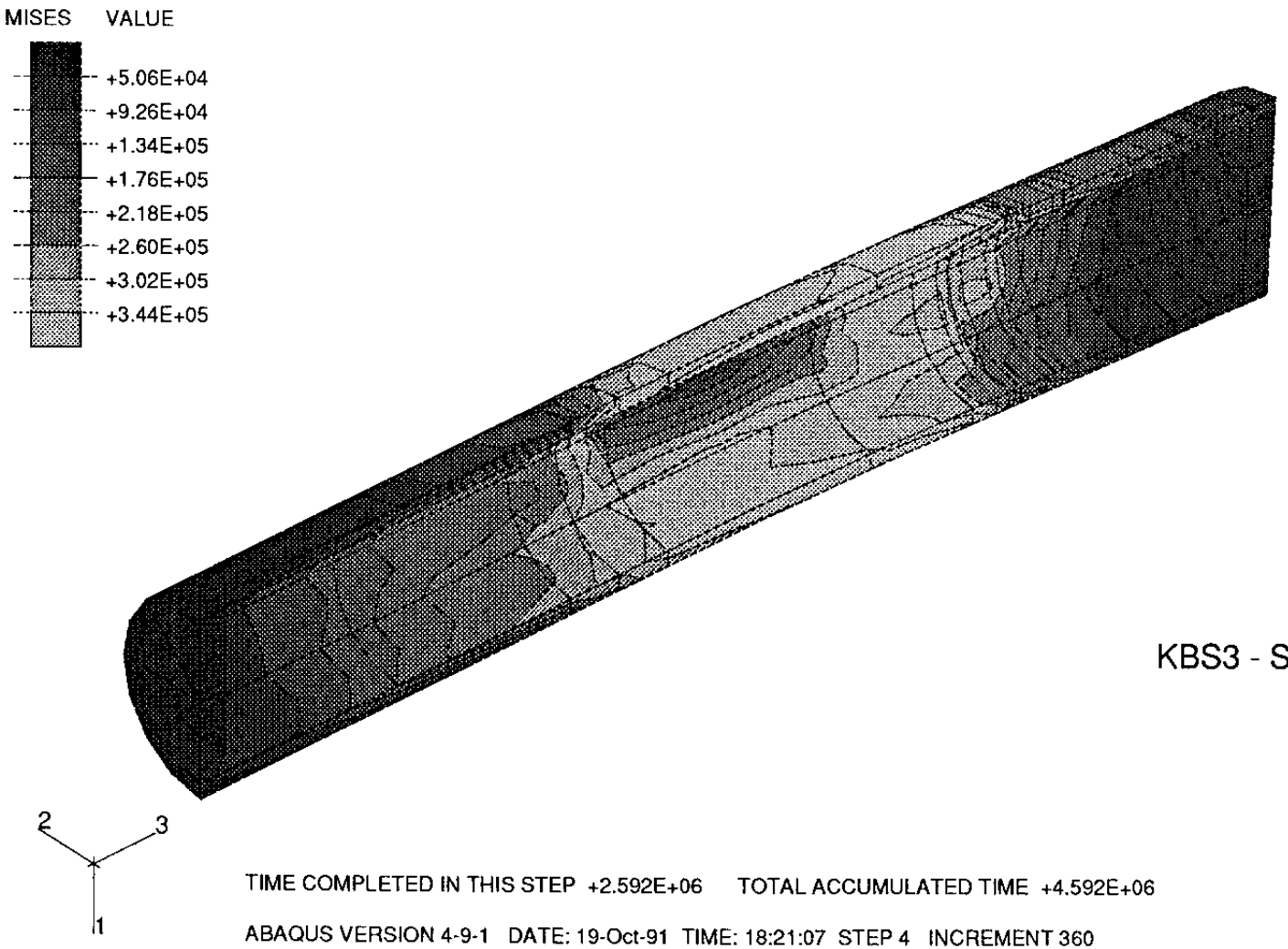

KBS3 - Steel

TIME COMPLETED IN THIS STEP +2.592E+06 TOTAL ACCUMULATED TIME +4.592E+06

ABAQUS VERSION 4-9-1 DATE: 19-Oct-91 TIME: 18:21:07 STEP 4 INCREMENT 360

ABAQUS

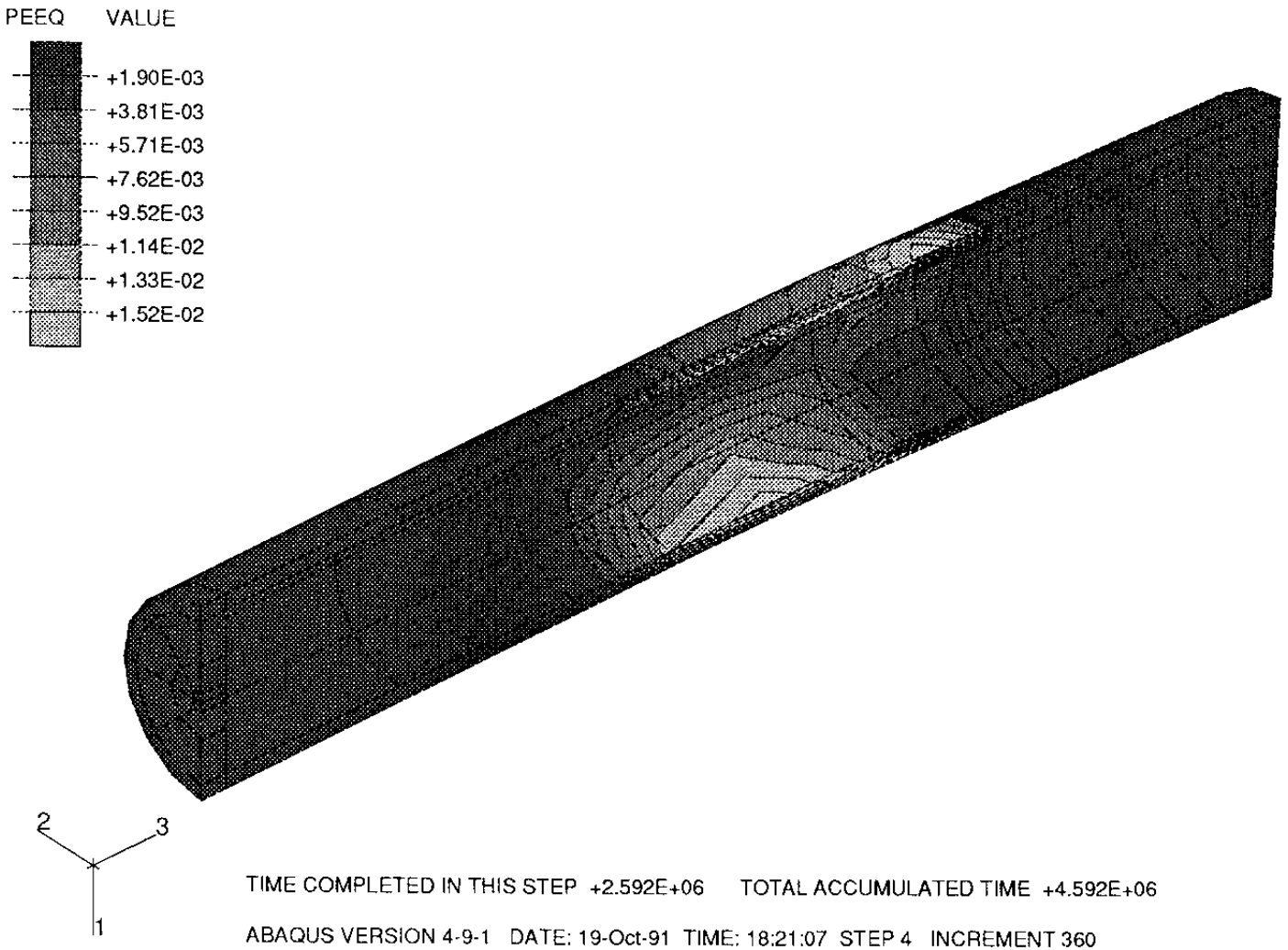

TIME COMPLETED IN THIS STEP +2.592E+06 TOTAL ACCUMULATED TIME +4.592E+06

ABAQUS VERSION 4-9-1 DATE: 19-Oct-91 TIME: 18:21:07 STEP 4 INCREMENT 360

ABAQUS

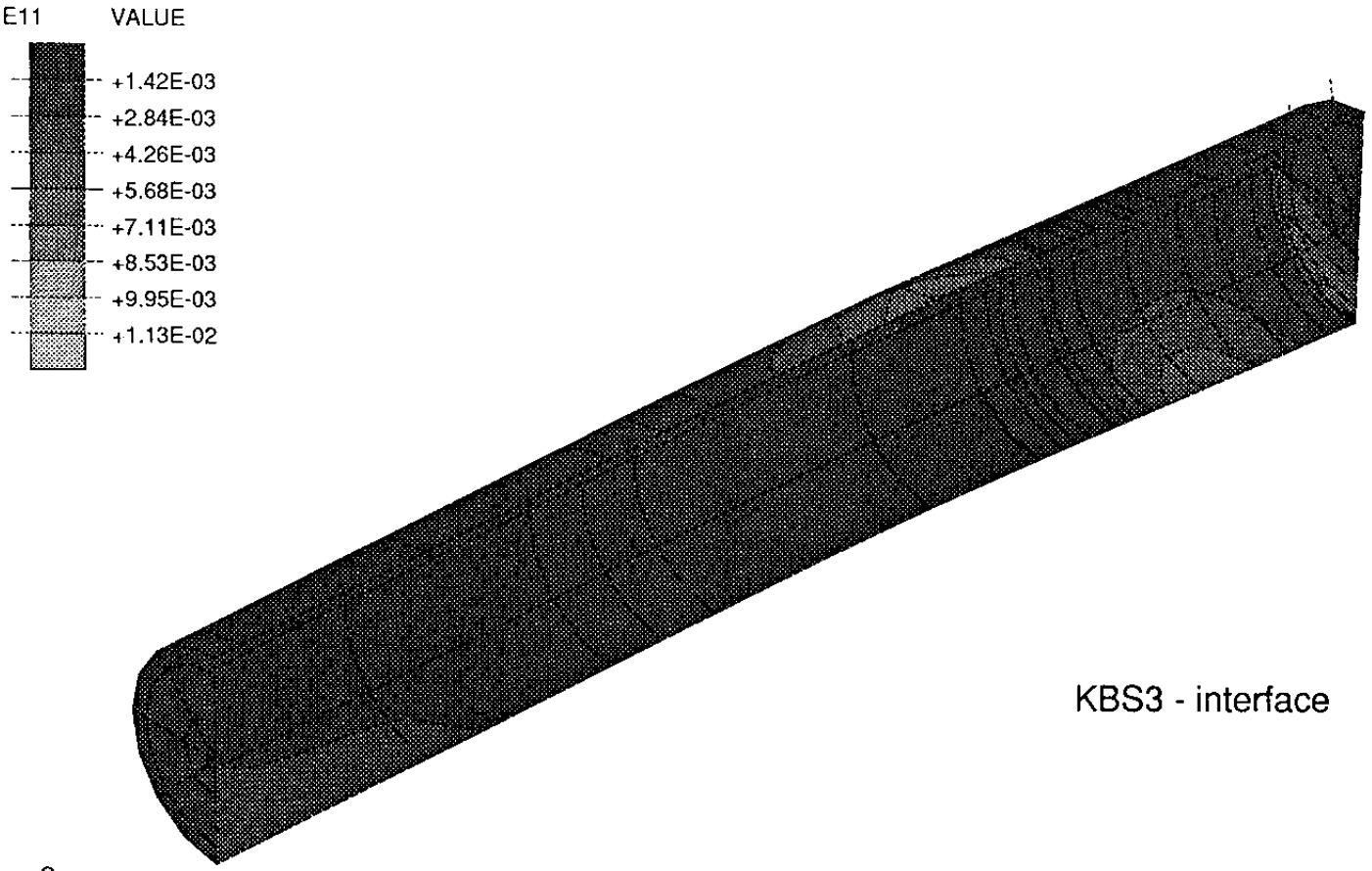

KBS3 - interface

TIME COMPLETED IN THIS STEP +2.592E+06 TOTAL ACCUMULATED TIME +4.592E+06

ABAQUS VERSION 4-9-1 DATE: 19-Oct-91 TIME: 18:21:07 STEP 4 INCREMENT 360

ABAQUS

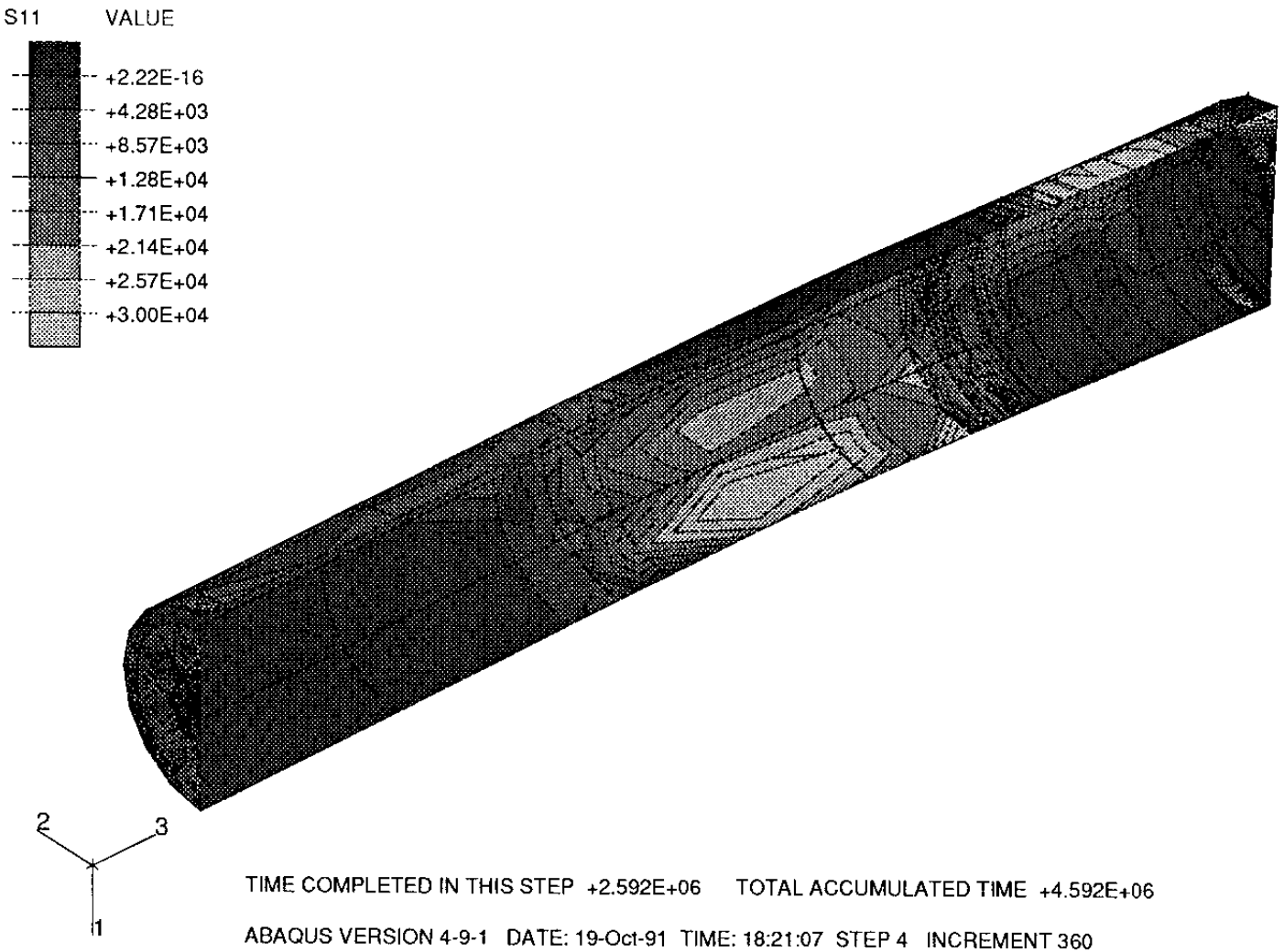

TIME COMPLETED IN THIS STEP +2.592E+06 TOTAL ACCUMULATED TIME +4.592E+06

ABAQUS VERSION 4-9-1 DATE: 19-Oct-91 TIME: 18:21:07 STEP 4 INCREMENT 360

APPENDIX VIII

Results from a swelling pressure calculation
VLH copper steel canister

VLH 910402

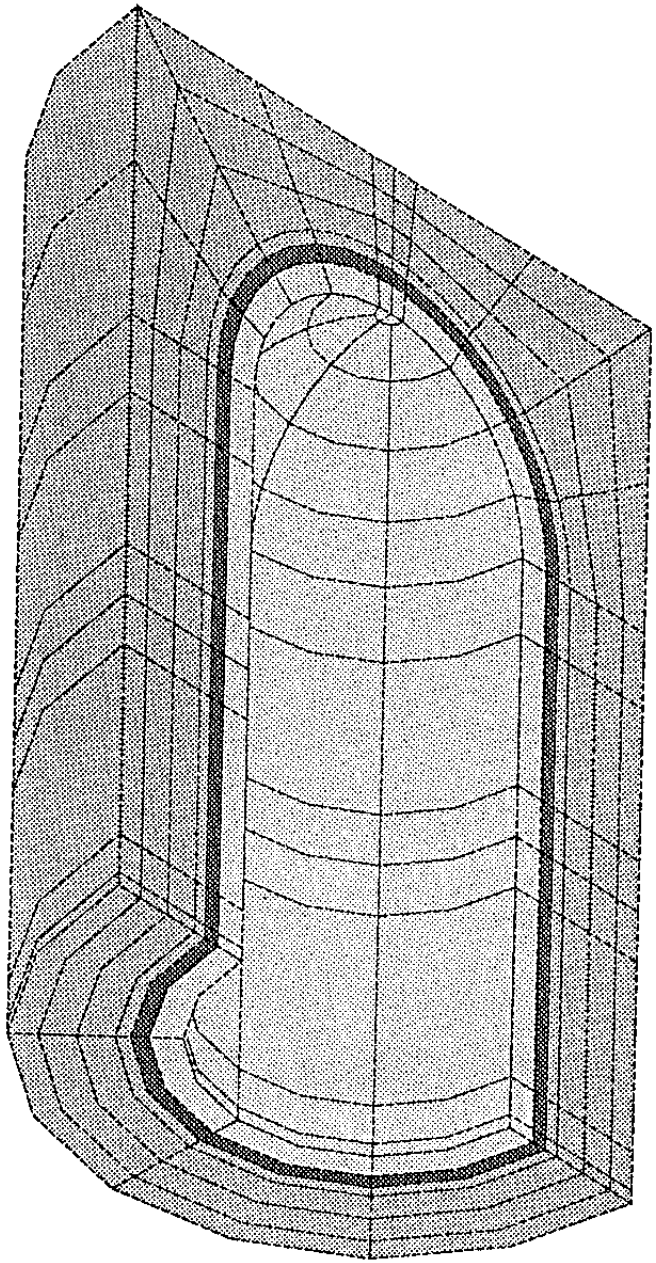

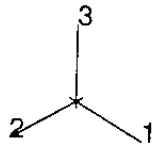

ABAQUS

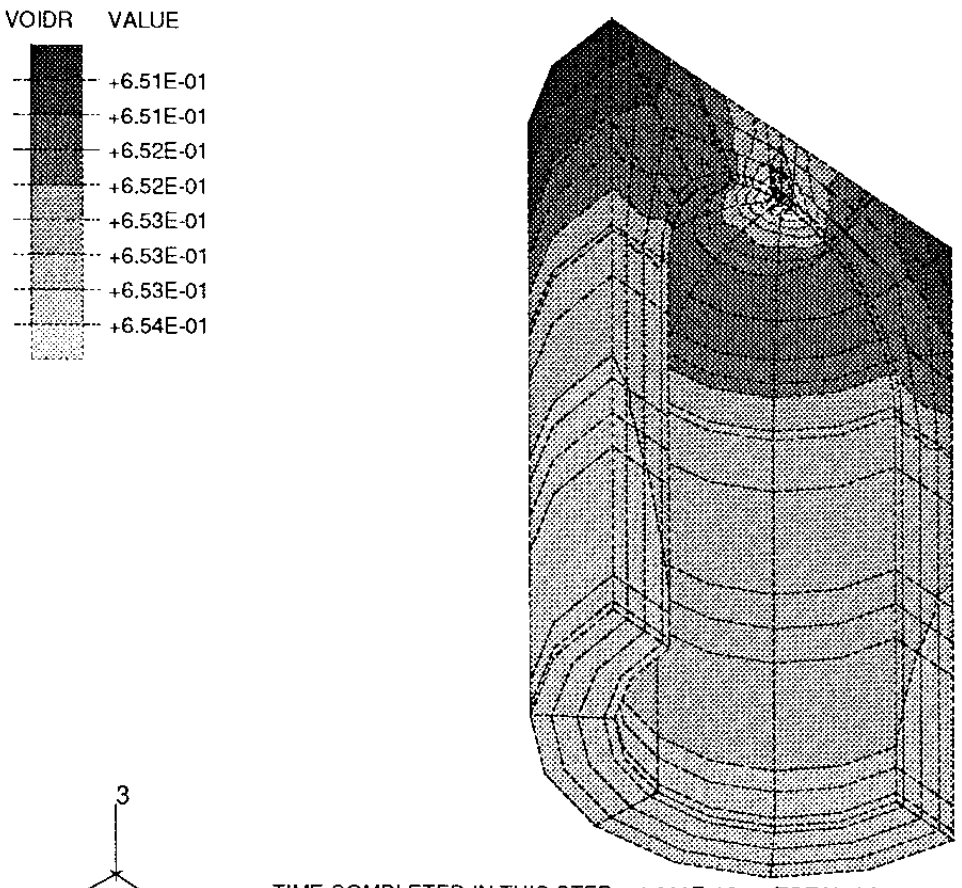

VLH - Clay

TIME COMPLETED IN THIS STEP +1.000E-06 TOTAL ACCUMULATED TIME +2.000E+00

ABAQUS VERSION 4-8-5 DATE: 7-Apr-91 TIME: 22:10:02 STEP 3 INCREMENT 1

VLH. Effect of bentonite swelling and additional hydrostatic water pressure. Clay geometry. Void ratio.

ABAQUS

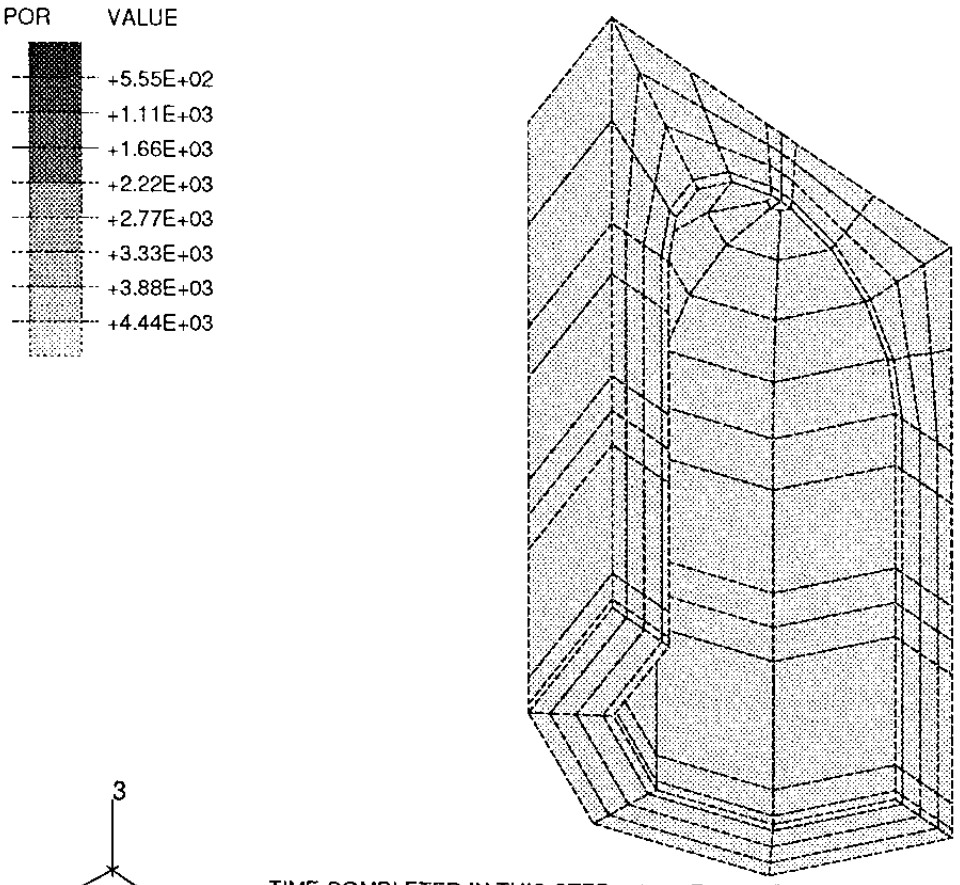

TIME COMPLETED IN THIS STEP +1.000E-06 TOTAL ACCUMULATED TIME +2.000E+00

ABAQUS VERSION 4-8-5 DATE: 7-Apr-91 TIME: 22:10:02 STEP 3 INCREMENT 1

VLH. Effect of bentonite swelling and additional hydrostatic water pressure. Clay geometry. Pore pressure.

ABAQUS

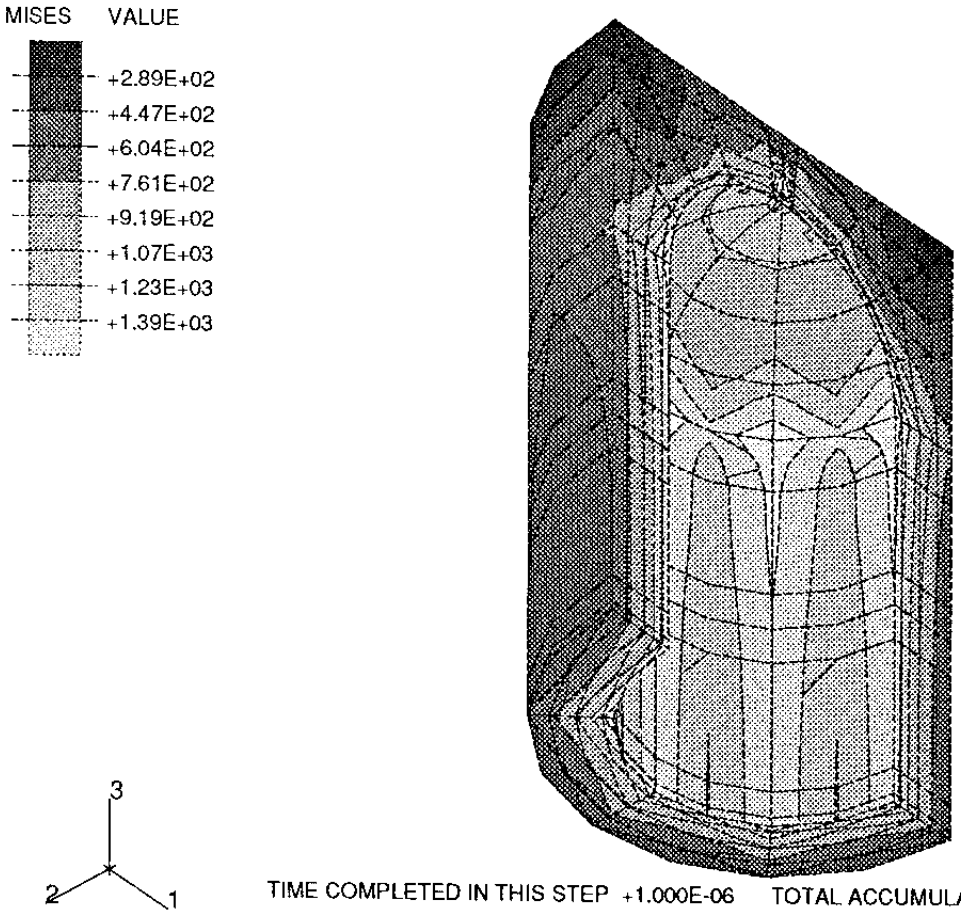

TIME COMPLETED IN THIS STEP +1.000E-06 TOTAL ACCUMULATED TIME +2.000E+00

ABAQUS VERSION 4-8-5 DATE: 7-Apr-91 TIME: 22:10:02 STEP 3 INCREMENT 1

VLH. Effect of bentonite swelling and additional hydrostatic water pressure. Clay geometry. Mises stress.

ABAQUS

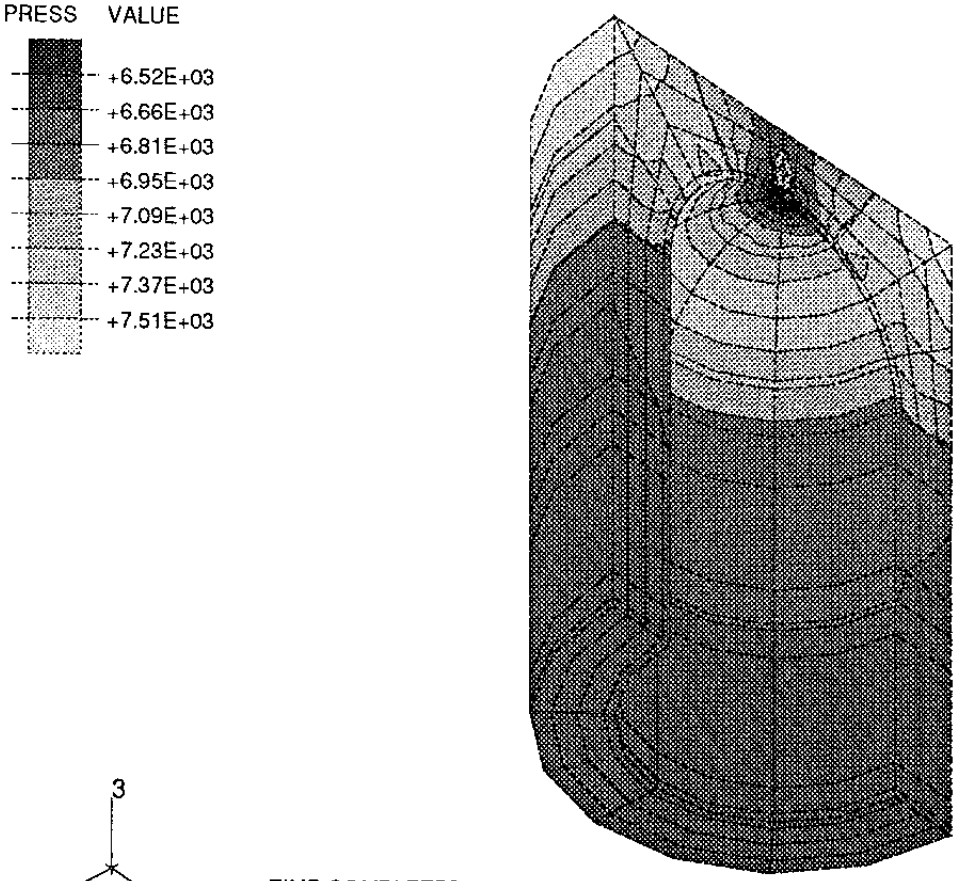

TIME COMPLETED IN THIS STEP +1.000E-06 TOTAL ACCUMULATED TIME +2.000E+00

ABAQUS VERSION 4-8-5 DATE: 7-Apr-91 TIME: 22:10:02 STEP 3 INCREMENT 1

VLH. Effect of bentonite swelling and additional hydrostatic water pressure. Clay geometry. Average effective stress.

VLH. Effect of bentonite swelling and additional hydrostatic water pressure. Copper canister. Deformed structure.

ABAQUS

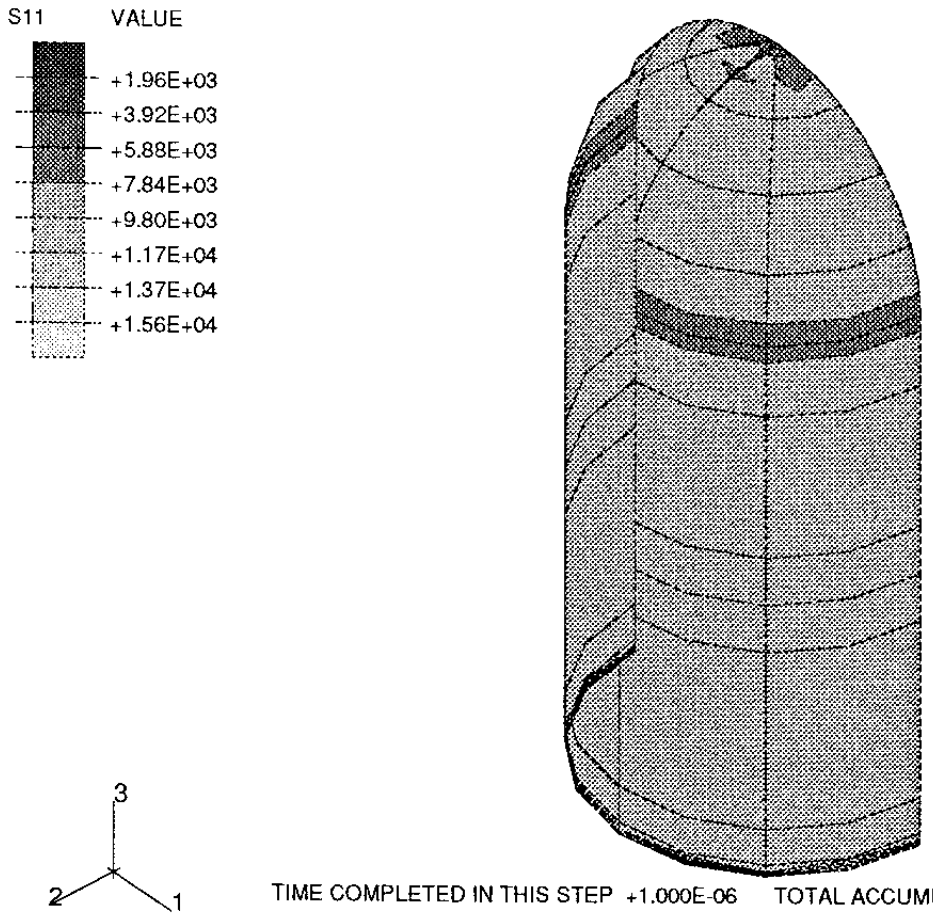

TIME COMPLETED IN THIS STEP +1.000E-06 TOTAL ACCUMULATED TIME +2.000E+00

ABAQUS VERSION 4-8-5 DATE: 7-Apr-91 TIME: 22:10:02 STEP 3 INCREMENT 1

5

VLH. Effect of bentonite swelling and additional hydrostatic water pressure. Slot. Contact pressure.

ABAQUS

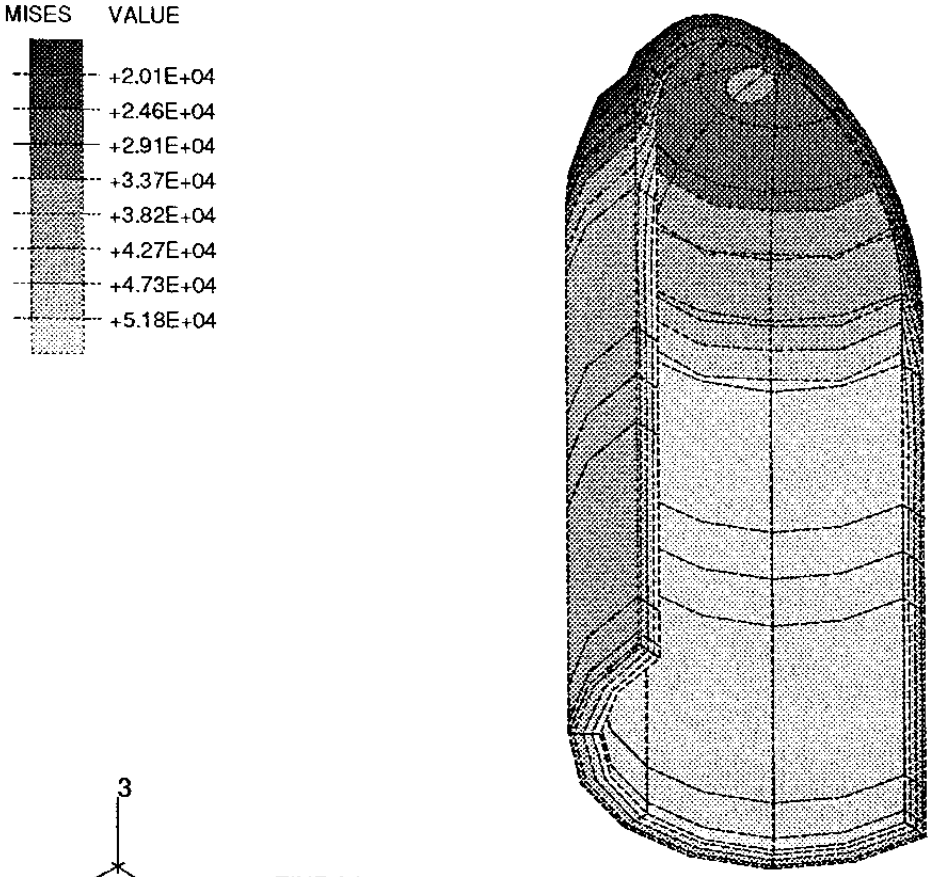

VLH - Steel

TIME COMPLETED IN THIS STEP +1.000E-06 TOTAL ACCUMULATED TIME +2.000E+00

ABAQUS VERSION 4-8-5 DATE: 7-Apr-91 TIME: 22:10:02 STEP 3 INCREMENT 1

11

VLH. Effect of bentonite swelling and additional hydrostatic water pressure. Steel cylinder. Mises stress.

APPENDIX IXb

Results from a rock shear calculation
Symmetric shear
VLH copper/steel canister

After 20 cm rock displacement

ABAQUS

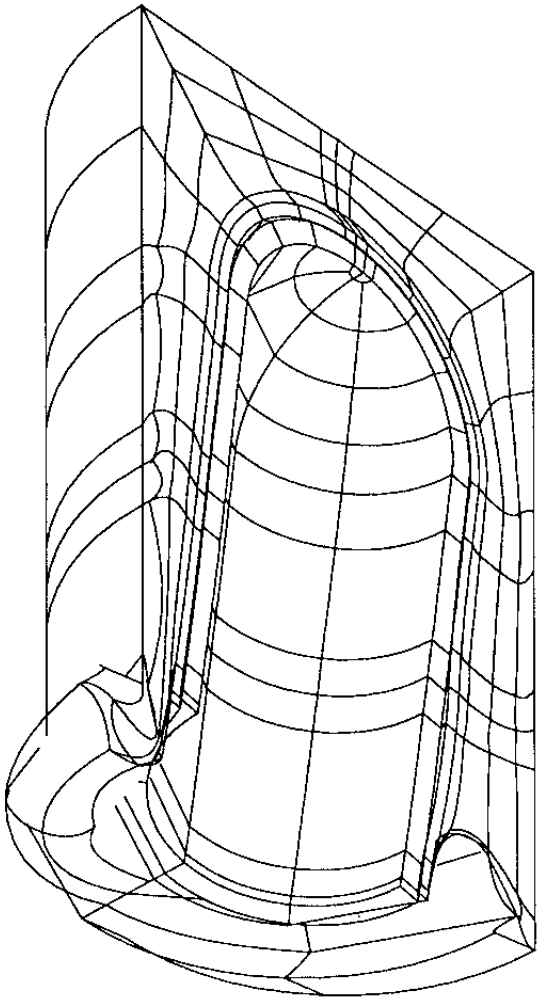

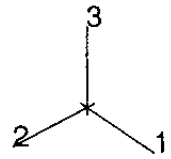

MAG. FACTOR =+2.5E+00

ABAQUS

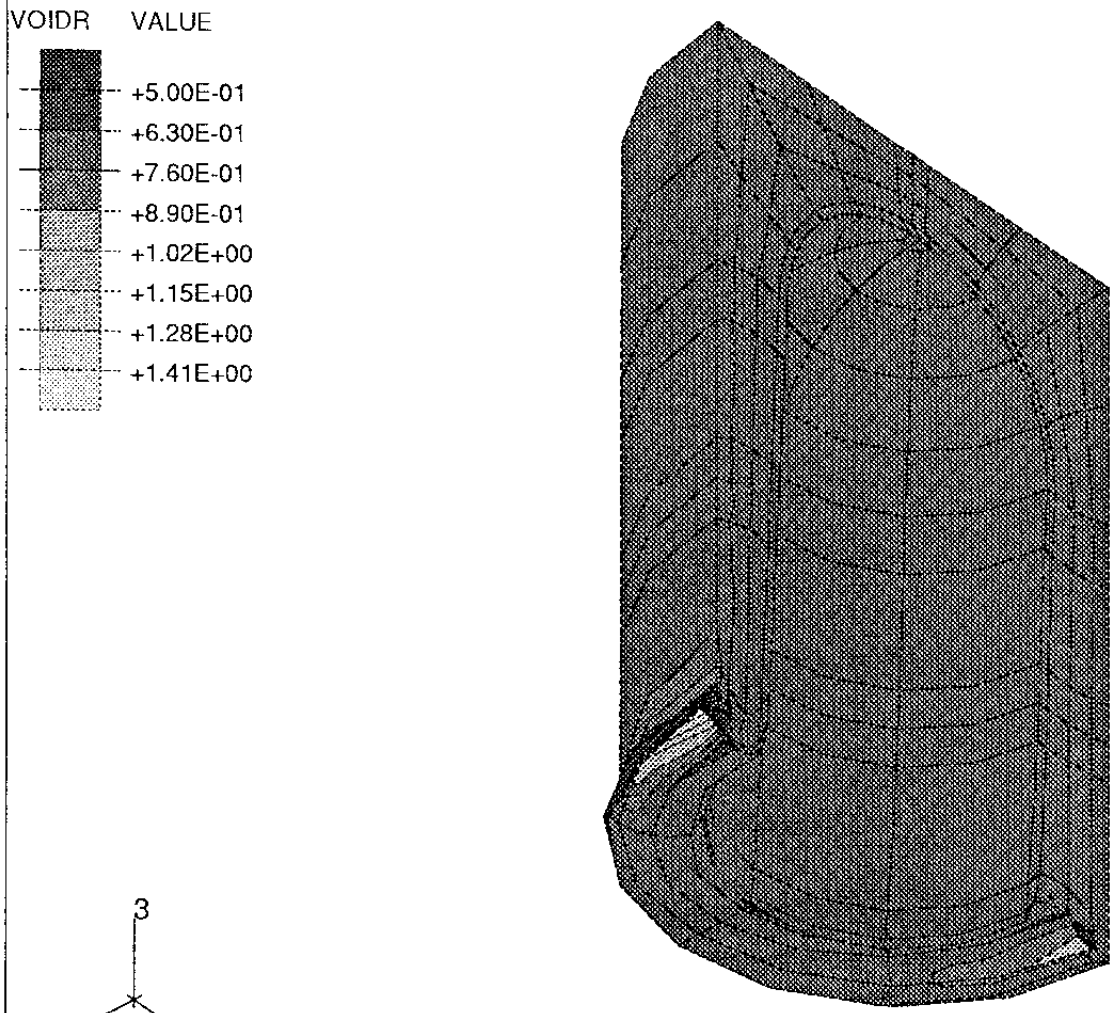

VLH - Clay

TIME COMPLETED IN THIS STEP +2.487E+06 TOTAL ACCUMULATED TIME +3.146E+06

ABAQUS VERSION 4-8-5 DATE: 29-Apr-91 TIME: 08:29:25 STEP 7 INCREMENT 320

ABAQUS

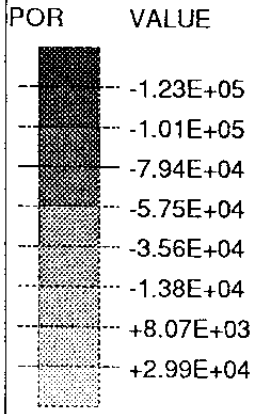

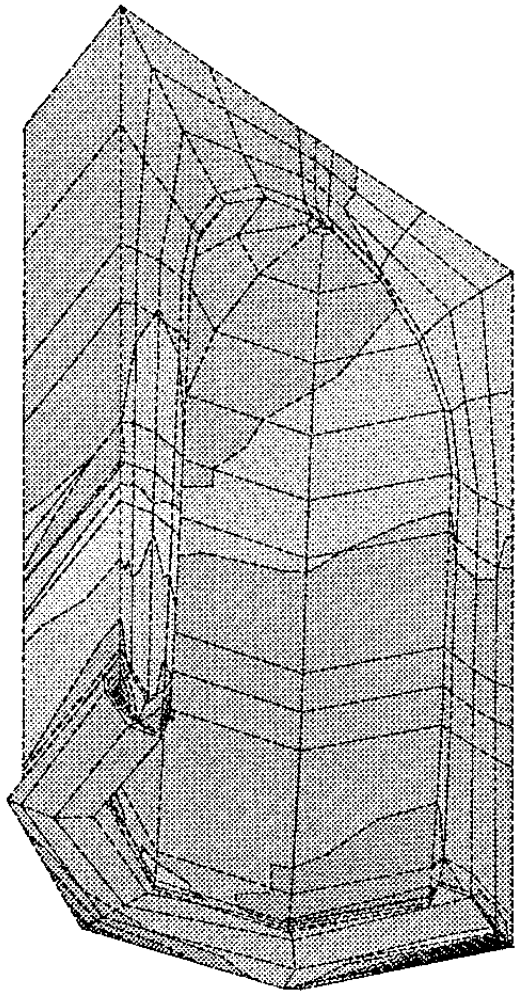

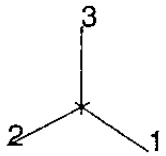

TIME COMPLETED IN THIS STEP +2.487E+06 TOTAL ACCUMULATED TIME +3.146E+06

ABAQUS VERSION 4-8-5 DATE: 29-Apr-91 TIME: 08:29:25 STEP 7 INCREMENT 320

ABAQUS

MISES VALUE

+7.92E+03
+1.54E+04
+2.30E+04
+3.05E+04
+3.81E+04
+4.56E+04
+5.32E+04
+6.07E+04

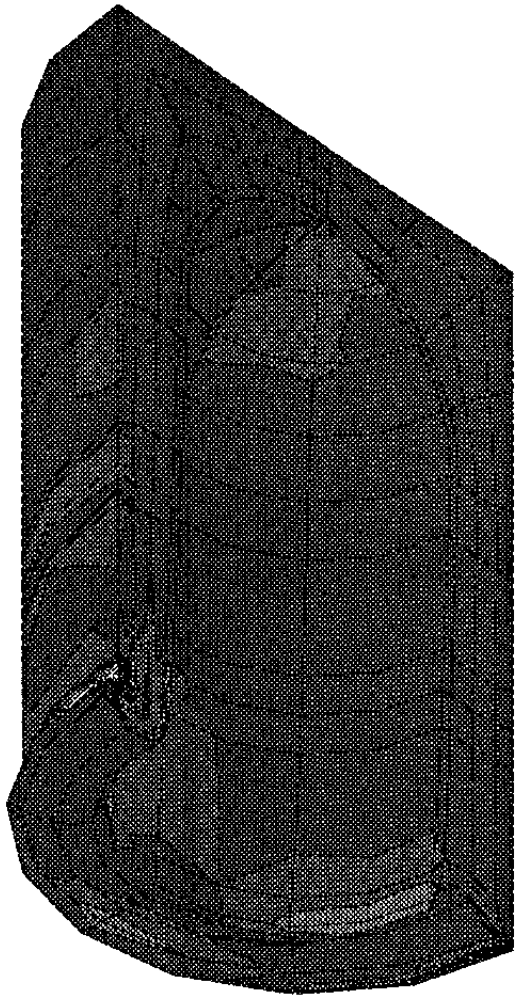

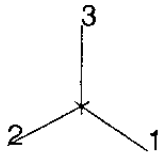

TIME COMPLETED IN THIS STEP +2.487E+06 TOTAL ACCUMULATED TIME +3.146E+06

ABAQUS VERSION 4-8-5 DATE: 29-Apr-91 TIME: 08:29:25 STEP 7 INCREMENT 320

ABAQUS

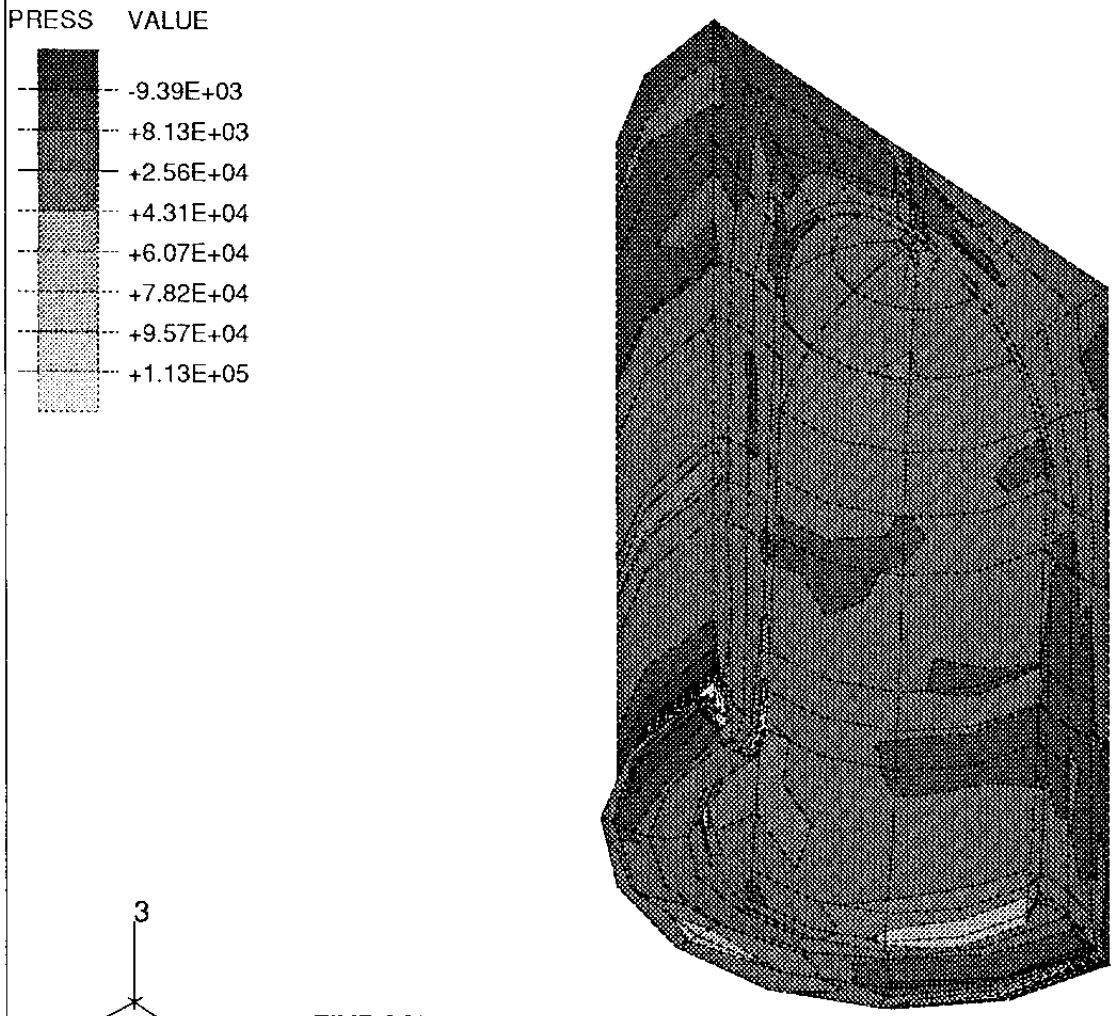

TIME COMPLETED IN THIS STEP +2.487E+06 TOTAL ACCUMULATED TIME +3.146E+06

ABAQUS VERSION 4-8-5 DATE: 29-Apr-91 TIME: 08:29:25 STEP 7 INCREMENT 320

ABAQUS

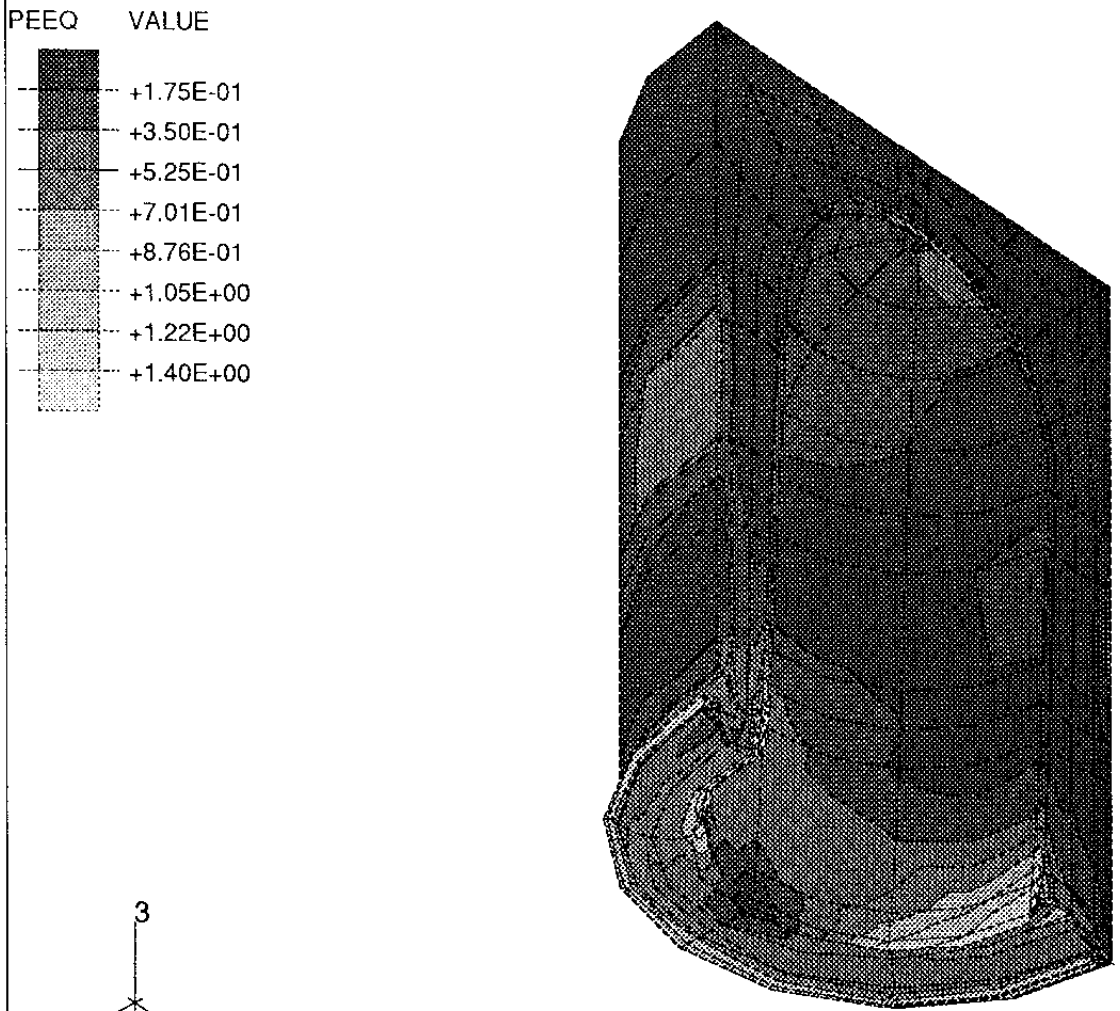

TIME COMPLETED IN THIS STEP +2.487E+06 TOTAL ACCUMULATED TIME +3.146E+06

ABAQUS VERSION 4-8-5 DATE: 29-Apr-91 TIME: 08:29:25 STEP 7 INCREMENT 320

ABAQUS

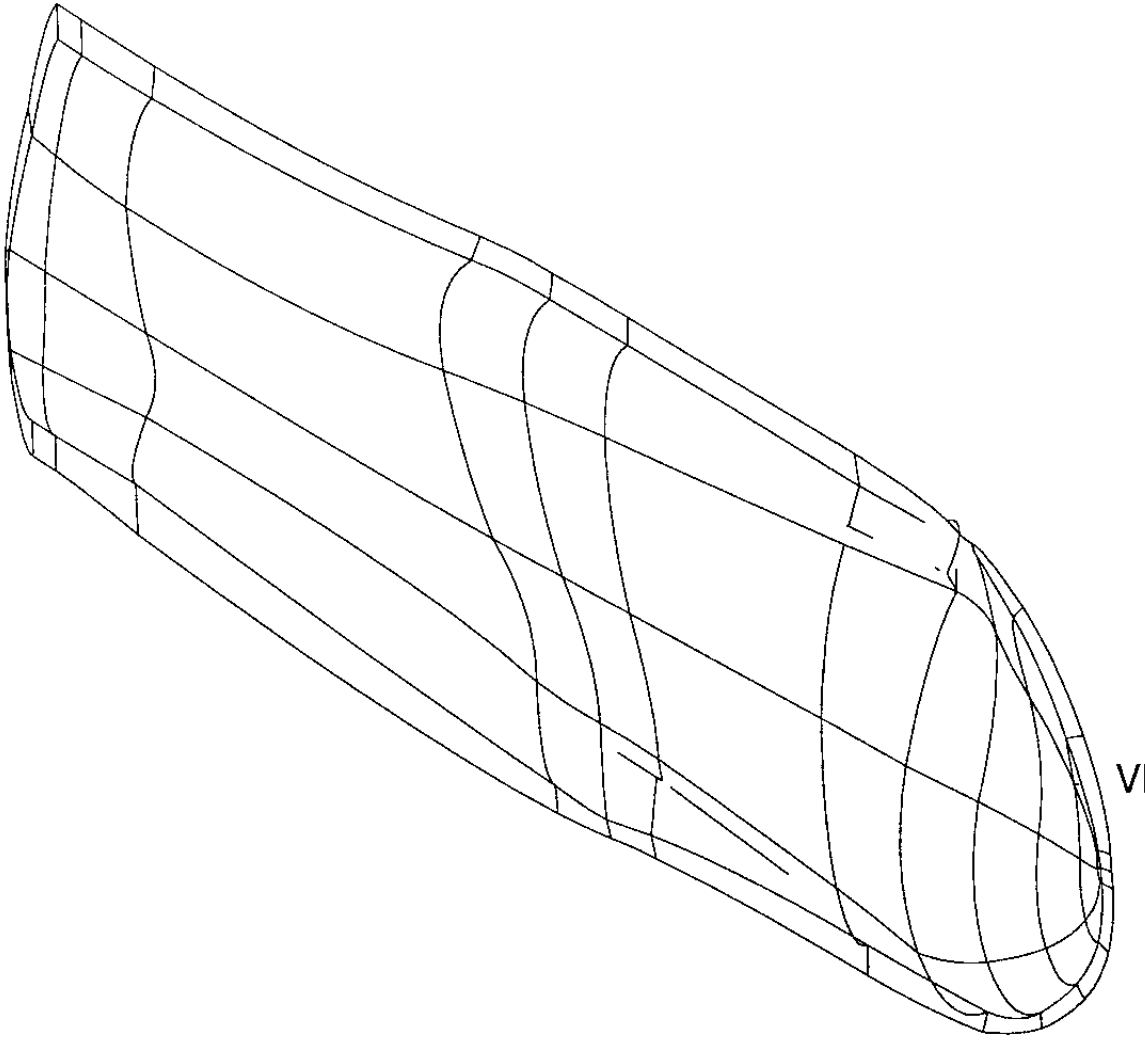

VLH - Copper

3
2
1

MAG. FACTOR =+2.0E+02

ABAQUS

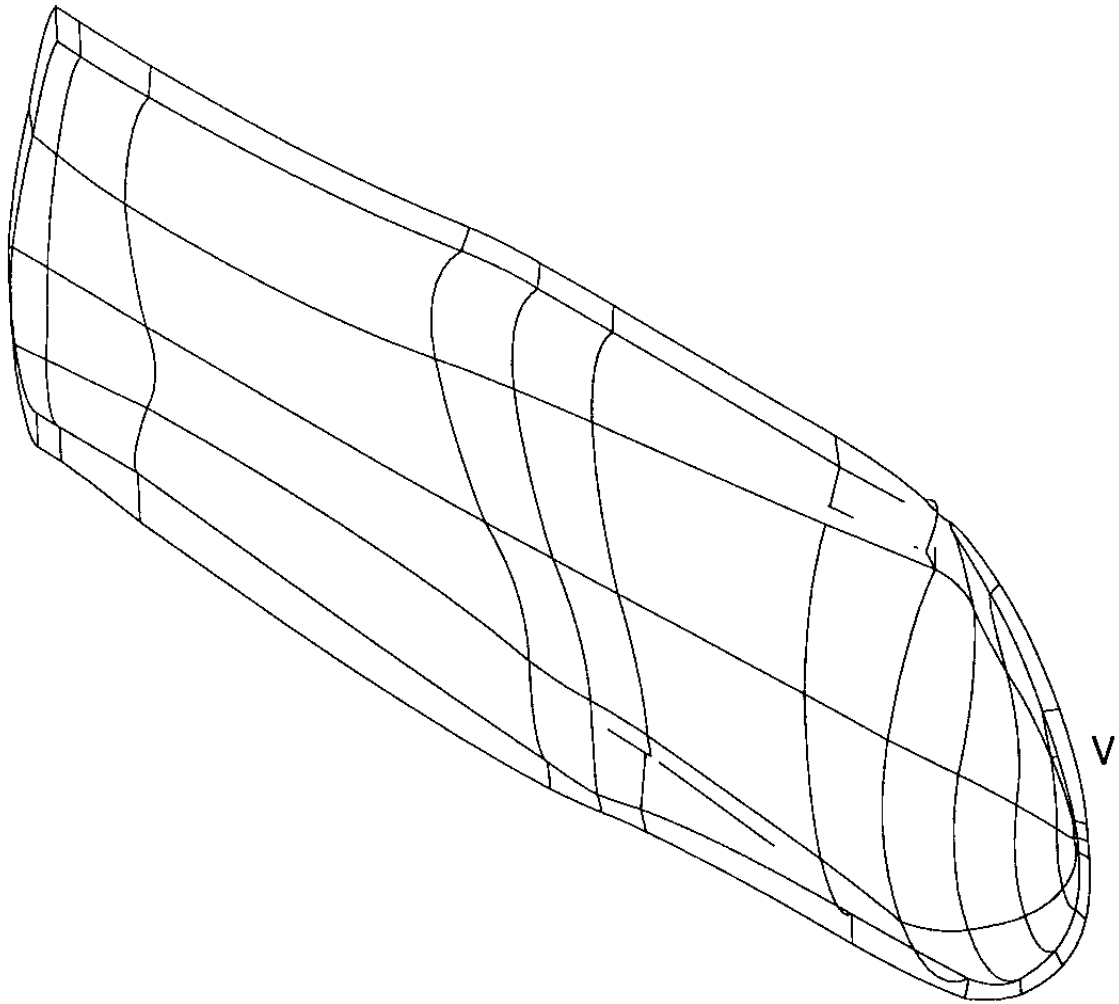

VLH - Copper

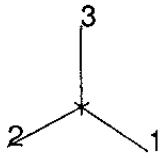

MAG. FACTOR =+2.0E+02

ABAQUS

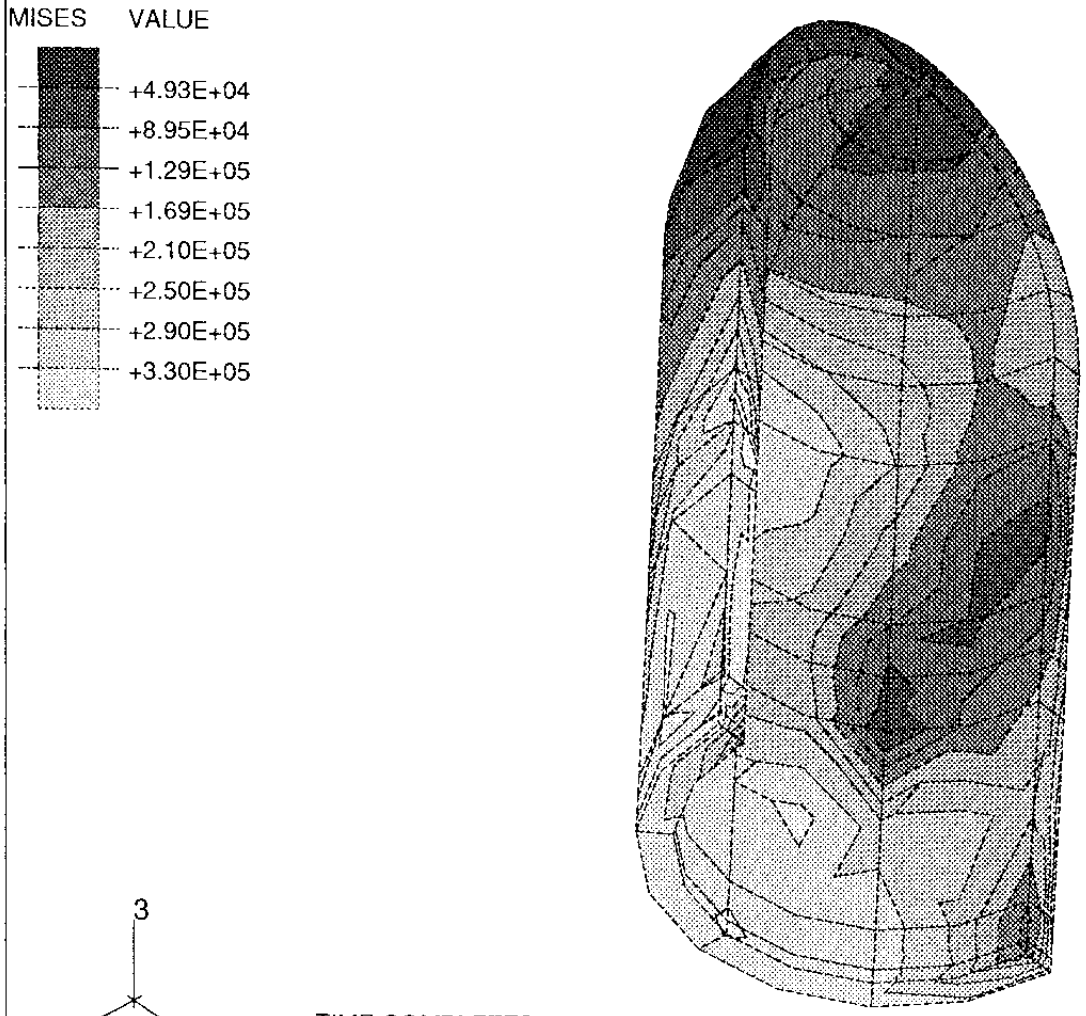

VLH - Steel

TIME COMPLETED IN THIS STEP +2.487E+06 TOTAL ACCUMULATED TIME +3.146E+06

ABAQUS VERSION 4-8-5 DATE: 29-Apr-91 TIME: 08:29:25 STEP 7 INCREMENT 320

ABAQUS

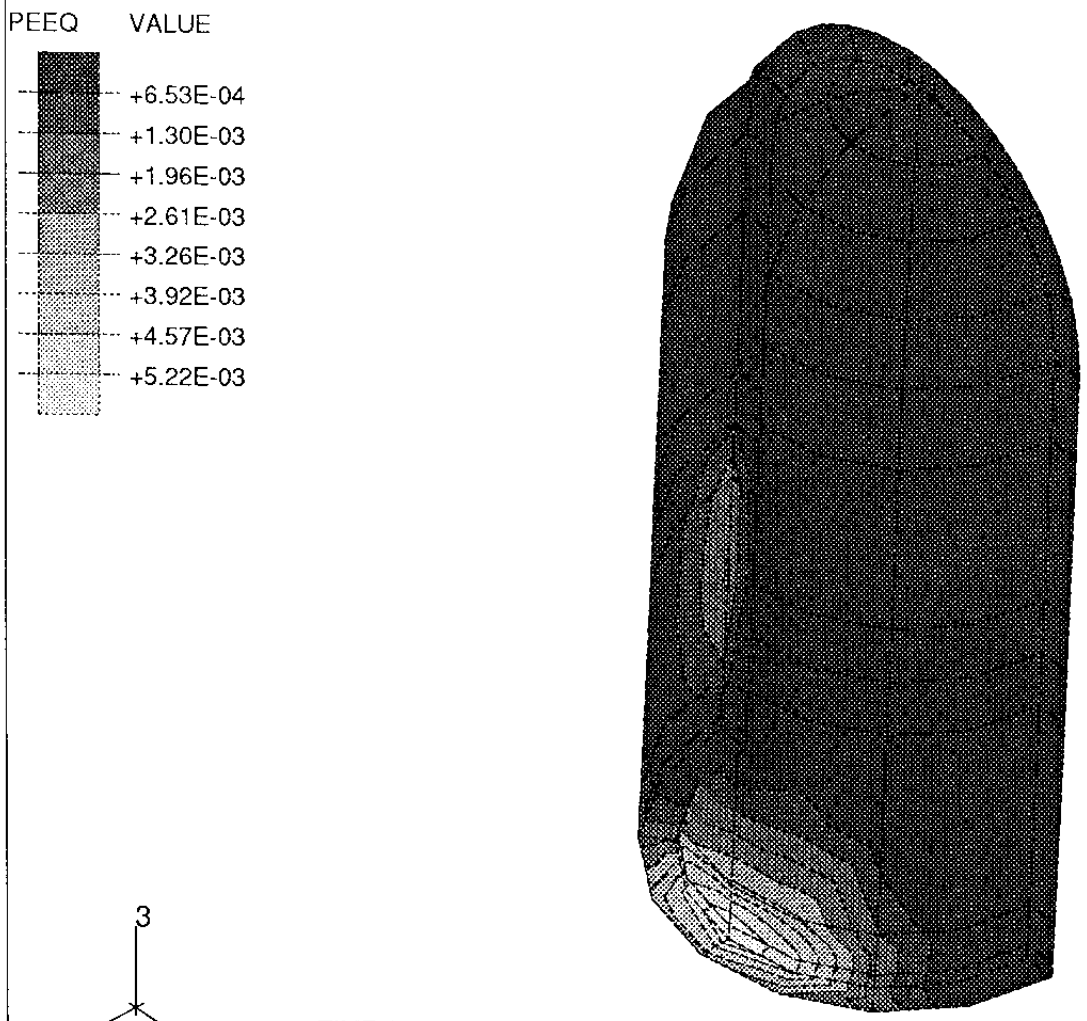

TIME COMPLETED IN THIS STEP +2.487E+06 TOTAL ACCUMULATED TIME +3.146E+06

ABAQUS VERSION 4-8-5 DATE: 29-Apr-91 TIME: 08:29:25 STEP 7 INCREMENT 320

ABAQUS

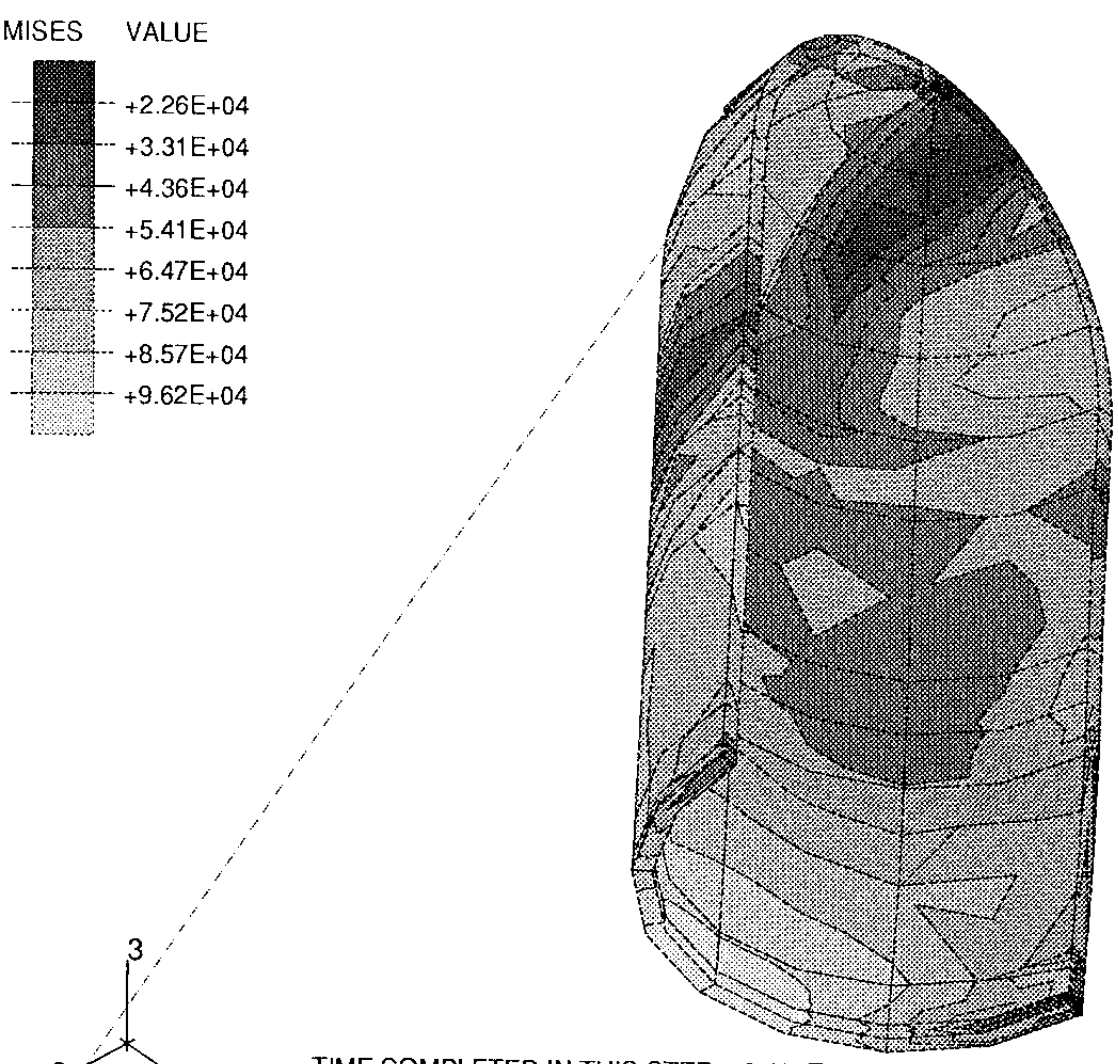

TIME COMPLETED IN THIS STEP +2.487E+06 TOTAL ACCUMULATED TIME +3.146E+06

ABAQUS VERSION 4-8-5 DATE: 29-Apr-91 TIME: 08:29:25 STEP 7 INCREMENT 320

ABAQUS

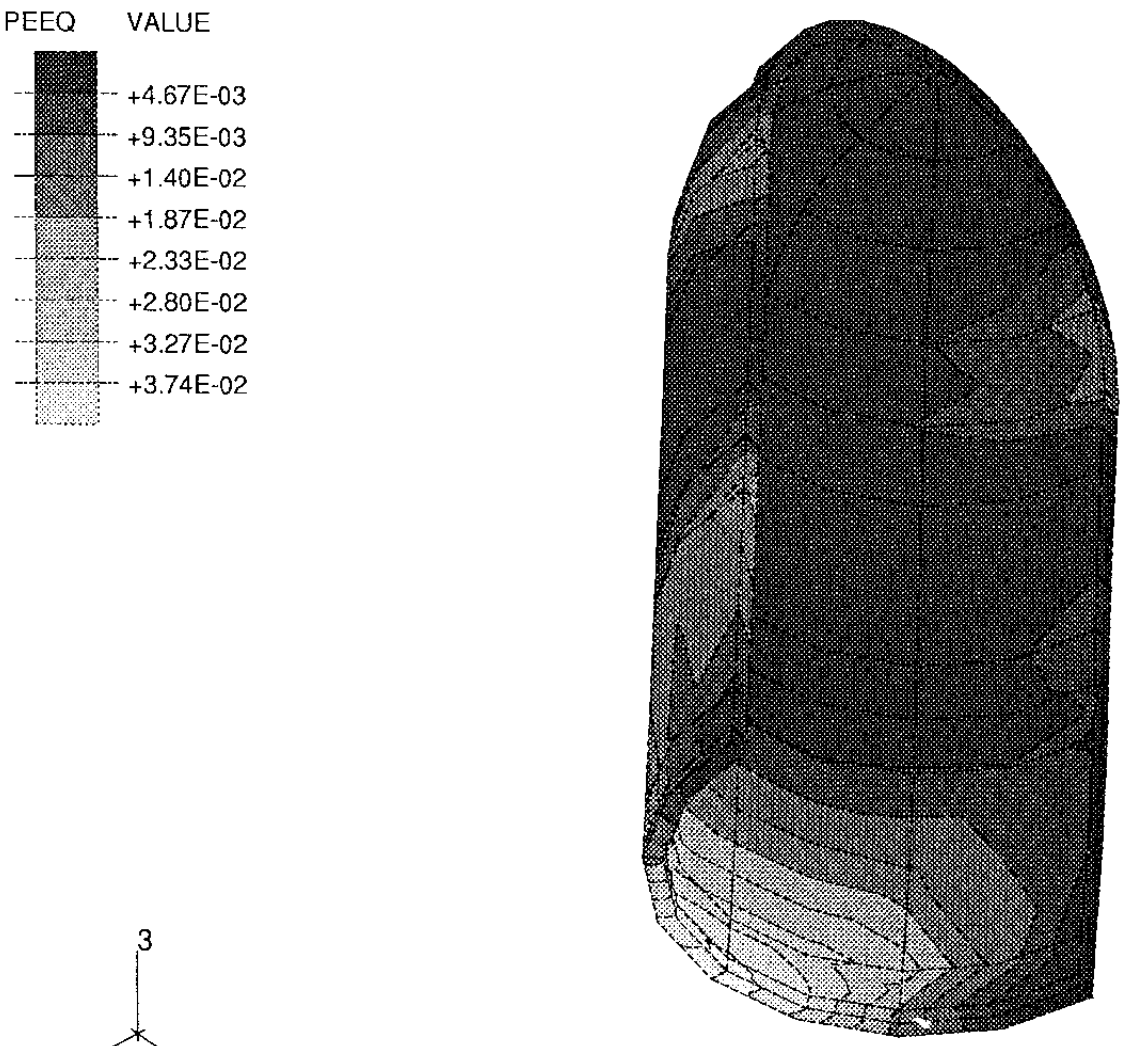

TIME COMPLETED IN THIS STEP +2.487E+06 TOTAL ACCUMULATED TIME +3.146E+06

ABAQUS VERSION 4-8-5 DATE: 29-Apr-91 TIME: 08:29:25 STEP 7 INCREMENT 320

ABAQUS

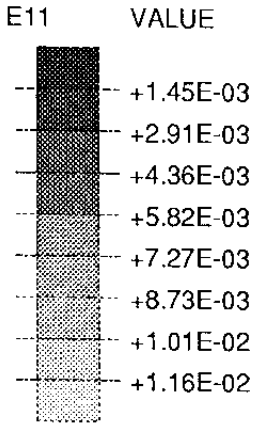

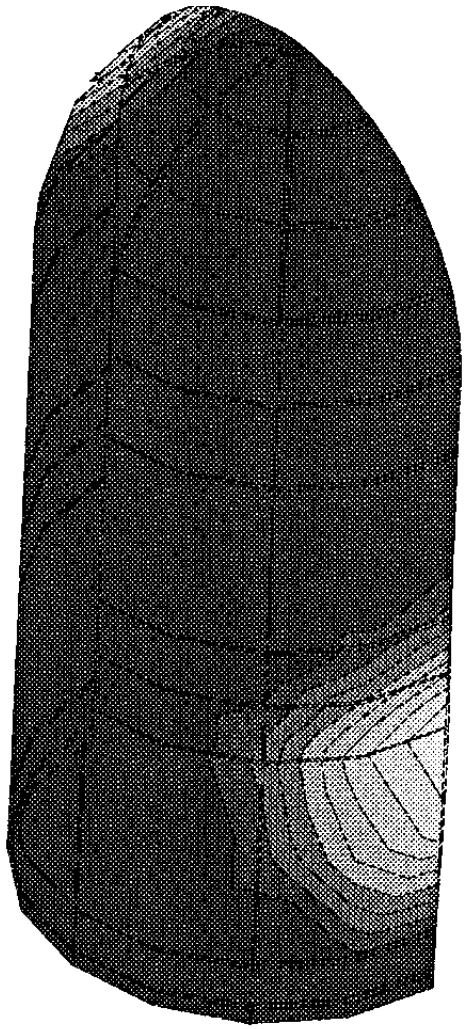

VLH - interface

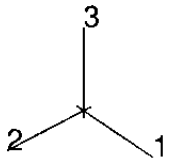

TIME COMPLETED IN THIS STEP +2.487E+06 TOTAL ACCUMULATED TIME +3.146E+06

ABAQUS VERSION 4-8-5 DATE: 29-Apr-91 TIME: 08:29:25 STEP 7 INCREMENT 320

ABAQUS

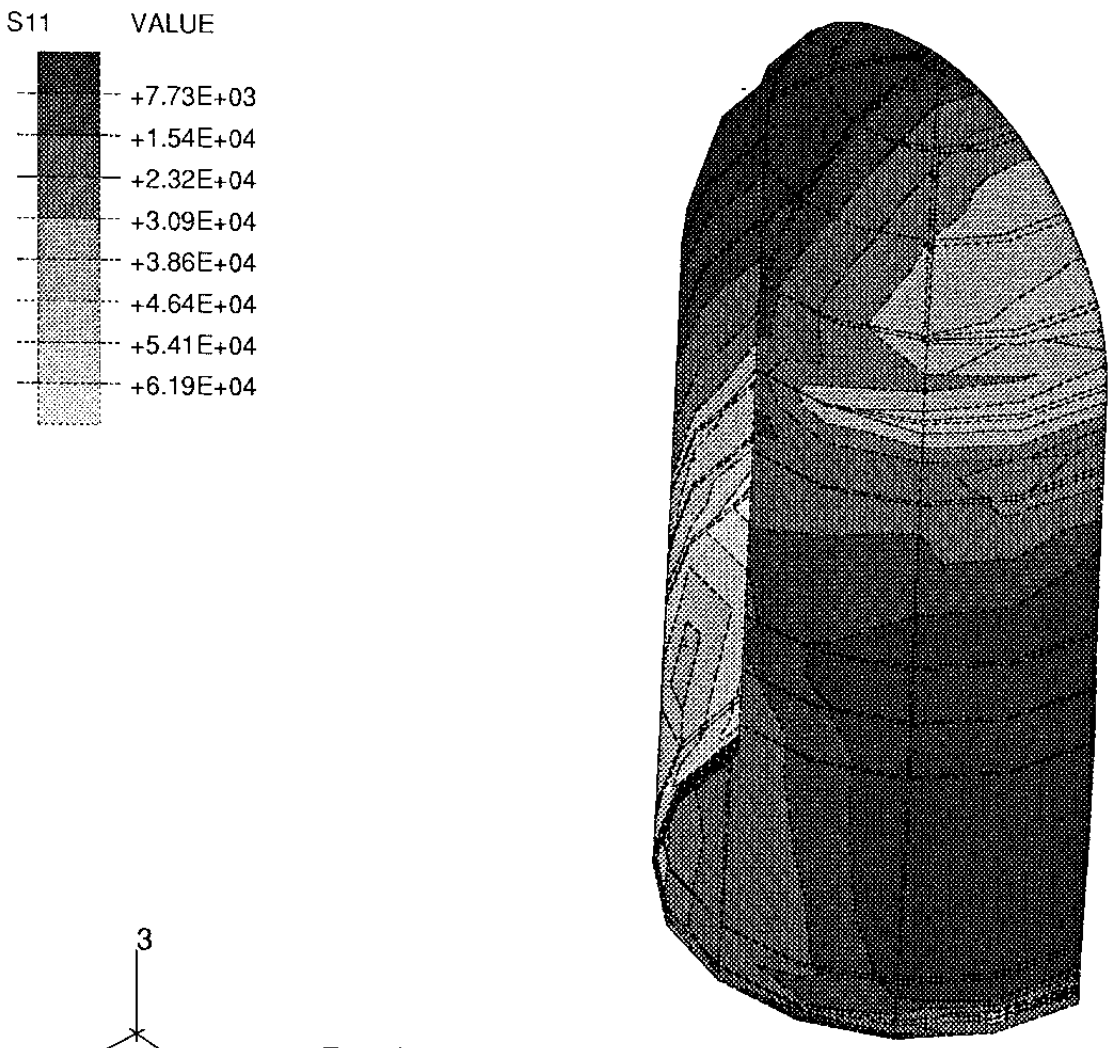

TIME COMPLETED IN THIS STEP +2.487E+06 TOTAL ACCUMULATED TIME +3.146E+06

ABAQUS VERSION 4-8-5 DATE: 29-Apr-91 TIME: 08:29:25 STEP 7 INCREMENT 320

APPENDIX IXa

Results from a rock shear calculation
Symmetric shear
VLH copper/steel canister

After 5 cm rock displacement

VLH. Effect of rock shear.

Deformed structure.

VLH. Effect of rock shear.
Clay geometry. Void ratio.

ABAQUS

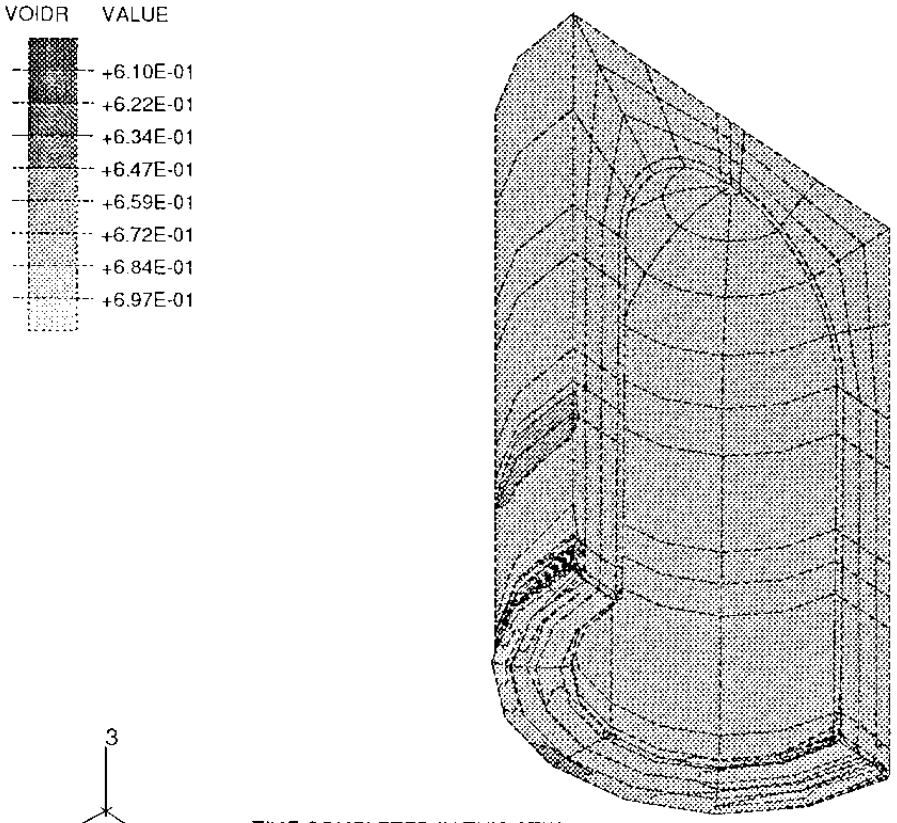

VLH - Clay

TIME COMPLETED IN THIS STEP +4.546E+05 TOTAL ACCUMULATED TIME +6.583E+05

ABAQUS VERSION 4-8-5 DATE: 15-Apr-91 TIME: 18:45:54 STEP 6 INCREMENT 50

VLH. Effect of rock shear.
Clay geometry. Pore pressure.

ABAQUS

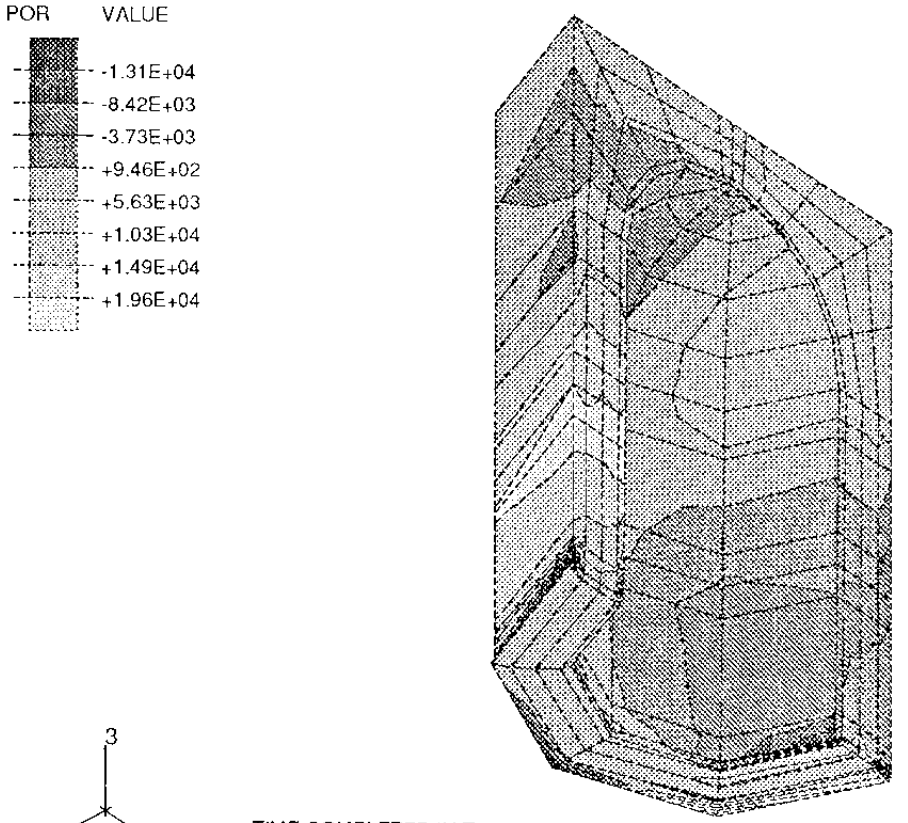

TIME COMPLETED IN THIS STEP +4.546E+05 TOTAL ACCUMULATED TIME +6.583E+05

ABAQUS VERSION 4-8-5 DATE: 15-Apr-91 TIME: 18:45:54 STEP 6 INCREMENT 50

ABAQUS

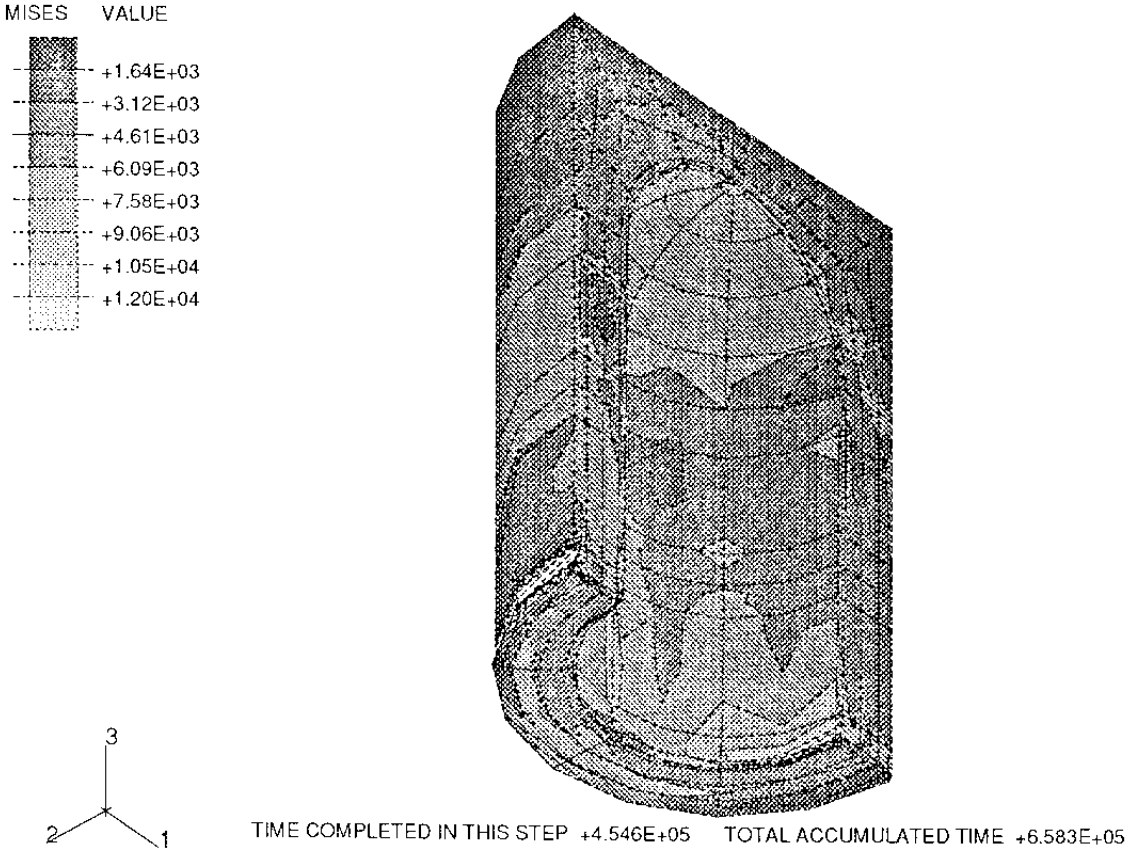

VLH. Effect of rock shear.
Clay geometry. Mises stress.

ABAQUS

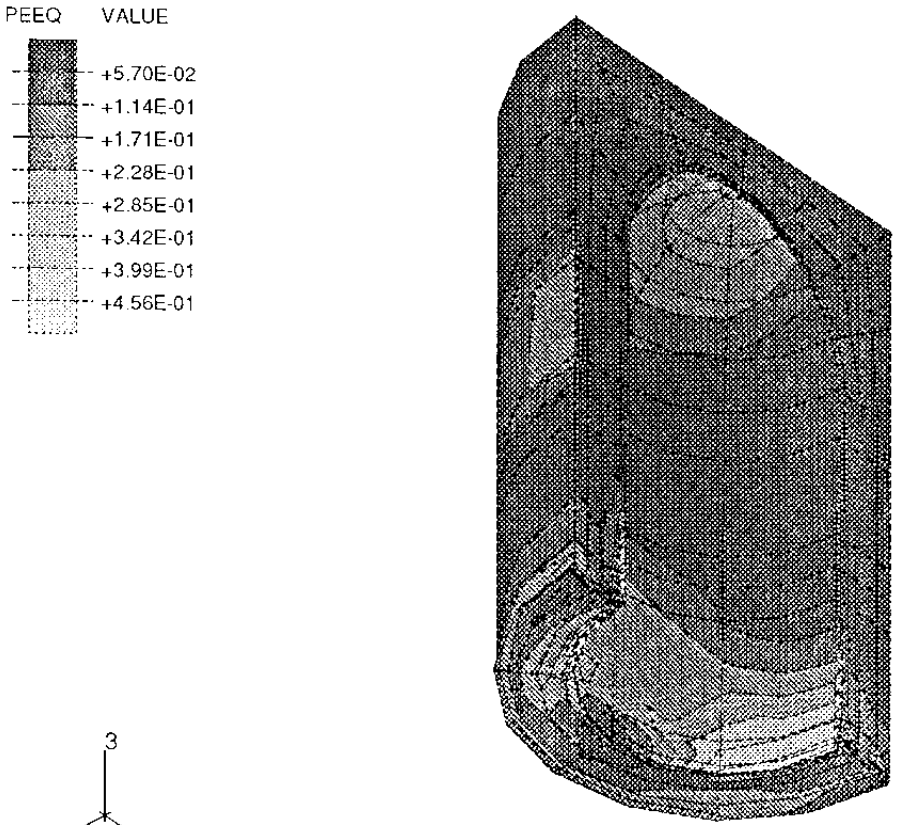

TIME COMPLETED IN THIS STEP +4.546E+05 TOTAL ACCUMULATED TIME +6.583E+05

ABAQUS VERSION 4-8-5 DATE: 15-Apr-91 TIME: 18:45:54 STEP 6 INCREMENT 50

ABAQUS

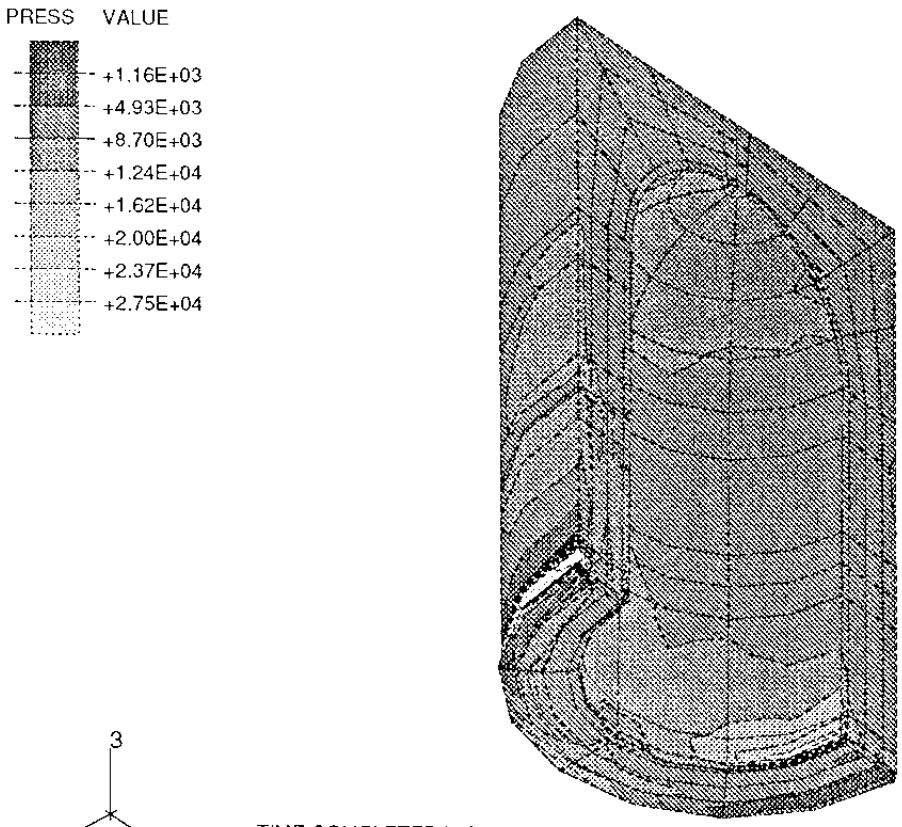

TIME COMPLETED IN THIS STEP +4.546E+05 TOTAL ACCUMULATED TIME +6.583E+05

ABAQUS VERSION 4-8-5 DATE: 15-Apr-91 TIME: 18:45:54 STEP 6 INCREMENT 50

VLH. Effect of rock shear.
Clay geometry. Average stress.

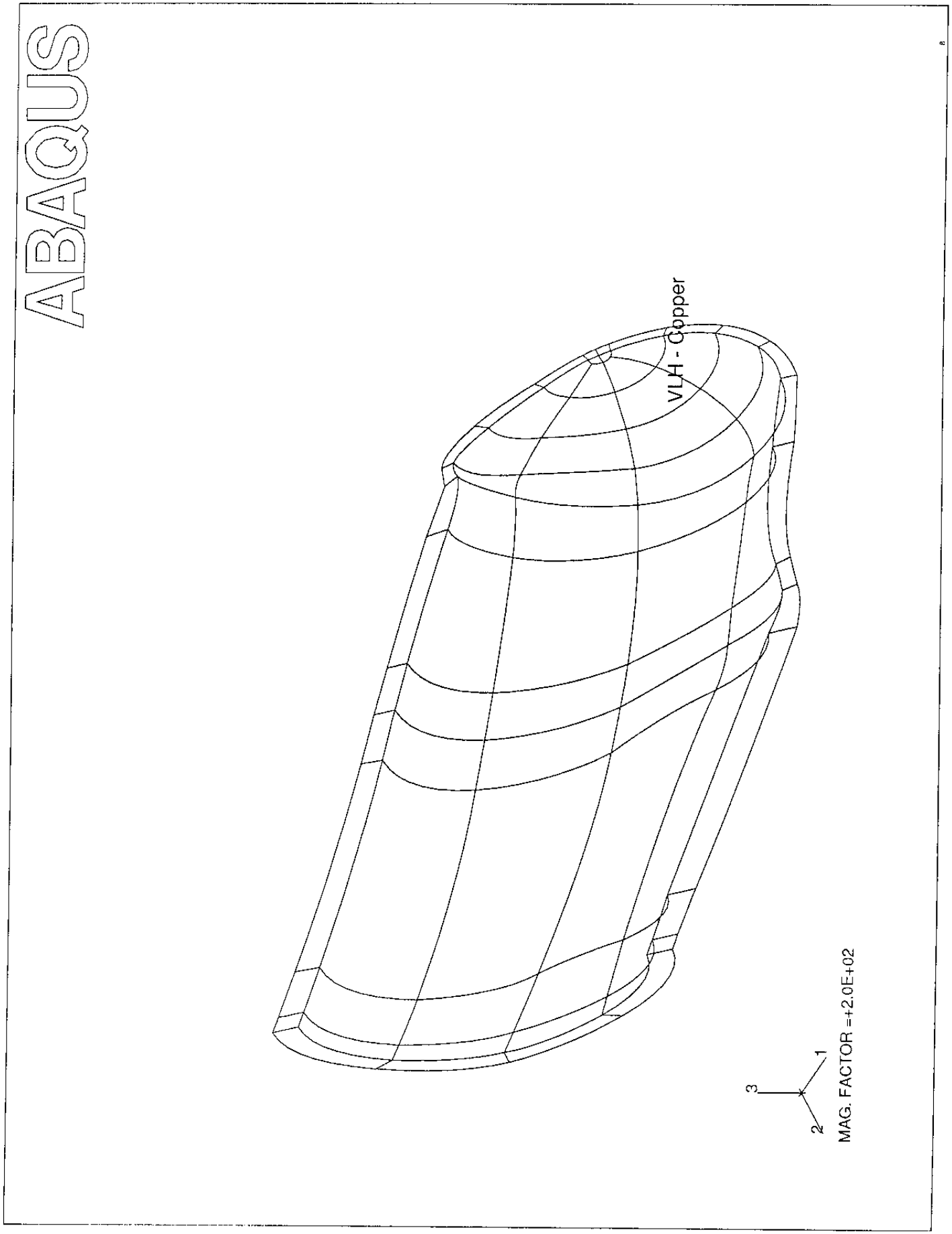

VLH. Effect of rock shear.
Copper canister. Deformed structure.

ABAQUS

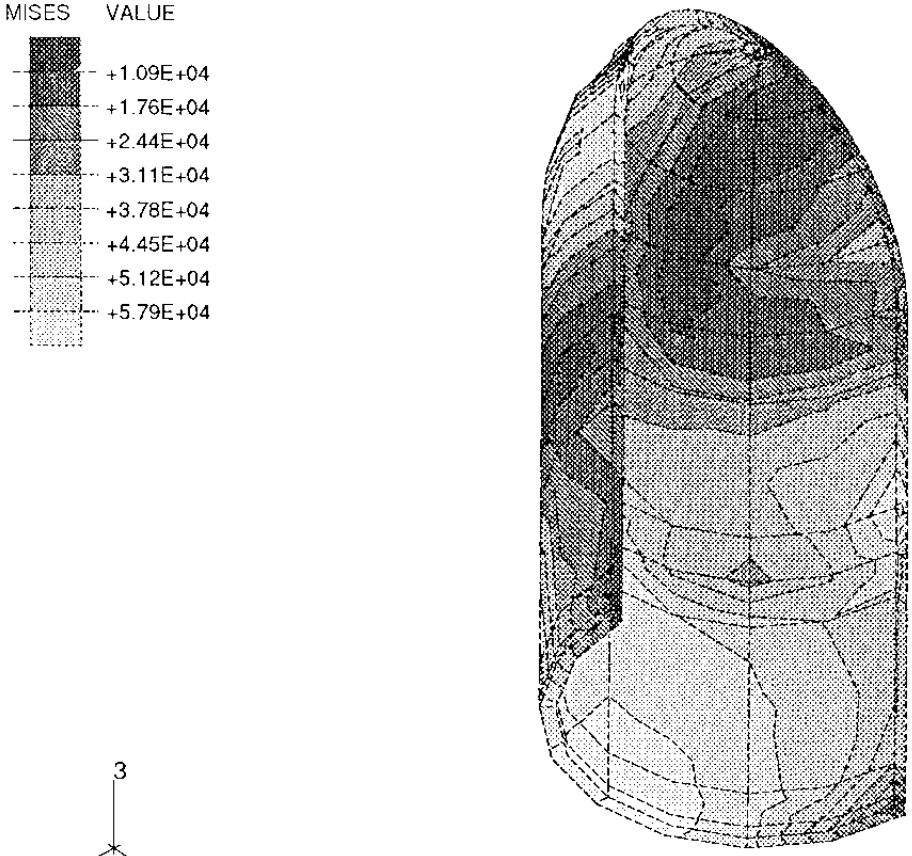

TIME COMPLETED IN THIS STEP +4.546E+05 TOTAL ACCUMULATED TIME +6.583E+05

ABAQUS VERSION 4-8-5 DATE: 15-Apr-91 TIME: 18:45:54 STEP 6 INCREMENT 50

VLH. Effect of rock shear.
Copper canister. Mises stress.

VLH. Effect of rock shear.
Copper canister. Plastic strain.

ABAQUS

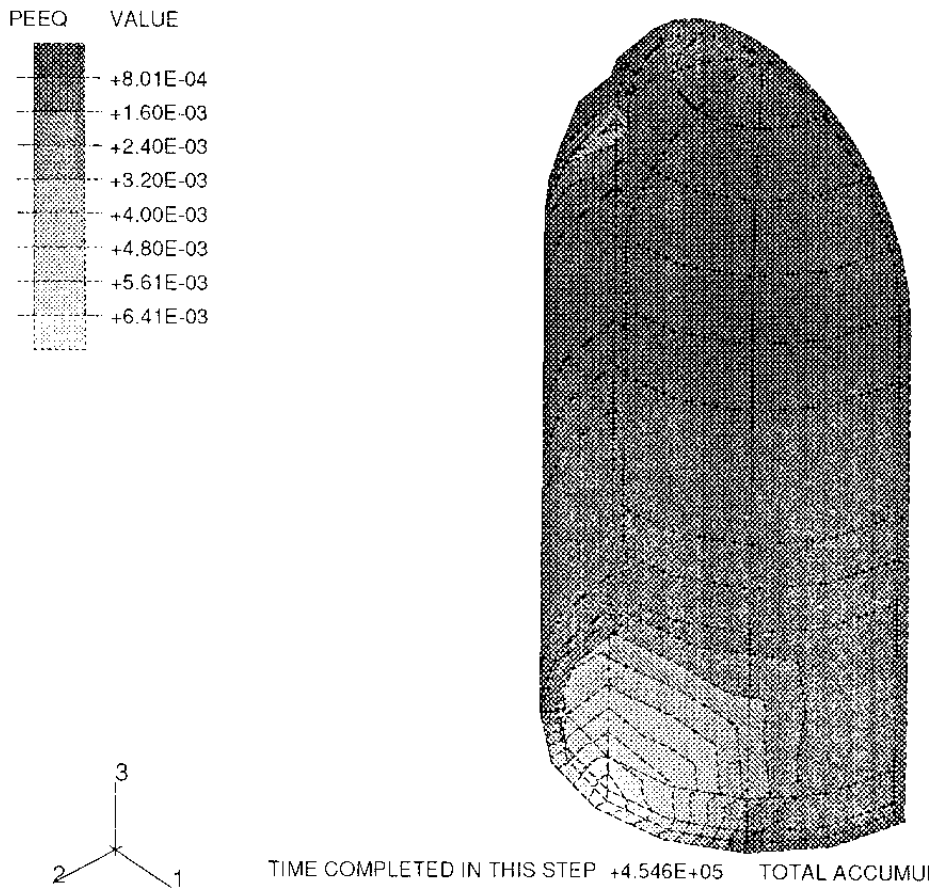

TIME COMPLETED IN THIS STEP +4.546E+05 TOTAL ACCUMULATED TIME +6.583E+05

ABAQUS VERSION 4-8-5 DATE: 15-Apr-91 TIME: 18:45:54 STEP 6 INCREMENT 50

ABAQUS

Stress_axi VLH 911203

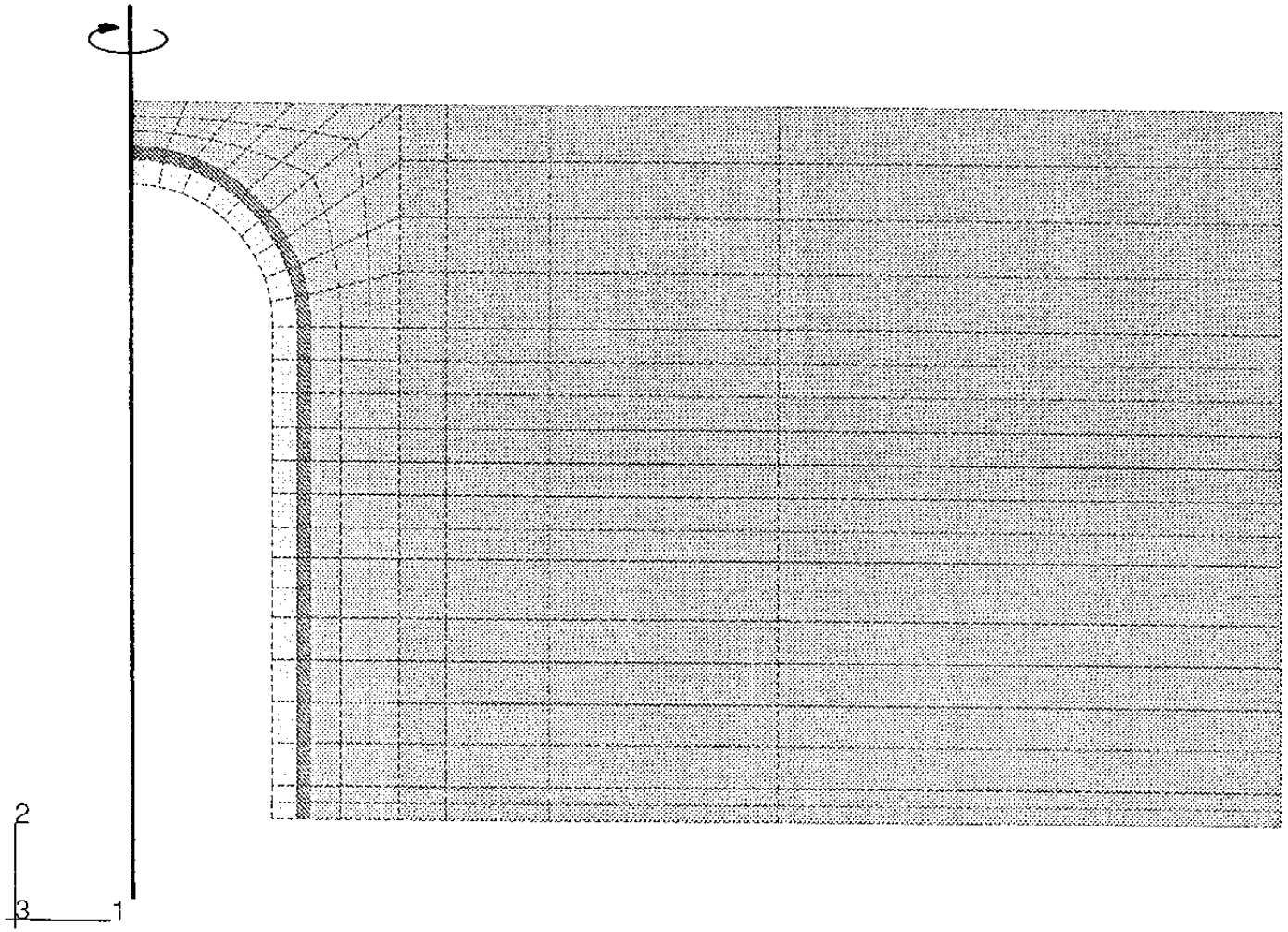

ABAQUS

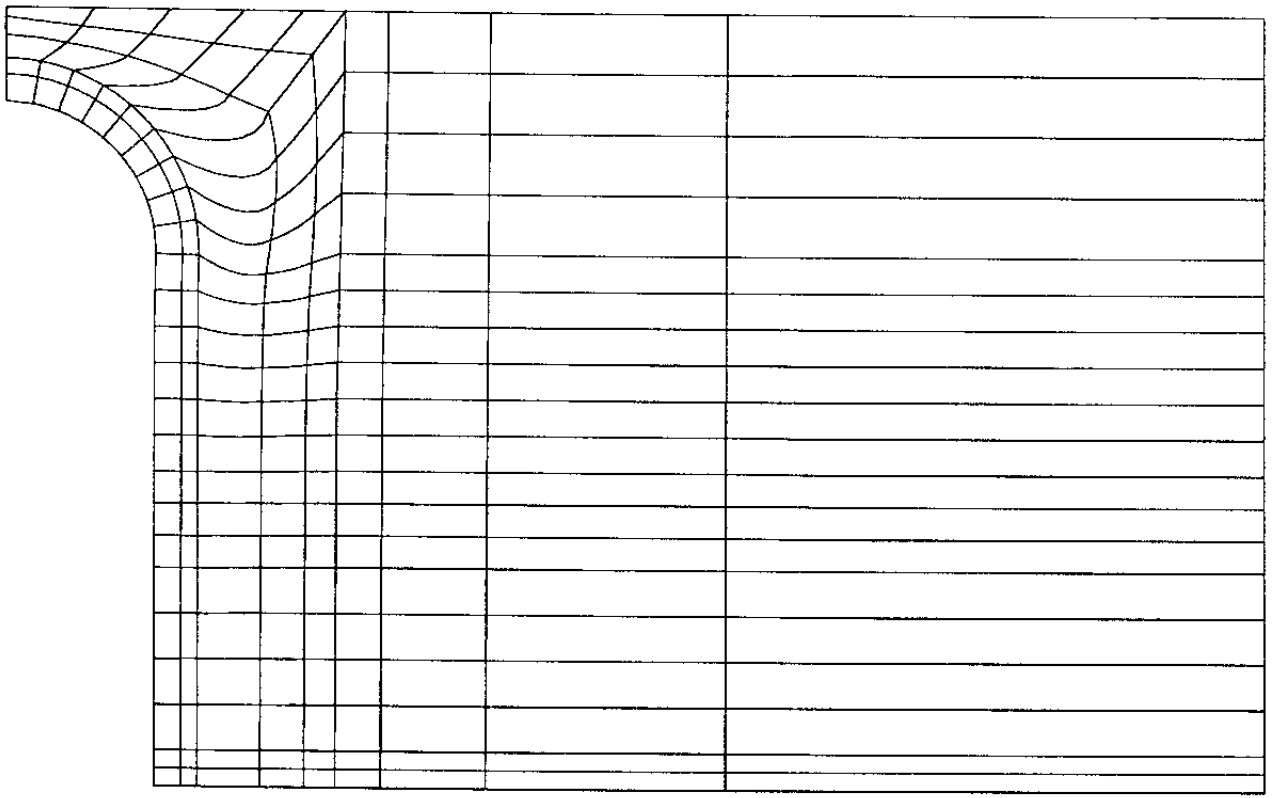

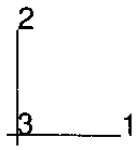

MAG. FACTOR =+5.0E+01

ABAQUS

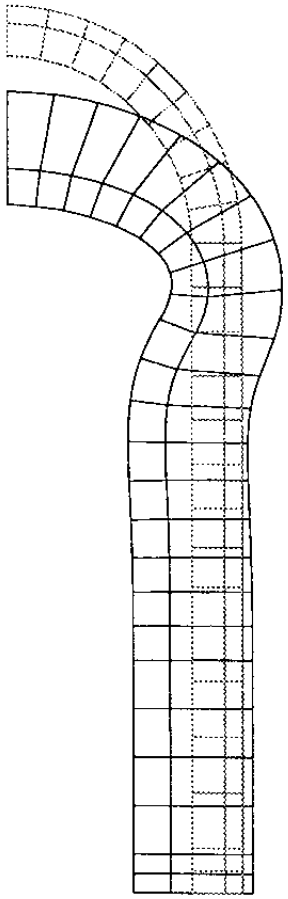

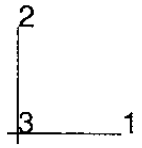

MAG. FACTOR =+1.3E+03

DISPLACED MESH

ORIGINAL MESH

ABAQUS

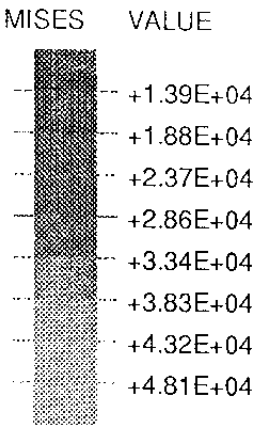

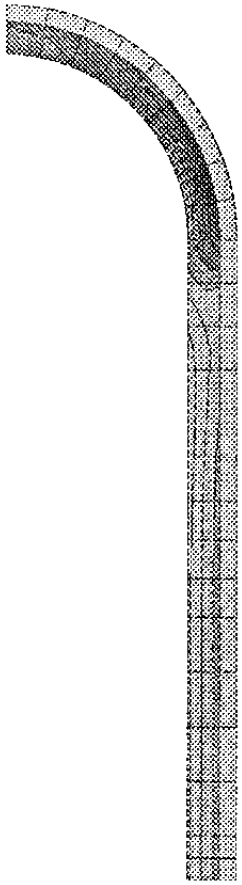

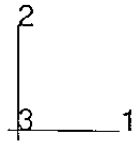

TIME COMPLETED IN THIS STEP +1.268E+07 TOTAL ACCUMULATED TIME +1.268E+07

ABAQUS VERSION 4-9-1 DATE: 3-Dec-91 TIME: 18:58:27 STEP 3 INCREMENT 300

ABAQUS

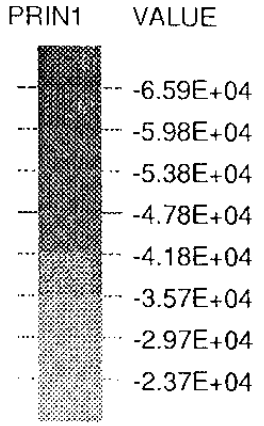

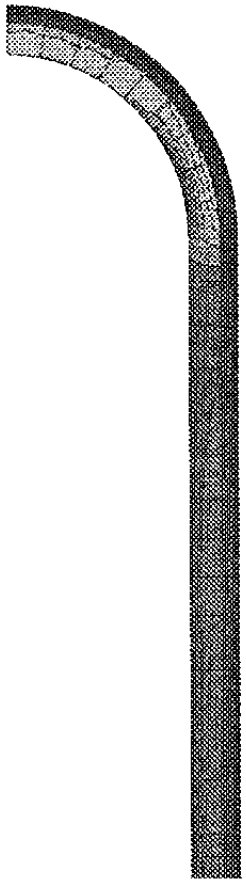

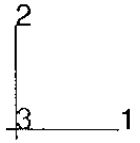

TIME COMPLETED IN THIS STEP +1.268E+07 TOTAL ACCUMULATED TIME +1.268E+07

ABAQUS VERSION 4-9-1 DATE: 3-Dec-91 TIME: 18:58:27 STEP 3 INCREMENT 300

ABAQUS

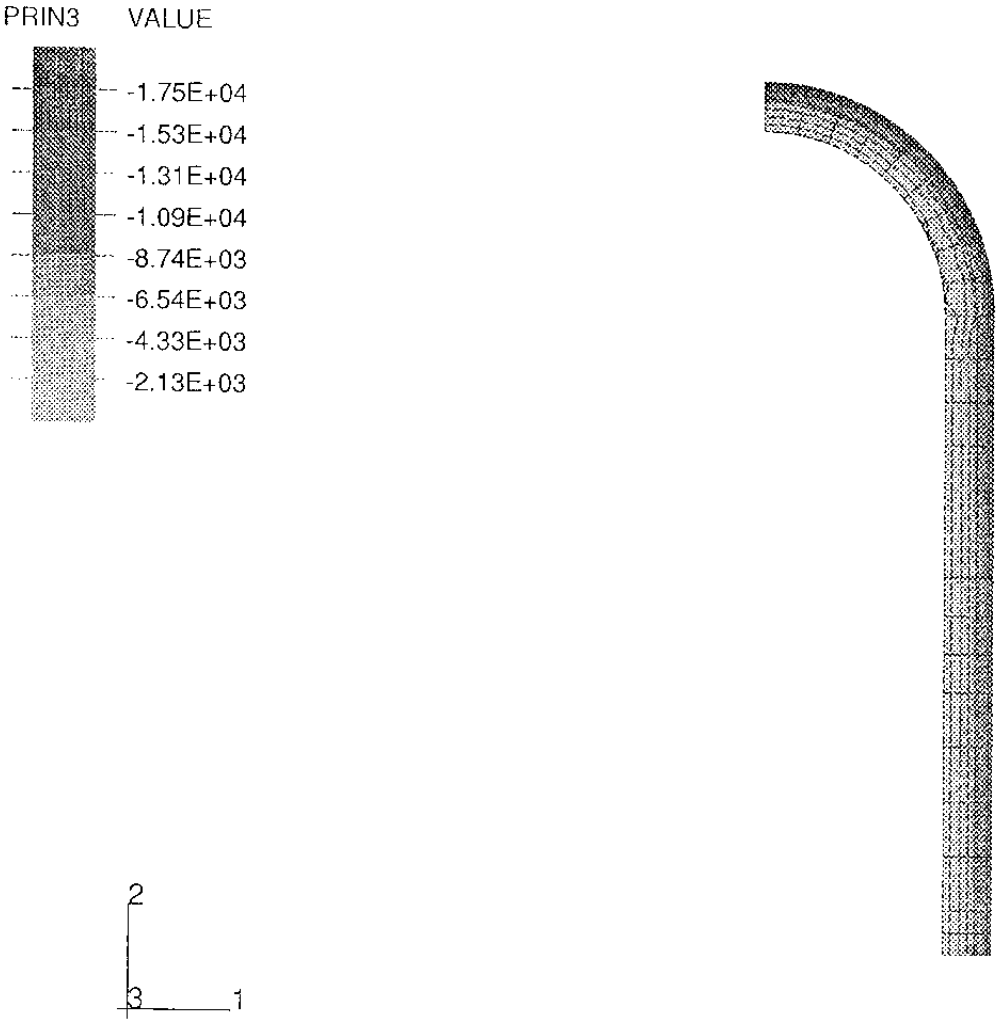

TIME COMPLETED IN THIS STEP +1.268E+07 TOTAL ACCUMULATED TIME +1.268E+07

ABAQUS VERSION 4-9-1 DATE: 3-Dec-91 TIME: 18:58:27 STEP 3 INCREMENT 300

ABAQUS

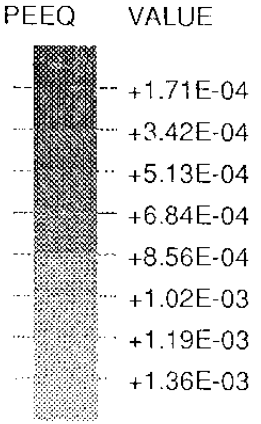

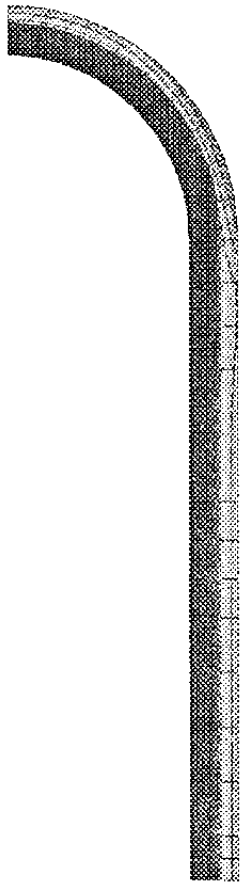

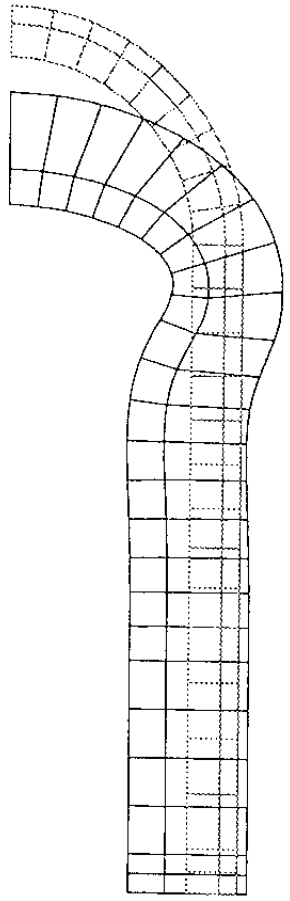

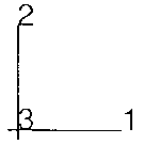

TIME COMPLETED IN THIS STEP +1.268E+07 TOTAL ACCUMULATED TIME +1.268E+07

ABAQUS VERSION 4-9-1 DATE: 3-Dec-91 TIME: 18:58:27 STEP 3 INCREMENT 300

ABAQUS

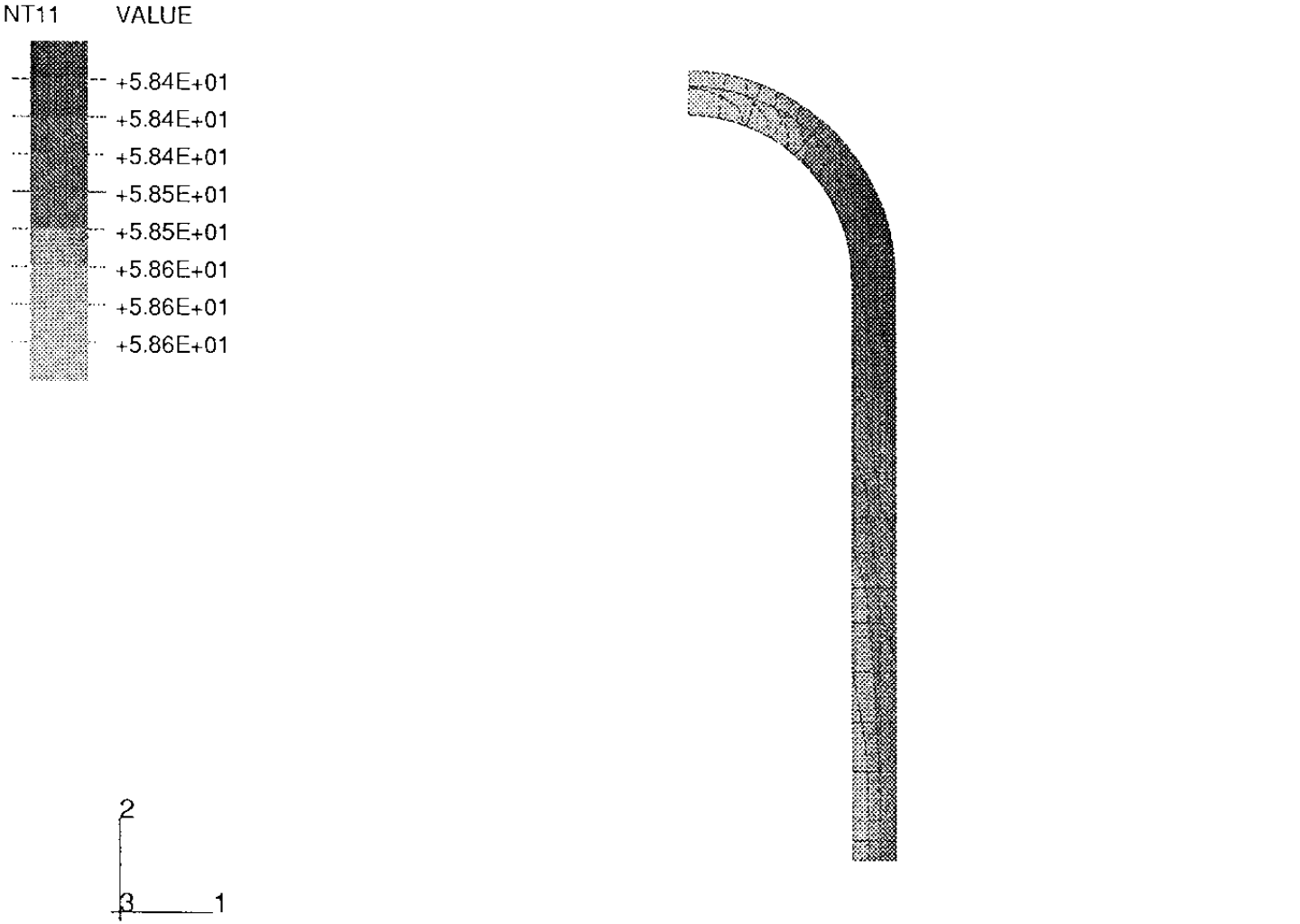

TIME COMPLETED IN THIS STEP +1.268E+07 TOTAL ACCUMULATED TIME +1.268E+07

ABAQUS VERSION 4-9-1 DATE: 3-Dec-91 TIME: 18:58:27 STEP 3 INCREMENT 300

ABAQUS

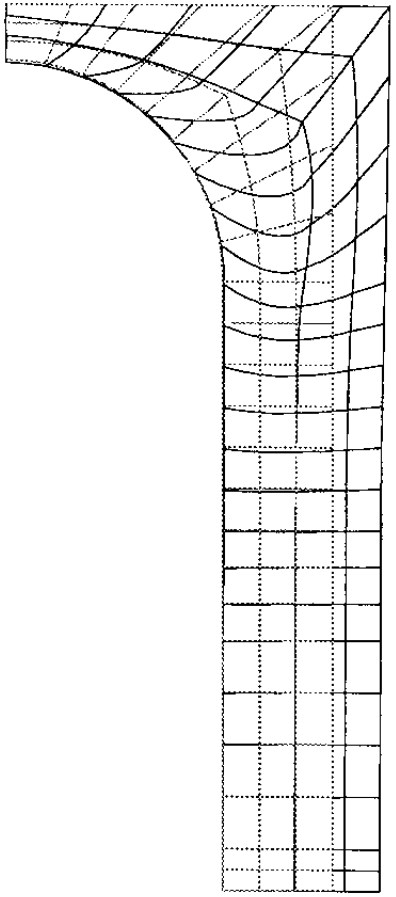

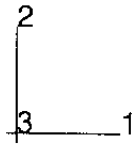

MAG. FACTOR =+5.0E+01

DISPLACED MESH

ORIGINAL MESH

ABAQUS

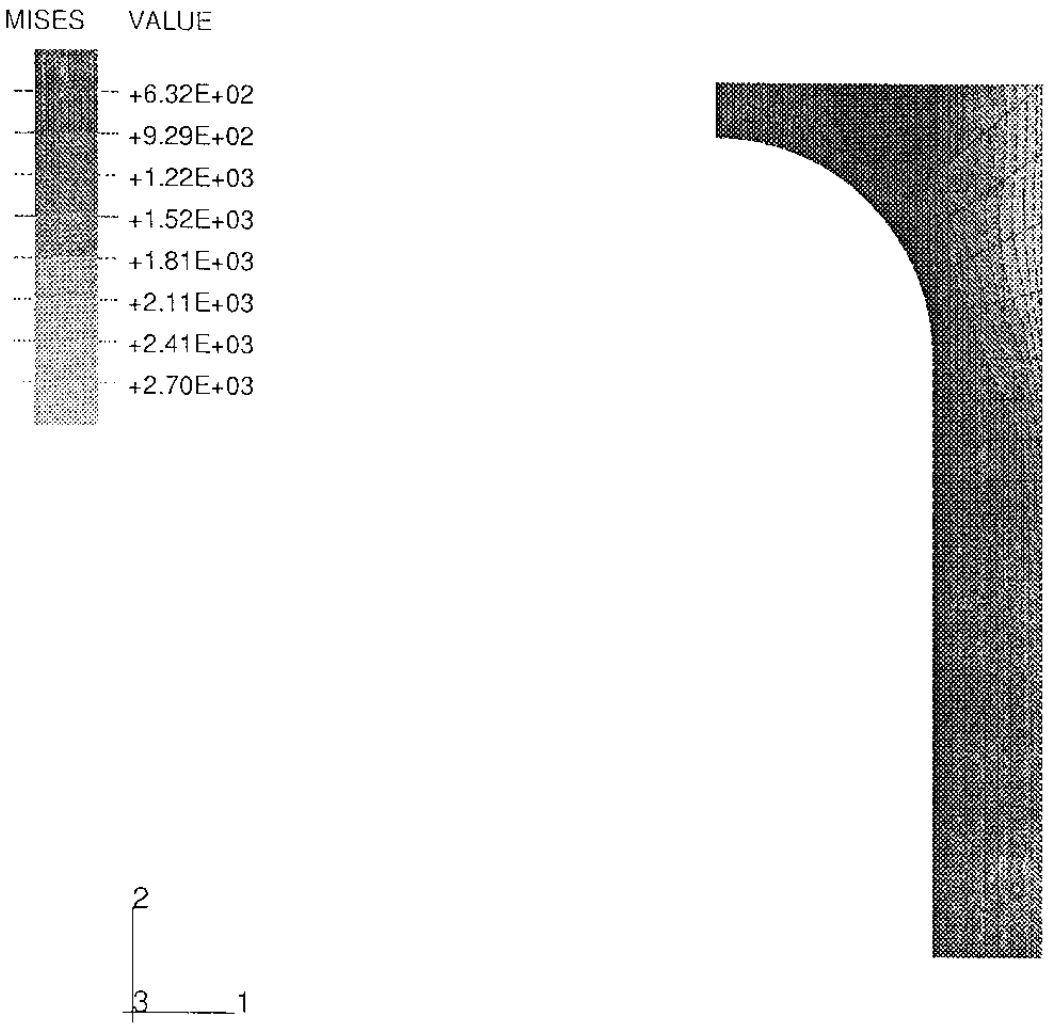

TIME COMPLETED IN THIS STEP +1.268E+07 TOTAL ACCUMULATED TIME +1.268E+07

ABAQUS VERSION 4-9-1 DATE: 3-Dec-91 TIME: 18:58:27 STEP 3 INCREMENT 300

ABAQUS

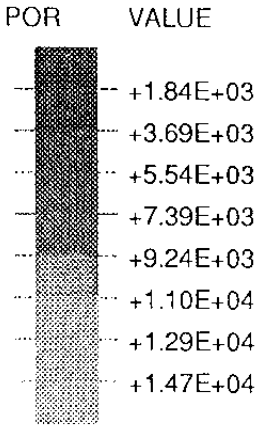

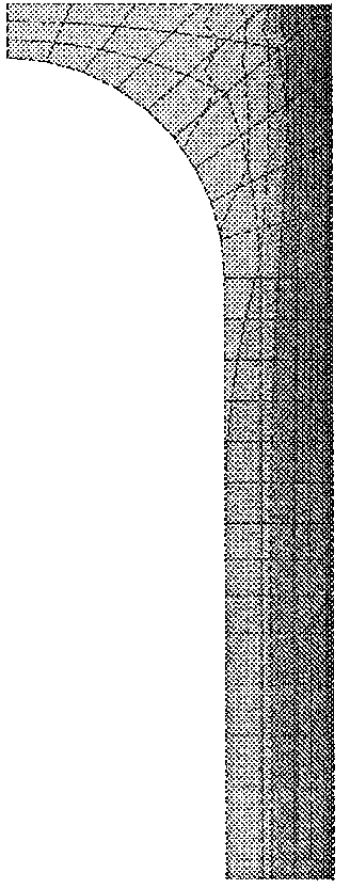

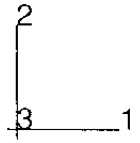

TIME COMPLETED IN THIS STEP +1.268E+07 TOTAL ACCUMULATED TIME +1.268E+07

ABAQUS VERSION 4-9-1 DATE: 3-Dec-91 TIME: 18:58:27 STEP 3 INCREMENT 300

ABAQUS

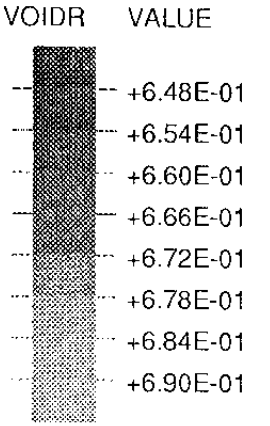

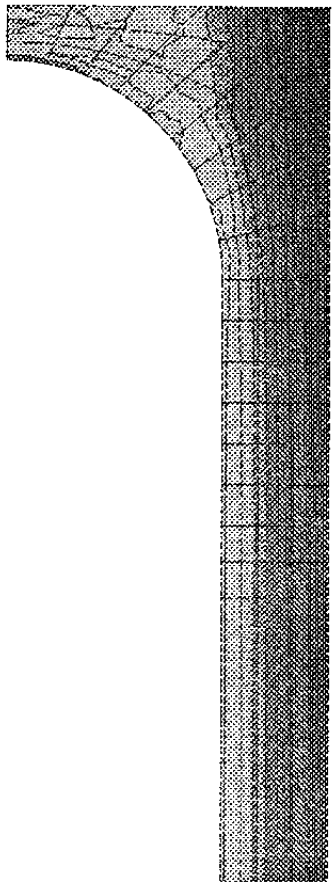

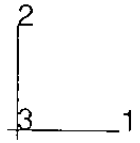

TIME COMPLETED IN THIS STEP +1.268E+07 TOTAL ACCUMULATED TIME +1.268E+07

ABAQUS VERSION 4-9-1 DATE: 3-Dec-91 TIME: 18:58:27 STEP 3 INCREMENT 300

ABAQUS

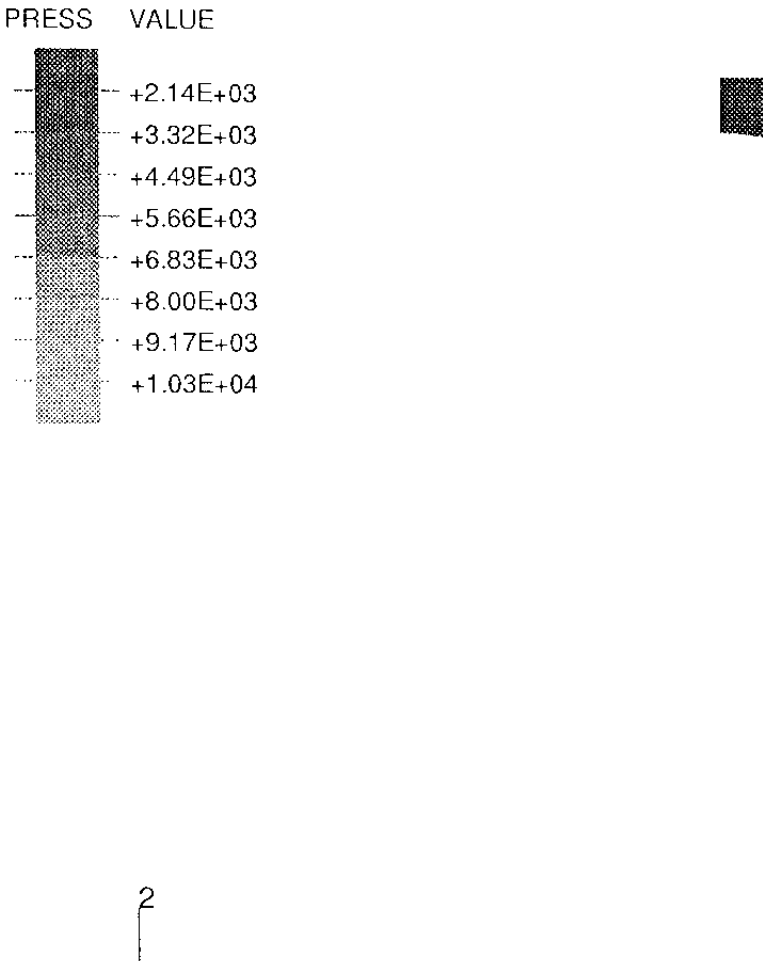

TIME COMPLETED IN THIS STEP +1.268E+07 TOTAL ACCUMULATED TIME +1.268E+07

ABAQUS VERSION 4-9-1 DATE: 3-Dec-91 TIME: 18:58:27 STEP 3 INCREMENT 300

ABAQUS

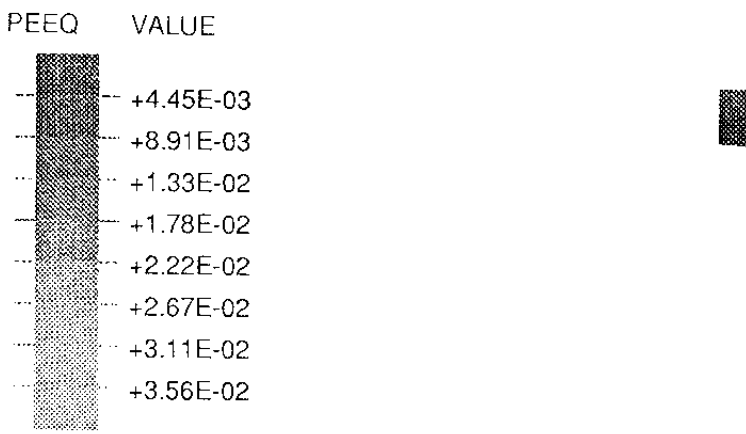

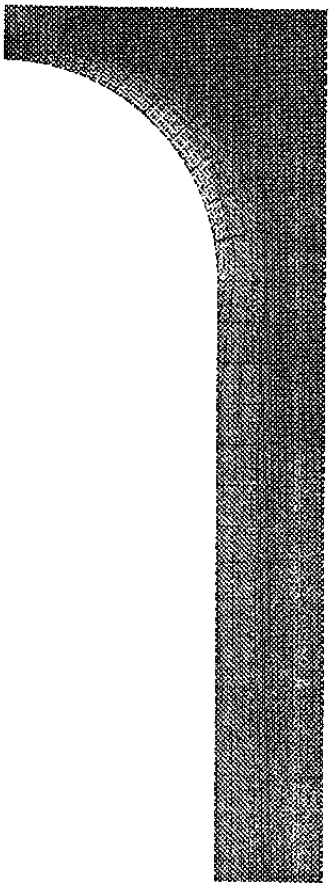

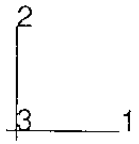

TIME COMPLETED IN THIS STEP +1.268E+07 TOTAL ACCUMULATED TIME +1.268E+07

ABAQUS VERSION 4-9-1 DATE: 3-Dec-91 TIME: 18:58:27 STEP 3 INCREMENT 300

ABAQUS

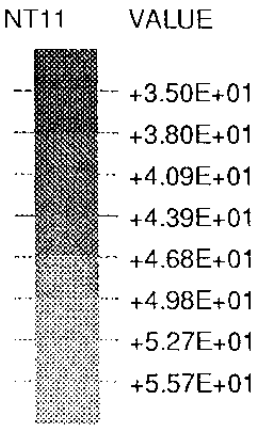

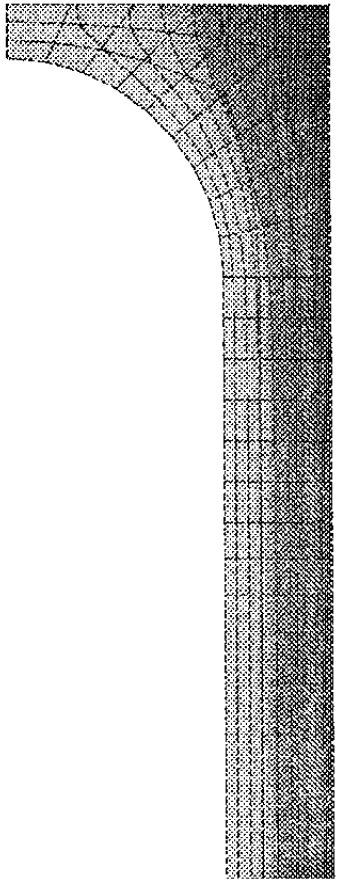

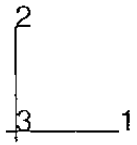

TIME COMPLETED IN THIS STEP +1.268E+07 TOTAL ACCUMULATED TIME +1.268E+07

ABAQUS VERSION 4-9-1 DATE: 3-Dec-91 TIME: 18:58:27 STEP 3 INCREMENT 300

ABAQUS

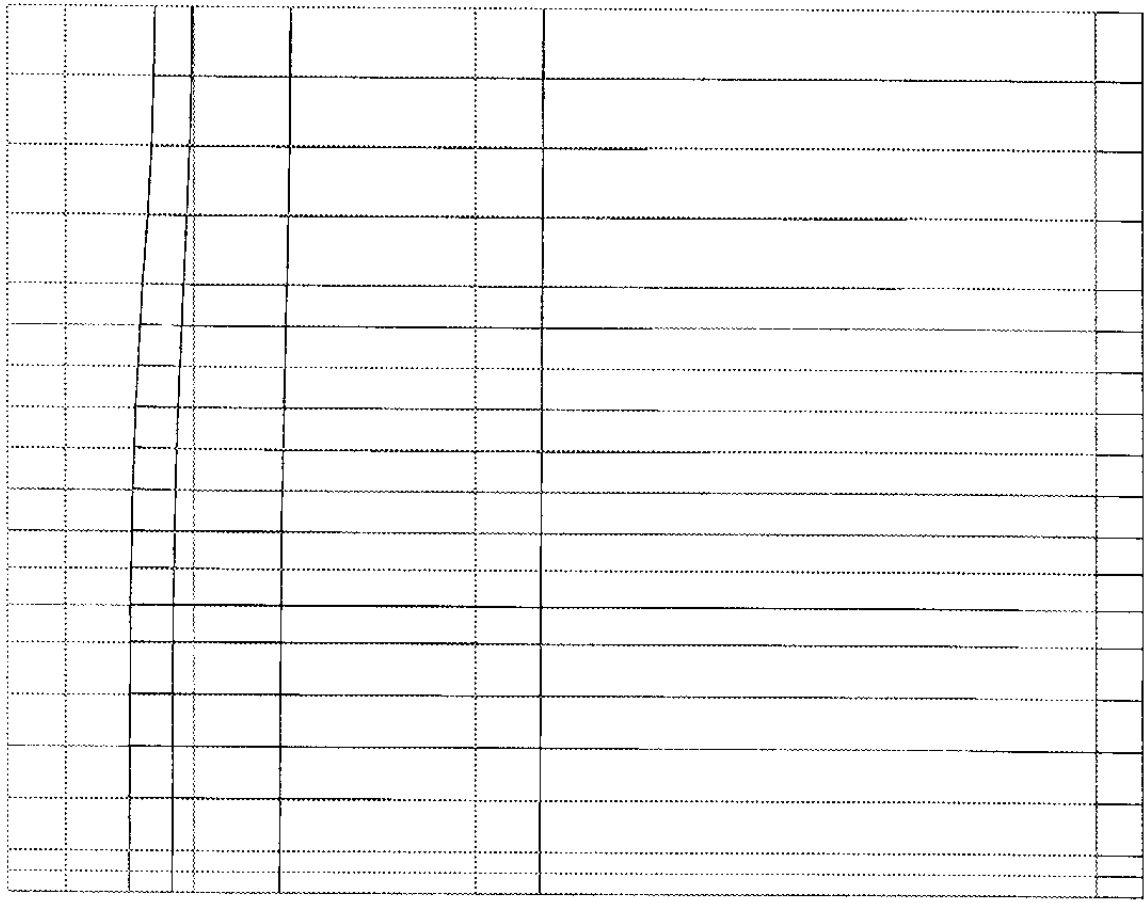

MAG. FACTOR =+1.2E+02

DISPLACED MESH ORIGINAL MESH

ABAQUS

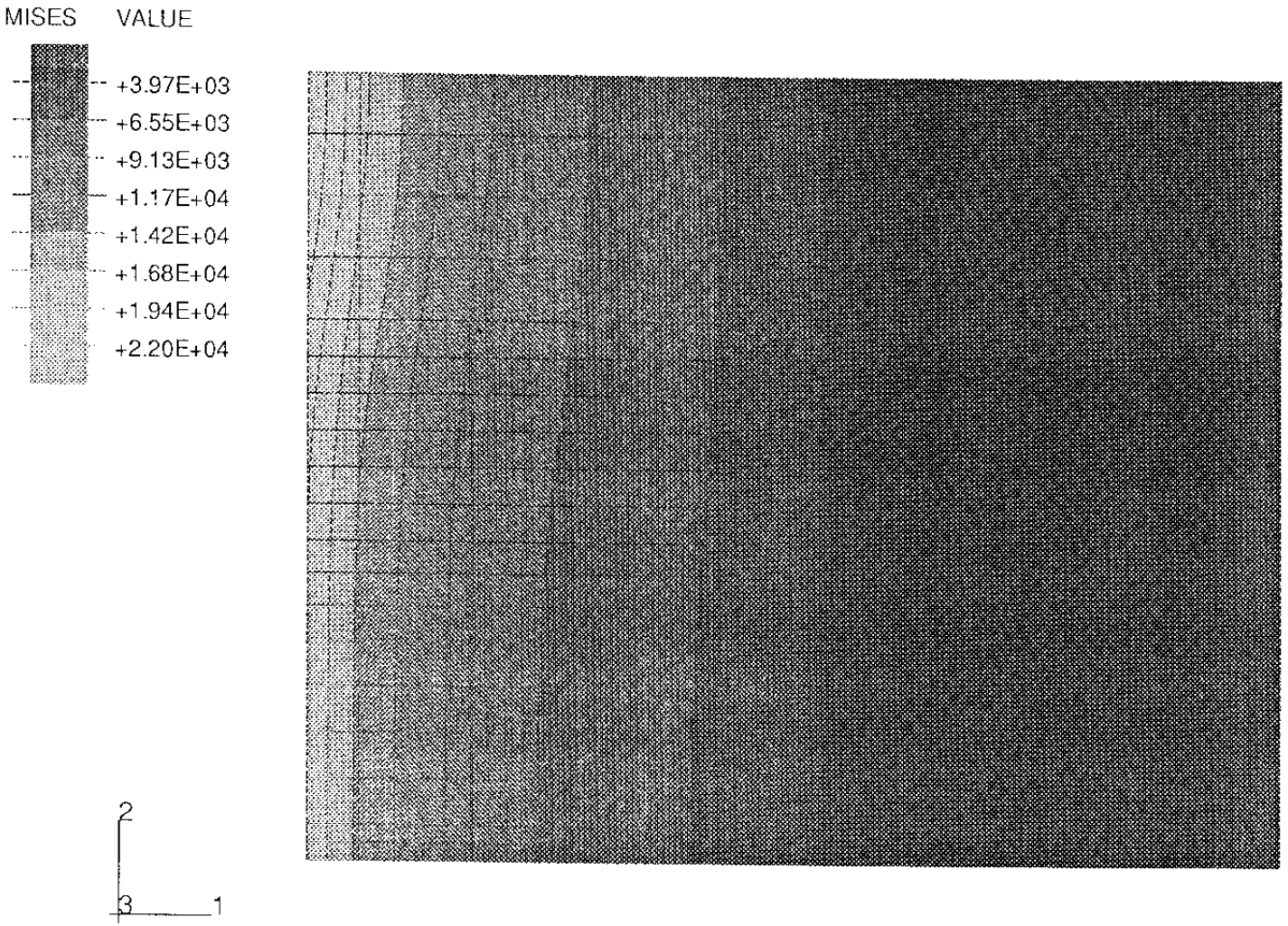

TIME COMPLETED IN THIS STEP +1.268E+07 TOTAL ACCUMULATED TIME +1.268E+07

ABAQUS VERSION 4-9-1 DATE: 3-Dec-91 TIME: 18:58:27 STEP 3 INCREMENT 300

ABAQUS

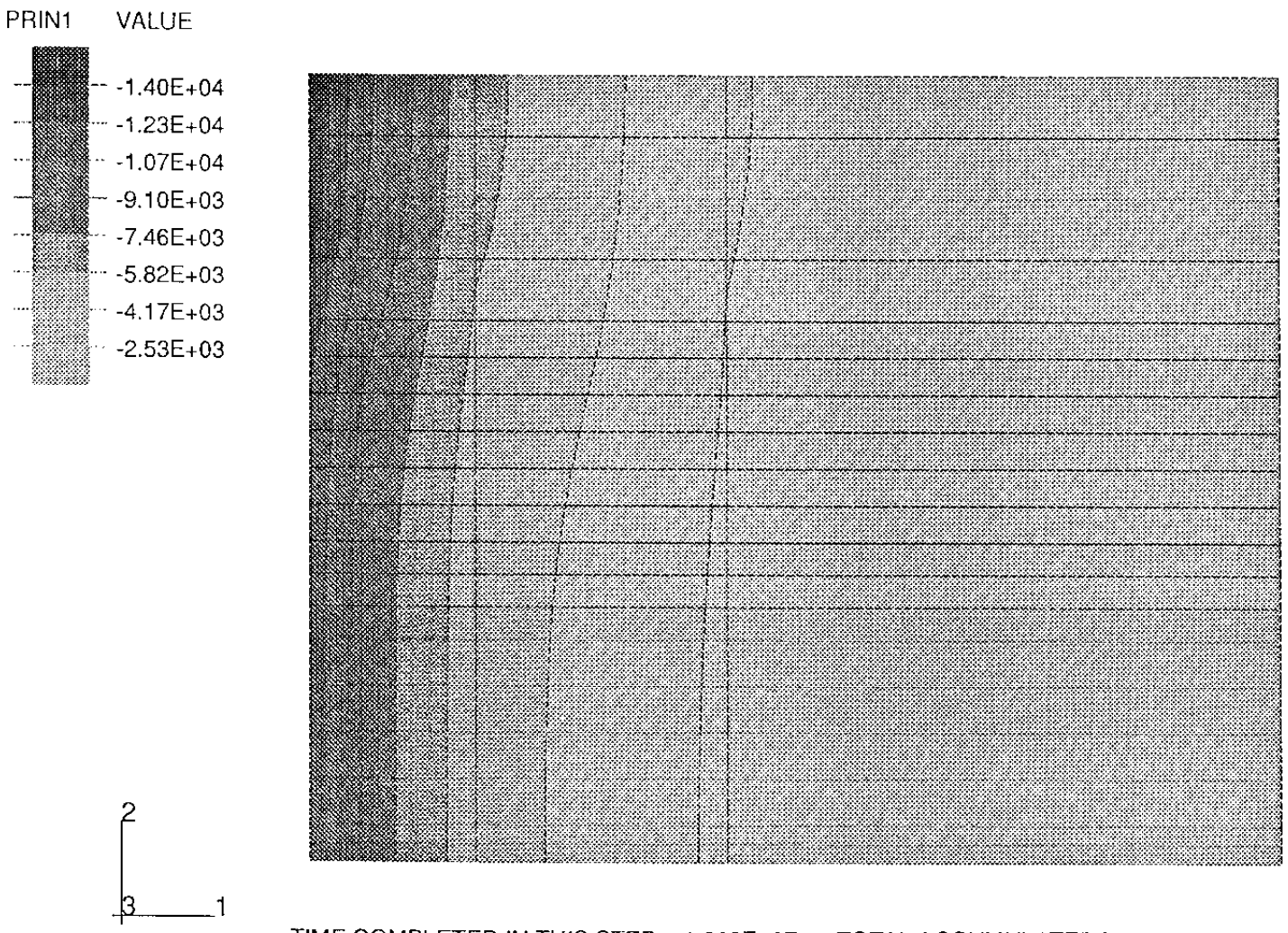

TIME COMPLETED IN THIS STEP +1.268E+07 TOTAL ACCUMULATED TIME +1.268E+07

ABAQUS VERSION 4-9-1 DATE: 3-Dec-91 TIME: 18:58:27 STEP 3 INCREMENT 300

ABAQUS

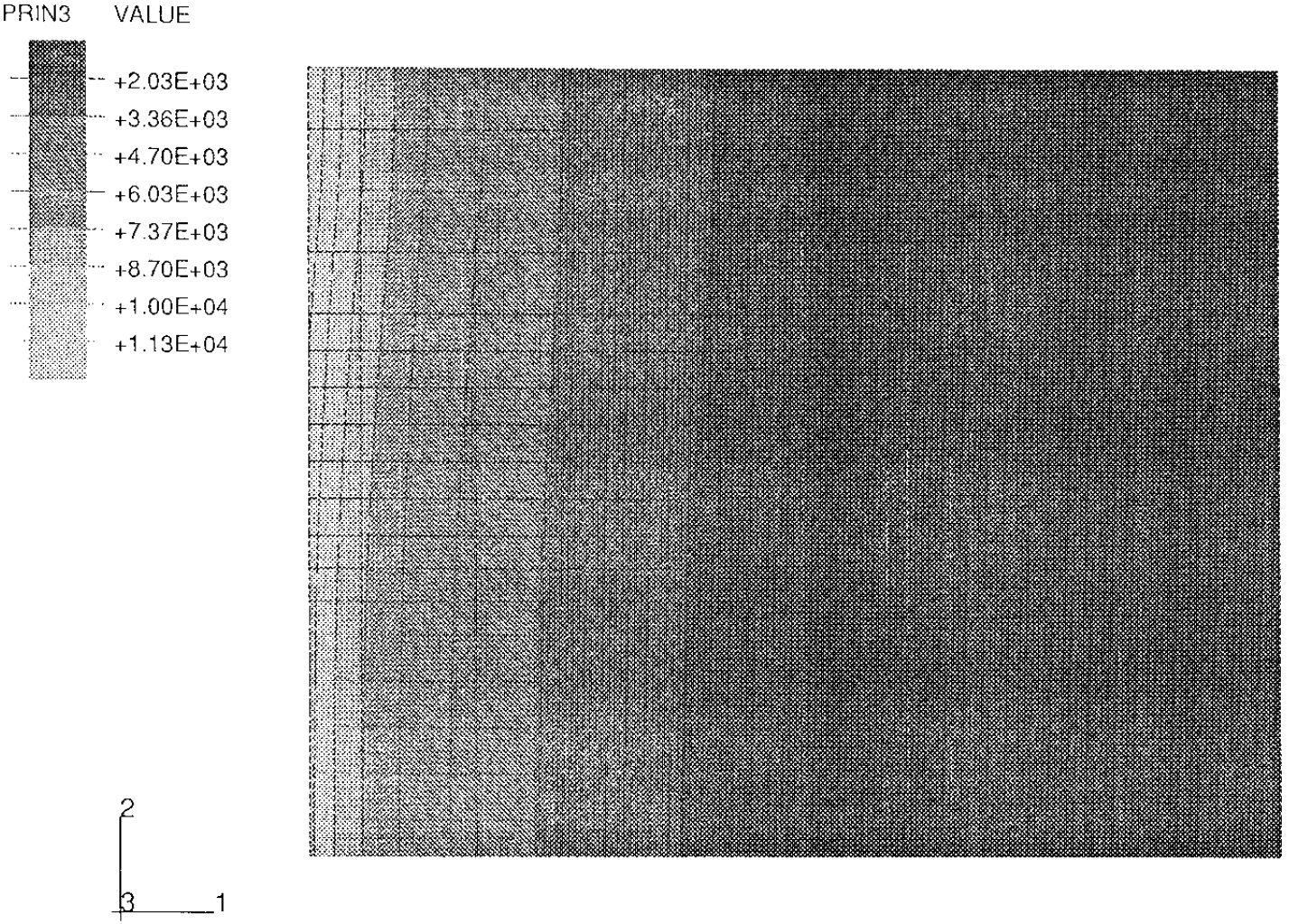

TIME COMPLETED IN THIS STEP +1.268E+07 TOTAL ACCUMULATED TIME +1.268E+07

ABAQUS VERSION 4-9-1 DATE: 3-Dec-91 TIME: 18:58:27 STEP 3 INCREMENT 300

ABAQUS

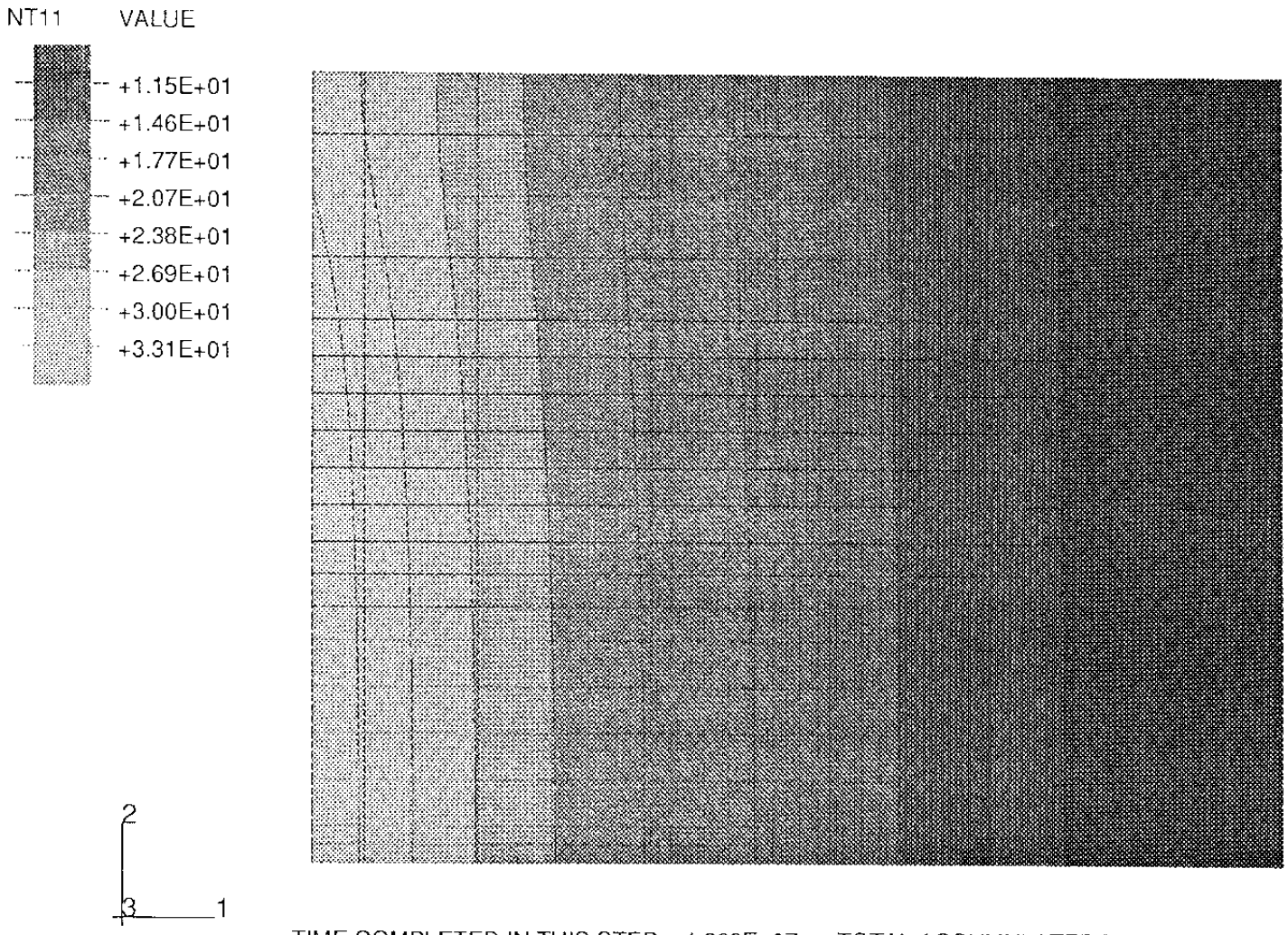

TIME COMPLETED IN THIS STEP +1.268E+07 TOTAL ACCUMULATED TIME +1.268E+07

ABAQUS VERSION 4-9-1 DATE: 3-Dec-91 TIME: 18:58:27 STEP 3 INCREMENT 300

APPENDIX X

Results from the thermomechanical calculation
VLH copper/steel canister

148 days after deposition

VLH. Effect of rock shear.
Slot. Aperture.

ABAQUS

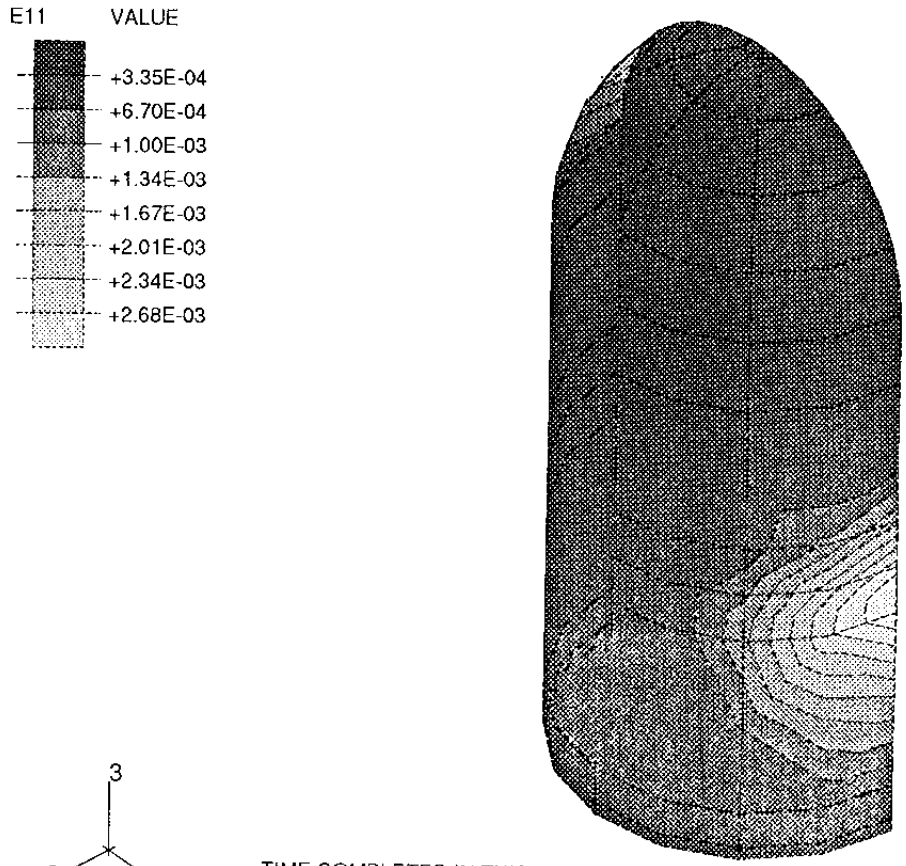

VLH - interface

TIME COMPLETED IN THIS STEP +4.546E+05 TOTAL ACCUMULATED TIME +6.583E+05

ABAQUS VERSION 4-8-5 DATE: 15-Apr-91 TIME: 18:45:54 STEP 6 INCREMENT 50

VLH. Effect of rock shear.
Slot. Contact pressure.

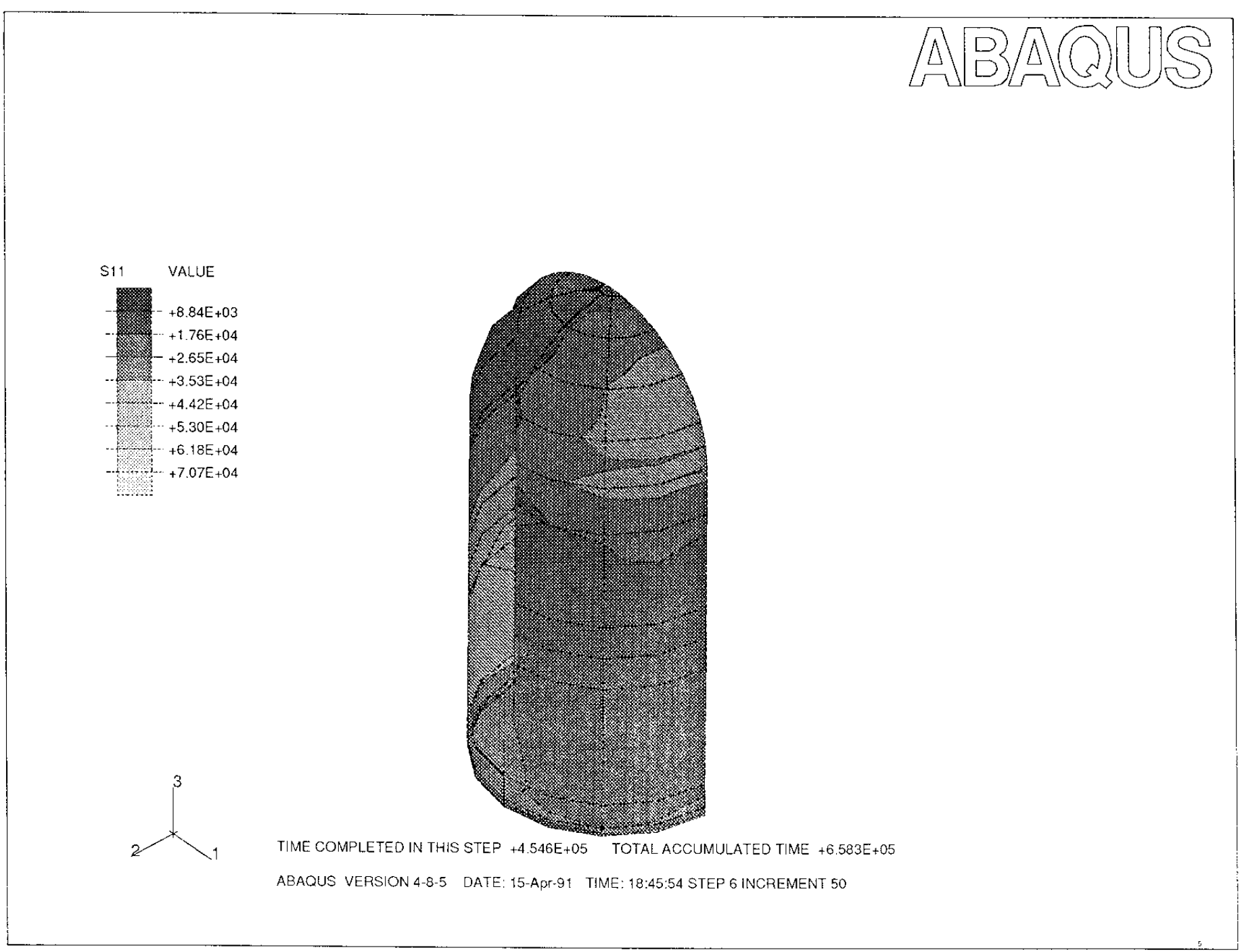

KBS-3. Effect of rock shear.
Steel canister. Mises stress.

ABAQUS

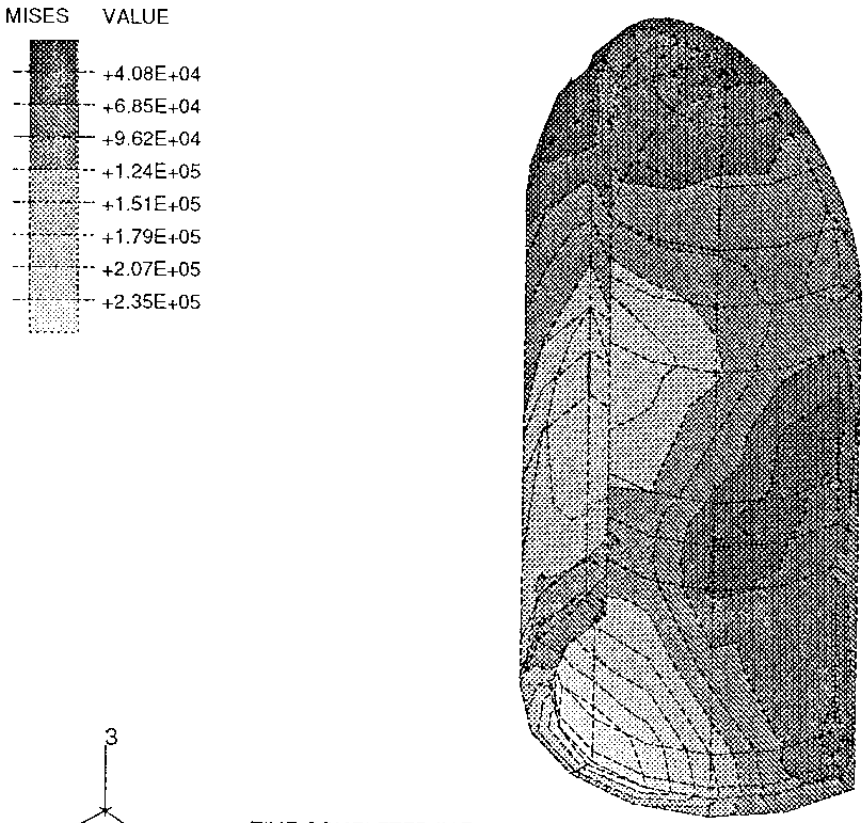

VLH - Steel

TIME COMPLETED IN THIS STEP +4.546E+05 TOTAL ACCUMULATED TIME +6.583E+05

ABAQUS VERSION 4-8-5 DATE: 15-Apr-91 TIME: 18:45:54 STEP 6 INCREMENT 50

List of SKB reports

Annual Reports

1977-78
TR 121
KBS Technical Reports 1 – 120
Summaries
Stockholm, May 1979

1979
TR 79-28
The KBS Annual Report 1979
KBS Technical Reports 79-01 – 79-27
Summaries
Stockholm, March 1980

1980
TR 80-26
The KBS Annual Report 1980
KBS Technical Reports 80-01 – 80-25
Summaries
Stockholm, March 1981

1981
TR 81-17
The KBS Annual Report 1981
KBS Technical Reports 81-01 – 81-16
Summaries
Stockholm, April 1982

1982
TR 82-28
The KBS Annual Report 1982
KBS Technical Reports 82-01 – 82-27
Summaries
Stockholm, July 1983

1983
TR 83-77
The KBS Annual Report 1983
KBS Technical Reports 83-01 – 83-76
Summaries
Stockholm, June 1984

1984
TR 85-01
Annual Research and Development Report 1984
Including Summaries of Technical Reports Issued during 1984. (Technical Reports 84-01 – 84-19)
Stockholm, June 1985

1985
TR 85-20
Annual Research and Development Report 1985
Including Summaries of Technical Reports Issued during 1985. (Technical Reports 85-01 – 85-19)
Stockholm, May 1986

1986
TR 86-31
SKB Annual Report 1986
Including Summaries of Technical Reports Issued during 1986
Stockholm, May 1987

1987
TR 87-33
SKB Annual Report 1987
Including Summaries of Technical Reports Issued during 1987
Stockholm, May 1988

1988
TR 88-32
SKB Annual Report 1988
Including Summaries of Technical Reports Issued during 1988
Stockholm, May 1989

1989
TR 89-40
SKB Annual Report 1989
Including Summaries of Technical Reports Issued during 1989
Stockholm, May 1990

1990
TR 90-46
SKB Annual Report 1990
Including Summaries of Technical Reports Issued during 1990
Stockholm, May 1991

1991
TR 91-64
SKB Annual Report 1991
Including Summaries of Technical Reports Issued during 1991
Stockholm, April 1992

Technical Reports

List of SKB Technical Reports 1992

TR 92-01
GEOTAB. Overview
Ebbe Eriksson[1], Bertil Johansson[2], Margareta Gerlach[3], Stefan Magnusson[2], Ann-Chatrin Nilsson[4], Stefan Sehlstedt[3], Tomas Stark[1]
[1]SGAB, [2]ERGODATA AB, [3]MRM Konsult AB
[4]KTH
January 1992

TR 92-02
Sternö study site. Scope of activities and main results
Kaj Ahlbom[1], Jan-Erik Andersson[2], Rune Nordqvist[2], Christer Ljunggren[3], Sven Tirén[2], Clifford Voss[4]
[1]Conterra AB, [2]Geosigma AB, [3]Renco AB,
[4]U.S. Geological Survey
January 1992

TR 92-03
Numerical groundwater flow calculations at the Finnsjön study site – extended regional area
Björn Lindbom, Anders Boghammar
Kemakta Consultants Co, Stockholm
March 1992

TR 92-04
Low temperature creep of copper intended for nuclear waste containers
P J Henderson, J-O Österberg, B Ivarsson
Swedish Institute for Metals Research, Stockholm
March 1992

TR 92-05
Boyancy flow in fractured rock with a salt gradient in the groundwater – An inititial study
Johan Claesson
Department of Building Physics, Lund University, Sweden
February 1992

TR 92-06
Characterization of nearfield rock – A basis for comparison of repository concepts
Roland Pusch, Harald Hökmark
Clay Technology AB and Lund University of Technology
December 1991

TR 92-07
Discrete fracture modelling of the Finnsjön rock mass: Phase 2
J E Geier, C-L Axelsson, L Hässler,
A Benabderrahmane
Golden Geosystem AB, Uppsala, Sweden
April 1992

TR 92-08
Statistical inference and comparison of stochastic models for the hydraulic conductivity at the Finnsjön site
Sven Norman
Starprog AB
April 1992

TR 92-09
Description of the transport mechanisms and pathways in the far field of a KBS-3 type repository
Mark Elert[1], Ivars Neretnieks[2], Nils Kjellbert[3], Anders Ström[3]
[1]Kemakta Konsult AB
[2]Royal Institute of Technology
[3]Swedish Nuclear Fuel and Waste Management Co
April 1992

TR 92-10
Description of groundwater chemical data in the SKB database GEOTAB prior to 1990
Sif Laurent[1], Stefan Magnusson[2],
Ann-Chatrin Nilsson[3]
[1]IVL, Stockholm
[2]Ergodata AB, Göteborg
[3]Dept. of Inorg. Chemistry, KTH, Stockholm
April 1992

TR 92-11
Numerical groundwter flow calculations at the Finnsjön study site – the influence of the regional gradient
Björn Lindbom, Anders Boghammar
Kemakta Consultants Co., Stockholm, Sweden
April 1992

TR 92-12
HYDRASTAR – a code for stochastic simulation of groundwater flow
Sven Norman
Abraxas Konsult
May 1992

TR 92-13
Radionuclide solubilities to be used in SKB 91
Jordi Bruno[1], Patrik Sellin[2]
[1]MBT, Barcelona Spain
[2]SKB, Stockholm, Sweden
June 1992

TR 92-14
Numerical calculations on heterogeneity of groundwater flow
Sven Follin
Department of Land and Water Resources, Royal Institute of Technology
June 1992

TR 92-15

Kamlunge study site.
Scope of activities and main results

Kaj Ahlbom[1], Jan-Erik Andersson[2],
Peter Andersson[2], Thomas Ittner[2],
Christer Ljunggren[3], Sven Tirén[2]
[1]Conterra AB
[2]Geosigma AB
[3]Renco AB
May 1992

TR 92-16

Equipment for deployment of canisters with spent nuclear fuel and bentonite buffer in horisontal holes

Vesa Henttonen, Miko Suikki
JP-Engineering Oy, Raisio, Finland
June 1992

TR 92-17

The implication of fractal dimension in hydrogeology and rock mechanics. Version 1.1

W Dershowitz[1], K Redus[1], P Wallmann[1],
P LaPointe[1], C-L Axelsson[2]
[1]Golder Associates Inc., Seattle, Washington, USA
[2]Golder Associates Geosystem AB, Uppsala, Sweden
February 1992

TR 92-18

Stochastic continuum simulation of mass arrival using a synthetic data set. The effect of hard and soft conditioning

Kung Chen Shan[1], Wen Xian Huan[1], Vladimir Cvetkovic[1], Anders Winberg[2]
[1] Royal Institute of Technology, Stockholm
[2] Conterra AB, Gothenburg
June 1992

TR 92-19

Partitioning and transmutation.
A review of the current state of the art

Mats Skålberg, Jan-Olov Liljenzin
Department of Nuclear Chemistry,
Chalmers University of Technology
October 1992

TR 92-20

SKB 91
Final disposal of spent nuclear fuel.
Importance of the bedrock for safety.

SKB
May 1992

TR 92-21

The Protogine Zone.
Geology and mobility during the last 1.5 Ga

Per-Gunnar Andréasson, Agnes Rodhe
September 1992

TR 92-22

Klipperås study site.
Scope of activities and main results

Kaj Ahlbom[1], Jan-Erik Andersson[2],
Peter Andersson[2], Tomas Ittner[2],
Christer Ljunggren[3], Sven Tirén[2]
[1]Conterra AB
[2]Geosigma AB
[3]Renco AB
September 1992

TR 92-23

Bedrock stability in Southeastern Sweden. Evidence from fracturing in the Ordovician limestones of Northern Öland

Alan Geoffrey Milnes[1], David G Gee[2]
[1]Geological and Environmental Assessments (GEA), Zürich, Switzerland
[2]Geologiska Institutionen, Lund, Sweden
September 1992

TR 92-24

Plan 92
Costs for management of the radioactive waste from nuclear power production

Swedish Nuclear Fuel and Waste Management Co
June 1992

TR 92-25

Gabbro as a host rock for a nuclear waste repository

Kaj Ahlbom[1], Bengt Leijon[1], Magnus Liedholm[2],
John Smellie[1]
[1]Conterra AB
[2]VBB VIAK
September 1992

TR 92-26

Copper canisters for nuclear high level waste disposal. Corrosion aspects

Lars Werme, Patrik Sellin, Nils Kjellbert
Swedish Nuclear Fuel and Waste Management Co, Stockholm, Sweden
October 1992

TR 92-27

Thermo-mechanical FE-analysis of butt-welding of a Cu-Fe canister for spent nuclear fuel

B L Josefson[1], L Karlsson[2], L-E Lindgren[2], M Jonsson[2]
[1]Chalmers University of Technology, Göteborg, Sweden
[2]Division of Computer Aided Design, Luleå University of Technology, Luleå, Sweden
October 1992

TR 92-28

A rock mechanics study of Fracture Zone 2 at the Finnsjön site

Bengt Leijon[1], Christer Ljunggren[2]
[1]Conterra AB
[2]Renco AB
January 1992

TR 92-29

Release calculations in a repository of the very long tunnel type

L Romero, L Moreno, I Neretnieks
Department of Chemical Engineering,
Royal Institute of Technology, Stockholm, Sweden
November 1992